

63-4-1

CATALOGED BY DDC
AS AD NO. ~~407~~ 505

407 505

Columbia University
in the City of New York

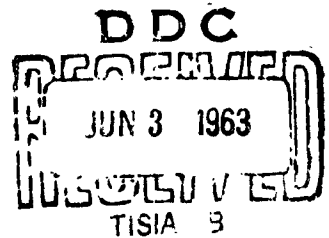
AN EXPERIMENTAL STUDY OF HEAT TRANSFER AT
HIGH TEMPERATURE DIFFERENCES IN TURBULENT
AIR FLOW BETWEEN A ROTATING CYLINDER
AND A STATIONARY CONCENTRIC OUTER CYLINDER

by

G. S. Longobardo and H. G. Elrod

Sponsored by the Air Force Office of Scientific Research
Contract No. AF 49(638)-1001
Final Report No. AFOSR 3207

August 1962



DEPARTMENT OF MECHANICAL ENGINEERING
SCHOOL OF ENGINEERING AND APPLIED SCIENCE
NEW YORK 27, N.Y.

**Best
Available
Copy**

Abstract

A study has been made of convective heat transfer between a rotating cylinder and a stationary, concentric outer cylinder for the Taylor number range 2000 to 9000, and for rotor surface temperatures in the range 80 F to 430 F.

Measurements were made of overall heat transfer, and velocity and temperature distributions in the gap between the two cylinders. A hot wire anemometer was used to determine whether secondary flows exist in the gap in the Taylor number range of the investigation.

The principal results are as follows:

1. That turbulent flow can exist in the gap without an axial flow of air in the range of Taylor number 3000 to 9000.
2. That the correlation offered by Kays and Bjorklund for the heat transfer in the gap, $Nu/Nu_{cond.} = 0.175 (Ta)^{1/2}$ can be extended for low temperature differences from Taylor numbers of 2000 to Taylor numbers of 9000. At higher temperature differences the heat transfer is reduced but still varies as $(Ta)^{1/2}$.
3. That V_{θ}^+ vs. y^+ follows the universal curve for pipe flow out to $y^+ = 10$, and levels off.
4. That the friction factor follows a relation

$$f_{rotor} = \frac{0.3342}{Ta^{0.358}}$$

5. a. That near the walls and out to $y^+ = 50$, two curves, one for the rotor, and one for the stator, suffice to describe $\epsilon_M/\nu f$ vs, y^+ for $3000 < Ta < 9000$, and for temperature differences of from 60 F to 330 F.

b. That the eddy diffusivity in the middle of the channel can be expressed by the relation

$$(1 + \epsilon_M/\nu) = 0.0894 \left(\frac{r_{\text{rotor}}}{r}\right)^2 \left(\frac{1}{d/r_{\text{rotor}}}\right)^{3/2} f_{\text{rotor}} \left(1 + \frac{T_{\text{stator}}}{T_{\text{rotor}}}\right) T_a$$

1.75 < r" < 1.95

6. That the ratio ϵ_H/ϵ_M equals 1.4 for the conditions studied.

7. That the correlations obtained can be used to determine overall friction factors and heat transfer for the apparatus in the ranges of Taylor number and temperature differences studied when given the temperature of the rotor, the temperature of the stator, and the rpm of the rotor.

Table of Contents

	Page
Acknowledgements	
List of Tables	
List of Illustrations	
Nomenclature	
Chapter	
I Introduction	1
1.1 Purpose of Investigation	1
1.2 Summary of Previous Work	2
1.2.1 Flow between Rotating Cylinders	
1.2.2 Determination of Eddy Diffusivities for Momentum and Heat	
II Development of Basic Equations	20
2.1 General Equations of Motion	20
2.1.1 Equation of Motion for Laminar Flow	
2.1.2 Equation of Motion for Turbulent Flow	
2.1.3 The Determination of ϵ_H/GM	
III Experimental Apparatus	36
3.1 General Arrangement	36
3.2 Inner Rotating Cylinder	
3.2.1 Rotor Outer Shell	
3.2.2 Rotor Heating Element	
3.2.3 Rotor Shaft	

	Page
3.2.4 Rotor End Plates	44
3.2.5 Slip Ring Assembly for Rotor. Temperature Measurement	46
3.3 Outer Stationary Cylinder and Cooling Jacket	49
3.3.1 The Outer Cylinder	
3.3.2 Cooling Jacket	
3.3.3 End Plates	
3.4 Bearing Housings and Base-Plate	54
3.5 Motor	58
3.6 Cooling Water Arrangement	58
IV Instrumentation	61
4.1 The Experimental Apparatus	61
4.2 Temperature Measurements	62
4.2.1 Stator Temperature	
4.2.2 Rotor Thermocouples	
4.2.3 Reference Junction	
4.2.4 Temperature Indication	
4.2.5 Thermocouple Corrections	
4.3 Pressure Measurements	76
4.3.1 Total Pressure Measurement	
4.3.2 Static Pressure Measurement	
4.3.3 Micromanometer for the Indication of Total and Static Pressures	
4.4 Temperature Distribution in the Gap Between the Two Cylinders	92
4.4.1 Introduction	

	Page
4.4.2 The Design of the Mechanical Parts	
4.4.3 Corrections Required	
4.5 The Use of the Hot Wire Anemometer	109
V Experimental Procedures	
5.1 Introduction	110
5.2 Overall Heat Transfer	110
5.3 Measurement of Total Pressure Distribution	111
5.4 Determination of Density Distribution	115
5.4.1 Alignment of the Interferometer with the Test Piece	
5.4.2 Obtaining "Flow" and "No-Flow" Photographs	
5.5 Use of the Hot-Wire Anemometer	120
VI Processing the Data	121
6.1 Overall Heat Transfer	121
6.1.1 The Determination of Q_c	
6.1.2 The Determination of A_{rotor}	
6.1.3 The Determination of $(T_{rotor} - T_{stator})$	
6.2 Velocity Distributions	125
6.3 The Determination of Temperature Distribution	127
6.3.1 Density Differences	
6.3.2 The Determination of Radial Position on the Interferometer Plate	

	Page
6.4 The Determination of V_{θ}^+ vs. y^+	136
6.5 The Determination of Friction Factor, f	
6.6 The Determination of ϵ_M/ν	
 VII Estimate of Systematic Errors	 149
7.1 Overall Heat Transfer	161
7.1.1 The Error in the Determination of θ_c	
7.1.2 The Error in the Determination of A_{rotor}	
7.1.3 The Error in the Determination of ΔT	
7.2 Velocity Distribution	157
7.2.1 The Error in the Determination of V_{θ}	
7.2.2 The Error in the Determination of radial position r	
7.2.3 The Error in Determination of $r \frac{dV_{\theta}/r}{dr}$	
7.2.4 The Error in Determination of $(1 + \epsilon_M/\nu)/f$	
7.2.5 The Error in Determination of f	
7.2.6 The Error in Determination of ϵ_M/ν	
7.3 The Error in Determination of ϵ_H/ϵ_M	161
7.3.1 The Error in Determination of $\frac{dT}{dr}$	
7.4 The Error in Determination of T_a	165
7.4.1 The Error in RPM	

	Page
VIII Experimental Results	167
8.1 Hot-Wire Measurements to Establish that Turbulent Flow Exists in the Gap	168
8.2 Overall Heat Transfer	172
8.3 Velocity Distributions	175
8.3.1 V_{ϕ}/r versus r	
8.3.2 $V_{\phi} r$ versus r	
8.3.3 V_{ϕ}^+ versus y^+	
8.4 Friction Factor	190
8.5 Eddy Diffusivity for Momentum	195
8.5.1 ϵ_m/z Near the Wall	
8.5.2 ϵ_m/z in the Center of the Gap	
8.6 Temperature Measurements	219
8.6.1 T vs. r	
8.6.2 T vs. V_{ϕ}/r ; The Determination of α	
IX Reconstruction of the Experimental Data and Prediction of Overall Heat Transfer and Friction Factors	227
9.1 Introduction	227
9.2 Reconstruction of Experimental Data from the Correlation $\epsilon_m/\nu f^2$ vs. y^+	
9.2.1 Derivation of Equations	
9.2.2 Reconstruction of Experimental Data	

	Page
9.3 Prediction of Overall Heat Transfer and Factors	240
Appendix	
I Description of Operation of a Mach-Zehnder Interferometer	247
II Experimental Determination of Temperature Gradient in the Windows at the Ends of the Gap	258
III Experiments Performed to Determine the Accuracy of the Slip-Ring Assembly	262
IV Tables of Data	266
V Fluid Properties used in Computations	
Bibliography	

Nomenclature

A	area of surface, ft^2 ; A_{rotor} , area of rotor, ft^2
c_p	specific heat, Btu/lb.-deg. F
d	gap width, ft.
a^E_b	electromotive force between metals a and b
f	friction factor, dimensionless
G	defined in text, equation (9-7)
G_c	temperature gradient in quartz windows, deg/inch
H	stagnation enthalpy Btu/lb.
h	unit convective conductance on surface of heated cylinder, $\text{Btu/hr-ft}^2\text{-deg F}$
k	thermal conductivity, $\text{Btu/hr-ft}^2\text{-deg F/ft}$
K	Gladstone-Dale constant, ft^3/lb
L	length of rotor, ft
l	mixing length
M	magnification factor on interferometric plates
n	index of refraction
P_t	total pressure, lbs/ft^2
p	static pressure lbs/ft^2
Q_c	heat transferred by convection, Btu/hr
q_r	heat transferred at radius r, Btu/hr-ft^2 , in r direction
r	radius, ft; r_{rotor} , rotor radius; r_{stator} , stator radius; r_c , radius at center of gap
T	temperature, deg R
U	mean velocity of flow in x direction
V	velocity, ft/sec

V_{θ}	velocity in θ -direction
$V_{\theta, \text{rotor}}$	velocity of rotor surface
$V_{\theta, c}$	velocity at center of gap
V_r	velocity in r-direction
V_z	velocity in z-direction
y	distance from wall, ft
y_t	distance from wall, thousandths of inches
$y_{t,m}$	distance from wall, as indicated by total pressure probe. N . displacement correction

Greek letter symbols

α	ratio between eddy diffusivity for heat and eddy diffusivity for momentum
α_g	coefficient of thermal expansion for quartz windows inches/inch-deg F
Δ	fringe shift, inches
Δ_{Fringe}	spacing of no-flow fringes
ϵ	fringe shift measured in wavelengths of light
ϵ_H	eddy diffusivity for heat, ft ² /sec
ϵ_M	eddy diffusivity for momentum, ft ² /sec
κ	thermal diffusivity,
λ	wavelength of light, Angstrom units, \AA
λ_{vac}	wavelength of light in vacuum, Angstrom units \AA
μ	viscosity, (lbs)(sec)/ft ²
ν	kinematic viscosity, ft ² /sec
ρ	density, lbs/ft ³ or slugs/ft ³

τ	shear stress, lbs/ft ²
ω	angular velocity radians/sec; ω_c critical angular velocity at which Taylor vortices develop

Dimensionless Numbers

f_{rotor}	friction factor on rotor surface, defined by $f_{rotor} = \frac{2 T_{rotor}}{\rho_{rotor} V_{\theta,c}^2}$
f_{stator}	friction factor on stator surface, defined by $f_{stator} = \frac{2 T_{stator}}{\rho_{stator} V_{\theta,c}^2}$
N_u	Nusselt Number, hd/k
Nu_{cond}	Conduction value of Nusselt number in the gap, defined by $(d/r_{rotor}) / \ln(1 + d/r_{rotor})$
Pr	Prandtl number, $\mu c_p / k$
Re	Reynolds number, Ud/ν ; $Re_{d,rotor} = \frac{2 V_{\theta,rotor} r_{rotor}}{2 \nu_{rotor}}$
Ta	Taylor number, $\sqrt{d/r_{rotor}} \frac{V_{\theta,rotor} d}{\nu_c}$
u_*	friction velocity, $\sqrt{\tau_w / \rho_w}$
v_{θ}^+	non-dimensionalized velocity, V_{θ} / u_*
y^+	non-dimensionalized distance from the wall, $y u_* / \nu$

Unless otherwise stated, properties in dimensionless numbers are evaluated at the average between the rotor and stator temperatures.

The barred and primed quantities refer to time mean and fluctuating quantities in turbulent flow and are defined by equations (2-9) to (2-12) and (2-14) to (2-16).

Chapter I

Introduction

1.1 Purpose of Investigation

The purpose of this study is to determine experimentally velocity and temperature distributions, and overall heat transfer in the annulus between a rotating, hot cylinder, and a concentric, stationary outer cylinder under conditions such that the properties of the separating air are markedly variable. Emphasis is placed on the turbulent regime of flow.

These data are useful since they enable the prediction of overall heat transfer rates in turbulent flow from a knowledge of the velocity field; this through the concept of the eddy diffusivities for momentum and heat transfer.

The concentric cylinder apparatus was chosen for this work because it provides a means for obtaining high rates of energy transfer, and relatively high temperature differences in a small apparatus. Further, in the absence of secondary flow effects this apparatus is capable of producing one of the few possible examples of established, compressible flow. Analysis of the data is then simple in certain respects.

Other problems are introduced, however, such as the existence of Taylor Vortices, a three-dimensional secondary flow, which, if persisting at ranges of speed covered by the

present experiment would complicate the analysis.

1.2 Summary of Previous Work:

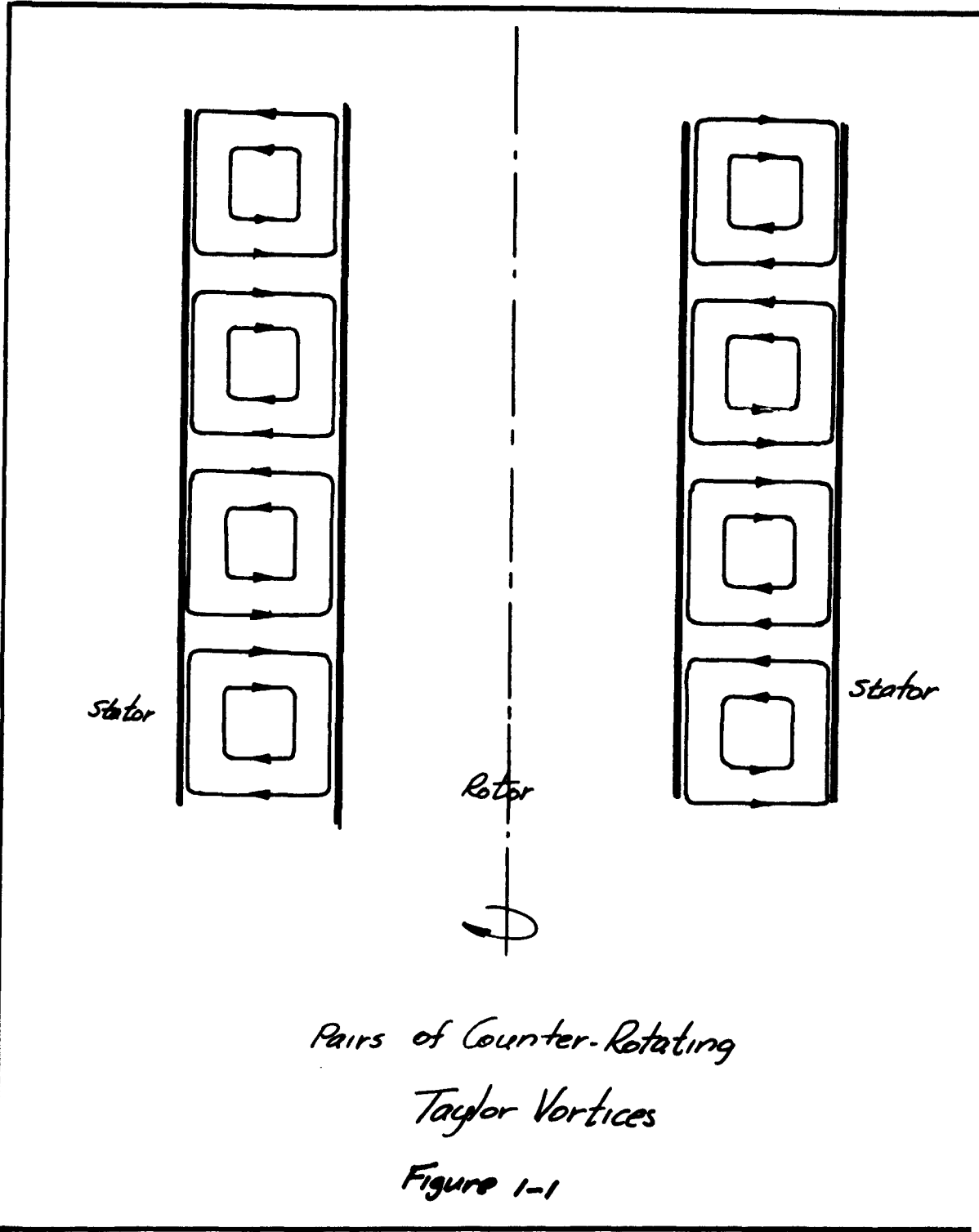
1.2.1 Flow Between Rotating Cylinders

A discussion of previous investigations of flow between rotating cylinders can be conveniently divided into three parts; one concerned with the flow regimes within the annulus; the second with the heat transfer; and the third with velocity and temperature measurements in the annulus.

1.2.1.1 Flow Regimes

The breakdown to turbulent flow of the curved Couette flow existing between the cylinders at low speeds of rotation of the inner cylinder does not occur in the same manner as in pipes or on flat plates. In these the laminar flow, at a critical Reynolds Number Re_{cr} , becomes unstable to disturbances existing in the flow. These disturbances increase with time and change the character of the flow from the well-behaved laminar to the random fluctuations of turbulent flow.

The curved Couette flow on the other hand responds to small disturbances in a different manner. At a critical value of the parameter $\frac{V \omega r_m}{\nu}$, called the Taylor number, the laminar flow breaks down. This breakdown is not into the random fluctuations which typify turbulent flow but into a new type of laminar flow containing torroidal cells of secondary motion looping the inner cylinder, as shown in Fig. 1-1.



In a classical paper G. I. Taylor¹ predicted not only the development of these vortices but also the conditions of cylinder rotational speeds and fluid properties at which they would occur. Taylor superimposed on the velocity components for laminar flow small sinusoidal disturbances.

Substitution of the resultant velocities into the conservation equations and the solution of these yielded, for an incompressible fluid, and for $d/r_{\text{in}} \rightarrow 0$, a critical speed of rotation for the inner cylinder, beyond which the perturbations would grow.

The vortices formed are called Taylor Vortices. This flow is laminar in nature and represents a secondary flow superimposed on the circumferential flow.

For the case where the outer cylinder is stationary Taylor found that the laminar vortex motion sets in at a critical speed given by

$$\omega_c^2 = \frac{\pi^4 \nu^2 (r_{\text{outer}} + r_{\text{in}})}{2 \rho d^3 r_{\text{in}}^2} \quad (1-1)$$

where

$$P = 0.0571 \left(1 - 0.652 \frac{d}{r_{\text{in}}}\right) + \frac{0.00056}{\left(1 - 0.652 \frac{d}{r_{\text{in}}}\right)}$$

For the case $d/r_{\text{in}} \rightarrow 0$, $P = 0.0577$

and

$$\frac{\omega_c^2 r_{\text{in}}^2 d^2}{\nu^2 r_{\text{in}}} = 1697$$

or,

$$T_{\text{critical}} = 41.2 \quad (1-2)$$

¹"Stability of a Viscous Fluid Contained between Two Rotating Cylinders," G. I. Taylor, Philosophical Trans. of the Royal Society of London, series A, vol. 223, 1923, pp. 289-343.

Taylor also predicted the vortex spacing, which he found to be equal to the annulus width. Experiments conducted by him, using water as the fluid, confirmed the analytical value of to within 2%. Further, the vortex spacing measured by Taylor was 1.05 cm, for an annulus width of 1.105 cm.

J. W. Lewis¹ also investigated experimentally this type of motion and found that the vortices themselves were stable to arbitrary small disturbances, such as changes in the speed, much as in pipe flow where a turbulent flow persists at Reynolds Numbers below the critical as the speed is reduced. He further found that for $d/r_{\text{rot}} = 0.17$, the laminar vortex flow became "irregularly turbulent" at a speed twice the critical value. He did not observe this breakdown at speeds up to five times the critical for the values $d/r_{\text{rot}} = 0.43$, and 0.71.

The turbulent flow which ensues at speeds much higher than the critical has not yet been analysed. Pai Shih-I,² however, has investigated experimentally the case for air flow between the cylinders at Taylor numbers from 10-20,000. He concluded from hot wire velocity measurements and pressure distributions that secondary vortices persist even at speeds several hundred times beyond the critical. He also determined

¹"An Experimental Study of the Motion of a Viscous Liquid Contained Between Two Coaxial Cylinders," Proc. Roy. Soc. London, Ser. A, 117, pp. 388-407 (1927-1928).

²"Turbulent Flow between Rotating Cylinders," Pai Shih-I, NACA TN-892, March 1943.

that the vortices occur in pairs and their number decreases with the speed of the inner cylinder; that in certain areas the initial vortex motion breaks down into smaller eddices which degenerate further to produce regions where turbulent fluctuations predominate. Pai's conception of the flow pattern is shown in Fig. 1-2.

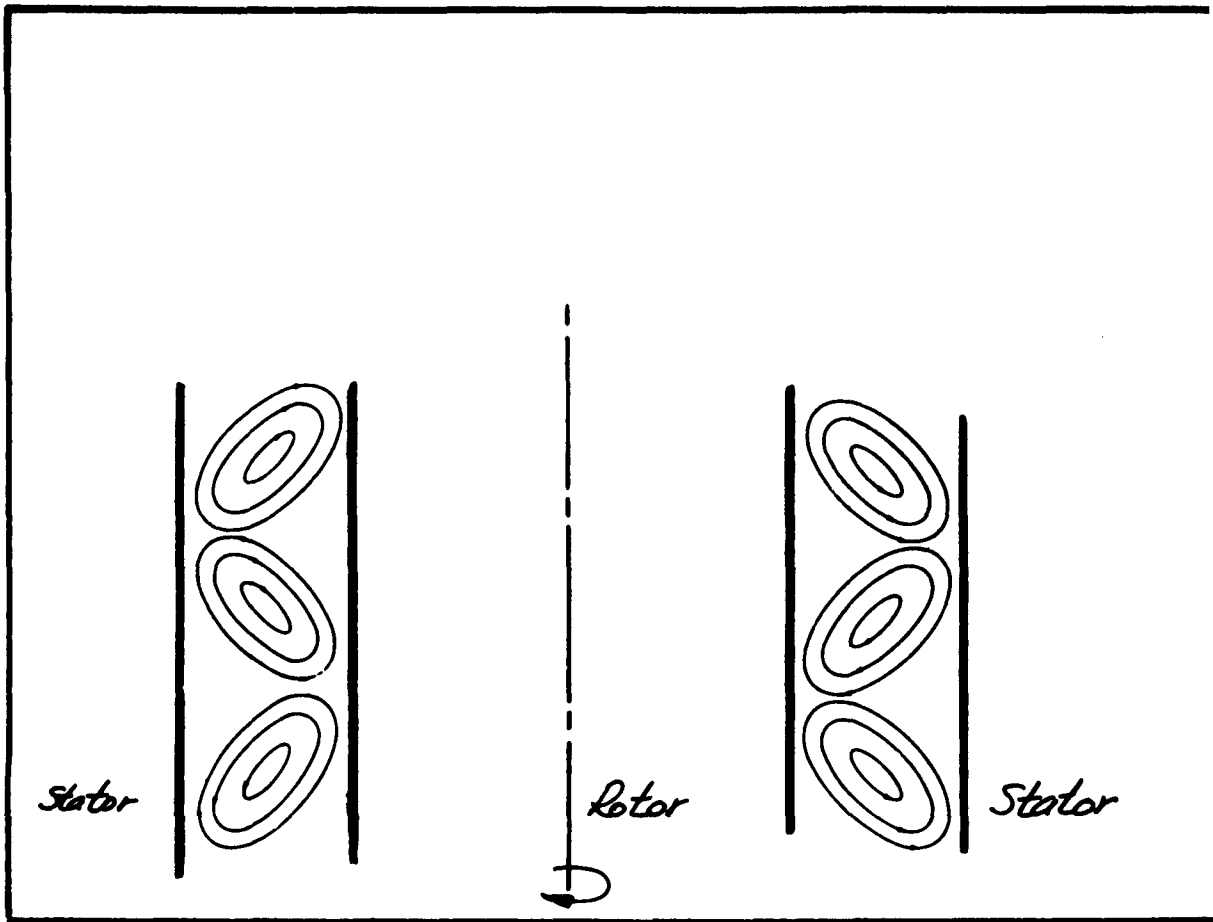
Pai's conclusions were based on two experimental observations; a non-uniform axial pressuredistribution and two different types of mean velocity distribution observed at different axial locations.

He further observed at high speeds sudden changes in the velocity distribution at a given axial location from one type to another, typified by a sudden drop in mean speed.

Pai associated each of the two types of velocity distributions with a region in the flow; one type in those regions where the secondary flow predominates, the other type, the region in which the random turbulent fluctuation predominate. The latter velocity distribution, he found was of a logarithmic type.

The findings of Pai were extended by Kaye and Elgar¹ who studied the turbulent vortical flow with smoke tracer and hot-wire techniques. Their experiments were performed both with and without axial air flow through the annulus. They

¹"Modes of Adiabatic and Diabatic Fluid Flow in an Annulus with an Inner Rotating Cylinder," J. Kaye and E. C. Elgar, ASME Paper #57-HT-14, 1957.



*Distorted Taylor Vortices
Hypothesized by Pai*

Figure 1-2

suggest that four modes of flow exist in the annulus, depending on the axial flow Reynolds Number and the Taylor Number. Fig. 1-3 shows a schematic representation of their results, in which the four regimes, laminar, laminar-plus-vortices, turbulent, and turbulent-plus-vortices, are delineated. Included also as dashed lines, are the separation loci conjectured by Becker in his dissertation.^{1,2}

Becker's work will be discussed later in connection with the heat transfer results of the present experiment. Included in his dissertation is an excellent review of the literature for the flow under discussion together with an extensive bibliography for both the diabatic and adiabatic cases.

¹"An Experimental and Theoretical Study of Heat Transfer in an Annulus with an Inner Rotating Cylinder," Sc. D. Thesis, Kurt Becker, Massachusetts Institute of Technology, Aug. 1957.

²In a subsequent paper Becker and Kaye suggest a different arrangement of the regimes for the diabatic and adiabatic case as concerns the transition from laminar flow to turbulent flow and laminar-plus-vortices flow to turbulent-plus-vortices flow. This is apparently a reevaluation of the work of Kaye and Elgar in this region since Becker and Kaye state "Based on these [temperature] profiles [taken by Kaye and Becker in each of these regions] and upon the difficulties of interpretation of hot-wire data for the adiabatic case, we recommend the use of a nearly horizontal demarcation line, between the laminar and turbulent regimes, ... for both adiabatic and diabatic flows." See "K. M. Becker, J. Kaye, "Measurements of Diabatic Flow in an Annulus with an Inner Rotating Cylinder." ASME paper No. 61-SA-19, August, 1961

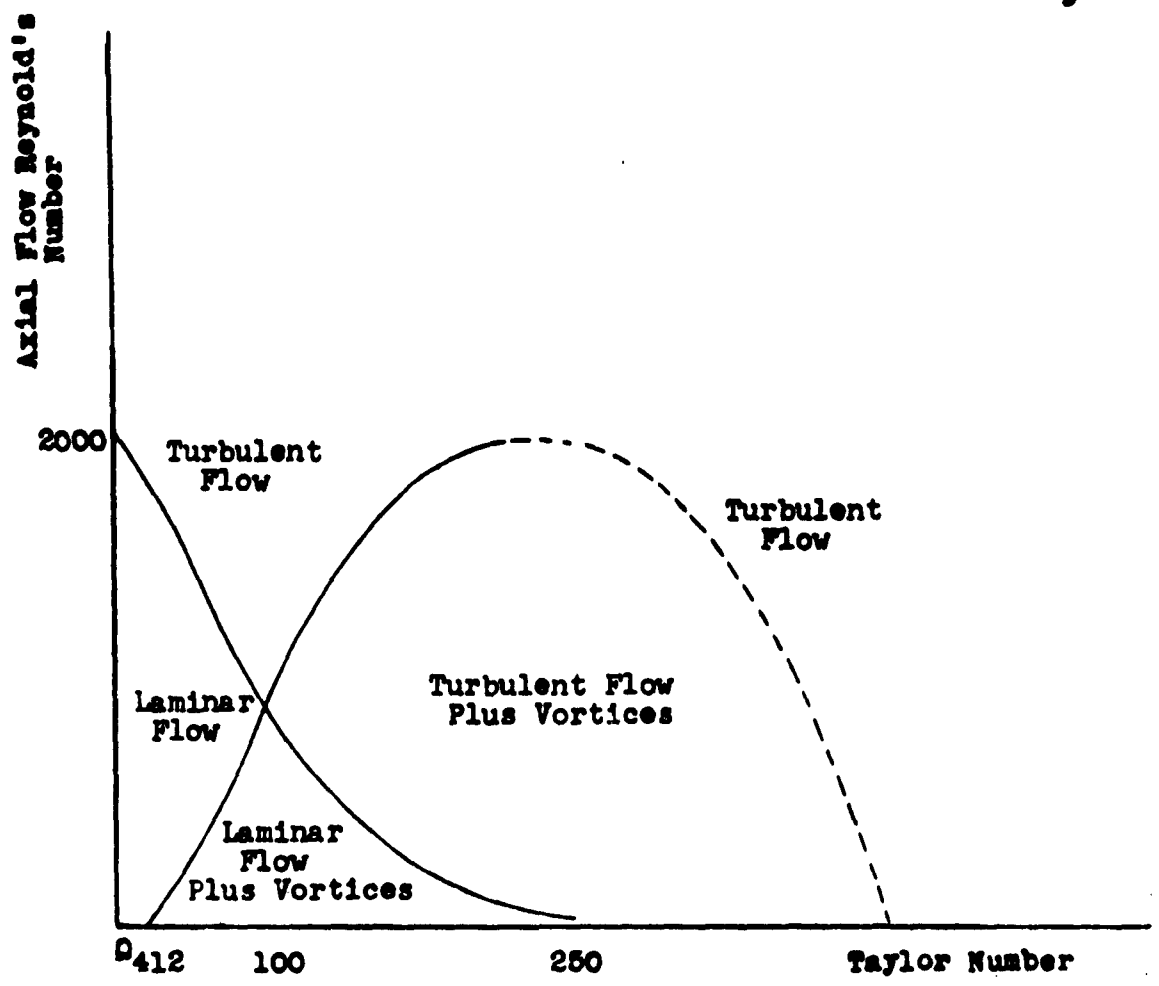


Figure 1-3

Schematic Representation of Different Regions of Flow in the Annulus (dashed line: Becker's Hypothesis)

To summarize this section, one can say:

1. The breakdown of the curved Couette motion under discussion does not proceed directly from laminar to turbulent flow but rather from laminar to a vortical flow, still laminar, superimposed on the mean circumferential flow. This transition occurs at a critical value of the Taylor number.

2. At speeds much higher than the critical these vortices still persist.

3. Indications are that at still higher Taylor Numbers the vortices break up completely and a random turbulent motion occurs.

1.2.1.2 Overall Heat Transfer

Most prior studies of heat transfer from a rotating inner cylinder to a concentric outer cylinder have been limited to a determination of overall heat transfer coefficients. The earlier studies are reported by Kaye and Elgar,¹ Becker,⁴ Gazley,² and Kays and Bjorklund.³ These latter three works are the most extensive to date. Gazley measured the heat transfer

¹Kaye and Elgar, ASME paper #57-HT-14.

⁴Becker, Sc.D., Thesis, MIT, 1957.

²"Heat Transfer Characteristics of Rotational and Axial Flow between Concentric Cylinders," Carl Gazley, Jr., A.S.M.E. Paper #56-A-128, 1956.

³"Heat Transfer between Concentric Rotating Cylinders," I. S. Bjorklund and W. M. Kays, ASME Paper #58-A-99, 1958.

in the gap for smooth and slotted rotors and stators with and without axial through flow. The length of the annulus was 10 inches, and air gap diameter was about 5 inches. Different rotors were used, with air gaps of either 0.017 inches or 0.24 inches. Rotational speeds varied from 540 to 4700 rpm with temperature differences of about 100 to 150 deg F.¹ The Taylor Number range was about 20 to 80 for $d/r_{rotor} = 0.0068$ and from about 250 to 3000 for $d/r_{rotor} = 0.095$.

Becker performed similar studies with a smooth rotor, and was mainly concerned with obtaining the lines of demarcation for the four flow regimes mentioned earlier.

The experiments of Kays and Bjorklund involved smooth surfaces without axial airflow but with provision for rotation of the stator as well as the rotor.

The results of Kays and Bjorklund, and Becker (considering only his results with no axial air flow) for $Ta > 90$ can be placed on a line

$$Nu_{rotor}/Nu_{cond} = 0.175 Ta^{1/2} \quad (1-3)$$

where

$$Nu_{cond} = \frac{(d/r_{rotor})}{\ln(1 + d/r_{rotor})} \quad (1-4)$$

and Ta is based on r_{rotor} , and fluid properties evaluated at a temperature halfway between the temperatures of the two cylinders.

¹Personal communication, C. Gazley, Jr. to G. S. Longobardo, June 24, 1959.

The data of Gazley follow the same trend but are higher, possibly because, as Becker suggests, he did not take into account radiation between the two cylinders.

The physical dimensions and ranges of temperature difference between the rotor and stator, and Ta for the three works cited and the present work are given in the following Table:

Table I.1

Investigator	Ta	$\Delta t, \text{deg F}$	d/r_{rotor}	L/d	Length L, inches
Gazley	20-80	100-150	0.0068	0.0017	10
	250-3000		0.095	0.024	
Becker	0-575	30-62	0.233	0.0058	56
Kays & Bjorklund	0-2000	60	0.054-	0.0067-	18.25
			0.246	0.0305	
Longobardo	3000-7000	60-350	0.227	0.084	4.5

As shown later, the overall heat transfer results for low temperature differences obtained in the present experiment, although at higher Taylor Numbers can be placed on the line represented by eq. (1-3).

1.2.1.3 Velocity and Temperature Distribution Data

Detailed time-mean velocity distributions for purely

rotational flow have been obtained by Taylor,¹ Pai,² and Wattendorf.³

Taylor's experiments were conducted to differentiate between his vorticity transfer theory and the momentum transfer theory of Prandtl. The results for only one rotational speed are reported in detail, that corresponding to a Taylor Number of 60,000. Taylor's "raw" pitot tube data gave the result that \sqrt{v} increased toward the stator in the middle of the channel. Taylor, noting the small magnitude of the variation (about 6%) tried to determine how much of the variation was contributed by pitot tube. He then reran the experiment using a larger pitot tube (by a factor of 2 on outside diameter) and obtained a greater variation in \sqrt{v} .

Using these data to extrapolate to a pitot tube of zero diameter, he obtained the result $\sqrt{v} = \text{constant}$ in the central 85% of gap width. Unfortunately, Taylor's data do not approach the wall sufficiently close for further evaluation.

¹"Distribution of Velocity and Temperature between Concentric Rotating Cylinders," G. I. Taylor, Proc. Royal Society of London, ser. A, vol. 157, no. 892, Dec. 2, 1936, pp. 494-512.

²Pai Shih-I, NACA TN 892.

³"A Study of the Effect of Curvature on Fully Developed Turbulent Flow," F. L. Wattendorf, Proc. Royal Society of London, ser. A, no. 865, vol. 148, Feb. 1935, pp. 565-598.

Pai Shih-I's experiments were conducted to investigate the validity of Taylor's extrapolation, and have already been discussed in Section 1.2.1.1. Again, no data were obtained close to the wall, but Pai found that away from the wall the velocity obeyed a logarithmic law.

1.2.2 Determination of Eddy Diffusivities for Momentum and Heat

Consider a laminar, incompressible flow with a mean velocity \bar{U} in the x direction. One writes for the shear stress

$$\tau/\rho = \nu \frac{d\bar{U}}{dy}$$

In a turbulent flow an augmentation of the transfer of momentum occurs and it is customary to write

$$\tau/\rho = \nu \left(1 + \frac{\epsilon_M}{\nu}\right) \frac{d\bar{U}}{dy} \quad (1-4)$$

where ϵ_M is the "eddy diffusivity for momentum." Similarly, for the heat-transfer one can write for the laminar case

$$\frac{q}{\rho c_p} = \frac{k}{\rho c_p} \frac{dT}{dy} \quad (1-5)$$

and for the turbulent case

$$\frac{q}{\rho c_p} = \frac{k}{\rho c_p} \left(1 + \frac{\epsilon_H}{k/\rho c_p}\right) \frac{dT}{dy} \quad (1-6)$$

where ϵ_H is the "eddy diffusivity for heat."

Defining α as

$$\alpha \equiv \epsilon_H/\epsilon_M \quad (1-7)$$

and noting that $R = \frac{Gk}{k}$ equation (1-6) can be written

Pai Shih-I's experiments were conducted to investigate the validity of Taylor's extrapolation, and have already been discussed in Section 1.2.1.1. Again, no data were obtained close to the wall, but Pai found that away from the wall the velocity obeyed a logarithmic law.

1.2.2 Determination of Eddy Diffusivities for Momentum and Heat

Consider a laminar, incompressible flow with a mean velocity \bar{U} in the x direction. One writes for the shear stress

$$\tau/\rho = \nu \frac{d\bar{U}}{dy}$$

In a turbulent flow an augmentation of the transfer of momentum occurs and it is customary to write

$$\tau/\rho = \nu \left(1 + \frac{\epsilon_M}{\nu}\right) \frac{d\bar{U}}{dy} \quad (1-4)$$

where ϵ_M is the "eddy diffusivity for momentum." Similarly, for the heat-transfer one can write for the laminar case

$$\frac{q}{\rho c_p} = \frac{k}{\rho c_p} \frac{dT}{dy} \quad (1-5)$$

and for the turbulent case

$$\frac{q}{\rho c_p} = \frac{k}{\rho c_p} \left(1 + \frac{\epsilon_H}{k/\rho c_p}\right) \frac{dT}{dy} \quad (1-6)$$

where ϵ_H is the "eddy diffusivity for heat."

Defining α as

$$\alpha \equiv \epsilon_H / \epsilon_M \quad (1-7)$$

and noting that $R = \frac{c_p \mu}{k}$ equation (1-6) can be written

$$\frac{q}{\rho q} = \frac{k}{\rho q} \left(1 + \alpha \rho \frac{e_m}{2} \right) \frac{dT}{dy} \quad (1-8)$$

The value of α now takes on an added significance since with a knowledge of α and the velocity field the temperature field and hence the heat transfer can be determined.

Mechanistic theories of turbulence such as Prandtl's Mixing Length Theory,¹ and Taylor's Vorticity Transport Theory² have been offered to arrive at a useful formulation for $e_m/2$ and subsequently, α

Prandtl, on the assumption that a "lump" of fluid in moving from a position y in the fluid to a position $y + \delta y$ conserves not only its identity but its momentum as well arrives at

$$e_m = \ell^2 \frac{dU}{dy}$$

where ℓ is called the mixing length and is analagous to the mean free path in kinetic theory.

The theory has its limitations;³ one such being that

¹L. Prandtl, Essentials of Fluid Dynamics (Hafner Publishing Company, Inc., New York, 1952), p. 117 to 121.

²S. Goldstein, Modern Developments in Fluid Mechanics (Oxford at the Clarendon Press, 1938) vol. I, pp. 209-214.

³R. W. Stewart, "A New Look at the Reynolds Stresses," Canadian Journal of Physics, vol. 34, 1956, pp. 722-725.

it requires ϵ_m to go to zero at points of maximum velocity, such as at the center of a pipe. This is not borne out experimentally. Another is that values of l obtained from experimental data are large in a given flow, contrary to what has been assumed in the theory.

Hinze¹ has calculated the value of the mixing length from measured velocity distributions in the wake of a circular cylinder. He found that l is infinite at the axis of the wake, zero at the boundary, and obtained an average value of l equal to 1/5 to 1/4 the wake width.

If, using this theory, it is assumed that heat is transferred in the same manner as momentum it can be shown that

$$\epsilon_H = l^2 \frac{dU}{dy}$$

and

$$\epsilon_H / \epsilon_m = \alpha = 1$$

The assumption $\alpha = 1$ has been used by Deissler,^{2,3,4} Lyon⁵

¹J. O. Hinze, Turbulence (New York: McGraw-Hill Book Co., Inc., 1958), p. 394.

²R. G. Deissler, and C. S. Eian, "Analytical and Experimental Investigation of Fully Developed Turbulent Flow of Air in a Smooth Tube with Heat Transfer with Variable Fluid Properties," NACA TN 2629, 1952.

³R. G. Deissler, "Analysis of Turbulent Heat Transfer, Mass Transfer and Friction in Smooth Tubes at High Prandtl and Schmidt Numbers," NACA TN 3145, 1954.

⁴R. G. Deissler and M. F. Taylor, "Analysis of Turbulent Flow and Heat Transfer in Non-Circular Passages," NACA TN 4384, 1958.

⁵R. N. Lyon, "Liquid Metal Heat Transfer Coefficients," Chemical Engineering Progress, vol. 47, 1951, pp. 75-79.

and Seban and Shimizaki,¹ for example, to calculate the temperature distribution in a fluid from a known velocity distribution.

However, the assumption $\alpha = 1$ is not borne out by experimental evidence.² In a pioneering experiment Isakoff and Drew³ found that α was a function of Reynolds Number and radial position in the tube. Further there seemed to be a trend toward unity as the turbulence increased.

¹R. A. Seban and T. T. Shimizaki, "Heat Transfer to a Fluid Flowing Turbulently in a Smooth Pipe with Walls at Constant Temperature," Trans. ASME, Vol. 73, 1951, pp. 803-809.

²In "The Principles of Turbulent Heat Transfer," NACA TM 1408, 1957, H. Reichardt states, "In this connection [the ratio]... a far reaching congruence was obtained of the temperature and velocity profiles in friction layers [from the results of F. Elias "Heat Transfer from a Heated Plate to Flowing Air," NACA TM 614, originally published in 1930]. This result was looked upon as a confirmation of the previously held conception of the identity between momentum exchange and heat transport [i.e. $\alpha = 1$].

This conclusion from the measurement results of Elias was, however, in error, as was shown by the author [Reichardt] in the year 1940." Elias' reported results, $\alpha = 1$, were based on $\beta = 1$ whereas, as Reichardt pointed out, $\beta = 0.72$, leading to a result, $\alpha = 1.4$.

³S. E. Isakoff and T. B. Drew, "Heat and Momentum Transfer in Turbulent Flow of Mercury," General Discussion on Heat Transfer, The Institution of Mechanical Engineers, London, 1951, pp. 405-409.

Similarly, Brown, Amstead, and Short,¹ again using mercury as the fluid found α between 0.7 and 0.9 for $200,000 < Re < 800,000$ in the center of the pipe, dropping rapidly near the wall.

Seban and Shimizaki² using air in a heated pipe found α to be about 1.2 for $90 < y^+ < 300$, and about unity for $y^+ > 300$, where y^+ is the non-dimensionalized distance from the wall.

Corcoran, Page, et. al.³ studying the flow of air at small temperature differences in a rectangular channel found $\alpha = \frac{1}{R_{air}} = 1.4$ near the wall, and decreasing with increasing Reynold's number in the middle of the channel.

More recently, Sleicher,⁴ using air in a heated pipe found α to be greater than unity to vary with Reynold's number and position, and approach 1.4 near the walls.

None of these experiments was made under conditions of property variation of the fluid.

¹H. E. Brown, B. H. Amstead, and B. E. Short, "The Transfer of Heat and Momentum in a Turbulent Stream of Mercury," Trans. ASME, vol. 79, 1957, pp. 279-285.

²R. A. Seban and T. T. Shimazaki, "Temperature Distribution for Air Flowing Turbulently in a Smooth Heated Pipe," General Discussion on Heat Transfer, The Institution of Mechanical Engineers, London, England, 1951, pp. 122-126.

³W. H. Corcoran, F. Page, Jr., W. G. Schlinger, and B. H. Sage, "Temperature Gradients in Turbulent Gas Streams," Industrial and Engineering Chemistry, vol. 44, 1952, pp. 410-430.

⁴C. A. Sleicher, Jr., "Experimental Velocity and Temperature Profiles for Air in Turbulent Pipe Flow," Trans. ASME, vol. 80, 1958, pp. 693-704.

Under conditions of high property variation, Deissler and Eian¹ report total pressure profiles taken for air flowing in a heated tube at tube wall temperatures up to 1500 F, and $8000 < Re < 500,000$, and temperature profiles taken up to wall temperatures of only 300 F because of the delicacy of the thermocouple probe used. Based on the experimental data shown for u^+ vs. y^+ (their Fig. 9) and z^+ vs. y^+ (their Fig. 11) the scatter of the data appears too great to permit an evaluation of α . Certainly they report no data near the wall

"...because the distributions were measured at high Reynolds numbers where the severe velocity gradients and the presence of the hole in the tube wall make the accuracy of the measurement doubtful" (TN 2629 p. 17); and for temperature -- "The distributions shown for the region close to the wall may be subject to errors due to conduction along the thermocouple probe prongs" (TN 2629 p. 18.).

Values of α have been obtained from experiments with heated jets of air issuing into still air.

Hinze and VanderHeggeZijnen² report an average value ≈ 1.36 .

Corrsin³ obtained a ratio of 1.43 independent of the magnitude of the temperature differential up to 300 C.

These results are for turbulence not affected by the presence of a solid boundary.

¹R. G. Deissler and C. S. Eian, NACA TN 2629.

²J. O. Hinze, Turbulence, p. 426.

³S. Corrsin, M. S. Uberoi, NACA TN 2124, 1950

Chapter II

Development of Basic Equations¹

2.1 General Equations of Motion

The transient equations of linear momentum are written as

$$\frac{\partial \rho v_i}{\partial t} + \frac{\partial}{\partial x_i} (\rho v_i v_j) = \frac{\partial}{\partial x_i} P_{ij} \quad (2-1)$$

where body forces are neglected, and P_{ij} is given by

$$P_{ij} = \tau_{ij} - \delta_{ij} \left[p - \frac{2}{3} \mu (\nabla \cdot \mathbf{v}) \right]$$

where τ_{ij} is given as

$$\tau_{ij} = -\mu \left[\frac{\partial v_i}{\partial x_j} \right]$$

and

$$\delta_{ij} = \begin{cases} 1, & i=j \\ 0, & i \neq j \end{cases}$$

The continuity equation is

$$\frac{\partial \rho}{\partial t} + \frac{\partial}{\partial x_i} (\rho v_i) = 0$$

When these equations are transformed to cylindrical coordinates, (r, θ, z) in terms of the shear stresses, defined below, there results

¹The equations in this chapter are to a great extent developed from course notes in fluid mechanics and convective heat transfer taught by Professor H. G. Elrod at Columbia University.

r - component

$$\rho \left(\frac{\partial v_r}{\partial t} + v_r \frac{\partial v_r}{\partial r} + \frac{v_\theta}{r} \frac{\partial v_r}{\partial \theta} - \frac{v_\theta^2}{r} + v_z \frac{\partial v_r}{\partial z} \right) = -\frac{\partial p}{\partial r} \rightarrow$$

$$-\left(\frac{1}{r} \frac{\partial}{\partial r} (r T_{rr}) + \frac{1}{r} \frac{\partial T_{r\theta}}{\partial \theta} - \frac{T_{\theta\theta}}{r} + \frac{\partial T_{rz}}{\partial z} \right) \quad (2-1)$$

θ - component

$$\rho \left(\frac{\partial v_\theta}{\partial t} + v_r \frac{\partial v_\theta}{\partial r} + \frac{v_\theta}{r} \frac{\partial v_\theta}{\partial \theta} + \frac{v_r v_\theta}{r} + v_z \frac{\partial v_\theta}{\partial z} \right) = -\frac{\partial p}{\partial \theta} \rightarrow$$

$$-\left(\frac{1}{r^2} \frac{\partial}{\partial r} (r^2 T_{r\theta}) + \frac{1}{r} \frac{\partial T_{\theta\theta}}{\partial \theta} + \frac{T_{r\theta}}{r} \right) \quad (2-2)$$

z - component

$$\rho \left(\frac{\partial v_z}{\partial t} + v_r \frac{\partial v_z}{\partial r} + \frac{v_\theta}{r} \frac{\partial v_z}{\partial \theta} + v_z \frac{\partial v_z}{\partial z} \right) = -\frac{\partial p}{\partial z} \rightarrow$$

$$-\left(\frac{1}{r} \frac{\partial}{\partial r} (r T_{rz}) + \frac{1}{r} \frac{\partial T_{r\theta}}{\partial \theta} + \frac{\partial T_{zz}}{\partial z} \right) \quad (2-3)$$

T_{ij} is given by

$$T_{rr} = -\mu \left[2 \frac{\partial v_r}{\partial r} - \frac{2}{3} (\nabla \cdot \vec{v}) \right]$$

$$T_{\theta\theta} = -\mu \left[2 \left(\frac{1}{r} \frac{\partial v_\theta}{\partial \theta} + \frac{v_r}{r} \right) - \frac{2}{3} (\nabla \cdot \vec{v}) \right]$$

$$T_{zz} = -\mu \left[2 \frac{\partial v_z}{\partial z} - \frac{2}{3} (\nabla \cdot \vec{v}) \right]$$

$$T_{r\theta} = T_{\theta r} = -\mu \left[r \frac{\partial}{\partial r} \left(\frac{v_\theta}{r} \right) + \frac{1}{r} \frac{\partial v_r}{\partial \theta} \right]$$

$$T_{\theta z} = T_{z\theta} = -\mu \left[\frac{\partial v_\theta}{\partial z} + \frac{1}{r} \frac{\partial v_z}{\partial \theta} \right] \quad (2-4)$$

$$T_{rz} = T_{zr} = -\mu \left[\frac{\partial v_z}{\partial r} + \frac{\partial v_r}{\partial z} \right]$$

and

$$(\nabla \cdot \vec{v}) = \frac{1}{r} \frac{\partial}{\partial r} (r v_r) + \frac{1}{r} \frac{\partial v_\theta}{\partial \theta} + \frac{\partial v_z}{\partial z}$$

The Continuity Equation is

$$\frac{\partial \rho}{\partial t} + \frac{1}{r} \frac{\partial}{\partial r} (\rho r v_r) + \frac{1}{r} \frac{\partial}{\partial \theta} (\rho v_\theta) + \frac{\partial}{\partial z} (\rho v_z) = 0$$

(2-5)

2.1.1 Equations of Motion for Laminar Flow

For steady state, incompressible, Couette-type laminar flow in the gap between the inner, rotating cylinder and the outer stationary cylinder,

$$\frac{\partial}{\partial t}, \frac{\partial}{\partial \theta}, \frac{\partial}{\partial z}, v_z = 0$$

The Equation of Continuity becomes

$$\frac{1}{r} \frac{\partial}{\partial r} (\rho r v_r) = 0 \quad (2-6)$$

$$(\rho r v_r) = \text{constant}$$

At $r = r_{\text{rotor}}$, $v_r = 0$, and $v_r = 0$ everywhere.

The θ -component of the Equation of Motion gives

$$0 = \frac{1}{r^2} \frac{d}{dr} r^2 \tau_{r\theta}'$$

and since

$$\tau_{r\theta} = -\mu r \frac{d}{dr} (v_\theta / r)$$

there results

$$\mu r^3 \frac{d}{dr} (v_\theta / r) = \text{constant} \quad (2-7)$$

or

$$r^2 \left[\frac{dv_\theta}{dr} - v_\theta / r \right] = \text{constant}$$

¹ Thus $r^2 \tau_{r\theta} = \text{constant}$, and $\tau_{r\theta, \text{static}} r_{\text{static}}^2 = \tau_{r\theta, \text{rotor}} r_{\text{rotor}}^2$ which is a statement of Conservation of Angular Momentum.

Solving for V_θ ,

$$V_\theta = Ar + \frac{B}{r}$$

with Boundary Conditions

$$r = r_{\text{rotor}}, V_\theta = \omega_{\text{rotor}} r_{\text{rotor}}$$

$$r = r_{\text{stator}}, V_\theta = 0$$

There results

$$V_\theta = \left(- \frac{\omega_{\text{rotor}} r_{\text{rotor}}^2}{r_{\text{stator}}^2 - r_{\text{rotor}}^2} \right) r + \frac{\omega_{\text{rotor}} r_{\text{stator}} r_{\text{rotor}}^2}{(r_{\text{stator}}^2 - r_{\text{rotor}}^2)} \frac{1}{r}$$

(2-8)

A plot of V_θ for the present apparatus at $\omega_{\text{rotor}} = \pi$ radians/sec (30rpm) is shown in Fig. 2-1. Here, $V_{\theta, \text{rotor}} = 0.43$ ft/sec, and $Ta = 36$, just below the critical.

2.1.2 Equations of Motion for Turbulent Flow

The equations that describe turbulent flow are derived from those of Section 3.1 through the substitution of a time mean plus a fluctuating component for the fluctuating quantities.

The substitutions made for incompressible turbulent flow are of the form

$$u = \bar{u} + u' \quad (2-9)$$

such that

$$\bar{u} = \int_{t-\frac{T}{2}}^{t+\frac{T}{2}} \frac{u dt}{T} \quad (2-10)$$

Solving for V_θ ,

$$V_\theta = Ar + \frac{B}{r}$$

with Boundary Conditions

$$r = r_{\text{rotor}}, V_\theta = \omega_{\text{rotor}} r_{\text{rotor}}$$

$$r = r_{\text{stator}}, V_\theta = 0$$

There results

$$V_\theta = \left(- \frac{\omega_{\text{rotor}} r_{\text{rotor}}^2}{r_{\text{stator}}^2 - r_{\text{rotor}}^2} \right) r + \frac{\omega_{\text{rotor}} r_{\text{stator}} r_{\text{rotor}}^2}{(r_{\text{stator}}^2 - r_{\text{rotor}}^2)} \frac{1}{r}$$

(2-8)

A plot of V_θ for the present apparatus at $\omega = \pi$ radians/sec (30rpm) is shown in Fig. 2-1. Here, $V_{\theta, \text{rotor}} = 0.43$ ft/sec, and $Ta = 36$, just below the critical.

2.1.2 Equations of Motion for Turbulent Flow

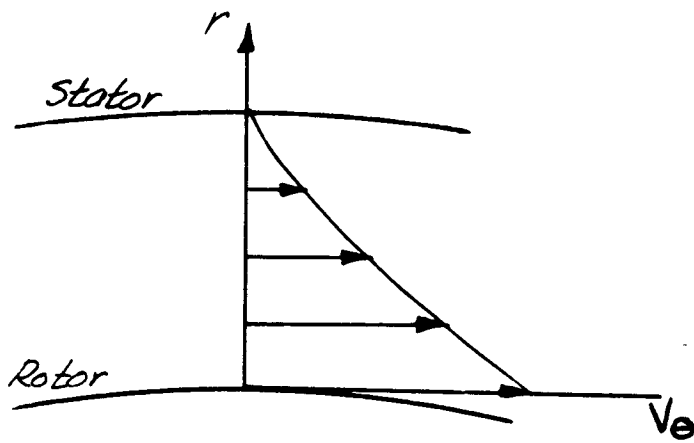
The equations that describe turbulent flow are derived from those of Section 3.1 through the substitution of a time mean plus a fluctuating component for the fluctuating quantities.

The substitutions made for incompressible turbulent flow are of the form

$$u = \bar{u} + u' \quad (2-9)$$

such that

$$\bar{u} = \int_{t-\frac{T}{2}}^{t+\frac{T}{2}} \frac{u \, dt}{T} \quad (2-10)$$



*V_e vs. r in the Annulus
Taylor Number Below Critical
Figure 2-1*

from which it follows that

$$\overline{u'} = \int_{t-\tau/2}^{t+\tau/2} \frac{u'}{\tau} dt = 0 \quad (2-11)$$

Similarly then

$$\begin{aligned} V_\theta &= \overline{V_\theta} + V_\theta' \\ V_r &= \overline{V_r} + V_r' \\ p &= \overline{p} + p' \end{aligned} \quad (2-12)$$

The result when these are substituted into the Equations of Motion is that the equations for the turbulent case are exactly as those for the laminar, except that:

1. V_i is changed to \overline{V}_i and p to \overline{p} and
2. τ_{ij} is changed to $\tau_{ij}^{(t)}$

which is now

$$\tau_{ij}^{(t)} = (\overline{\tau}_{ij} + \rho \overline{V_i V_j'}) \quad (2-13)$$

Thus

$$\tau_{r\theta}^{(t)} = -\mu \left[r \frac{\partial \overline{V}_\theta}{\partial r} + r \frac{\partial \overline{V}_r}{\partial \theta} \right] + \rho \overline{V_r' V_\theta'} \quad (2-13)a$$

The averaging procedure is rather straight forward and is described by Goldstein.¹ The terms $\rho \overline{V_i V_j'}$ act in the equations just as the stresses due to viscous forces, and are called

¹S. Goldstein, Modern Developments in Fluid Mechanics (1st ed; Oxford at the Clarendon Press, 1938), I, pp. 191-193.

Reynolds stresses. They represent the transport of momentum across a surface that is due to velocity fluctuations; for example, the term $\overline{\rho v_0' v_r'}$ represents the transport of momentum $\rho v_0'$ across the surface $r = \text{constant}$, by v_r' in equation (2-13)a.

For a turbulent compressible flow the result is not in so neat a form.

Adding to equation (2-12)

$$\rho = \bar{\rho} + \rho'$$

results in the same expressions as before plus many new ones resulting from double and triple correlations among density fluctuations and turbulent components of the velocities. These are listed by Hinze.¹ The resulting equation of mean motion can no longer be put into the same form as the equation for incompressible turbulent flow.

Further, the continuity equation becomes with the notation used

$$\frac{\partial}{\partial t} (\bar{\rho} + \rho') + \frac{1}{r} \frac{\partial}{\partial r} [r (\bar{\rho} + \rho') (v_r + v_r')]]$$

which, when averaged, for steady flow becomes

$$\frac{1}{r} \frac{\partial}{\partial r} [r (\bar{\rho} v_r + \overline{\rho' v_r'})] = 0$$

The effect of the density fluctuations is seen to

¹J. O. Hinze, Turbulence (McGraw-Hill Book Company, Inc., New York, 1959), pp. 23, 24.

be an apparent source contributing a quantity $\frac{\partial}{\partial r} r(\bar{\rho} v_r')$

To overcome these difficulties, Professor H. G. Elrod has suggested in his lectures at Columbia the use of the following: Define a new time mean of some flow property u as

$$\underline{u} = \int_{t-\tau/2}^{t+\tau/2} \frac{\rho u}{\bar{\rho}} dt \tag{2-14}$$

such that

$$u = \underline{u} + u'' \tag{2-15}$$

Integrating equation (2-14) results in

$$\begin{aligned} \underline{u} &= \frac{1}{\tau} \int_{t-\tau/2}^{t+\tau/2} \frac{(\bar{\rho} + \rho')(u + u'')}{\bar{\rho}} dt \\ &= \underline{u} + \frac{\overline{\rho' u'}}{\bar{\rho}} \end{aligned} \tag{2-16}$$

From equations (2-15) and (2-16) it is seen that

$$u'' = u' - \frac{\rho' u'}{\bar{\rho}}$$

Although $\overline{u'} = 0$, $\overline{u''} \neq 0$, except for the case of $\rho = \text{constant}$

Applying the new averaging technique to the Continuity Equation, equation (2-5)

$$\begin{aligned} \frac{\partial \rho}{\partial t} + \frac{1}{r} \frac{\partial}{\partial r} [r \rho v_r] &= 0 \\ \frac{\partial}{\partial t} (\bar{\rho} + \rho') + \frac{1}{r} \frac{\partial}{\partial r} [r (\bar{\rho} + \rho') (v_r + v_r')] &= 0 \end{aligned}$$

¹Ting-Yi Li, H. T. Nagamatsu, "Effect of Density Fluctuations on the Turbulent Skin Friction on a Flat Plate at High Supersonic Speeds," Guggenheim Aeronautical Laboratory, California Institute of Technology, Pasadena, California, Memorandum No. 11, Nov. 1, 1952, p. 4.

when time averaged this becomes, for steady flow

$$\begin{aligned} \frac{1}{r} \frac{\partial}{\partial r} [r(\bar{p}V_r + \overline{p'v_r'})] &= 0 \\ &= \frac{1}{r} \frac{\partial}{\partial r} [r(\bar{p})(V_r + \frac{\overline{p'v_r'}}{\bar{p}})] = \\ &= \frac{1}{r} \frac{\partial}{\partial r} [r\bar{p}V_r] \end{aligned}$$

That is

$$r\bar{p}V_r = \text{Constant} = 0 \text{ on the stator.}$$

$$\text{Therefore } V_r = 0$$

If this substitution is made into the equations for momentum, the equations resulting are identical in form with the original transient form except that:

1. V_i is changed to \underline{V}_i and p to \bar{p} , and
2. π_{ij} is changed to $\pi_{ij}^{(v)}$ which is now

$$\pi_{ij}^{(v)} = \bar{\pi}_{ij} + \overline{\rho v_i v_j} \quad (2-17)$$

The terms $\overline{\rho v_i v_j}$ are the virtual stresses as contrasted to $\rho v_i v_j$ for the incompressible case.

In the case of a fluid of uniform density $\overline{\rho v_i v_j}$ reduces to $\rho \overline{v_i v_j}$

2.1.2.1 The Shear Stress, $\tau_{r\theta}$

In accordance with the previous section $\tau_{r\theta}^{(2)}$ is therefore

$$\tau_{r\theta}^{(2)} = \overline{\tau_{r\theta}} + \rho \overline{v_r'' v_\theta''} \quad (2-18)$$

where $\overline{\tau_{r\theta}}$ is developed below:

$$\begin{aligned} \overline{\tau_{r\theta}} &= -\overline{\mu \left[r \frac{\partial}{\partial r} \left(\frac{v_\theta}{r} \right) + r \frac{\partial v_r}{\partial \theta} \right]} \\ &= -\overline{\mu \left[r \frac{\partial}{\partial r} \frac{v_\theta}{r} \right]} \\ &= -\overline{(\mu + \mu') r \frac{\partial}{\partial r} \left[\frac{v_\theta}{r} + \frac{v_\theta'}{r} \right]} \\ &= -\overline{\mu r \frac{\partial}{\partial r} \frac{v_\theta}{r}} - \overline{\mu' r \frac{\partial}{\partial r} \frac{v_\theta'}{r}} \\ &= -\overline{\mu r \frac{\partial}{\partial r} \left(\frac{v_\theta}{r} \right)} + \overline{\mu r \frac{\partial}{\partial r} \left(\frac{\rho' v_\theta'}{r} \right)} - \overline{\mu' r \frac{\partial}{\partial r} \left(\frac{v_\theta'}{r} \right)} \end{aligned}$$

The last two terms represent interaction between molecular and turbulent transport. They are of higher order

than the first term and can be neglected.^{1,2,3}

Equation (2-18) becomes

$$\tau_{10}^{(t)} = -\bar{\mu} r \frac{d(V_0/r)}{dr} + \overline{\rho V_r'' V_0''} \quad (2-18)a$$

If an eddy diffusivity for momentum is defined as

$$\epsilon_M = \frac{\bar{\mu}}{\rho} \frac{\overline{\rho V_r'' V_0''}}{\tau_{10}} \quad (2-19)$$

$\tau_{10}^{(t)}$ becomes

$$\begin{aligned} \tau_{10}^{(t)} &= \bar{\tau}_{10} \left(1 + \frac{\epsilon_M}{\bar{\mu}}\right) \\ &= -\bar{\mu} r \frac{d(V_0/r)}{dr} \left(1 + \frac{\epsilon_M}{\bar{\mu}}\right) \end{aligned} \quad (2-20)$$

From a knowledge of the velocity distribution and

¹Ting-Yi Li, and H. T. Nagamatsu, "Effect of Density Fluctuations on the Turbulent Skin Friction on a Flat Plate at High Supersonic Speeds," pg. 3.

²R. G. Deissler, and A. L. Loeffler, Jr., "Turbulent Flow and Heat Transfer on a Flat Plate at High Mach Number with Variable Fluid Properties," ASME Paper Number 55-A-33, 1955, p. 20.

³For example, if characteristic values are taken for the velocity, length, density and viscosity, say V_0, r_0, ρ_0, μ_0 and the differential equations non-dimensionalized then in the stream,

$$V_0'/V_0, r_0 \approx O(1), V_0''/V_0, r_0 \approx \ll 1, \mu_0'/\mu_0 \approx O(1), \rho_0'/\rho_0 \approx O(1).$$

On this basis the molecular viscous effects are of order $O(1/Re)$ and interaction between fluctuations and viscosity are of order $O(1/Re)(V_0'/V_0, r_0)$ and are negligible.

the shear stress $\tau_{r\theta}^{(t)}$, $\frac{\text{dyn}}{\text{cm}^2}$ can be found.

The θ component of the Momentum Equation, equation (2-1), for the present case reduces to

$$0 = -\frac{1}{r^2} \frac{\partial}{\partial r} r^2 \tau_{r\theta}^{(t)}$$

or,

$$r^2 \tau_{r\theta}^{(t)} = \text{constant}$$

That is

$$\tau_{r\theta} r^2 = \tau_{r\theta} r_{\text{rotor}} r_{\text{rotor}}^2 = \tau_{\text{stator}} r_{\text{stator}}^2 \quad (2-21)$$

A knowledge of the shear stress at one wall therefore yields the shear stress throughout the flow.

2.1.2.2 The Energy Equation

The differential equation for the stagnation enthalpy H , is given as

$$\rho \frac{DH}{Dt} = \frac{\partial \rho}{\partial t} + \frac{\partial}{\partial x_i} \left[-\frac{2}{3} \mu V_i (\nabla \cdot \vec{V}) \right] + \frac{\partial}{\partial x_i} \left[\mu V_j \left(\frac{\partial x_i}{\partial x_j} + \frac{\partial x_j}{\partial x_i} \right) \right] - \frac{\partial q_i}{\partial x_i} \quad (2-22)$$

where the stagnation enthalpy is, neglecting body forces,

$$H = c_p T + \frac{V^2}{2}$$

and

$$q_i = -k \frac{\partial T}{\partial x_i}$$

Applying the definitions given in equations (2-14) and (2-15) for the time averages of the quantities involved and again neglecting all interaction between molecular and turbulent transport, the resulting equation is

$$\begin{aligned} \bar{p} \frac{DH}{Dt} &= \frac{\partial \bar{p}}{\partial t} - \frac{\partial}{\partial x_i} (\bar{q}_i + \overline{\rho v_i'' H''}) + \frac{\partial}{\partial x_i} \left\{ \bar{\mu} \frac{\partial v_i^2 / 2}{\partial x_i} \right\} + \\ &+ \frac{\partial}{\partial x_i} \left\{ \bar{\mu} v_j \frac{\partial v_i}{\partial x_j} \right\} + \frac{\partial}{\partial x_i} \left[-\frac{2}{3} \bar{\mu} v_i (\nabla \cdot \vec{v}) \right] \end{aligned} \quad (2-23)$$

The term of interest in this equation is

$$\bar{q}_i + \overline{\rho v_i'' H''} \quad \text{since in cylindrical coordinates this term is}$$

$$\bar{q}_r + \overline{\rho v_r'' H''}$$

and is the radial heat flux from the rotor to the stator, $q_r^{(t)}$.

Thus

$$q_r^{(t)} = \bar{q}_r + \overline{\rho v_r'' H''} \quad (2-24)$$

To formulate an expression for \bar{q}_r consider the time average of $q_r = -k \frac{\partial T}{\partial r}$.

$$\begin{aligned} \bar{q}_r &= -(\bar{k} + k') \frac{d}{dr} (\bar{T} + T') \\ &= -\bar{k} \frac{d\bar{T}}{dr} - \overline{k' \frac{dT'}{dr}} \\ &= -\bar{k} \frac{d\bar{T}}{dr} + \bar{k} \frac{d\overline{\frac{\rho' T'}{\rho}}}{dr} - \overline{k' \frac{dT'}{dr}} \end{aligned}$$

Neglecting interaction between molecular and turbulent transport and terms of higher order magnitude

$$\bar{q}_r = -\bar{k} \frac{d\bar{T}}{dr}$$

If an eddy diffusivity for heat is defined as

$$\epsilon_H = \frac{\bar{k}}{\rho \bar{c}_p} \frac{\overline{\rho v_r'' H''}}{\bar{q}_i} \quad (2-25)$$

we have for $\frac{g_r}{g_r^{(t)}}$

$$\frac{g_r}{g_r^{(t)}} = -\bar{k} \left(1 + \frac{\epsilon_H}{\bar{\epsilon}}\right) \frac{dI}{dr} \quad (2-26)$$

To obtain ϵ_H , a knowledge of g_r and I is required.

The relation between g_r at r and g_{wall} is

$$g_r r = g_{r, rotor} r_{rotor} = g_{r, stator} r_{stator} \quad (2-27)$$

2.1.3 The Determination of ϵ_H/ϵ_M

With a knowledge of P_{wall} , g_{wall} , $V_0(r)$ and $I(r)$ one can determine ϵ_M and ϵ_H .

To determine ϵ_H/ϵ_M , the following equations are used:

From equation (2-20)¹

$$P_{ro} = -\bar{\mu} r \left(1 + \frac{\epsilon_M}{\bar{\epsilon}}\right) \frac{d(V_0/r)}{dr}$$

From equation (2-26)

$$\frac{g_r}{g_r^{(t)}} = -\bar{k} \left(1 + \frac{\epsilon_H}{\bar{\epsilon}}\right) \frac{dI}{dr}$$

Also

$$P_{ro} r^2 = P_{wall} r_{wall}^2 \quad (2-21)$$

and

$$g_r r = g_{wall} r_w \quad (2-27)$$

Dividing the latter two equations results in

$$\frac{P_{ro} r^2}{g_r r} = \frac{\bar{\mu} \left(1 + \frac{\epsilon_M}{\bar{\epsilon}}\right) r^2 \frac{d(V_0/r)}{dr}}{\bar{k} \left(1 + \frac{\epsilon_H}{\bar{\epsilon}}\right) dI}$$

¹Henceforth the superscript "(t)" will be omitted.

or

$$P_r^{-1} \left(\frac{T_w/r_w}{\rho_w/\bar{\rho}} \right) = \frac{(1 + \epsilon M/\bar{x})}{(1 + \epsilon H/\bar{x})} r^2 \frac{d(V_0/r)}{dr} \quad (2-28)$$

Define \mathcal{Z} as

$$\mathcal{Z} \equiv \frac{1}{r^2} \frac{1}{P_r} \left(\frac{T_w/r_w}{\rho_w/\bar{\rho}} \right) \frac{dI}{dV_0/r} \quad (2-29)$$

By algebra

$$P_r \frac{\epsilon H}{\epsilon M} = \alpha P_r = \frac{\bar{x}}{\epsilon M} (1 - \mathcal{Z}) + 1 \quad (2-30)$$

$$\text{Also } \frac{\mathcal{Z}}{\mathcal{Z}_w} = \frac{dI/d(V_0/r)}{\{dI/d(V_0/r)\}_w} \frac{r_w^2}{r^2}$$

Since $\mathcal{Z}_w = 1$

$$\mathcal{Z} = \frac{dI/d(V_0/r)}{\{dI/d(V_0/r)\}_w} \frac{r_w^2}{r^2}$$

(2-31)

Thus, a plot of \mathcal{Z} vs V_0/r yields \mathcal{Z} .

Note, more importantly that, since close to the wall $(r_w/r)^2 \approx 1$, if \mathcal{Z} vs. V_0/r in that region is a straight line then $\mathcal{Z} = 1$, and from equation (2-30)

$$\alpha P_r = 1$$

Since $1/P_r$ for air ≈ 1.4 ,

$$\alpha = 1.4$$

To summarize, what is required for a determination of α is

1. From equation (2-20)

a. $\frac{dV_0/r}{dr}$, which will be obtained from a total pressure traverse in the gap between the two cylinders

b. T_w , which will be obtained through a knowledge of the shear stress at the wall (see equation (2-21)). The determination of T_w is described in Chapter VI, Section 6.4.

2. From equation (2-26)

a. $\frac{dI}{dr}$ or I which is obtained from interferometric measurements of density in the gap

b. f_r which is obtained from f_w (equation (2-27)), which in turn is measured.

Chapter III

Experimental Apparatus

3.1 General Arrangement

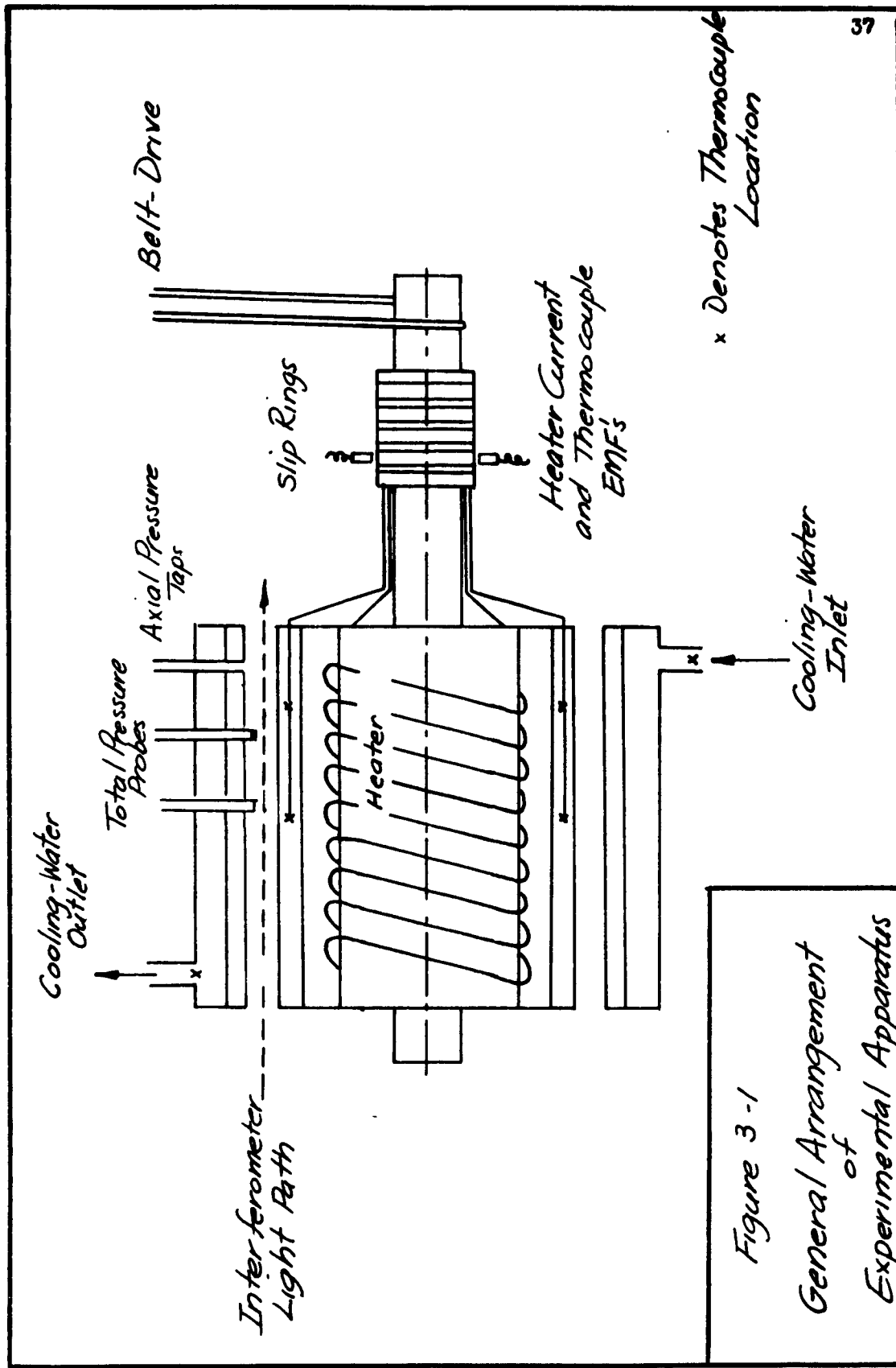
The apparatus from which the experimental data were obtained consists of an electrically heated, motor-driven rotor and a water cooled stator. Auxiliary equipment was provided for heater power and cooling water.

Provision was made for the measurement of the following:

1. Rotor temperature
2. Stator temperature
3. Rate of flow of cooling water
4. Temperature rise of cooling water
5. Heater power input
6. Static pressure distribution axially along the stator wall
7. Radial total pressure distribution in the gap between the two cylinders
8. Root mean square values of the radial and stream-wise turbulent velocity fluctuation components
9. Radial density distribution in the gap between the two cylinders.

A schematic diagram of the apparatus is shown in Fig. 3-1.

The instrumentation of the experimental apparatus



is discussed in Chapter IV.

3.2 Inner Rotating Cylinder

The inner cylinder is shown schematically in Fig. 3-2. It is composed of a stainless steel shell, a heater element, two end plates, a stainless steel shaft, and a slip ring assembly which is used for transmitting power to the heater element, and also for transmitting thermocouple from the thermocouples embedded in the rotor.

3.2.1 Rotor Outer Shell

Because of the temperature requirements (up to 800 F) and strength requirements (up to 10,000 rpm) the outer shell is made of austenitic stainless steel, available as commercial pipe.¹ The shell was machined to a length of 4 inches, an outside diameter of 3.320 inches, ± 0.0005 inches, and an inside diameter of 2.938 inches ± 0.001 inches. The surface finish of the outside surface is 5 microinches rms, as measured with a Profilometer.²

Four thermocouples are located at ninety degree intervals in the wall of the outer shell, two at an axial distance of 2-1/4 inches ($x/L = 1/2$) and two at an axial distance of one inch ($x/L \approx 1/4$), as measured from the end of the

¹Austenitic stainless steel is typified by high strength at elevated temperatures and has excellent scale resistance where conditions of high temperatures and corrosion are met.

²Manufactured by Physicists Research Corp., Ann Arbor, Michigan.

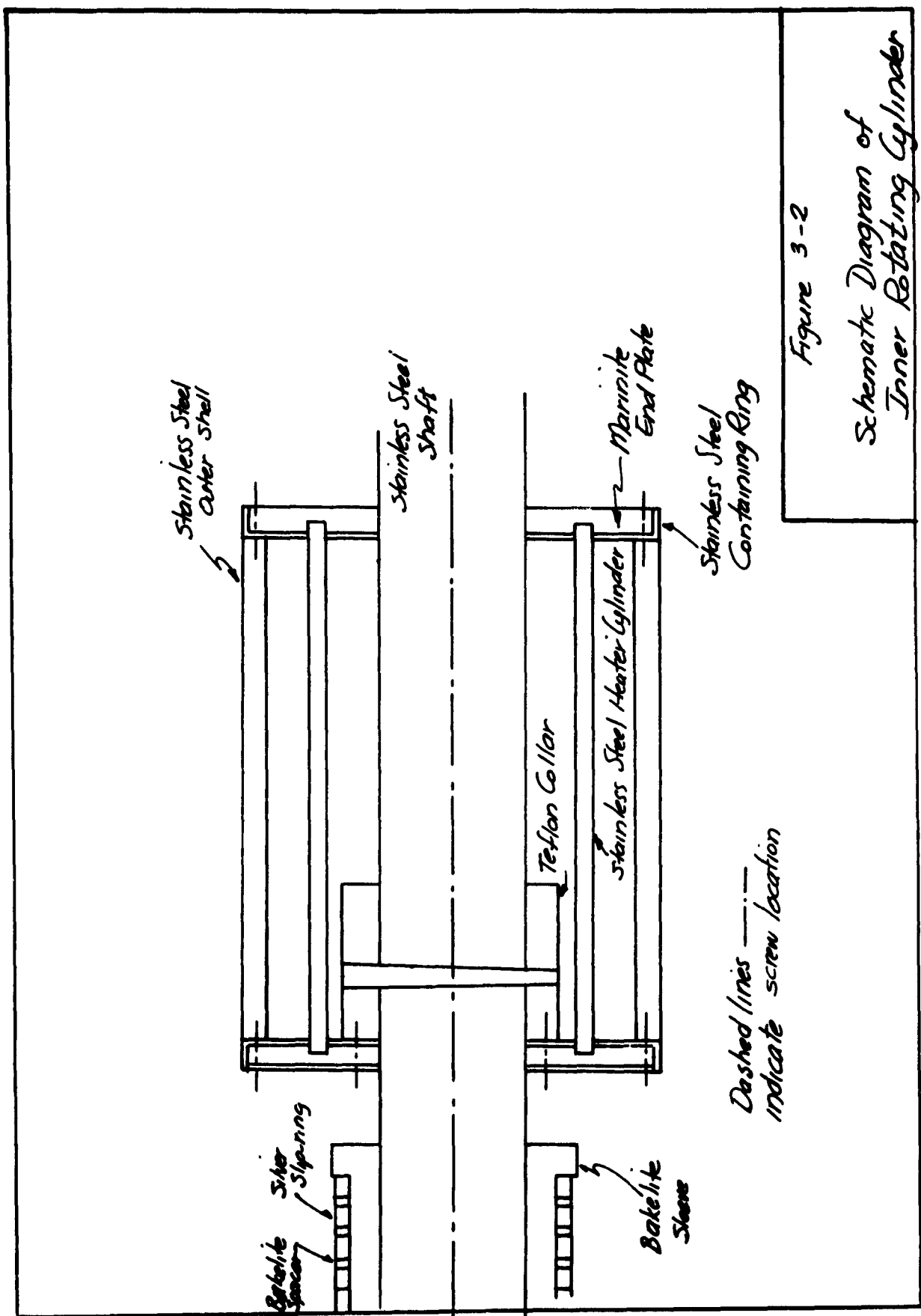


Figure 3-2

Schematic Diagram of Inner Rotating Cylinder

rotor nearest the slip rings.

The holes in which the thermocouples are placed were drilled axially to minimize errors in measurement which would be caused by temperature gradients and insufficient length of thermocouple wire in the parent metal. The installation was made according to procedures outlined by Baker, Ryder and Baker.¹

A further discussion of the thermocouple installation and the slip-ring arrangement is found in Chapter IV.

3.2.2 Rotor Heating Element

The rotor heating element is composed of a stainless steel tube 4-1/4 inches long, outside diameter of 2 inches and a 3/32 inch wall thickness. This tube is covered with two layers of mica sheet approximately 0.004 inches thick and wound with heater wire. The wire used was "Alloy K", purchased from C. O. Jellif Mfg. Corp., Southport, Connecticut, and had a resistance of 0.48 ohms/ft.

Winding was done on an engine lathe, holding the tube in a three-jaw chuck and the wire in the tool post where it was constrained so as to be under tension. The carriage

¹H. D. Baker, E. A. Ryder, and N. H. Baker, Temperature Measurement in Engineering (New York: John Wiley and Sons, 1953), Vol. I.

was then given such a motion as to produce six wraps per inch, corresponding to a heater resistance of 13 ohms.

Control of heater power during a run was by means of a Powerstat¹. Provision was made for measurement of heater power and

3.2.3 Rotor Shaft

The rotor shaft is shown in Fig. 3-3. The shaft material is stainless steel.

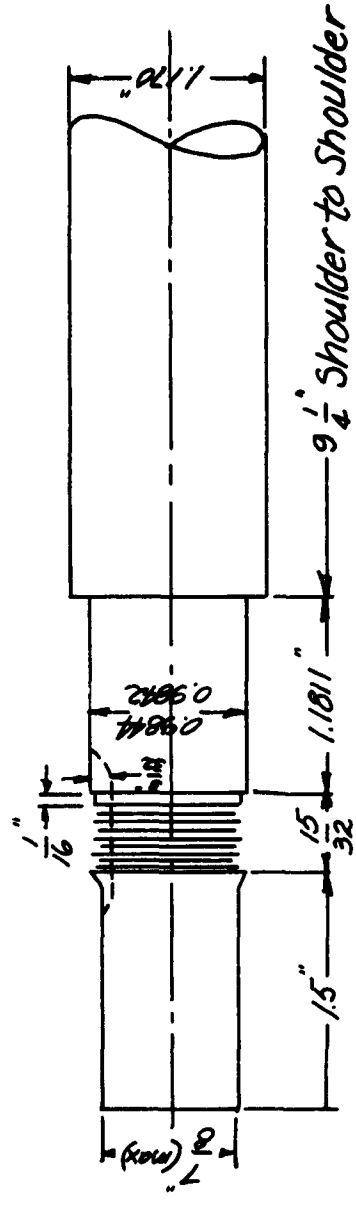
Axial grooves placed about the circumference of the shaft receive thermocouple leads from the outer shell of the rotor and thus enable the shaft to pass through the stator end plates (see Section 3.4) with a clearance of 0.005 inches.

The shaft was ground to an accuracy of 0.0001 inches as required by the ball bearings selected for the shaft.

The ball bearings were "D-B Mounted", a type of mounting whereby the backs of two bearings are preground and then placed together. This mounting eliminates the eccentricity in the bearings and is generally recommended by bearing manufacturers for high speed, high accuracy grinding spindles.

The light bearing loads (about three pounds per bearing) and the method of mounting assures high rotational speeds with a minimum of run-out (0.0001 inches on the shaft).

¹Manufactured by the Superior Electric Company (Bristol, Connecticut).



Thread Detail
 Major Diameter 0.9636
 Pitch Diameter 0.9487
 Maximum Minor Diameter 0.9307
 52 threads/inch

Fig. 3-3a
 Rotor Shaft
 Bearing End Detail
 Matl: Stainless Steel

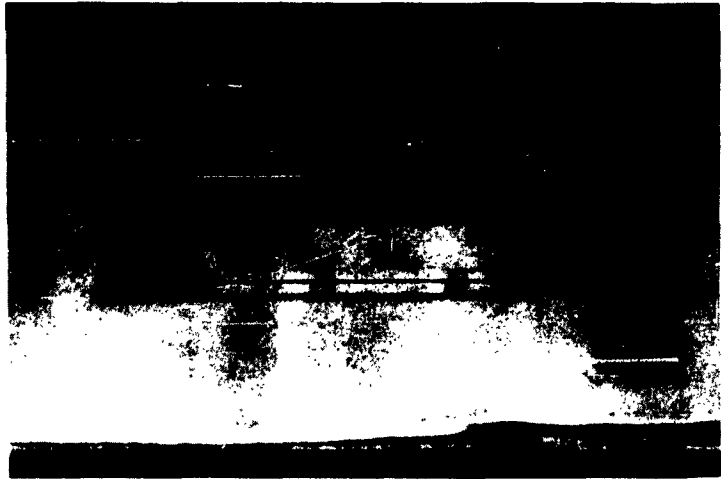


Figure 3-3b
Stainless Steel Rotor shaft

3.2.4 Rotor End Plates

The end plates provided to hold together the rotor assembly are shown in Fig. 3-4.

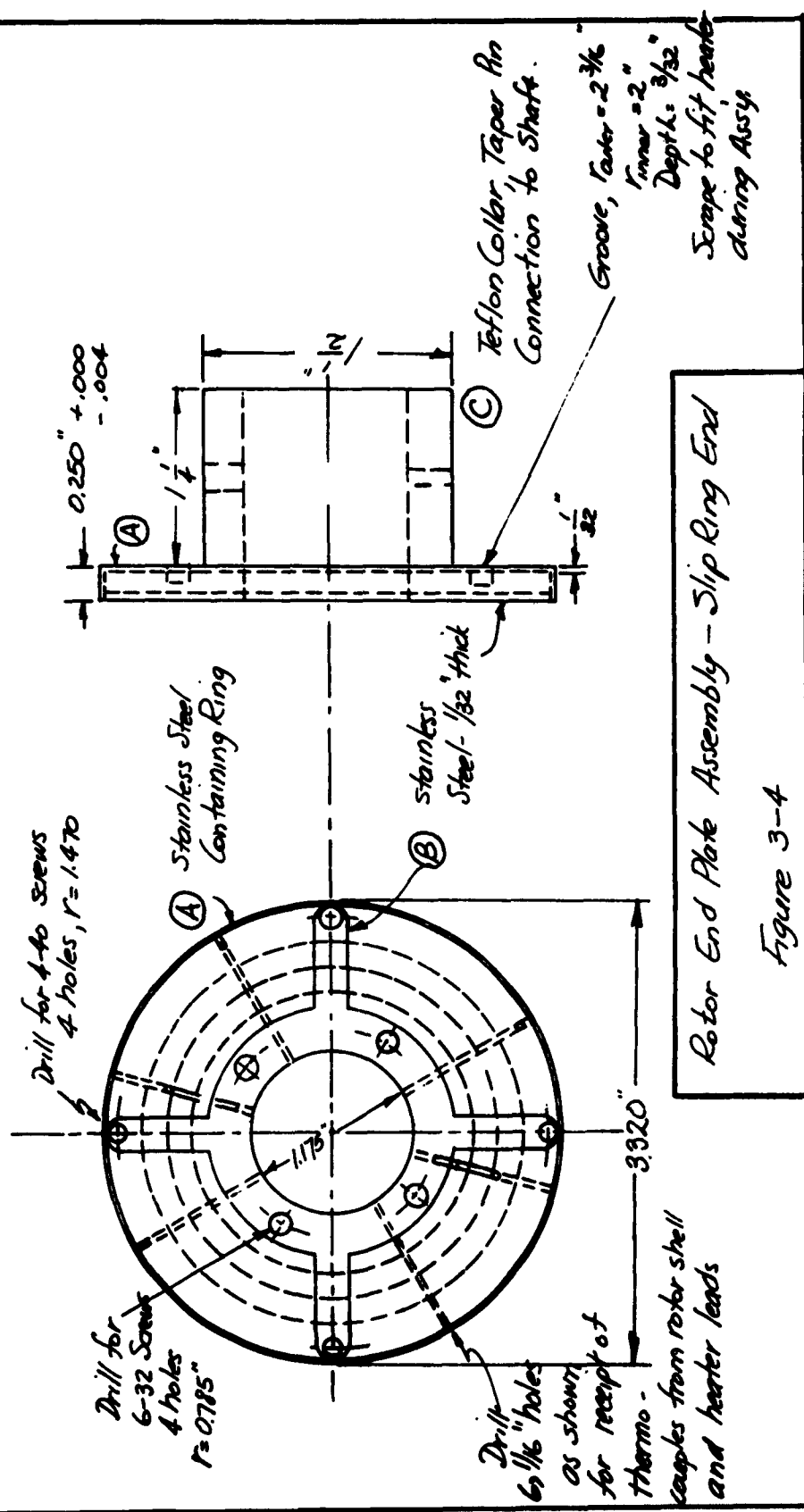
The requirements of a suitable end plate material are 1. That it have sufficient strength at high temperatures to withstand the centrifugal stresses at high speeds.

2. That it have low thermal conductivity to inhibit heat losses from the outer rotor shell and heater to the shaft.

3. That it be easily machined, since holes and grooves were required for the passage of thermocouple and heater leads from the rotor outer shell and the heater to the slip rings.

A first attempt was made to use a product of the American Lava Corporation of Chatanooga, Tennessee, called Lava Grade A, an aluminum silicate. This product was easily machined before firing. By trial and error the decrease in size because of firing was determined and it was possible to have the end plate in final form to size within 0.001 inches. This material was rejected, however, because of cracks which developed during assembly because of loads imposed by fastening screws.

A second material, Marinite, manufactured by the Johns-Manville Corporation of New York, New York was found to be satisfactory. The containing ring A and the spider like member B in Fig. 3-4 were provided so that the Marinite would



Rotor End Plate Assembly - Slip Ring End
Figure 3-4

Scrape to fit heater during Assy.

not be a load bearing member. The two end plates and their containing rings are each $1/4$ inch wide.

Further, only one end plate was fastened to the shaft by means of the Teflon collar C . The second end plate made no connection with the shaft to allow for axial thermal expansion of the rotor assembly to be taken up in this direction (much as the floating tube-sheets in commercial heat exchanger design).

3.2.5 Slip-Ring Assembly for Rotor Temperature Measurement

The slip-ring assembly for rotor temperature measurement is shown in Fig. 3-5. The brushes, brush holders and coin silver slip rings were purchased from the Graphite Metallizing Corporation of Yonkers, New York.¹

The slip rings were pressed over a bakelite bushing, as shown in Fig. 3-5, with bakelite spacers between the rings. The bushing was grooved to receive copper lead wires which at one end were soldered to the coin silver slip rings and at the other end to the iron and constantan thermocouple wires at points in the ambient air external to the rotor and rotating with it. The copper lead wires from the silver GRAPHALLOY brushes were returned to form compensating junctions with iron

¹From Graphite Metallizing Corporation, catalog No. 3, General Brushes: Silver GRAPHALLOY, $5/32$ inches square.

Brush Holders: No. 11509

Coin silver slip rings: No. 1165-27, 1- $11/16$ inches O.D., machined to $5/32$ inches wide.

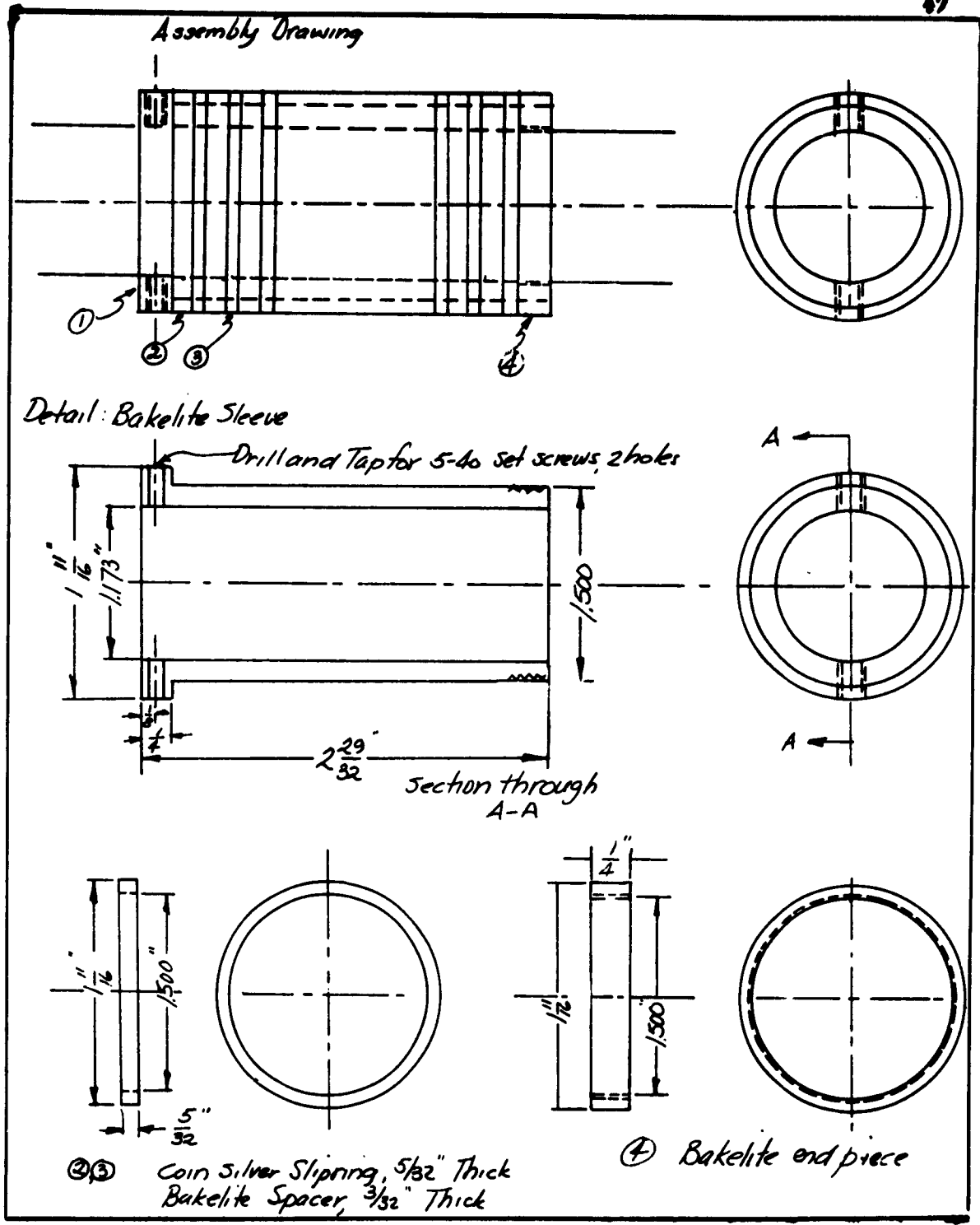


*Figure 3-5 (a)
Slip Ring Assembly*

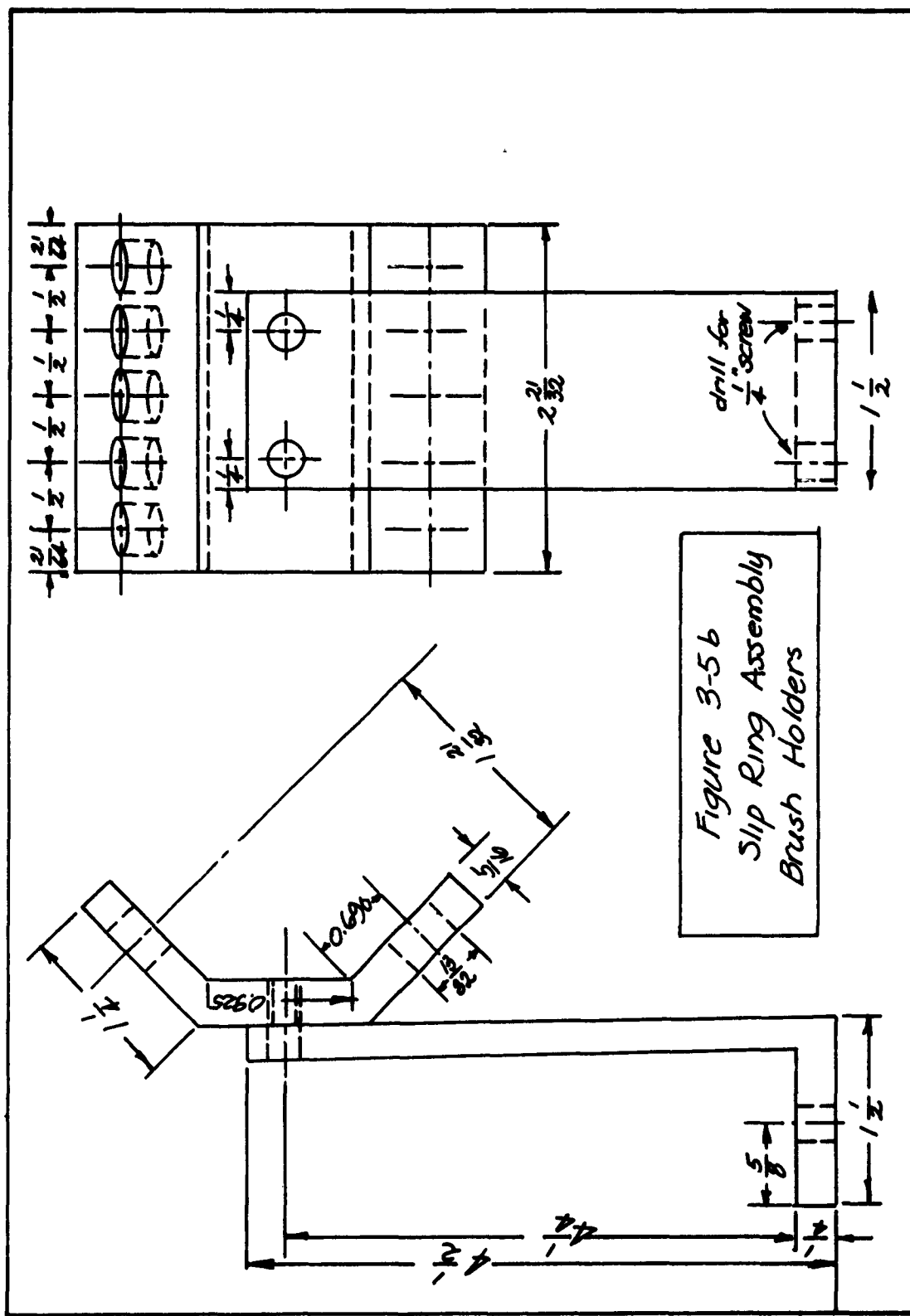


Figure 3-5b
Slip Ring Assembly
Brush Holders

and with constantan at points close to the path of rotation of the previously mentioned copper-and-iron and copper-and-constantan junctions.

The brushes are spring loaded in such a way that so that contact with the slip rings was only momentary during measurement. In this manner spurious thermoelectric effects are minimized. A more detailed discussion of the accuracy of emf measurement with the slip ring assembly is given in the next chapter.

3.3 Outer Stationary Cylinder and Cooling Jacket

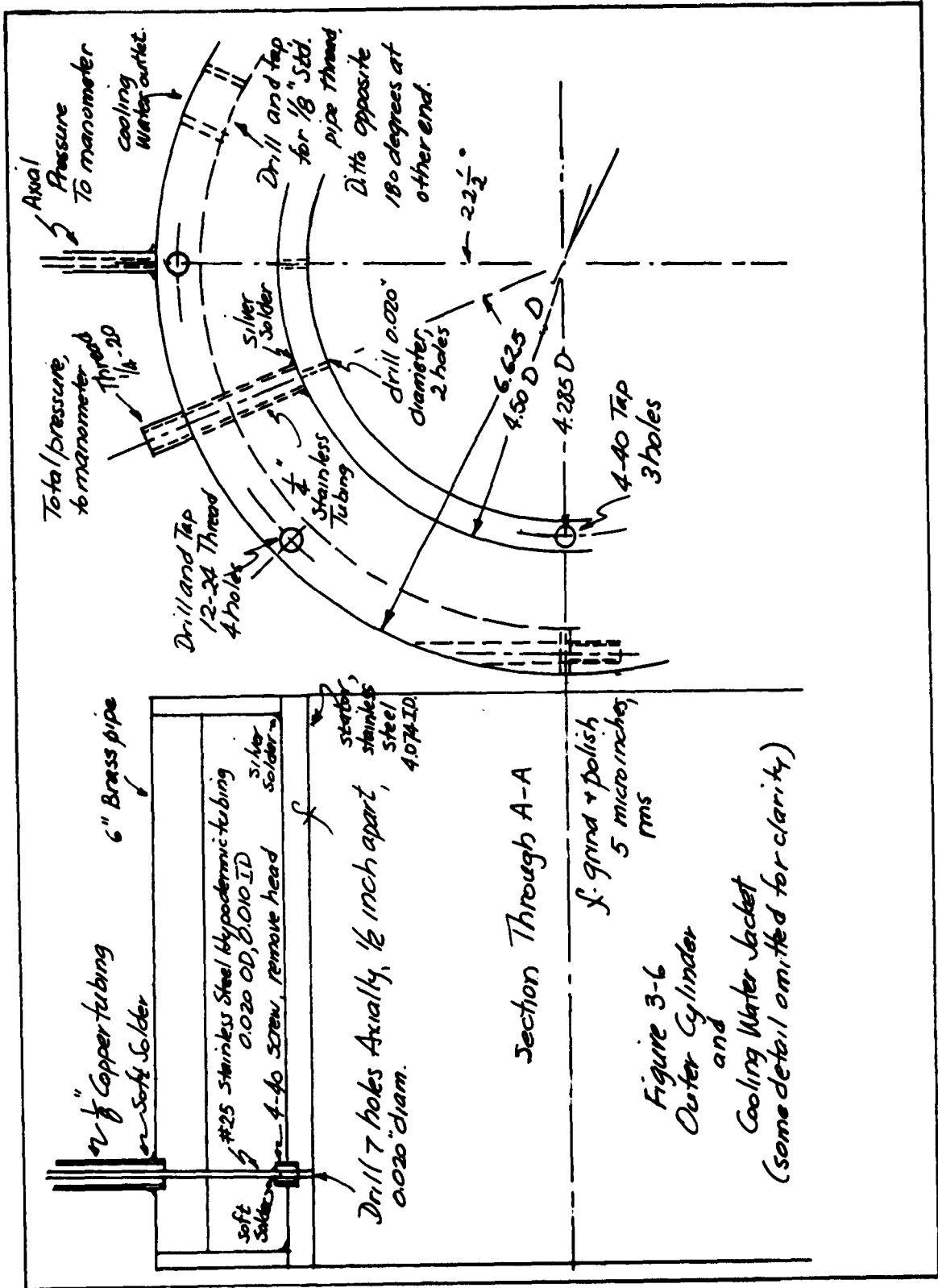
The outer stationary cylinder and cooling jacket is shown in Fig. 3-6a and b.

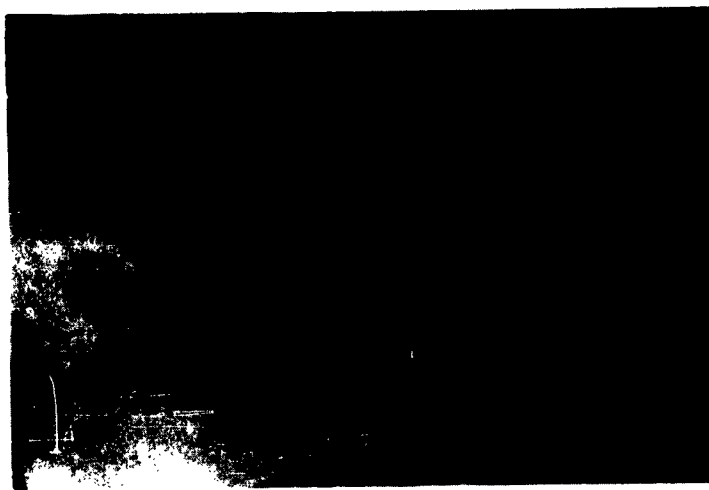
3.3.1 The Outer Cylinder

The outer cylinder is made of austenitic stainless steel available as commercial pipe and machined to an inside diameter of 4.074 \pm 0.001 inches. It was ground to a surface finish of 7 microinches rms.

Seven holes, 0.020 inches in diameter were drilled through the stator walls as shown in Fig. 3-6 to allow the insertion of 0.020 inches outside diameter, 0.010 inches inside diameter stainless steel hypodermic tubing¹ to serve as axial static pressure taps.

¹No. 25 Stainless steel hypodermic tubing, purchased from Becton and Dickenson and Co., Inc., Rutherford, New Jersey.





Outer Stationary Cylinder
and
Cooling Jacket

Figure 3-6 b

The hypodermic tubing was soldered into 4-40 stainless steel screws.

The stator holes were counter bored and tapped to receive the tubing and its fitting. Non-hardening Permatex (No. 2) was used at the joint to prevent cooling water leakage. The stainless steel tubing was counter sunk at the wall of the stator 0.010 inches to eliminate the effect of disturbances to the static pressure at the stator wall caused by the presence of the tap. This effect is discussed in Chapter IV.

Two holes 0.020 inches in diameter were drilled through the stator wall at a radial position, 22-1/2 degrees from the static pressure taps; one at an axial distance of 1-1/2 inches, the other at an axial position of 2-1/4 inches. The total pressure probes were later inserted into these holes. Suitable packing glands were silver soldered to the outer surface of the stator, concentric with these holes and are shown in Fig. 3-6c. The purpose of these glands is to prevent cooling water leakage into the gap between the concentric cylinders.

Two chromel-alumel thermocouples were embedded into the stator at approximately the same radial position but at different axial positions; one at an axial distance of 2-1/4 inches, the other at an axial distance of 1-1/2 inches. The details of the thermocouple installation are given in the next Chapter.

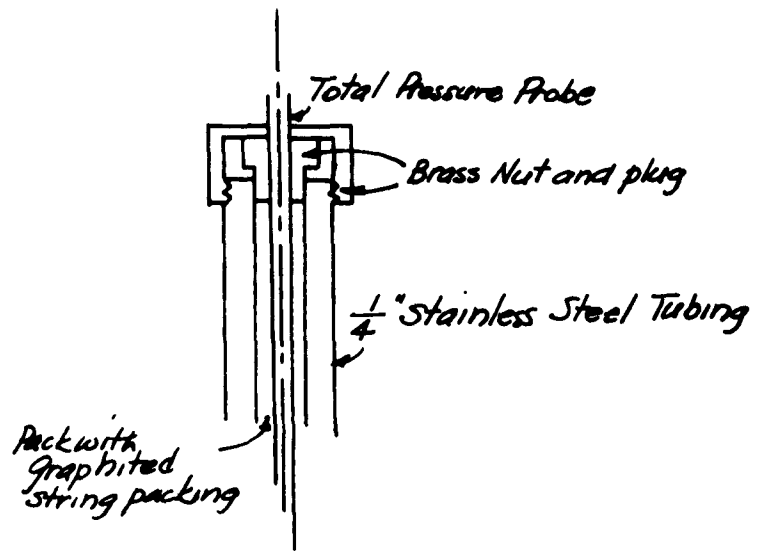


Figure 3-6 c
Packing Gland
used for
Total Pressure Probe

3.3.2 Cooling Jacket

The cooling jacket was made from 6 inch Schedule 80 brass pipe. Water inlet and outlet are through 3/8 inch copper tubing to pipe-thread brass elbows, in each of which is arranged a thermocouple well and thermocouple as shown in Fig. 3-7. These thermocouples are for the measurement of the temperature difference, entering and leaving, of the cooling water.

As a precaution against heat losses from the jacket, the jacket itself was covered with Johns-Manville 85% carbonate of magnesia, 15% asbestos insulation. Losses were further minimized by having the average cooling water temperature approximately equal to room temperature.

3.3.3 End Plates

Two stator end plates were provided to enclose the rotor-stator assembly. These are shown in Fig. 3-8. These were made of *Marinite*.

Fused quartz windows are seated in the rectangular openings shown to provide a light path for interferometric study of the density distribution in the gap between the rotor and stator.

3.4 Bearing Housings and Base Plate

Fig. 3-9 is a drawing of the bearing housings.

The base plate has levelling screws on which the

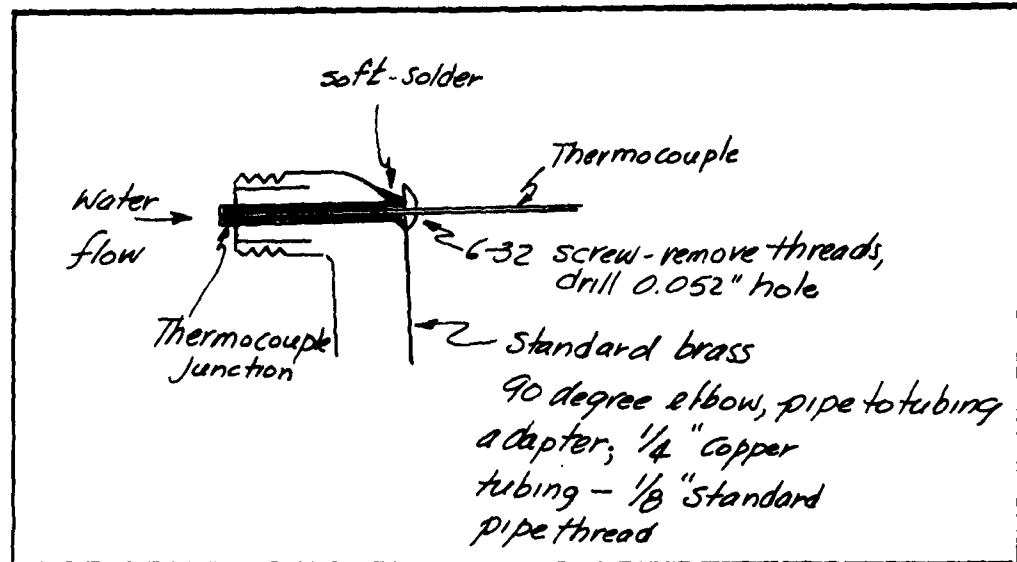


Figure 3-7

Cooling Water Thermocouple
Well

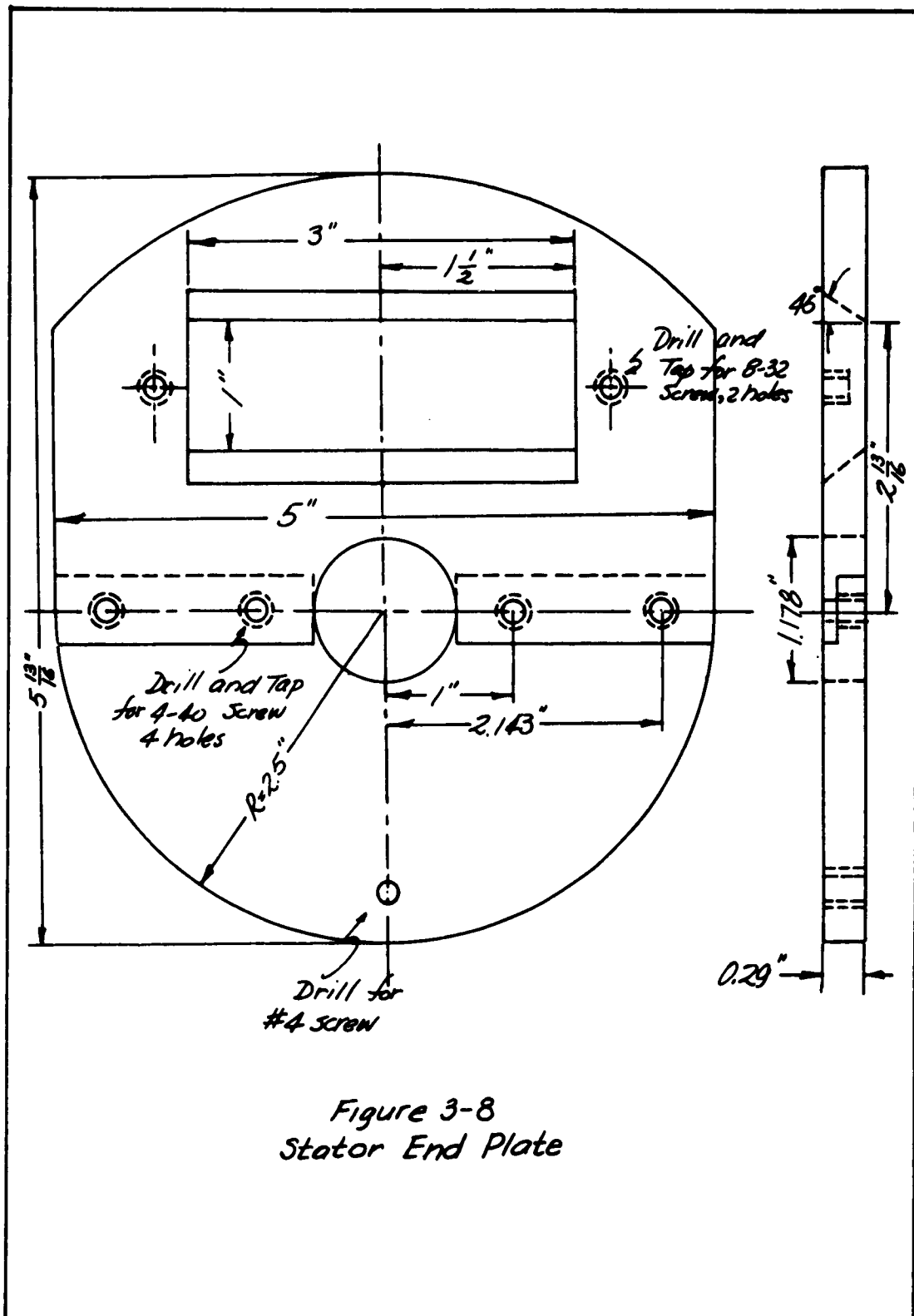


Figure 3-8
Stator End Plate

stator assembly is seated. The levelling screws enable adjustment of the stator position so that it can be made concentric to the rotor.

3.5 Motor

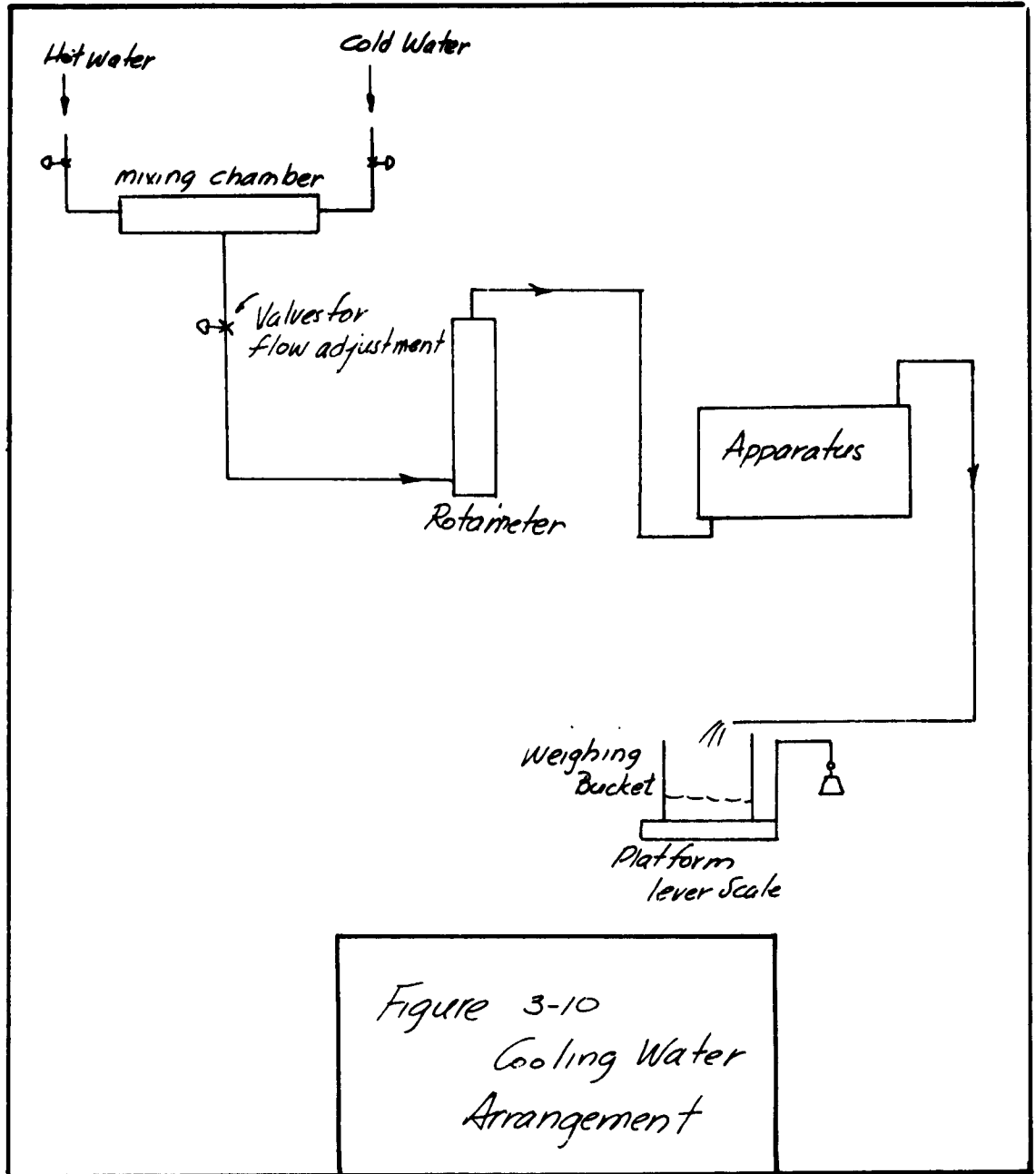
The rotating cylinder is driven by a D. C. motor. Alternating current is led through a constant voltage transformer and a rectifier to the motor. Speed adjustment is made by means of slide wire rheostates in the armature and field circuits of the motor.

A Strobotach¹ was used to determine variations from the desired speed. The Strobotach was not used as a speed measuring device because of its drift. A chronometric tachometer placed against the rotating shaft was used to set the Strobotach to the desired glimpse frequency. The setting of the Strobotach was checked through speed measurements with the Chronometric tachometer every fifteen minutes.

3.6 Cooling Water Arrangement

The cooling water arrangement is shown in Fig. 3-10. Hot and cold water were mixed in a chamber made from 2 inch, Schedule-40 steel pipe. A pressure regulating valve was supplied for both the hot water and cold water. After mixing, the water was led through another pressure regulating valve to a rotameter. The rotameter was used to determine variations from the desired flow settings. Variations from the settings were infrequent, generally occurring before noon and at 4:30 P.M.

¹Manufactured by the General Radio Company (Cambridge, Mass.).



when excessive demands were placed on the Pupin Building water supply. At these times, adjustment was required in control valve settings to maintain the desired temperature and flow rate. The adjustments were minor in nature. From the rotameter the water was led through Tygon tubing to the test-section and returned from the test-section, again in Tygon tubing, to a pail placed on a lever scale.¹ Here the flow rate was measured by weighing the water flow over a time interval. Thus, accurate calibration of the rotameter was not required.

¹The water outlet from the rotameter is through an expanded tube fitting from which only several inches of copper tubing extends. A tight joint was obtained between the Tygon tubing and the piece of copper tubing by selecting the Tygon size about 1/8 inch smaller in inside diameter than the outside diameter of the copper tubing. The Tygon was then immersed in Acetone for about one-half hour causing its diameter to increase. It was then placed over the copper tubing. When the Acetone evaporated from the Tygon a "shrink" fit resulted between the Tygon and copper.

CHAPTER IV

Instrumentation

4.1 The experimental apparatus described in Chapter III was instrumented so that ultimately the following were known:

1. Overall rate of heat transfer from the rotor to the stator under varying conditions of rotor speed and temperature. The required measurements were rotor and stator temperature, rate of flow of cooling water, and temperature rise of cooling water.

2. Velocity distribution in the gap between the rotor and stator. The required measurements were total pressure distribution, static pressure at the stator surface, and density distribution.

3. Temperature distribution in the gap. The measurements taken were density distribution in the gap as determined with a Mach-Zehnder interferometer.

4. Whether Taylor vortices persisted in the flow at rotational speeds of the experiment. The required measures were made with a hot-wire anemometer.

The measurements taken can then be grouped as temperature measurements, pressure measurement, water flow rates, fluctuating velocities and density measurements.

4.2 Temperature Measurements

Wherever possible, thermocouples were used to measure temperature. The emf outputs of the thermocouples were measured with a null-balance potentiometer. Thermocouple installation and error analysis, cold junctions and indication circuitry were generally as outlined by H. D. Baker et.al.¹

4.2.1 Stator Temperature

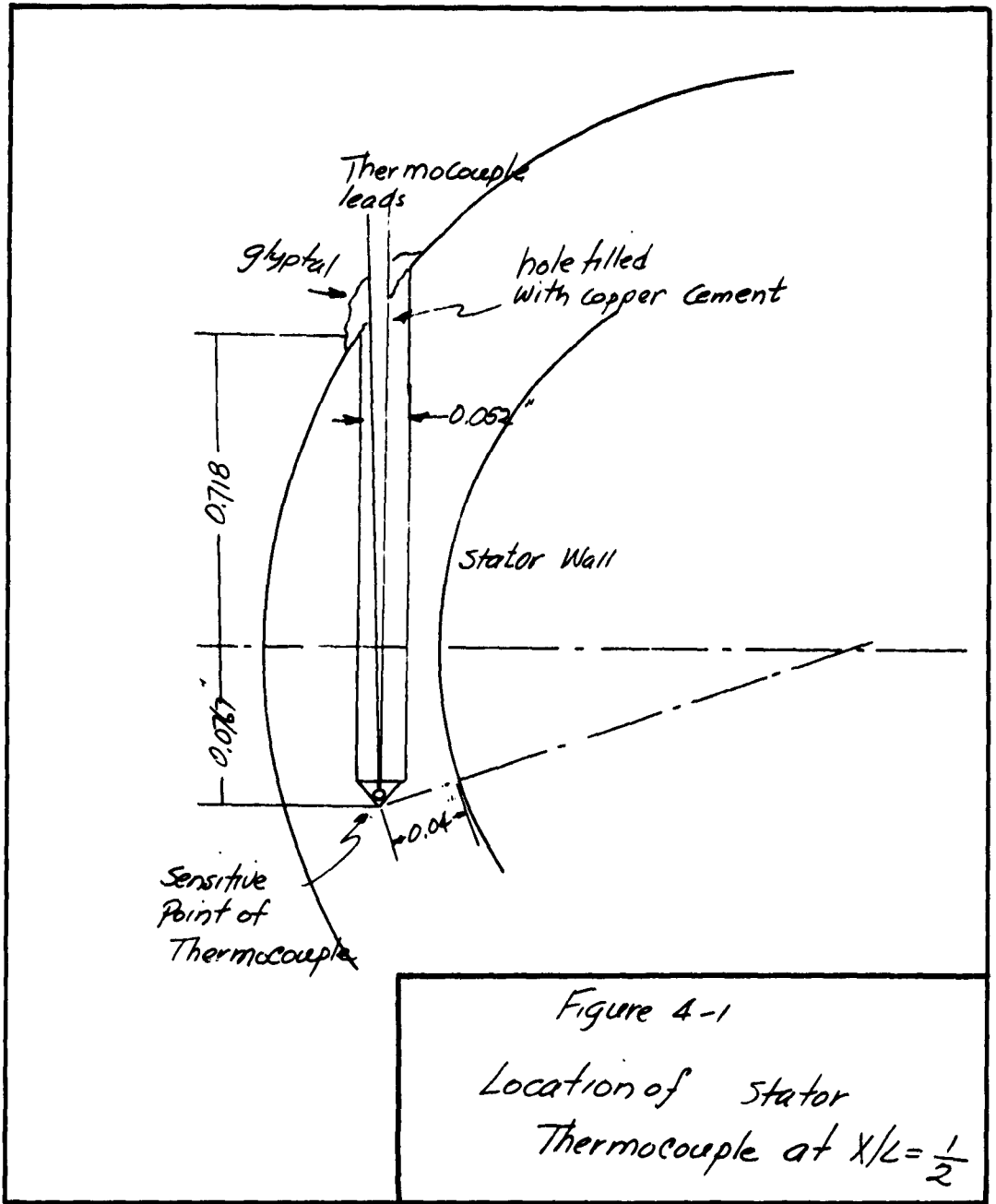
The stator temperature was measured with number 30 B and S gage, glass insulated chromel-alumel thermocouple wire obtained from the Leeds and Northrup Company of Philadelphia, Pennsylvania.

Two thermocouples were placed in the stator wall as shown in Fig. 4-1, one at an axial location, $X/L = 1/2$ the other at an axial location, $X/L = 1/3$. They were displaced from each other in the ϕ -direction by 22-1/2 degrees.

The installation was made exactly as outlined by Baker² except that the drill size used was 0.052 inches rather than 0.046 inches. The junction on these thermocouples as

¹H. D. Baker, E. A. Ryder, and N. H. Baker, Temperature Measurement in Engineering (New York: John Wiley and Sons, 1953), Vol. I.

²H. D. Baker, et.al., Temperature Measurement in Engineering, pp. 143-145.



on all those used was made by the arc method.¹

4.2.2 Rotor Thermocouples

The rotor temperature was measured with number 30 B and S gage glass insulated, duplex iron-constantan thermocouple wire obtained from the Leeds and Northrup Company of Philadelphia, with error of 1% of indication. The installation was made as for the stator thermocouples.

4.2.3.1 Slip Ring Assembly

The measurement of the emf of the rotor thermocouples was made through a brush and ring type slip ring. Other arrangements, such as a mercury slip ring, or magnetic coupling between a rotating and stationary coil were rejected because of the bulk of the installation for the former and the additional investment in electronic equipment required for the latter. The brush and ring type had the advantage that the component parts were available as stock items from the supplier, that the installation was mechanically simple and that several successful installations were described in detail in the literature.

One such installation is that discussed by

¹H. D. Baker, et.al., Temperature Measurement in Engineering, p. 50.

R. Chaplin¹ and it was this design that was paralleled in the present installation. Chaplin reports that his design made possible temperature measurements with errors of less than 1°C, with a chromel-alumel thermocouple.

4.2.3.2 Design of Brush and Ring Type Slip Ring

The most severe problem to be overcome in the design of a brush and ring type slip ring assembly is that of the electrical noise caused by the sliding contact between the brush and the ring. This "noise" is of two types; one caused by the variation of contact resistance, the other caused mainly by spurious thermal emfs from hot spots caused by frictional heating. Since a null balance method of emf measurement was used in the present experiment the variation of contact resistance is of negligible consequence so long as it remains small. The second type of noise was studied in detail by Horton² who measured the generated noise voltages of different brush materials such as natural graphite, silver-graphite, with both high and low silver content, and rhodium-graphite acting on rings of silver, rhodium, gold, copper,

¹R. Chaplin, "Multichannel Slip Rings for Stress and Temperature Measurement" National Gas Turbine Establishment, Pyestock, Hants, Great Britain, Memorandum Number M.289, (December, 1956), p. 7.

²B. M. Horton, "Sliding Contacts to Transmit Signals," Rev. Sci. Insts., Vol. 20, Number 12, (December 1949), pp. 930-932.

and electrographitic carbon.

Horton found that 1) "surfaces covered with corrosion films give much higher values of generated noise voltage than do clean surfaces", 2) "All of the contact combinations... [had]...a generated noise voltage that increased with speed", and he concludes by stating "metal-graphite brushes operating with low friction on clean metal surfaces can yield very low values of generated noise voltage in the frequency range considered [0.5 to 200 c.p.s.]".

For a clean silver ring acted on by 2 brushes of fine texture, high carbon content silver graphite brushes with a normal force of 50 grams, and a sliding speed of 35 cm/sec., (about 350 RPM on the present apparatus), Horton reports a generated noise of 0.3 microvolts. This value was the lowest reported in his Table I. Silver rings with silver-graphite brushes of low silver content were therefore chosen for the present assembly.

At first, the iron and constantan of the rotor thermocouples were soldered directly to the silver slip rings. Large errors were observed in the output emf when the brushes and rings were in continuous contact. Allowing compressed air to flow over the rings reduced this error to more reasonable proportions. When the brushes were allowed to contact the rings for a period of 1 or 2 seconds as necessary to make measurements, errors in emf varying with the time of contact were still observed.

Consequently, the iron and the constantan leads from the rotor thermocouples were joined to copper leads at points in the ambient air external to the rotor and rotating with it.

These form two new thermocouples, copper-constantan and copper-iron, and require compensation. This compensation is achieved by having the copper leads from the brushes returned to form the necessary junctions with iron and constantan at points close to the path of rotation of the copper-iron and copper-constantan junctions. This arrangement is shown schematically in Fig. 4-2 and comprises the final arrangement.

Copper was chosen as the intermediate material between the rings and the rotor thermocouples because of the low thermal emf generated between copper and silver as compared with iron or constantan with silver.¹ With copper as the

¹The data for the following was obtained from the International Critical Tables (first ed., McGraw-Hill Book Co., Inc., New York, 1929) Vol. VI, pp. 214-215.

For example, if the emf of a thermocouple composed of metals A and B, with one junction at 0 deg. C, the other at t deg C is denoted by E_{AB} , then for the metals mentioned

$$\begin{aligned} \text{Iron } E_{\text{silver}} &= 13.79t - 3.675t^2 \times 10^{-2} + 2.856t^3 \times 10^{-5} \\ \text{Constantan } E_{\text{silver}} &= -58.015t - 4.217t^2 \times 10^{-2} + 2.856t^3 \times 10^{-5} \\ \text{Copper } E_{\text{silver}} &= 0.09t + 0.225t^2 \times 10^{-2} \end{aligned}$$

Thus at 38 deg. C (about 100 deg. F) the "thermo-electric power," Q for each of these is

$$\begin{aligned} \text{Iron } Q_{\text{silver}} &= 0.011 \text{ mV/deg C} = 0.006 \text{ mV/deg F} \\ \text{Constantan } Q_{\text{silver}} &= 0.041 \text{ mV/deg C} = 0.023 \text{ mV/deg F} \\ \text{Copper } Q_{\text{silver}} &= 0.004 \text{ mV/deg C} = 0.0022 \text{ mV/deg F} \end{aligned}$$

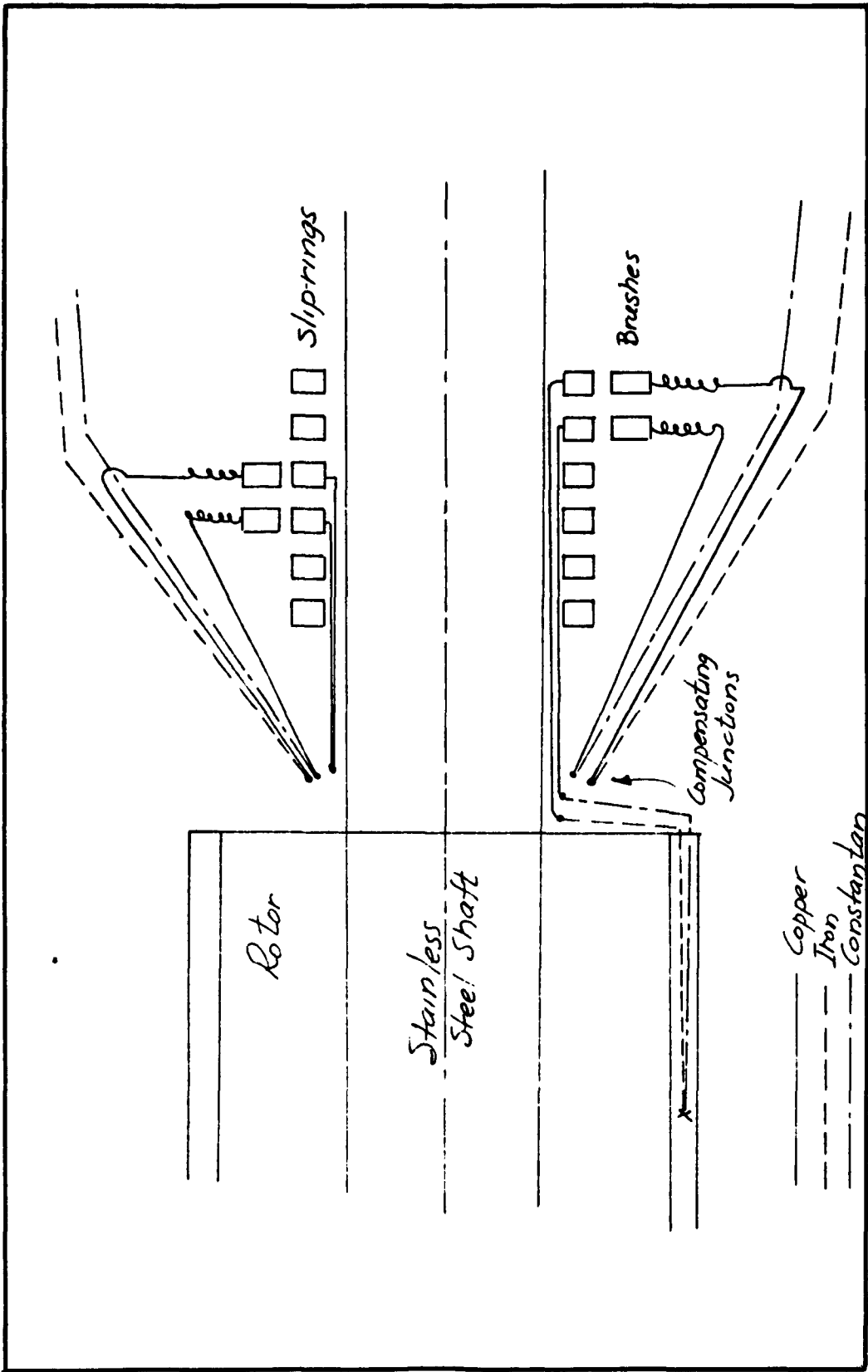


Figure 4-2
Schematic Diagram of Final
Slip-Ring Arrangement

Rotor

Stainless
Steel Shaft

Brushes

Compensating
Junctions

Sliprings

Copper
Iron
Constantan

intermediate metal between the rotor thermocouples and the slip rings the error in indication was reduced to the order of three degrees F. even with the brushes in continuous contact at 4000 to 6000 rpm.

Details of tests run to determine the stated error are reported in Appendix *III*.

4.2.3 Reference Junction

The reference junction used for the thermocouples was a quart thermos bottle filled with ice made from distilled water with enough water added so as to just fill the interstices between the pieces of ice. The two thermocouple junctions one iron-constantan the other chromel-alumel, were each placed in a 6 mm. glass tube, sealed at one end and filled with moisture-free kerosene. These were immersed into the thermos flask to a depth of about 6 inches with the sealed end of the tube about 3 inches from the bottom of the flask.

The thermos in turn was surrounded by slag wool for insulation purposes. The ice was replenished before every run.

4.2.4 Temperature Indication

A null-balance Leeds and Northrup No. 8662 Portable Precision Potentiometer was used as the indicating instrument for the rotor, stator and cooling water thermocouples. The instrument has two scales, one 0 to 16 millivolts, the other 0 to 80 millivolts, with provision for manual cold junction compensation. This latter was not used since a separate

reference junction was maintained during the experiments. The experiments reported here required the use of only the lower scale. The smallest division on that scale is 0.01 millivolts and can be read with confidence to 1/2 division, or 0.005 millivolts, or about 1/4 deg. F for a chromel-alumel thermocouple.

4.2.5 Thermocouple Corrections

Besides the error caused by the slip-ring installation, consideration must be given to errors caused by 1) conduction along the leads and 2) location of the thermocouples relative to the rotor and stator surfaces.

4.2.5.1 Conduction Along the Leads

This error is a result of heat transferred from the point of interest to the ambient using the thermocouple wires as the heat path. Since the transfer of heat implies a temperature difference the thermocouple junction may not be at the same temperature as the surrounding metal of the rotor or stator.

Baker¹ gives an expression for the heat transferred from the leads to the ambient as

¹H. D. Baker, et.al., Temperature Measurement in Engineering, Vol. I, p. 71.

$$q_0 = \sqrt{UCkA} \theta \quad (4-1)$$

where q_0 is the heat transferred, Btu/hr,
 C is the circumference of the leads, ft
 k is the mean value of the thermal
conductivity of the thermocouple lead materials,
Btu/hr-ft²-degF/ft

A is the cross-sectional area of the leads,
ft²,

U is the effective value of the surface
boundary conductance referred to C , Btu/hr-ft²-
deg F and

θ_0 is the surface temperature of the body
minus the ambient temperature.

The value for kA is given with sufficient accuracy
by averaging kA for each of the wires.

The value of U includes the thermal resistance
of the glass sheathing about the wires.

The quantity q_0 must be supplied by the parent
metal. One then computes the temperature difference between
the point of interest and the temperature of the sensitive
junction. This difference, the error, is given by

$$\text{Error} = \frac{q_0}{\sqrt{UCkA}} \operatorname{csch} ml + \frac{q}{m} \operatorname{coth} ml \quad (4-2)$$

where $m = \frac{\sqrt{D'c'}}{k'A'}$

The primed quantities refer to the parent metal,

l is the depth of immersion, ft, and

g is the thermal gradient, deg./ft, along the leads in the parent metal.

Looking at these equations qualitatively, one sees that the error can be reduced by

1. Inhibiting heat transferred to the ambient, g , by suitable choice of small wires, low thermal conductivity metals, and, if necessary, additional insulation over the leads.

2. Encouraging that heat transfer, g_0 which must occur inside the parent metal, by assuring good thermal contact between the parent metal and the thermocouple, and by providing a large depth of immersion, l . These allow to be transferred with small temperature difference and hence small error.

4.2.5.1 Estimation of the Conduction Error

4.2.5.1.1 Stator Thermocouple

A sketch of the thermocouple installation used given in Fig. 4-/.

The hourly heat leaving the installation is given by eq. (4-1).

Where $\theta_0 = (T_{\text{stator}} - T_{\text{cooling water}}) = 20$ degrees, maximum,
 $C = \pi (0.0141)/2 = 0.0037$ ft. based on the equivalent
diameter of the thermocouple metals, $k A = 0.4 \times 10^{-4}$
Btu/hr - degF/ft, and $U = 8$ Btu/hr-ft²-degF. This latter
value is obtained by using a value of h , the surface con-
ductance between the leads and the water of 8.8, referred to
the diameter of the wire, and considering the thermal resistance
of the glyptal-coated glass braid insulation ($k = 0.2$) over
the leads. The thermal resistances of the latter can be
calculated by the conventional equations.

$$\begin{aligned} \text{Using these values, } \theta_0 &= 20 \quad 8(0.0037)(0.4 \times 10^{-4}) \\ &= 0.021 \text{ Btu/hr} \end{aligned}$$

To find m of eq. (4-2),

$$m = UC'/k'A'$$

U is the overall heat transfer conductance between
the thermocouple leads and portions of the body sufficiently
distant so that the isotherms there are not disturbed by the
installation. Consequently, it is composed of two parts; one,
the conductance between the thermocouple leads and the wall
of the hole, this volume being filled with copper cement; the
other part between the wall of the hole and those regions
mentioned.

$$U' \text{ is then given as } \frac{1}{\frac{1}{\mu_{\text{cement}}} + \frac{1}{\mu_{\text{body}}}}$$

$$\text{For a value of } k_{\text{cement}} = 2, \quad \frac{1}{\mu_{\text{cement}}} = \frac{1}{2000}$$

From Baker's Chart A, Fig. 7-6, $1/\mu_{\text{body}} = 1/2000$

since the depth of immersion is 1 inch for the stator, $V = 1000$

$$\text{and } m = \sqrt{\frac{(1000)(0.037)}{0.4 \times 10^{-7}}} = 305 \text{ per ft}$$

$$ml = 25.4.$$

The value of $\text{csch } ml$ in eq. (4-2) is negligible, and the error in the absence of gradient g is therefore negligible.

The temperature gradient in the stator from the inside wall to the outside wall is given by

$$Q = -kA \frac{dT}{dr}$$

The maximum Q/A to be passed is of the order 2000 Btu/hr. The thermal conductivity, k for stainless is 15. Thus,

$$\frac{2000}{15} = 133.3 \text{ degrees/ft.}$$

and the temperature difference between the two walls is, since the stator cylinder is $1/4$ inch thick,

$$\frac{dT}{dx} = \frac{133}{12} \times 0.25 = 2.77 \text{ degrees}$$

The gradient g , in the direction of the thermocouple is therefore 2.77 degrees/inch = 33.24 degrees/ft.

With this value of g , length of immersion, l
 = 1 inch = 0.0833 ft, and $m = 305$,

the conduction error due to g is 0.13 F, and the total conduction error is $0 + 0.13 = 0.13$ F.

4.2.5.1.2 Rotor Thermocouples¹

For the thermocouples embedded in the rotor the conditions inside the parent affecting the accuracy of the thermocouples are the same except that $f = 0$ since the thermocouples were placed axially, and g is higher because of higher θ_0 , and σ . However, the value of n is unchanged, and l is 1 inch for two of the thermocouples and 2-1/4 inches for the other two. Thus, ml is of the same order of magnitude as for the stator thermocouple and the conduction error is negligible.

4.2.5.1.3 Cooling Water Thermocouples

Similar considerations show this error to be negligible.

4.2.5.2 The Error due to Location in the Stator or Rotor Wall

For the stator it was found that ΔT across the wall was 2.77 degrees.

Measurements show that the sensitive point of the thermocouple was approximately 0.040 inches from the wall of interest. The correction to be made is

$$\frac{2.77}{0.25} \times 0.040 = 0.4 \text{ degrees at the most}$$

extreme conditions encountered during the experiment.

This correction was applied throughout the

¹In the computation of the conduction errors, perfect contact was assumed between the thermocouple, copper cement, and the solid body. This assumption may be incorrect for one of the rotor thermocouples. See Section 6.1.3.

computations for overall heat transfer.

For the rotor thermocouples the heat transferred per square foot of surface is of the same order of magnitude. Since their radial location is in the middle of the wall slightly higher errors result and are of the order 1.5 F at rotor temperatures of 400 F. A correction of this error was made in the computation of overall heat-transfer.

4.3 Pressure Measurements

4.3.1 Total Pressure Measurement

Total pressure probes were used to determine the streamwise velocity in the gap between the rotating and stationary cylinder.

4.3.1.1 Manufacture of the Total Pressure Probe

The total pressure probes were made as follows:

A random length of stainless steel hypodermic tubing with dimensions 0.020 inches outside diameter and 0.010 inches inside diameter was deburred on its end with a fine honing stone.

The tube was washed in acetone and blown clear with compressed air. One end of the tubing was then heated to a dull red to prevent splitting of the tubing during subsequent bending operations. A sliver of 0.002 inches shim stock was inserted to a depth of approximately 1/8 inches into the hole.

A small crescent wrench was clamped shut over the end in which the shim stock was inserted, flattening the tube about the shim stock for a length of approximately $1/8$ inches. This flattened portion was then bent 90 degrees to the main stem, and the wrench was removed.

The piece of shim stock was removed, and the probe tip honed to the desired dimensions. Measurements were made of the probe tip dimensions with a toolmaker's microscope, to an accuracy of 0.0001 inches. Fig. 4-4 shows a probe used for the present experiment.

The pressure probes were mounted in the apparatus shown in Fig. 4-5. Pressure in the probe was transmitted through the manifold shown to the manometer.

A $1/4$ inch steel ball was partially enfolded in the top of the manifold. The manifold was spring loaded to bear on a micrometer spinder and barrel which was mounted in a pedestal bolted to the base plate. Rotary motion of the barrel caused an axial motion of the spindle which moved the manifold through contact at the steel ball.

4.3.1.2 Determination of the Radial Position of the Total Pressure Probe in the Gap

To determine the probe distance from the rotor or stator at a given micrometer setting the probe was brought close to the rotor or stator until contact was made using a

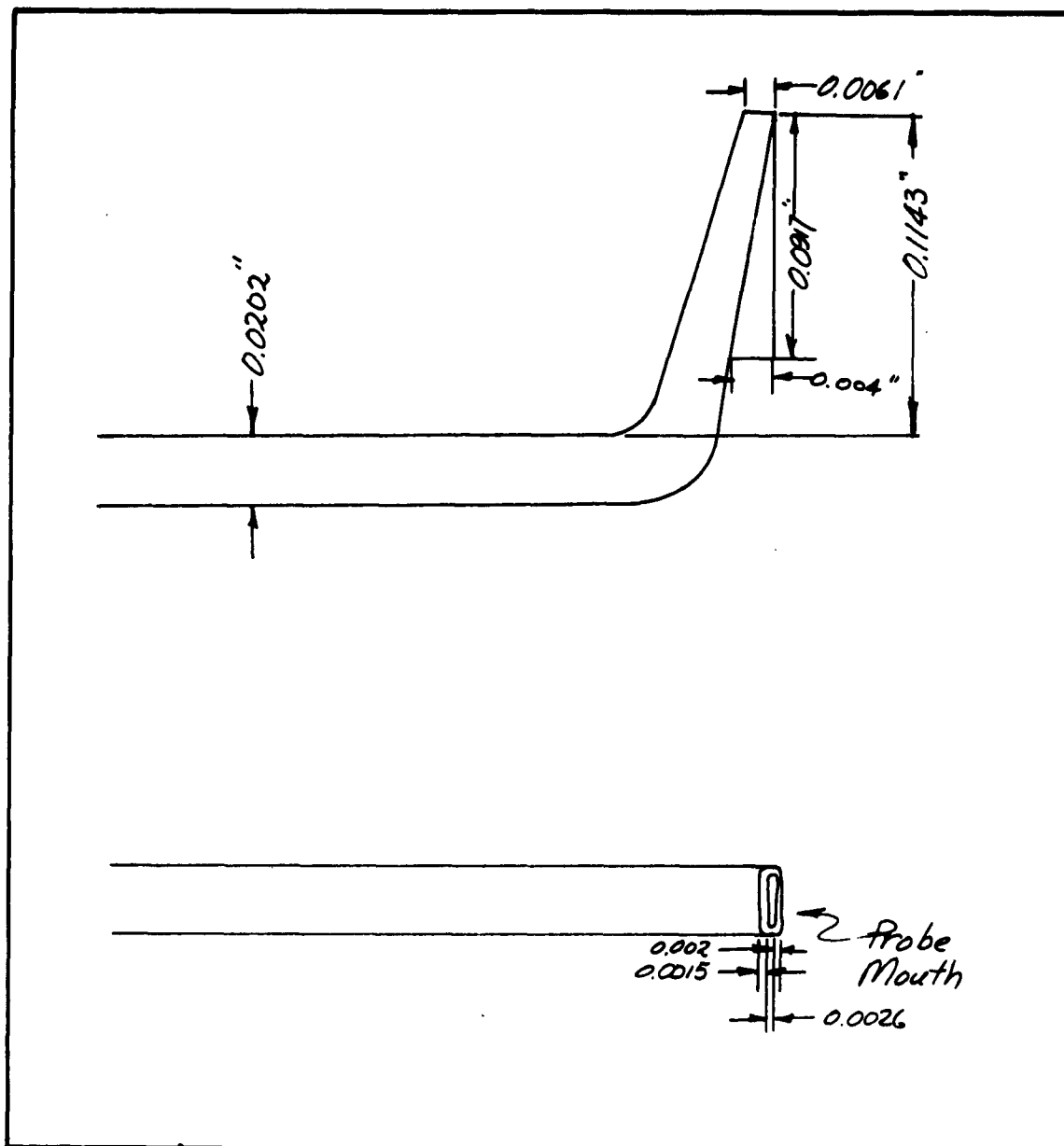


Figure 4-4

Sketch of a Probe Used for Velocity
Measurements Over the Rotor
(Not to scale)

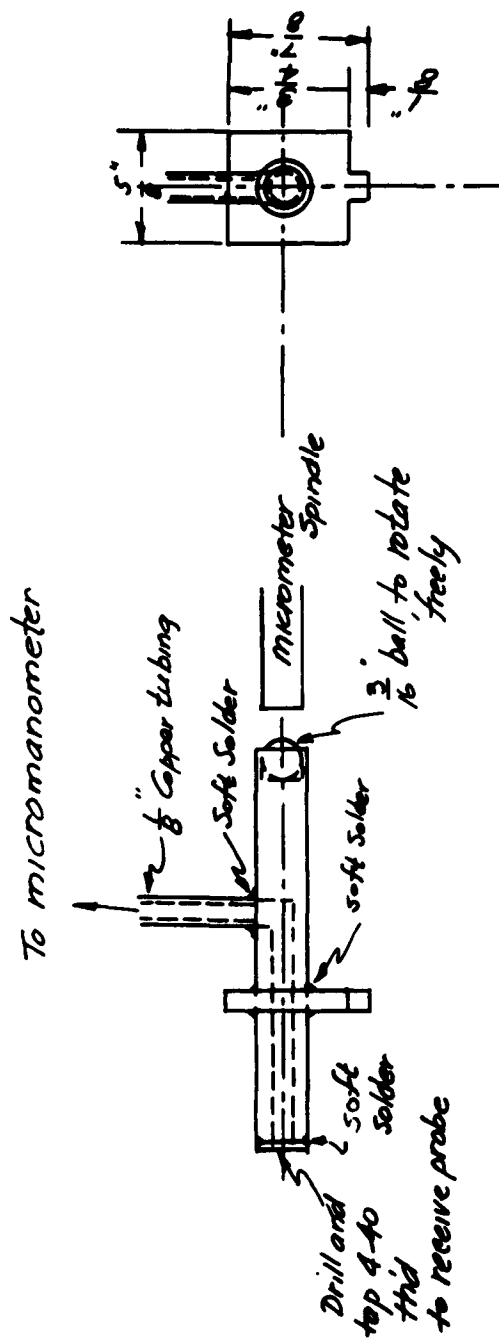


Fig. 4-5
Manifold for Transmitting
Total Pressure to Micromanometer

0.001 inch piece of cigarette paper as a feeler gage. The center of the probe opening relative to the probe height was known, the measurements having been taken with the toolmaker's microscope. In this manner it was possible to determine the distance from the rotor or stator surface to the center of the probe opening.

The probe was used to determine the change in rotor radius with temperature. With the rotor stationary, and heated, the following relationship was determined:

$$r_{\text{rotor}} = 1.660 + 0.000563(MV) - 0.000294$$

where MV is the millivolt reading from the rotor thermocouple connected to the rings furthest from the rotor.

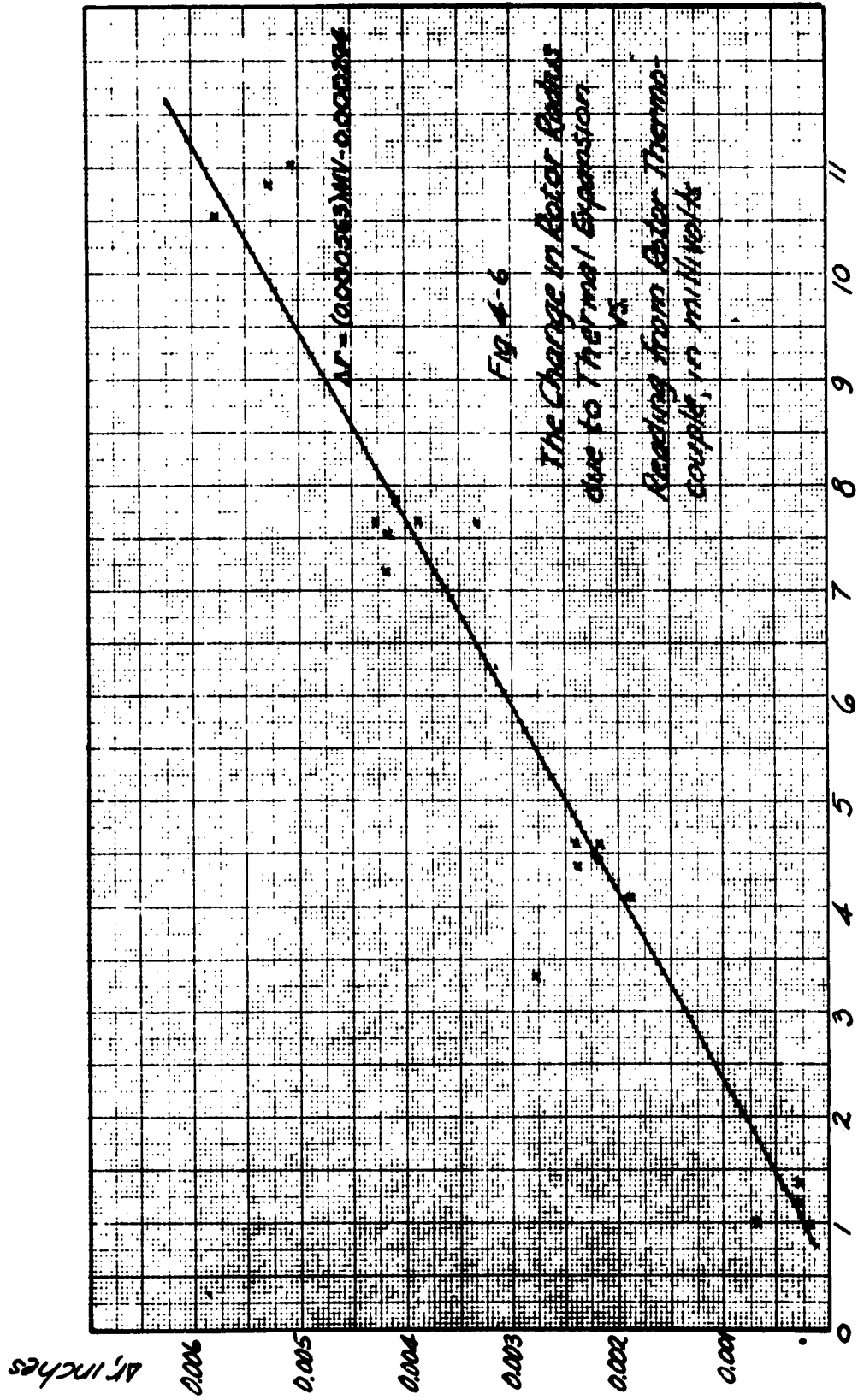
A plot of the data taken to obtain this relation is shown in Fig. 4-6.

4.3.1.3 Total Pressure Probe Corrections

Total pressure probes are subject to several effects which may cause errors in measurement.

4.3.1.3.1 Viscous Effects

So long as the Reynolds number based on a probe dimension such as radius or height is sufficiently large (for example > 100) the indication of a total pressure probe will not be influenced by viscous effects.



For Reynolds numbers between 30 and 100, the indication will be about 0.99 the true total pressure.

For Reynolds numbers less than 30, viscous forces play a more dominant role and the measured impact pressure increases as the Reynolds Number decreases.

This effect has been studied analytically^{1, 2} and experimentally^{3, 4}.

Hurd, Chesky and Shapiro recommend from experiments

$$\frac{P_{\text{stagnation, indicated}} - P_{\text{stagnation}}}{\frac{1}{2} \rho_0 V^2} = 1 + 5.6/Re$$

($Re < 10$)

The results of MacMillan, for probes of different

¹Barker, M. "On the Use of Very Small Pitot Tubes for Measuring Wind Velocity", Proc. Royal Soc. London, A101, (1922), pp. 435-445.

²R. W. Ladenburg, B. Lewis, R. N. Pease, H. S. Taylor, Physical Measurements in Gas Dynamics and Combustion (Princeton, New Jersey: Princeton University Press, 1954), pp. 112-118.

³C. W. Hurd, K. P. Chesky, and A. H. Shapiro, "Influence of Viscous Effects on Impact Tubes", J. Appl. Mech., Vol. 20, (1953), pp. 253-256.

⁴F. A. MacMillan, "Viscous Effects on Flattened Pitot Tubes at Low Speeds", Aeronautical Research Council, Fluid Motion Sub-Committee, FM2081a, Oct. 1954.

width to height ratios indicate a Reynolds Number effect starting at about $Re = 20$. The data of MacMillan are shown in Fig. 4-7. For a width to internal height ratio of about 4 to 1 as for the present probes, the data show a correction of 2% for a Reynolds Number of 9. This corresponds to a velocity of about 4 ft/second in atmospheric air. No velocities this low were measured during the present experiment.

4.3.1.3.2 The Effect of Transverse Shear and Wall Interference

When a total pressure probe is placed in a flow in which there is a transverse velocity gradient the indication given by the probe is the total pressure not at the geometric center of the probe but at some "effective center", displaced from the geometric center toward the higher velocity because the presence of the probe causes a distortion of the probe streamlines toward the region of lower velocities.

In a boundary layer, wall interference effects further confuse the situation.

Some experimental work has been done on the "displacement" correction applicable to total pressure probes in

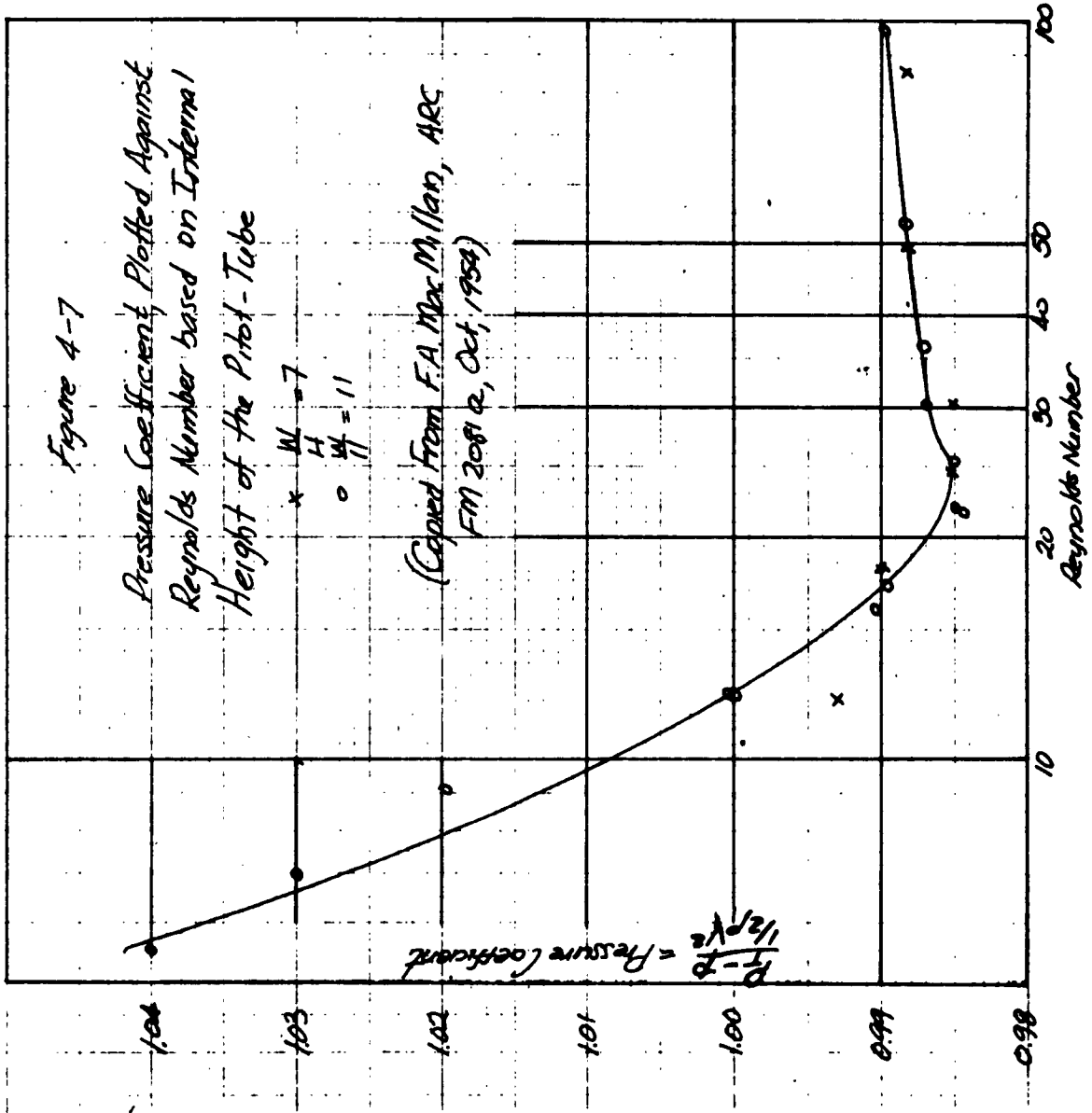
width to height ratios indicate a Reynolds Number effect starting at about $Re = 20$. The data of MacMillan are shown in Fig. 4-7. For a width to internal height ratio of about 4 to 1 as for the present probes, the data show a correction of 2% for a Reynolds Number of 9. This corresponds to a velocity of about 4 ft/second in atmospheric air. No velocities this low were measured during the present experiment.

4.3.1.3.2 The Effect of Transverse Shear and Wall Interference

When a total pressure probe is placed in a flow in which there is a transverse velocity gradient the indication given by the probe is the total pressure not at the geometric center of the probe but at some "effective center", displaced from the geometric center toward the higher velocity because the presence of the probe causes a distortion of the probe streamlines toward the region of lower velocities.

In a boundary layer, wall interference effects further confuse the situation.

Some experimental work has been done on the "displacement" correction applicable to total pressure probes in



turbulent boundary layers.¹

Livesey^{2, 3} has apparently studied the displacement corrections for flat-end pitot tubes in a turbulent boundary layer after it had been thickened by a wire cloth screen.

Livesey states that the displacement correction is a function of the solidity of the cross-section and the aspect ratio of the probe tip. He further comments "So far, work on compressible sub- and supersonic flow has not given any consistent indication of that [displacement] error".

¹ A. D. Young and J. N. Maas, in "The Behaviour of a Pitot Tube in a Transverse Total Pressure Gradient," Aeronautical Research Council, R. and M 1770 1936; I. M. Hall in "The Displacement Effect of a Sphere in Two Dimensional Shear Flow", Journal of Fluid Mechanics, Vol. 1, Part 2, (July, 1956), 142-162, and M. J. Lighthill in "Contributions to the Theory of Pitot-Tube Displacement Effect", Journal of Fluid Mechanics, Vol. 2, Part 5, (July, 1957), pp. 493-512, concerned themselves with the displacement corrections applicable to flow in a wake. The corrections described are not applicable here. This is mentioned because in the literature one finds the Young and Maas experimentally determined displacement correction incorrectly applied to boundary layer total pressure traverses.

² J. L. Livesey, "Design of Total Pressure Probes for Minimum Interference with Measured Flow," J. Aero. Sci., Vol. 21, (Sept., 1954), p. 641.

³ Unpublished work by Livesey is referred to in the work by P. O. A. L. Davies, "The Behaviour of a Pitot Tube in Transverse Shear", Aeronautical Research Council, (December, 1957), F.M. 2619, Fluid Motion Sub-Committee, (December, 1957).

F. A. Macmillan¹ working with round pitots reports displacements of the order of $0.15D$, (where D is the probe height), in a pipe and a boundary layer on a flat plate.

Davies² found experimentally that for a flat-ended round pitot of conventional form no displacement corrections were necessary in a turbulent boundary layer even when the pitot was touching the wall.

Davies also suggests that because of the wire cloth screen Livesey used to thicken his turbulent boundary layer, the conditions Livesey studied were more nearly like those in a wake rather than in a turbulent boundary layer.

Deissler³ made velocity profile measurements in a tube with both round and flattened probe tips in the vicinity of the wall. Because no appreciable difference could be noticed between the measurements made with the two types of tips, he concluded that the aerodynamic and geometric centers of the probe coincided.

¹F. A. Macmillan, "Experiments on Pitot Tubes in Shear Flow", Aeronautical Research Council, R and M 3028, (Feb., 1956).

²Davies, ARC, F.M. 2619, December, 1957.

³R. G. Deissler, "Analytical and Experimental Investigation of Adiabatic Turbulent Flow in Smooth Tubes", NACA, TN 2138, (July, 1950).

The Staff of the Aerodynamics Division, National Physical Laboratory of the Ministry of Aviation¹ in establishing a calibration curve for skin friction determination on a flat plate with a Preston tube (a round pitot attached to the surface) show a curve (their figure 11) for y_e/d vs. Re

(where y_e is the effective center of the pitot and the diameter of the tube). They show that y_e/d , although varying with Reynolds Number, has a value about 0.62, and also that y_e is displaced toward the higher velocities.

Matting, Chapman, Nyholm and Thomas², from measurements of velocity profiles and separate measurements of skin friction on a flat plate at high Mach numbers, report an "increasing discrepancy [with increasing Mach numbers] between the slope deduced from skin-friction measurements and the apparent slope of the measured profiles", and attribute this to a displacement effect caused by the probe. They note that the apparent distortion is of the same order of magnitude as reported by Taylor³ and Von Doenoff⁴.

¹Staff of the Aerodynamics Division, N.P.L., Ministry of Aviation, "On the Measurement of Local Surface Friction on a Flat Plate by Means of Preston Tubes", Aeronautical Research Council, R. and M. No. 3185, May 1958, Published 1961.

²F. W. Matting, D. R. Chapman, J. R. Nyholm and A. G. Thomas, "Turbulent Skin-Friction at High Mach numbers and Reynolds Numbers in Air and Helium", NASA Technical Report R-82, 1961.

³G. I. Taylor, "Measurements with a Half-Pitot Tube", Proc. Roy. Soc. (London), Ser. A, Vol. 166, 1938, pp. 476-481.

⁴A. E. Von Doenhoff, "Investigation of the Boundary Layer About a Symmetrical Airfoil in a Wind Tunnel of Low Turbulence, NACA WR-L-507, 1940.

The velocity profiles for the present experiment also indicate a displacement effect. The method used for correcting the data for this effect is given in Section 6.4.

4.3.1.3.3 The Effects of Turbulent Fluctuations

The lag of the total pressure probe and micromanometer causes the probe to indicate some average value of the total head. The total head includes not only the dynamic head of the mean velocity V_0 but also the effect of the turbulent velocities V_0', V_r', V_z' .

Goldstein¹ for an incompressible fluid, suggests that the turbulent terms included in the reading of the total head probe be

$$P_{Total} = \bar{P}_{static} + \frac{1}{2} \rho \bar{V}^2 + \frac{1}{2} \rho \sqrt{V_x'^2 + V_y'^2 + V_z'^2}$$

Hinze and Van der Hegge Zijnen² as reported by Hinze³ neglected the effects of the lateral turbulence components because of lack of reliable data.

Alexander, Baron, and Comings⁴ observed that the total

¹S. Goldstein, Modern Developments in Fluid Mechanics (1st ed; Oxford at the Clarendon Press, 1938), I, p. 253.

²J. O. Hinze and B. G. Van Der Hegge Zijnen; Applied Science Research, Vol. 1A, p. 435, 1949.

³J. O. Hinze, "Turbulence," (1st ed; McGraw-Hill Book Company, Inc., New York, 1959), pp. 132-137.

⁴L. G. Alexander, T. Baron, and E. W. Comings, University of Illinois Experimental Station, Technical Report No. 8, 1950.

head tube reading decreased with an increase in relative turbulent intensity (contrary to expectations), so that they neglected the effect of turbulence completely and used

$$\bar{P}_{Total} = \bar{P}_{Static} + \frac{1}{2} \rho V^2$$

Hinze¹ states that "Neither of these two methods is entirely correct but...at present no better method can be suggested". In Section 6-2 is presented an analysis which shows that the terms neglected in the equation above for the present case are 1. interaction between molecular and turbulent terms and 2. terms such as $\frac{\rho}{\sigma} \overline{v^2}$ which include second and third order correlation and are much smaller than everywhere in the flow. The equation used as representing the reading of the total head probe is

$$\bar{P}_T = \bar{P} + \frac{1}{2} \bar{\rho} V_0^2$$

4.3.2 Static Pressure Measurement

For the purpose of determining the axial static pressure distribution at the stator wall, seven 0.010 inches static pressure taps were provided as described in Section 3.3.1.

4.3.2.1 Errors in Indication Caused by Pressure of Tap

The stainless steel tubing from which these taps

¹ J. O. Hinze, Turbulence, p. 136.

were made were countersunk 0.005 inches to eliminate the effects of disturbances to the static pressure at the stator wall caused by the presence of the tap, whereby the flow streamlines tend to dip into the tap hole.

Experiments conducted by R. E. Rayle^{1,2} show that a tap diameter 0.010 inches to 0.040 inches countersunk to a depth of 1/2 the diameter will substantially eliminate tap errors.

4.3.3 Micromanometer for the Indication of Total and Static Pressures.

The measurements of static and total pressures to within 0.001 inches of water were made with a micromanometer from a design by A. M. O. Smith and James S. Murphy³. The pressure to be determined is led through Tygon Tubing to an inclined sight tube which forms one leg of a U-tube manometer. The other leg is brought to a reservoir which is mounted on the arm of a Vernier height gage.

¹R. E. Rayle, "An Investigation of the Influence of Orifice Geometry on Static Pressure Measurements", MIT, SM Thesis, Dep't. of Mech. Eng'g., (1949).

²R. C. Dean, Jr., Aerodynamic Measurements (Boston; Eagle Enterprises, 1953), p. 60.

³A. M. O. Smith, and J. S. Murphy, "Micromanometer for Measuring Boundary Layer Profiles", Rev. Sci. Inst's., Vol. 26, Number 8 (Aug., 1955).

During operation, the reservoir is moved up or down so that the meniscus in the sight tube is brought to its zero position. This zero position is determined with a 40 power microscope fitted with a reticule. The inclined tube allows the vertical height of the meniscus to be determined with the microscope to well within 0.001 inches of fluid. The base of the instrument is fitted with levelling bubbles and levelling screws, and the reservoir is placed as close to the sight tube as possible. Thus, two important sources of error in U-tube manometers are eliminated; that caused by inaccuracy in the determination of the meniscus level and that resulting from tilt between the legs of the manometer.

Experiments by Smith and Murphy to determine a proper manometer fluid with regard to a) adhesion of the manometer fluid to the walls of the tube, b) low volatility and c) stable density, i.e., minimum tendency to absorb moisture from the air, resulted in a choice of DC-200 (DCS)¹ a silicone fluid manufactured by the Dow-Corning Corporation.

MacMillan² has suggested that to minimize manometer zero shift caused by ambient temperature change the expansion of the reservoir and manometer fluid be balanced against the change in the meniscus position caused by change in surface tension.

¹Dow-Corning DC200(DCS); density 0.818 gms/cm³, boiling point 152 deg. C, surface tension 17.0 dynes/cm and viscosity 0.818 centipoises.

²F. A. MacMillan, Liquid Manometers with High Sensitivity and Small Time Lag", J. Sci. Instr., V. 31, 1954, p. 17.

This was accomplished by Smith and Murphy by proper design of the component tubing and reservoir.

Smith and Murphy found that the micromanometer had an accuracy of 0.0002 inches due to random adherence of fluid to the tubing walls. However, the accuracy of the present manometer is 0.001 inches, the accuracy of the vernier height gage used to position the reservoir.

4.4 Temperature Distribution in the Gap Between the Two Cylinders

4.4.1 Introduction

The temperature distribution in the gap between the cylinders was determined from the density distribution as measured with a Mach Zehnder Interferometer.

An interferometer was chosen for this purpose because as an optical method it has several advantages over mechanical means such as a thermocouple probe.

The advantages of an interferometer are as follows:

- a) its use does not disturb stream conditions of temperature and flow, as would the use of a probe
- b) its use permits the entire flow field to be studied from a single interferogram.

It should be noted that in addition, a probe would have been difficult to calibrate because of radiation effects at the higher temperatures.

The disadvantages of the interferometer are that it is costly, difficult to build, adjust and align. Also, its use in the present experiment introduced a small error due to quartz-window heating effects.

The theory and application of the Mach-Zehnder Interferometer has been extensively covered in the literature^{1,2,3}. In Appendix I is given a brief description of the fundamentals of its operation and adjustment.

4.4.2 The Design of the Mechanical Parts

The principle mechanical components of the Mach-Zehnder Interferometer under discussion are

1. The base on which the mirror holders are mounted
2. The mirror holders
3. The holders
4. The light source, collimating lens, and camera.

¹See for example the extensive bibliographies in Ladenburg, et al, pp. 75-78 and Dean, pp. 270-271.

²L. H. Tanner, "The Optics of a Mach-Zehnder Interferometer", Aeronautical Research Council, R and M 3069, Oct. 1956.

³L. H. Tanner, "The Design and Use of Interferometers in Aerodynamics", Aeronautical Research Council, R and M No. 3131, Sept. 1957.

A photograph of the entire assembly is shown in Fig. 4-8.

4.4.2.1 The Base

A photograph of the base plate on which the mirrors are mounted is shown in Fig. 4-9.

The base consists of a 1/2 inch thick steel plate approximately 30 inches square to the back of which have been welded I-beam sections in a U-arrangement as shown.

Four blocks of steel 1 inch by 6 inches by 4 inches, their centers at the corners of a rectangle 20 inches by 10 inches, and oriented at 45 degrees to the legs of the rectangle were welded to the 1/2 inch thick steel plate and machined flat on a jig-borer. The interferometer mirror holders were bolted onto these blocks. No stress relief was provided other than that of allowing the base to stand at room temperature for about a month.

The rigidity of the base so designed has proved satisfactory. Indeed, the only precaution needed against distortion of the base is that it not be subjected to temperature gradients.¹

The base is bolted at three points to a triangular plate, and this plate is hung at its corners through vibration

¹Dean, p. 198 reports that for a similar interferometer at M.I.T. a temperature variation of 0.1 deg. F in one arm of the base displaces the bands about one band space, but observes that the principle precaution required is not to allow the base to be subject to direct sunlight.

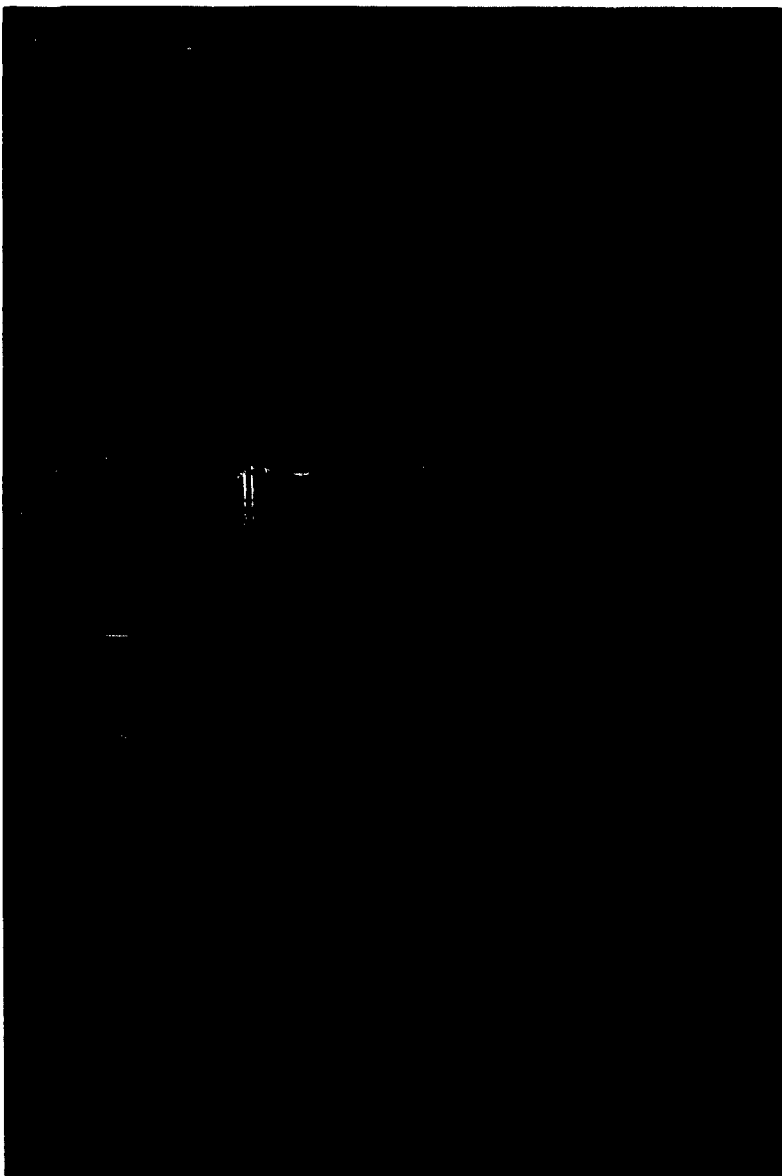


Figure 4-8
Interferometer Assembly

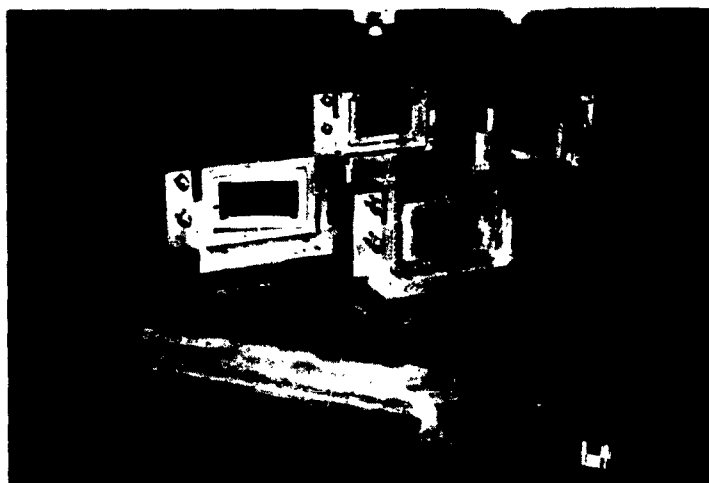


Figure 4-9
Interferometer Base-Plate
and
Mirror Holders

isolators from a frame made of 2 inch pipe. This frame has been sufficient to prevent major disturbances to the mirrors and plates once they have been adjusted to produce fringes. The pipe frame is mounted on wheels.

The arrangement described has been satisfactory since from day to day and month to month, only minor adjustments to fringe spacing are necessary. Indeed, the fringes have disappeared but once accidentally, when a mirror holder inadvertently was given a direct, sharp blow.

4.4.2.2 The Mirror Holders

The mirrors must be mounted so that they are free to rotate in any plane and also so that they are stress free. A gimbal-type mounting is provided to meet the first condition. Such a mounting is shown in Fig. 4-10. The inner mount, in which lies the 2 inch by 4 inch mirror is made 3 or 4 thousandths of an inch larger on a side than the mirror. Scotch drafting tape is used as a gasketing material between the mirror and the frame. Scotch drafting tape is ideal for this application since its wrinkled surface allows for expansion and contraction of the mirror under diurnal temperature change and yet provides sufficient drag so that the mirrors do not shift about.

On each side of the mirror is placed a rectangular metal frame which fits over the mirror holder and is attached thereto with screws. Each metal frame has three protrusions

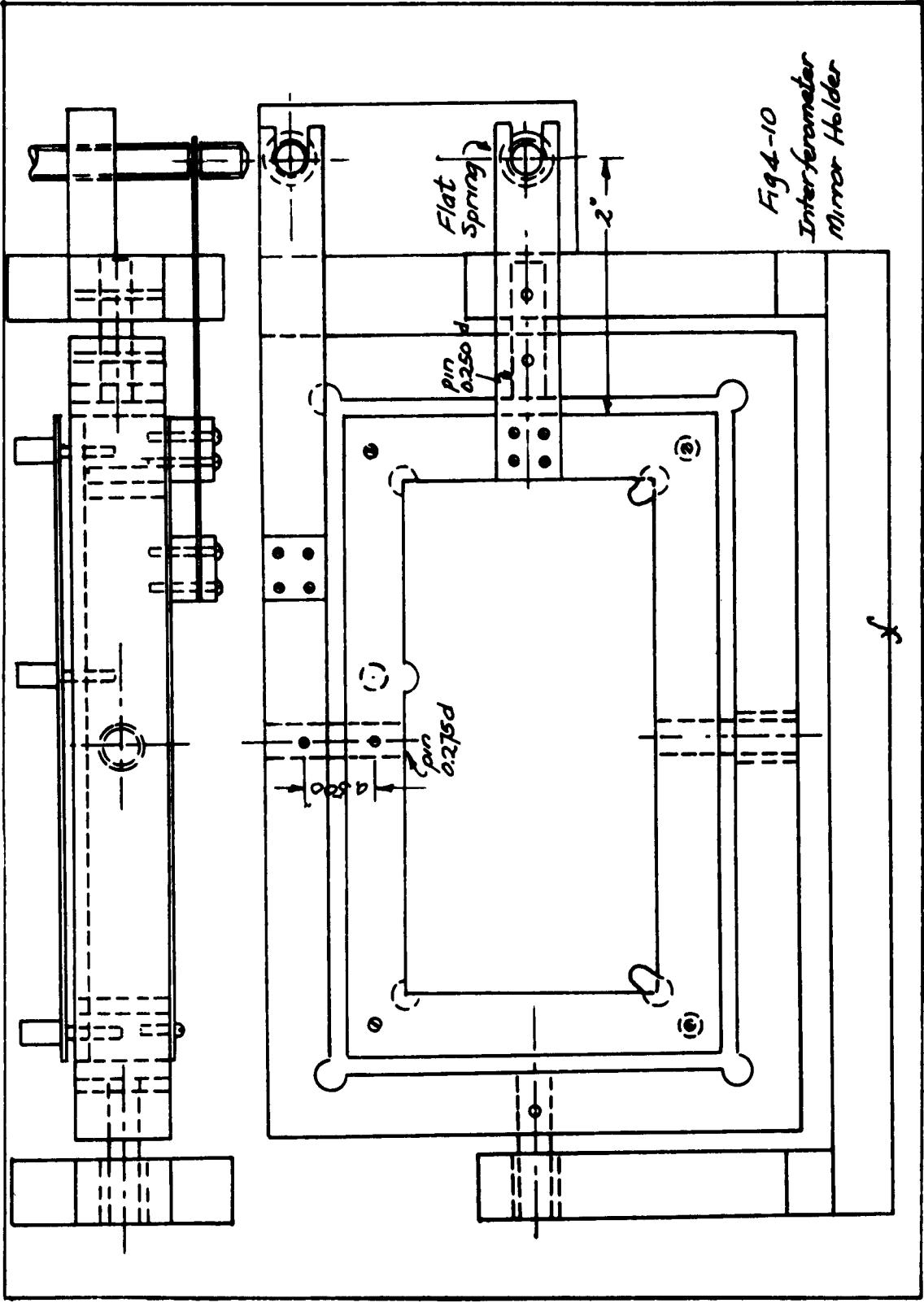


Fig 4-10
Interferometer
Mirror Holder

f

which extend over the mirror and serve as supports. Turning the screws by which the frame is attached to the mirror holder also allows rough positioning of the mirrors as needed during adjustment.¹ The small rotations required are accomplished on the present apparatus by having a flat spring attached to the frame loaded by a screw of small lead (0.025 inches per revolution). This load creates a moment which tends to twist the pieces on which the frame is supported. The system is so designed that one revolution of the screw rotates the frame 30×10^{-6} radians. Minute motions are provided very simply, as contrasted with complicated gear trains.

4.4.2.3 Mirrors

The plates and mirrors used are made from selected optical quality plate glass and were purchased from The Laboratory Optical Company, Plainfield, New Jersey. They are 2 inches by 4 inches by $3/4$ inches thick and are flat to within 0.1 wavelength of mercury green light.²

4.4.2.4 The Light Source, Collimating Lens, and Camera

The light source used is a General Electric B-H6

¹If the spacing between the fringes is to be one millimeter, so that they can be seen with the naked eye, and if mercury green light is used then the angle of rotation of a mirror to produce the fringes is

$$\frac{\delta}{2d} = \frac{5461 \times 10^{-8}}{2 \times 10^{-1}} = 2730.5 \times 10^{-7} \text{ radians}$$

²Verbal communication, from Mr. S. Brower, Laboratory Optical Company.

air-cooled Mercury vapor lamp in continuous operation or flashed, as needed. The rating of this lamp is as follows: Watts, 900; Lumens, 60,000; starting voltage (AC), 1200; Operating voltage, 900; starting amperes, 2.6; operating amperes, 1.25.

The percentage of the total energy output of the lamp in the wavelength range 5388-5536 Å is 16.8. The principle line in this region is 5461 Å.

A short distance from the lamp was mounted a piece of brass shimstock 0.0003 inches thick in which was drilled a hole 0.004 inches in diameter. This hole was placed at the focal point of an f/2.5 Aero Ektar lens, and thus served as the point source.

Between the source and the lens was placed a multi-layer interference filter¹ which passed the mercury green line, 5461Å, with approximately 70% transmission and half-band width of approximately 70 Å.

With this arrangement of light source, operating continuously, 0.004 inch hole filter, and collimating lens, 1/20 second exposure time was required to expose a 103 G Eastman-Kodak spectroscopic plate with 1/2 magnification of the test section.

For flashing operation of the lamp, a 2 microfarad

¹Manufactured by Baird Associates - Atomic Instrument Company, 33 University Road, Cambridge 38, Massachusetts. See Technical Circular RD 503.

capacitor at 3000 volts was discharged through the lamp. A circuit diagram of the arrangement is shown in Fig. 4-11. One flash of unfiltered light was sufficient to expose an Eastman-Kodak Super-Ortho press photographic plate, when an opening of 0.010 inches was used as the point source. For filtered light four flashes of the lamp were required to expose a similar plate.

To photograph the interference bands, another Aero-Ektar, $f/2.5$, 7 inch lens was mounted on a 4 inch x 5 inch Speed Graphic camera box.

4.4.3 Corrections Required

4.4.3.1 The Refraction Error

Because a density gradient exists in the gap a light ray passing axially through the gap is refracted away from the heated rotor.

On the photographic plate a refracted ray appears to originate at the same position in the gap as an unrefracted ray which would have struck the photographic plate at the same point.

There is, therefore, an error in fringe shift as read on the photographic plate occasioned by the difference in optical path lengths between the refracted ray and the unrefracted ray.

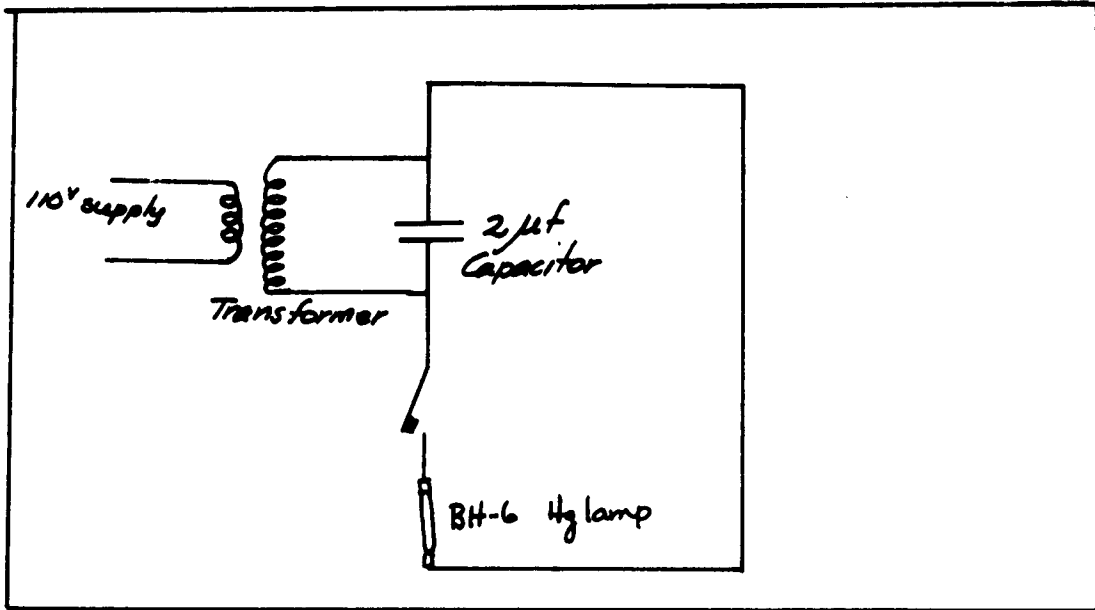


Figure 4-11
Electrical Circuit for Single Flash operation
of BH-6 Mercury Lamp

Wachtell^{1,2} has shown that to a first approximation the error vanishes if the camera is focused at a plane located at an axial distance $x/L = 1/3$, measured from the exit window; that is the window nearest the camera. Further, the error in using the first approximation was found to be less than 5 per cent of the density difference between the wall and free stream conditions for a boundary layer on a flat plate if

$$C = \frac{L}{\delta} \sqrt{K(\rho_e - \rho_w)} < 0.9, \text{ for a turbulent}$$

boundary layer.

In this equation L = span of the tunnel,

δ = boundary layer thickness

$(\rho_e - \rho_w)$ = density difference between
the free stream and the wall.

For the most severe situation in the present study, 7000 rpm, $T_{\text{rotor}} = 890$ F, conservatively estimating δ to be

¹R. Ladenburg, and D. Bershader, "Optical Studies of Boundary Layer Phenomena on a Flat Plate at Mach Number 2.35," Final Technical Report for Contracts NRO61 and N6ori-105 Task II, Palmer Physical Laboratory, Princeton, New Jersey, Dec. 15, 1952. See Chapter VIII, The Refraction Error by G. P. Wachtell.

²G. P. Wachtell, "Refraction Error in Interferometry of Boundary Layer in Supersonic Flow Along a Flat Plate", Ph.D. Dissertation Princeton University, 1951.

0.040 inches, $\rho_B = 0.0547$, $\rho_W = 0.0446$ and $K = 0.3635 \times 10^{-2}$.

Thus

$$C = \frac{L}{8} \sqrt{K(\rho_B - \rho_W)} = \frac{4.5}{0.040} \sqrt{0.3635 \times 10^{-2} (0.0547 - 0.0446)}$$

$$= 0.68 < 0.9$$

and the criterion is satisfied. In fact, the error decreases as C^4 so that the error here is negligible.

The camera was therefore focused in the plane $x/L = 1/3$ during the present experiments.

Another approach to the refraction error problem is given by DeFrate¹ and is useful when the criterion of Wachtell is not satisfied.

DeFrate suggests an iteration procedure as follows:

A density distribution is measured from the interferometric plate. Rays are traced through this density distribution. Noting the angle at which they leave the test section, one can calculate the y-position in the gap from which they appear to come to the photographic plate. Further, for each ray the change in optical path length from a no-flow condition can be calculated. For each ray one obtains a density and a y-position.

¹L. A. DeFrate, "Application of the Interferometer to the Study of Boundary Layers, Sc.D. Dissertation, M.I.T., 1950.

By tracing rays a density distribution can be obtained. This is compared with the measured distribution. If no agreement is obtained, rays are traced through the calculated density distribution and the process repeated until agreement is achieved between the assumed density distribution and the one calculated from ray tracing.

4.4.3.2 The Error Due to Temperature Gradient in the Quartz Windows

Consider, in Fig. 4-12, a drawing of one of the quartz windows over the ends of the gap. These windows provide a path for the interferometric test beam.

During the experiment the window experiences a temperature gradient since one end "sees" the ends of the hot rotor, and the other is in contact with the cooling water jacket. The quartz window undergoes a varying change in thickness across the light path as well as a change in its index of refraction. Thus, the optical path through a region in the quartz in the center of the gap differs from that through a region near the walls and an error in indicated density results. The error can be evaluated as follows: Consider the quartz window shown in Fig. 4-12. Under a temperature gradient expansion occurs as shown in the figure.

The optical path length at (1) in the cold condition is

$$OPL_{1,c} = t_{1,c} n_{1,c}$$

and in the hot condition

$$\text{where } OPL_{1,H} = t_{1,H} n_{1,H} = t_{1,c} (1 + \alpha_g \Delta T_1) (n_{1,c}) \left(1 + \frac{dn}{dT} \Delta T_1\right)$$

$$\Delta T_1 = T_{1,H} - T_{1,c}$$

At (2), the same can be written as

$$OPL_{2,c} = t_{2,c} n_{2,c}$$

and

$$OPL_{2,H} = t_{2,H} n_{2,H} = t_{2,c} (1 + \alpha_g \Delta T_2) (n_{2,c}) \left(1 + \frac{dn}{dT} \Delta T_2\right)$$

The difference in optical path lengths between the locations (1) and (2) in the hot condition, the optical path length of interest is ΔOPL .

$$\Delta OPL = t_{2,c} (1 + \alpha_g \Delta T_2) (n_{2,c}) \left(1 + \frac{dn}{dT} \Delta T_2\right) - t_{1,c} (1 + \alpha_g \Delta T_1) (n_{1,c}) \left(1 + \frac{dn}{dT} \Delta T_1\right)$$

Since

$$t_{1,c} = t_{2,c}$$

and

$$n_{2,c} = n_{1,c}$$

$$\Delta OPL = t_c n_c [T_{2,H} - T_{1,H}] \left[\alpha_g + \frac{dn}{dT} + \alpha_g \frac{dn}{dT} (\Delta T_2 - \Delta T_1) \right]$$

For the values

$$\alpha_g = 0.32 \frac{\text{inches}}{\text{inch-deg F}} \times 10^{-6}$$

$$\frac{dn}{dT} = 6.272 \text{ per deg F} \times 10^{-6}$$

$$t_{2,c} = 0.125 \text{ inches}$$

$$n_c = 1.46019 \text{ at } 75 \text{ deg F.}$$

$$\Delta OPL = 0.125 (1.46019) (T_{2,H} - T_{1,H}) \left\{ (0.32 + 6.272) 10^{-6} + 2.007 (\Delta T_1 - \Delta T_2) 10^{-12} \right\}$$

The term $2.007 \times 10^{-12} (\Delta T_1 - \Delta T_2)$ is negligible.

The result is

$$\Delta OPL = 1.203 \times 10^{-6} (T_{2,H} - T_{2,c})$$

Since $\lambda = 5460 \text{ \AA} = 21.496 \times 10^{-6} \text{ inches,}$

$$\epsilon / \text{degree temperature difference} = 0.055964$$

If the temperature difference between points (1) and (2) in the hot condition is known, the error in fringe shift as measured on an interferogram is known, and can be corrected.

In Appendix II is outlined the test procedure used to determine the temperature gradient in the glass. Tempilaq

¹
International Critical Tables (first ed., McGraw-Hill Book Company, New York, 1929) Vol. IV, p. 21, Vol. VI, p. 341, p. 342.

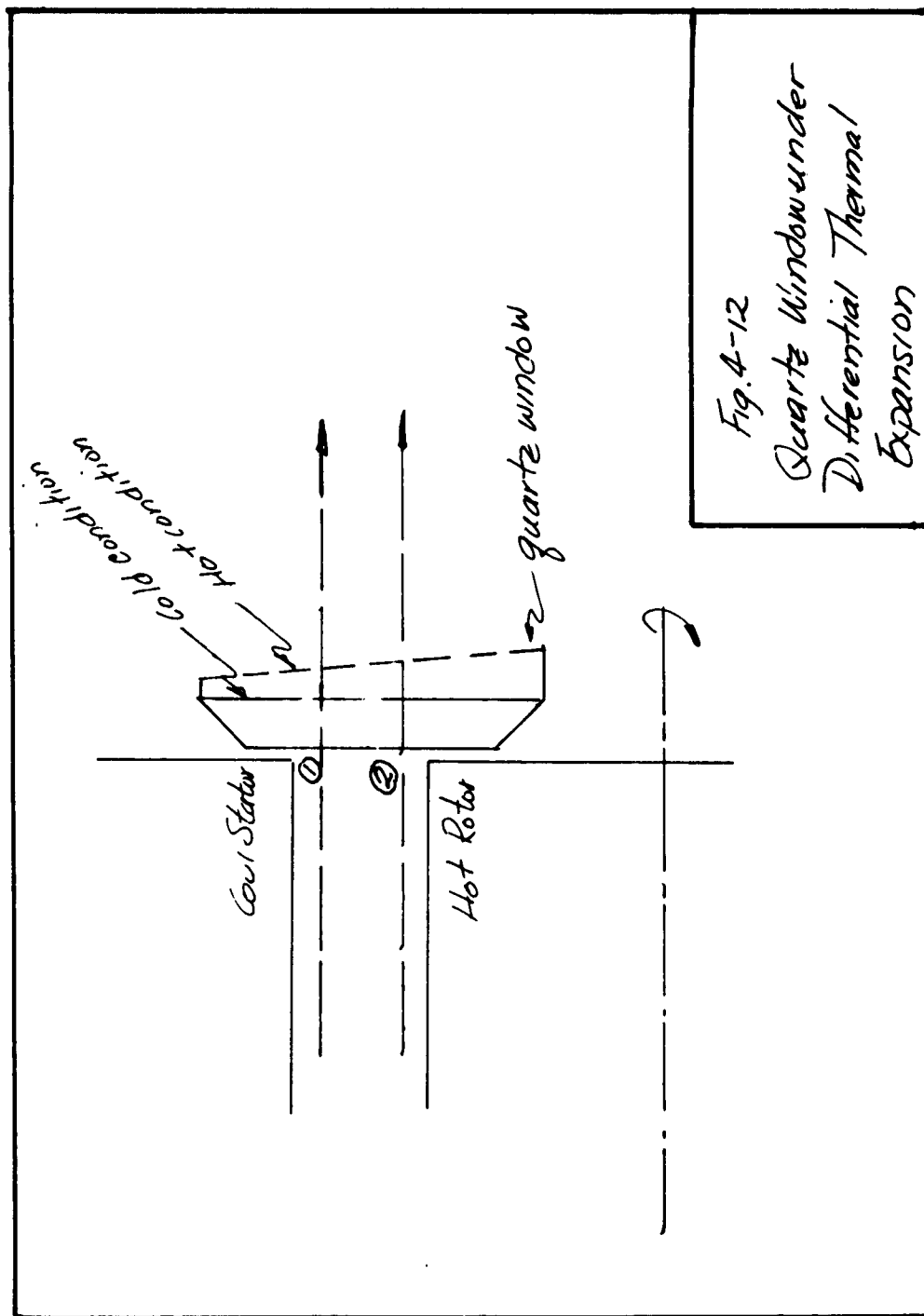


Fig. 4-12
Quartz Window under
Differential Thermal
Expansion

was used to determine the isotherms on the glass. The experiments showed the isotherms to be approximately concentric circles except for the corners of the glass.

The final corrections applied (see Section 6.3.1.2.1) are small over small distances from the rotor (the region of most interest) but are applied in the interest of consistency of the data obtained from the interferometer and the rotor and stator thermocouples.

4.5 The Use of the Hot-Wire Anemometer

A hot-wire anemometer purchased from the Flow Corporation of Cambridge, Massachusetts was used to study the turbulence characteristics of the flow.

A probe consisting of only one wire was placed in the stream so as to measure the θ or r-component of the turbulent fluctuations.

Operation and use of the hot-wire anemometer is described in detail elsewhere^{1,2} and specifically in the literature distributed by the Flow Corporation.

¹ R. W. Ladenburg, B. Lewis, R. N. Pease, and H. S. Taylor, Physical Measurements in Gas Dynamics and Combustion, (1st ed; Princeton University Press, Princeton, 1954), Article F, 2 by L. S. G. Kovasznay, pp. 219-276.

² See also the bibliography on pp. 283-285 in the same book.

Chapter V

Experimental Procedures

5.1 Introduction

The apparatus was operated at 3000, 5000 and 7000 rpm, with rotor temperatures of about 540 R, 600 R, 720 R, and 890 R. These conditions correspond to Taylor numbers of from 2500 to 9000, and temperature differences of 0 F to 330 F. This represents an extension in Taylor number and temperature difference over previous investigators. See Table I-1.

The experimental procedures followed are given below.

5.2 Overall Heat Transfer

For the measurement of overall heat transfer, the data required are rpm, rotor temperature, stator temperature, cooling water flow rate, and temperature rise of the cooling water.

After the start of rotation and the application of heater current, equilibrium conditions were reached in about one hour at lower temperatures and two hours at higher temperatures.

Equilibrium conditions were assumed to be established when three successive measurements of rotor temperature taken five minutes apart were within 1 deg F.

The cooling water flow rate and temperature rise were measured.

Cooling water flow rates were in the neighborhood of 50 lbs. per hour. The difference in temperature of the cooling water ranged from 5 to 10 deg F. depending on the heat input. Water flow from the apparatus was weighed for a period of about twenty minutes. During this time the temperature difference between the cooling water entering and leaving was measured every two minutes. In the intervals, water flow rate as indicated by a rotameter, heater power and rpm were checked for constancy. At the end of the water measurement period rotor and stator temperatures were again measured.

5.3 Measurement of Total Pressure Distribution

For the runs during which total pressure distribution in the gap was measured, the procedure was as for the overall heat-transfer runs. When equilibrium conditions were reached and the rotor temperature determined, the graph of Fig. 4-6 was used to establish the radial position of the probe. The stator diameter was assumed not to vary.

During the early velocity distribution runs, at 5000 and especially 3000 rpm, it was noticed that there could exist two axial pressure distributions, one uniform to within 2-1/2%, the other saw-toothed, much as those reported by Pai.¹

¹ Pai, Shih-I, NACA TN 892.

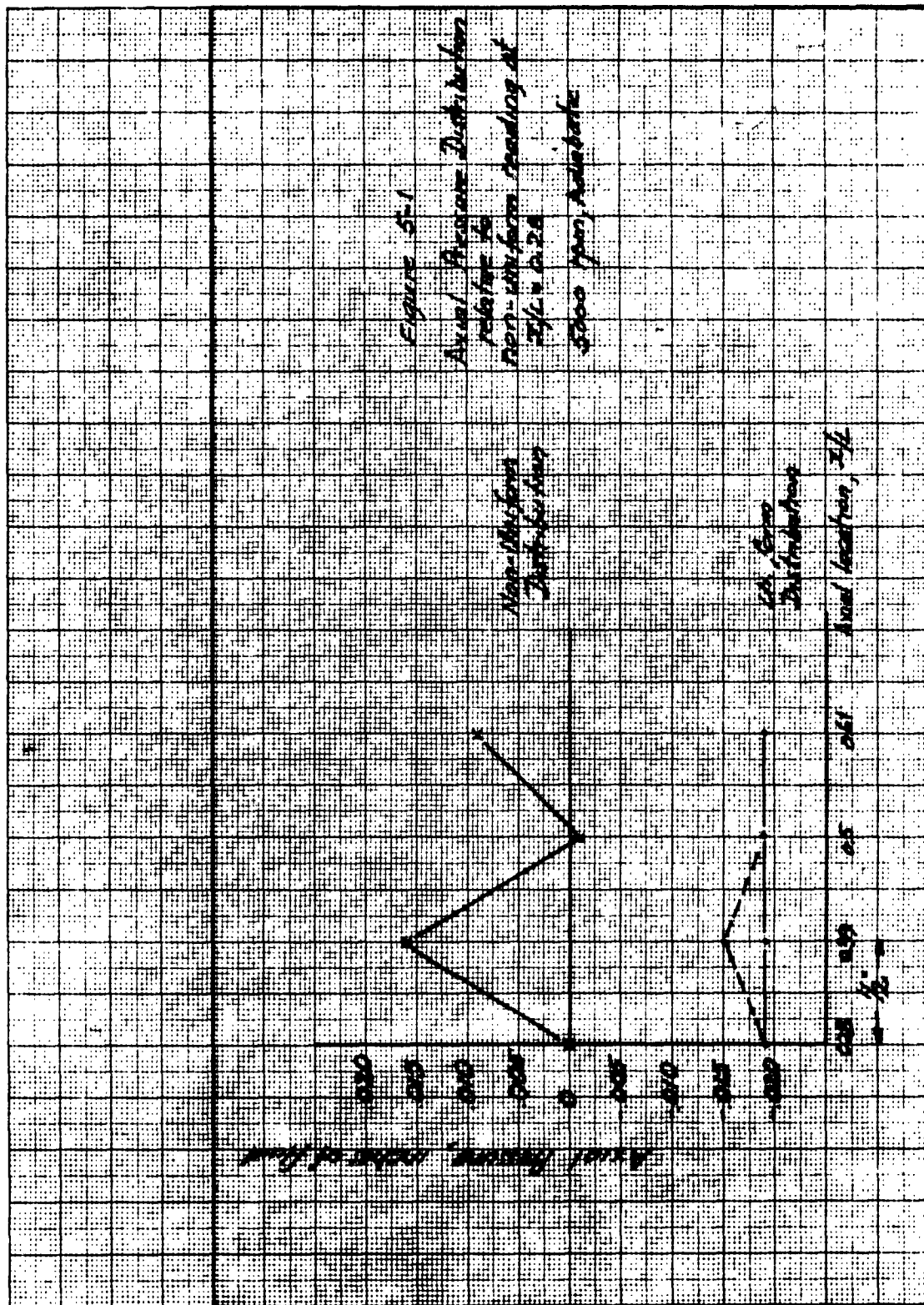
A typical distribution is shown in Fig. 5-1. Tests were made with a hot-wire anemometer to determine the characteristics of the flow. It was found that there could exist two types of flow at the same speed; one a vortical flow of the type reported by Pai, the other a random turbulent flow. These results are discussed in Chapter VIII.

The uniform axial pressure distribution was related to the conventional random, turbulent flow and the non-uniform axial pressure distribution to a flow in which Taylor vortices as discussed by Pai predominated.

At 5000 rpm it was found that if the probes were placed near the rotor surface at startup, generally a uniform axial pressure distribution would result. However, at times the flow would "flip" from the uniform to the non-uniform type during a run, in which case mechanical disturbances to the flow such as moving the probes down to the rotor and then to the stator would cause a return to the uniform type of flow. These experiences coincide with those reported by Pai.

At 3000 rpm, simple manipulation of the probes usually did not flip the flow from the non-uniform to the uniform type.

A more effective method was a sudden increase in rotor speed to about 8000 rpm, followed by a gradual reduction. This did not succeed at all times. In general, obtaining and maintaining a uniform axial pressure distribution was difficult at 3000 rpm.



At 7000 rpm, the non-uniform type of distribution was never encountered.

There was a possibility of a change in flow during a run, which could go undetected, especially while the probes were in the middle of the gap, where the total heads for the two types of flow were almost equal. Therefore, it was necessary to measure an axial pressure, move the probe to a new location, remeasure the axial pressure, measure the total pressure, re-measure the axial pressure and then move the probe. This was especially necessary at 3000 rpm, where velocities, axial pressures and total heads were low. At 5000 rpm, two or three total head readings were taken between axial pressure checks when the probes were in the center of the gap. Closer checks were made when the probes were near either wall.

The time constant of the probe and manometer was of the order of eight minutes, and of the axial pressure tubing and manometer of the order of five minutes. The method used for measurement was to bracket the reading to ± 0.004 inches and then setting the well to the mean value.

If there was no meniscus motion for 3 to 4 minutes the reading was accepted. If there was motion up or down, the well was set at the new mean value and the procedure repeated.

The average time for one reading was about twelve minutes, including the static pressure checks.

At 5000 rpm the average time for a run including

start up, was about eight hours. At 3000 rpm the average time was about 12 hours, because of the difficulties of maintaining a uniform flow.

5.4 Determination of Density Distribution with a Mach-Zehnder Interferometer

5.4.1 Alignment of the Interferometer with the Test Piece

The method for obtaining fringes in the Interferometer is given in Appendix I. Before use further alignment is required to make the test beam of the interferometer parallel to the rotor surface. Methods of making this alignment are given by DeFrate,¹ Wachtell² and Howes and Buchele.³

DeFrate and Wachtell suggest using the diffraction pattern caused by the edges of the test piece. Symmetry of the diffraction pattern indicates that the test beam is parallel to the rotor surface. Howes and Buchele suggest using a form of interference, similar to Lloyds mirror interference,⁴ which

¹L. A. DeFrate, "Application of the Interferometer to the Study of Boundary Layers," Sc.D. Dissertation, M.I.T., 1950.

²G. P. Wachtell, "Refraction Error in Interferometry of Boundary Layer in Supersonic Flow Along a Flat Plate," Ph.D. Dissertation, Princeton University, 1951.

³W. L. Howes, and D. R. Buchele, "Practical Considerations in Specific Applications of Gas Flow Interferometry," NACA TN 3507, July, 1955.

⁴F. A. Jenkins and H. E. White, Fundamentals of Optics (2nd ed; McGraw-Hill Book Company, Inc., 1950), pp. 238-239.

occurs between the feference and the reflection of the test beam from the mis-aligned surface. The results of this interference are fringes inclined to the main Mach-Zehnder fringes and superimposed on them at the surface. When the surface is aligned to the test beam this interference disappears.

The method of symmetry of the diffraction pattern was used here with an a posteriori check using the methods suggested by Howes and Buchele. The method was applied as follows:

To align the test section initially to a better approximation than obtained by eye, a frosted 100 watt, incandescent bulb was placed at the end of the test section away from the camera, so that its rays could pass through the test section. Thus, there appeared on the ground glass screen of the camera a black and white image of the gap as delineated by the rotor and stator surfaces. The camera lens was focused on the edge of the rotor nearest to it. Then, only the test beam of the mercury vapor lamp (with filter) was allowed to pass through the test section. This formed a green image on the ground glass screen. When the white image and green image were made to coincide by moving the test section, alignment was near. The test section was mounted on screw-jacks for this purpose.

The camera and the white light were then removed. The diffraction pattern around the gap was inspected with a

telescope set so that the edge of the rotor was out of focus. Adjustment was facilitated by the fact that the number of lines in the diffraction pattern changed rapidly with small motions of the test piece. When the diffraction pattern observed was uniform over the rotor and stator (five or six lines were observable) the test section was aligned.

The use of the 100 watt light bulb for the initial positioning facilitated alignment especially so far as yaw of the test piece was concerned.

A further check on the alignment was made after each run from the "no-flow" interferograms. In these, the "picket-fence" effect mentioned by Howes and Buchele,¹ and typifying alignment of the test section were clearly in evidence.

5.4.2 Obtaining "Flow" and "No-Flow" Photographs

After alignment of the test piece the conventional Mach-Zehnder interference pattern was adjusted for fringe spacing and orientation; further, with the filter removed, the zeroth order interference fringe was centrally located in the gap by moving the translation mount.

¹W. L. Howes and D. R. Buchele, NACA TN 3507, p. 45. Since the light source is always of finite size, not a geometric point, non-parallel rays do enter the test section and cause interference as described above. The "picket-fence" effect is caused by the combination of two opposed patterns of diagonal fringes, and is shown in Howes and Buchele's Fig. 6. A "No-Flow" plate from the present study is shown in Fig. 5-2.

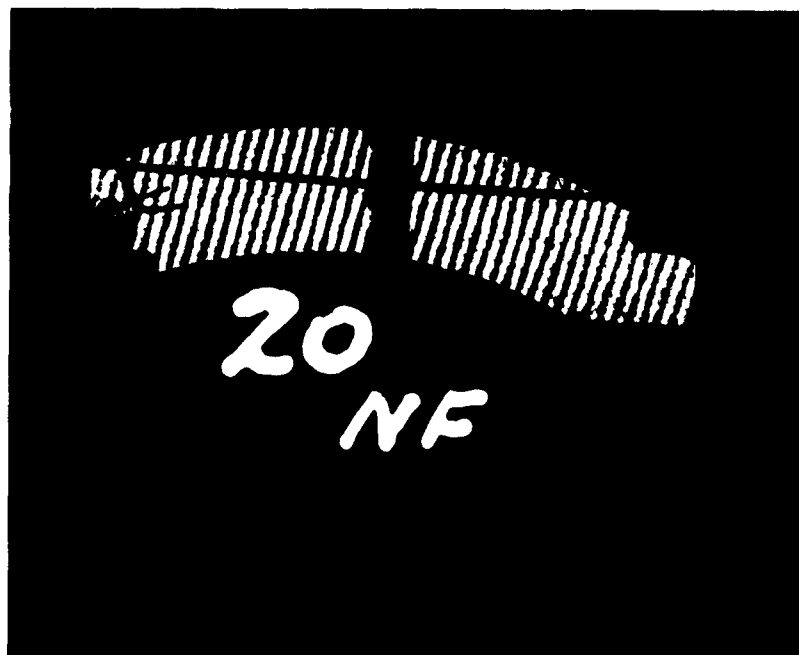


Figure 5-2

NO Flow Interferogram showing "Picket Fence" effect
and Diffraction Pattern

The interferometer was now ready for use.

The procedure followed was:

1. The camera was focused at an axial distance $x/L = 1/3$ as recommended by Wachtell.^{1,2}
2. A "no-flow" photograph was taken.
3. The equipment was started up, and equilibrium achieved.
4. A "flow" photograph was taken.

For the runs with rotor temperatures up to and including 700R, the "flow" and "no-flow" photographs were taken on separate plates with the filter in place. For the runs at rotor temperatures of 900R both were taken on the same plate, without the filter. The filter was removed because a single high intensity flash from the B-H6 lamp when it was operated by capacitor discharge, as it was for these runs, was not sufficient to expose a plate using green light.

Since only a few interference bands resulted because of the removal of the filter, and since the bands were translated as well as distorted by the density, the "no-flow" and "flow" fringes did not overlap and evaluation was possible.

¹G. P. Wachtell, "Refraction Error in Interferometry of Boundary Layer in Supersonic Flow," Ph.D. Dissertation, Princeton University, 1951.

²See Section 4.4.3.1.

The photographic plates so exposed were, after development, ready for evaluation.

5.5 Use of The Hot-Wire Anemometer

The hot-wire anemometer described in Chapter IV was used to show that two different types of flow can exist in the annulus. This was accomplished both with measurements of $\sqrt{V_o'^2}$ and $\sqrt{V_r'^2}$, and with photographs of oscilloscope traces of the signals from the hot-wire. During these runs, axial traverses were made with a single probe in the center of the gap at several different rpm and only under adiabatic conditions.

Chapter VI

Processing the Data

In this chapter are presented the methods used to process the experimental data.

6.1 Overall Heat Transfer

The overall heat transfer coefficient h is defined as

$$h = \frac{Q_c}{A_{rotor} (T_{rotor} - T_{stator})} \quad (6-1)$$

where $h = \text{Btu/hr-Ft}^2\text{-deg F}$

$A = \text{Area, ft}^2$

$T = \text{Temperature deg F}$

$Q_c = \text{Btu/hr. transferred from rotor to stator by convection}$

6.1.1 The Determination of Q_c

The rate of heat addition to the cooling water, Q Btu/hr, includes radiation transfer between the rotor and stator as well as convective heat transfer, as follows

$$Q = Q_c + Q_{\text{radiation}}$$

Q was determined from cooling water flow rate and temperature increase.

The cooling water flow rate was measured by weighing the water passing through the cooling jacket over a time interval.

The cooling water temperature difference was obtained from iron-constantan thermocouples placed as described in Section 3-6, so that the difference in millivolts was indicated directly.

As the cooling water temperature averaged 80 deg F, a value 0.0288 millivolts/degree was used to determine the temperature difference. The readings of Δt cooling water were taken at two minute intervals for approximately twenty minutes. The Δt used for computing Q was the time average of these 10 odd readings.

Thus

$$Q = [(lbs/hr)(\Delta t)]_{\text{cooling water}} \quad (6-2)$$

Q_{radiation} was determined from Stefan-Boltzmann's Law which for an annulus is

$$\frac{Q_{\text{radiation}}}{A_{\text{rotor}}} = \frac{0.172 \left[\left(\frac{T_{\text{rotor}}}{100} \right)^4 - \left(\frac{T_{\text{stator}}}{100} \right)^4 \right]}{\frac{1}{\epsilon_{\text{rotor}}} + \frac{\epsilon_{\text{rotor}}}{\epsilon_{\text{stator}}} \left[\frac{1}{\epsilon_{\text{stator}}} - 1 \right]}$$

Using a value of emissivity²

$$\epsilon_{\text{rotor}} = \epsilon_{\text{stator}} = 0.36$$

Q_{radiation} for the present apparatus becomes

$$Q_{\text{radiation}} = 0.013 \left[\left(\frac{T_{\text{rotor}}}{100} \right)^4 - \left(\frac{T_{\text{stator}}}{100} \right)^4 \right]$$

¹W. H. McAdams, Heat Transmission, (2nd ed; McGraw-Hill Book Company, Inc., New York, 1942), Table XIII, p. 59.

²Ibid, eq. (14), p. 394

Therefore $Q_{\text{convection}}$ can be determined.

6.1.2 The Determination of A_{rotor}

From the cylinder dimensions

$$L = 4.5 \text{ inches}$$

$$d_{\text{rotor}} = 3.320 \text{ inches to } 3.332$$

range caused by thermal expansion at the higher temperatures

$$\begin{aligned} A_{\text{rotor}} &= \frac{\pi(3.320)(4.5)}{144} \text{ to } \frac{\pi(3.332)(4.5)}{144} \\ &= 0.326 \text{ ft}^2 \text{ to } 0.327 \text{ ft}^2 \end{aligned}$$

The value used was

$$A_{\text{rotor}} = 0.326 \text{ ft}^2$$

6.1.3 The Determination of $(T_{\text{rotor}} - T_{\text{stator}})$

T_{rotor} was taken as the average of the readings from the three rotor thermocouple taken immediately before, and after measuring the water flow. At first, readings were taken every 3 minutes but the variation in temperature over these short periods was found to be negligible. When changes did occur to T_{rotor} they were generally accompanied by changes in T_{stator} so that $(T_{\text{rotor}} - T_{\text{stator}})$ was essentially constant. The change in $(T_{\text{rotor}} - T_{\text{stator}})$ during a run was about 3 degrees and this at the higher temperatures.

During these runs, three thermocouples were used two located 180 degrees apart at $X/L = 1/2$, the other at $X/L = 1/4$, and 90 degrees from either of the first two. Readings between one of the thermocouples at $X/L = 1/2$ and that at $X/L = 1/4$ agreed to within 1-2 degrees indicating that axially the rotor temperature was uniform. The third couple however, always read high, and was flux dependent, indicating perhaps a faulty mechanical installation. Since no reason was found for rejecting the reading from this couple its indications are included in the average. The deviation from the reading of the other two couples was never more than 10 degrees, this at the highest flux rate, which when averaged with the other two could result in an error of at most 1% in overall heat transfer.

6.2 Velocity Distributions

The velocity probe indicates total pressure that is local static pressure plus velocity pressure, modified in some way still undetermined analytically or experimentally by the turbulent fluctuations.¹ Unfortunately, direct computation of the velocity is impossible even if the turbulent fluctuations are ignored, since the local static pressure is unknown. A graphical integration procedure is required to determine the velocity in the gap and is developed below. This method has

¹See Section 4.3.1.3.3

been used by G. I. Taylor,¹ and F. L. Wattendorf.²

From the r - Component of the equations of motion one can show that

$$\frac{-\bar{p} V_0^2}{r} = \frac{\partial \bar{p}}{\partial r} - \frac{\partial}{\partial r} \overline{\rho V_r'^2} - \left[\overline{\rho \frac{V_r'^2 - V_0'^2}{r}} \right] \quad (6-3)$$

where interactions between molecular and convective fluctuation terms have been neglected.

The last term

$\rho (V_r'^2 - V_0'^2) \ll \bar{p} V_0^2$ everywhere in the

flow and can be ignored.

At the probe, it is difficult to state what effects the skin friction inside the probemouth and the lags of the manometric system will have regarding the effects of the turbulent fluctuations on the indication at the manometer.

Also, as discussed in Section 4.3.1.3.3 various investigators have treated the turbulent fluctuations at the probe in several ways, from ignoring them completely to including in the total pressure the total head of the total velocity vector.

¹G. I. Taylor, "Distribution of Velocity and Temperature Between Rotating, Concentric Cylinders," Proc. Royal Society of London, ser. A, vol. 157, no. 892, Dec. 2, 1936, p. 498.

²F. L. Wattendorf, "A Study of the Effect of Curvature on Fully Developed Turbulent Flow, Proc. Royal Society of London, ser. A, vol. 148, no. 865, Feb. 1935, p. 570.

If the total pressure at the probe mouth is taken as

$$\bar{P}_T = \bar{P} + \rho V_0^2 = \bar{P} + \frac{\rho V_0^2}{2} + \frac{\rho V_0''^2}{2} \quad (6-4)$$

then, equation (6-4) together with equation (6-3) yields

$$2(R-p) = -\frac{\partial \bar{P}}{\partial r} - \left[\frac{\partial}{\partial r} (\rho V_r''^2) + \rho V_0''^2 \right]$$

No statement can be made regarding the magnitude of the last term. It has been neglected by other investigators.

Therefore,

$$\frac{2}{r}(\bar{P} - \bar{P}) = \frac{\partial \bar{P}}{\partial r} \quad (6-5)$$

The value of \bar{P} at the stator is known and is a constant, \bar{P}_{stator} .

Therefore,

$$\frac{d(\bar{P} - \bar{P}_{\text{stator}})}{dr} = \frac{2}{r} [(\bar{P} - \bar{P}_{\text{stator}}) - (\bar{P} - \bar{P}_{\text{stator}})] \quad (6-6)$$

The solution of equation (6-6) is

$$(\bar{P} - \bar{P}_{\text{stator}}) = \frac{1}{r^2} \int_{r^2}^{r_{\text{stator}}^2} (\bar{P} - \bar{P}_{\text{stator}}) d(r^2)$$

Rearranging

$$\bar{P} = \frac{\bar{P}_{\text{stator}} r_{\text{stator}}^2 - \int_{r^2}^{r_{\text{stator}}^2} \bar{P} d(r^2)}{r^2} \quad (6-7)$$

Starting at the stator, this equation can be numerically integrated to give the distribution of static pressure in the gap. The trapezoidal rule was used.

Knowing \bar{P} and \bar{P} , using equation (6-5) one can find V_0 .

6.3 The Determination of Temperature Distributions

6.3.1 Density Differences

As shown in Appendix I, from point to point on an interferogram

$$\Delta\rho = \frac{\lambda_{\text{vacuum}}}{KL} \epsilon \quad (6-8)a$$

If the "no-flow" and "flow" interferograms in Fig. 6-1 a) and b) are superimposed, Fig. 6-1 c) results. If there were no density change the N^{th} fringe would go through point B. Instead, the 1st fringe passes through B. The fringe shift, ϵ is given by

That is,

$$\epsilon(N-1) \frac{\Delta}{\Delta_{\text{Fringe}}} = \rho_i - \rho = \frac{\lambda_{\text{vacuum}}}{KL} \frac{\Delta}{\Delta_{\text{Fringe}}} \quad (6-8)b$$

$$\lambda = 5460 \text{ \AA}$$

$$L = \frac{4.5}{12} \text{ ft}$$

and

$$K = 0.3635 \times 10^{-2} \frac{\text{ft}^3}{\text{lb}} \quad 1$$

thus

$$\Delta\rho = 13.1414 \times 10^{-4} \frac{\Delta}{\Delta_{\text{Fringe}}} = \rho_B - \rho_A \quad (6-8)c$$

6.3.1.1 The Measurement of Fringe Shift

The interferograms were evaluated in a Jones and Lamson Pedestal Comparator, of optical magnification 20x.

¹ G. M. Edelman, and M. H. Bright, "The Specific Refractivity of Gases for Various Wavelengths of Light," Gas Turbine Laboratory Report No. 6, Cambridge Massachusetts, M.I.T., May, 1948, p. 5.

The interferograms had a magnification factor of $1/2x$, so that the overall magnification from the gap to the screen of the comparator was $10x$. The comparator was capable of measurement of linear distances to 0.0001 inch.

Two ink lines were drawn on the outside of the quartz window nearest the camera,¹ in order to align the plates and also to serve as a reference mark to locate the surface of the rotor (see Sec. 6.3.1.2.) Therefore the angle θ in Fig. (6-1)c could be measured, as could Δ Fringe from the "no-flow" plate.

To determine Δ , let the measured coordinates of point B be (x, y) and those of point A be (x_A, y_A)

From Fig. (6-1)c, Δ is seen to be

$$\Delta = x - x_A - \frac{y - y_A}{\tan \theta}$$

or

$$\Delta = \left(x - \frac{y}{\tan \theta} \right) + \left(\frac{y_A}{\tan \theta} - x_A \right)$$

¹This technique was used by DeFrate, Sc.D. Dissertation, MIT, 1950, and G. P. Wachtell, Ph.D. Dissertation, Princeton University, 1951. Although the camera was not focussed on the reference mark, the image of the reference mark on the photographic plate was symmetrical since the image of an out-of-focus symmetrical object is symmetrical, depending, of course, on the quality of the camera lens. The camera lens used, an Aero-Ektar $f/2.5$, 7 inch lens is of excellent quality.

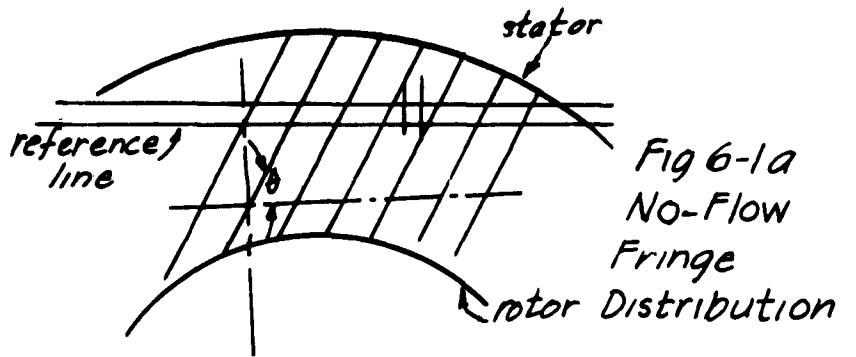


Fig 6-1 a
No-Flow
Fringe
Distribution

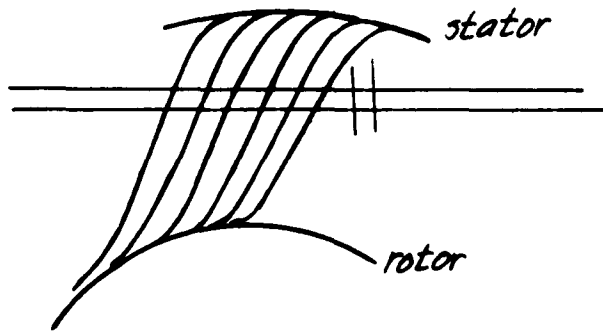


Fig 6-1 b
Distortion of
Fringes during
Flow

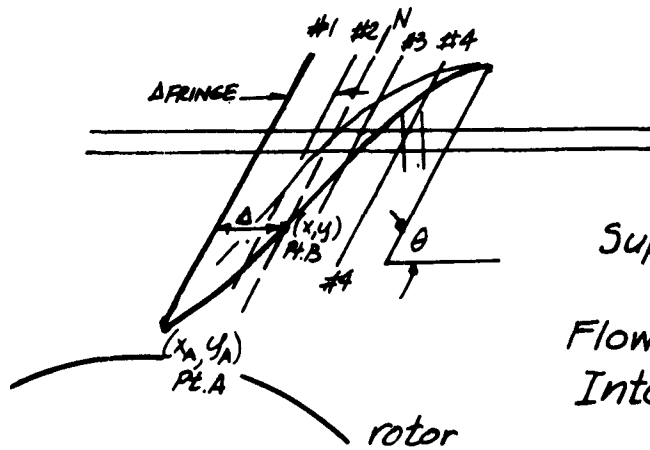


Fig 6-1 c
Superposition
of
Flow and No-Flow
Interferograms

6.3.1.2 The Determination of ρ_A , Reference Density

The ideal method of determination of ρ_A is one in which the interferometer alone is used. This can be accomplished if unfiltered mercury light is used as a means for assigning numbers to the filtered light fringes through means of no-flow and flow interferograms taken with the unfiltered light. In this manner, rotor temperature could be determined and checked against that measured from the rotor thermocouples

This was not done for two reasons: First, there existed a temperature gradient in the window (See Sections 4.4.3.2, 6.3.1.2.1, and Appendix II) which would prevent the numbering of the fringes, and secondly the location of the rotor surface on the "flow" interferogram is only apparent; that is, the rotor is not where it seems to be, because of refraction and diffraction in that region.

Because of the effects mentioned, the closest measurement to the rotor surface was of the order of 0.001 - 0.005 inches in the real plane, the low figure at low density gradients the high one at high density gradients.

Since near the wall $\frac{dT}{dr}$ is constant, it was calculated from overall heat transfer measurements and the rotor temperature as determined from the rotor thermocouples.

That is

$$\left(\frac{dT}{dr}\right)_{rotor} = - \frac{Q_c}{A_{rotor} L_{rotor}}$$

For $\Delta r = r_A - r_{rotor}$, $\Delta T = (T_A - T_{rotor})$ can be determined.

For the present experiments, Δr between 0 and 0.005 inches corresponds to at most y^+ between 0 and 6.5. In this region, and particularly for y^+ between 0 and 4, $u^+ \approx y^+$ to the best yet experimentally determined. That is, this region constitutes the so called "laminar sublayer".

In essence then the effects of turbulence are being ignored. This has been checked a posteriori, and there results little or no error.¹

Thus, ρ_A is determined and ρ_B is obtained from equation (6-8)c.

6.3.1.2.1 The Determination of the Glass Correction to

The value of the temperature gradient existing in the quartz windows has been determined experimentally for the different operating conditions. The results are presented in Appendix II. Equation (4-3) is used to determine the correction made to the measured densities.

The change in optical path lengths in the quartz window between points 1 and 2 caused by a temperature gradient in the quartz is

$$\Delta_2 OPL = L_c n_c (T_{2,H} - T_{1,H}) \left\{ \alpha_g + \frac{dn}{dT} (\Delta T_1 + \Delta T_2) + \frac{d^2n}{dT^2} \right\} \quad (4-3)$$

¹ Usually, there exists on the flow interferogram some area, and therefore, point whose density is known accurately, such as the free-stream density for the boundary layer on a flat plate.

From Section 4.4.3.2

$$\begin{aligned} n_e &= 1.46013 \text{ at } 18 \text{ C } (= 64.4 \text{ F}) \\ &= 1.46019 \text{ at } 75 \text{ F} \\ \alpha_g &= \frac{1.7}{3} \times 10^{-6} \text{ /deg C} \\ &= .32 \times 10^{-6} \text{ /deg F} \\ dn/dT &= 11.29 \times 10^{-6} \text{ /deg C} = 6.272 \times 10^{-6} \text{ /deg F} \end{aligned}$$

Since $t = 0.125$ inches

$$\begin{aligned} \Delta OPL &= 1.203 \times 10^{-6} (T_{2,N} - T_{1,N}) \\ &= \epsilon \text{ correction} = \epsilon_c \end{aligned}$$

$$\lambda = \frac{5460 \times 10^{-8} \text{ inches}}{2.54} = 21.496 \times 10^{-6} \text{ inches}$$

$$\begin{aligned} \text{Therefore, } \epsilon_c \text{ /degree temperature difference} &= \frac{1.203 \times 10^{-6}}{21.496 \times 10^{-6}} \\ &= 0.055964 \end{aligned}$$

If the gradient in the glass is expressed as G_c degrees/inch, then

$$\begin{aligned} \epsilon_c \text{ /inch} &= G_c (0.055964) \\ \text{since } \Delta \rho_c &= \epsilon_c (13.1414 \times 10^{-4}) \#/\text{ft}^3 \\ &= G_c (0.055964) 13.1414 \times 10^{-4} \\ \Delta \rho_c \text{ /0.001 inch} &= G_c (0.055964) 13.1414 \times 10^{-7} \\ &= G_c (.73544 \times 10^{-7}) \#/\text{ft}^3 / 0.001 \text{ inch} \end{aligned}$$

The correction is small for small differences in gap radius. For the case 7000 rpm, $T_{\text{rotor}} = 890 \text{ R}$, at a distance of 0.030 inches from the wall, the correction amounts to 2 deg F.

6.3.2 The Determination of Radial Position r on the Interferometric Plate

Consider the drawing of an interferometric plate shown in Fig. 6-2.

The reference lines can not be drawn absolutely parallel and perpendicular to the radius going through the reference point (A, F); hence the angularity effect when the long reference mark is placed on a horizontal center line in the comparator.

The point (A, F) is determined from average measurements of the points (1,2), (3,4), (5,6), and (7,8) and for all the runs measured the location of (A, F) relative to those points never varied by more than 0.0002 inches in about 0.012 inches.

The points (B, E), and (C, D) are likewise measured. On both the flow and no-flow interferograms the area through the gap about the reference point was blocked off in the reference path of the interferometer so that the interference fringes would not obscure the surfaces of the rotor and stator. The angle θ_{FL} is measured. This is of the order $0^{\circ}9'$. With these quantities the following can be determined:

$$(r_{\text{rotor}} - r_{\text{stator}})_{\text{plate}} = \Delta r = \frac{E-D}{\cos \theta}$$

The accuracy of measurement of θ is of no concern since $\cos 9' = 0.99999$, and θ can be measured to within $1'$ of arc.

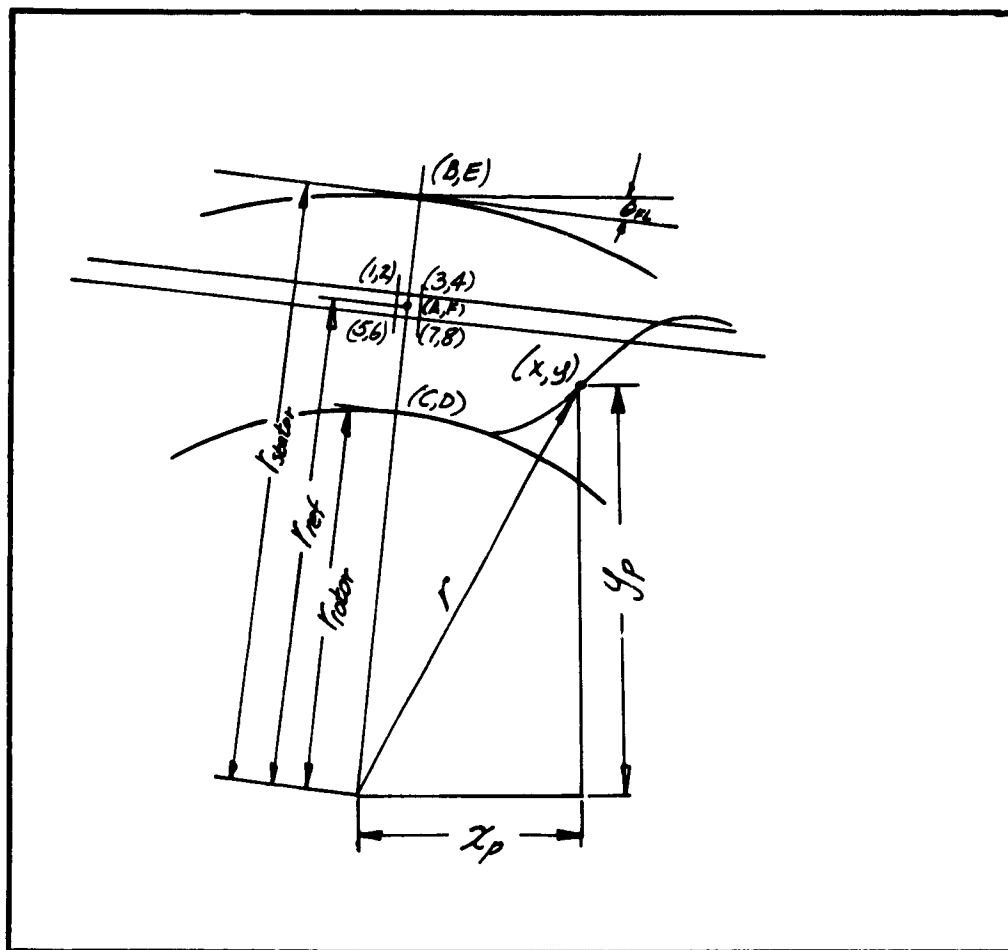


Fig. 6-2
Determination of
Radial position on an
Interferogram

The radial location of the reference point r_{ref} , is determined from

$$M = \text{Magnification Factor} = \frac{E - D}{\cos \theta} \frac{1}{(r_{\text{stator}} - r_{\text{rotor}})_{\text{True}}}$$

$$= \frac{E - D}{\cos \theta (.377)}$$

$$r_{\text{ref}} = 1.660 M + (r_{\text{ref}} - r_{\text{rotor}})_{\text{plate}}$$

Since

$$(r_{\text{ref}} - r_{\text{rotor}})_{\text{plate}} = \frac{F - D}{\cos \theta}$$

$$r_{\text{ref}} = 1.660 M + \frac{F - D}{\cos \theta}$$

Since the reference point lies in an area of very small density gradients (and hence is not subject to refraction effects), and since the camera location is unchanged from the no-flow plate to the flow-plate one can write, on the flow plate that

$$x_p = r_{\text{ref}} \sin \theta + (A - x)$$

$$\text{and } y_p = r_{\text{ref}} \cos \theta - (F - y)$$

where x and y are the location of the point of interest.

Consequently,

$$r_{\text{plate}}^2 = \sqrt{x_p^2 + y_p^2}$$

and

$$r = \frac{r_{\text{plate}}}{M}$$

In practice, x_p and y_p are taken as being on the centerline of a fringe.

6.4 The Determination of V_θ^+ vs. y^+

V_θ^+ is defined as

$$V_\theta^+ = \frac{V_\theta}{\frac{\tau_{stator}}{\rho \nu}} = \frac{V_\theta}{U_{\theta, stator}}$$

for the stator and as

$$V_\theta^+ = \frac{V_{\theta, rotor} - V_\theta}{\frac{\tau_{rotor}}{\rho \nu}}$$

for the rotor.

y^+ for the stator and rotor are defined as

$$y^+ = \frac{(\tau_{stator} - r) U_{\theta, stator}}{2 \tau_{stator}} = \frac{y U_{\theta, stator}}{z_{stator}}$$

at the stator, and

$$y^+ = \frac{y U_{\theta, rotor}}{z_{rotor}}$$

at the rotor.

To calculate these quantities, V_θ , T_w and T_w are required.

Direct measurements of shear stress were not made.

If T_w is evaluated by using the V_θ measured closest to the wall and forming $T_w = \mu r \left[\frac{dV_\theta}{dr} \right]_{\text{wall}}$ an error is made. First, the closest to the wall that V_θ was measured was 0.005 inches and 0.008 inches for the stator and rotor respectively. The value of $d(V_\theta/r)/dr$ at these points is different from the value at the wall. This is easily shown by using the

formulation by Deissler¹ for ϵ_m/ν near the wall which is

$$\epsilon_m/\nu = \eta^2 \frac{u y}{\nu} [1 - e^{-\eta^2 u y/\nu}]$$

and can be put in the form

$$\epsilon_m/\nu = \eta^2 u^+ y^+ [1 - e^{-\eta^2 u^+ y^+}]$$

where η is an experimental constant with the value 1/8.

Thus

$$\epsilon_m/\nu = x [1 - e^{-x}]$$

where

$$x = \eta^2 u^+ y^+$$

Using the data presented by Sleicher² for u^+ vs. y^+ , and estimating that $y^+ \sim y_T$ for the experimental run at 5000 rpm, no heat transfer, one finds that at a value of $y_T = 8$, $y^+ = 8$, $u^+ = 7$ and ϵ_m/ν has increased to the value 0.5.

Let τ_r represent the shear stress at a small distance from the rotor. Then

$$\tau_r r^2 = \tau_{rotor} r_{rotor}^2$$

Further

$$\tau_r = \mu r \left(1 + \frac{\epsilon_m}{\nu}\right) \frac{dV_0/r}{dr}$$

and

$$\tau_w = \mu_{rotor} r_{rotor} \left(\frac{dV_0/r}{dr}\right)_{rotor}$$

¹C. C. Lin, Turbulent Flows and Heat Transfer (Princeton University Press, Princeton, New Jersey, 1959), Section E by R. G. Deissler, p. 230.

²C. A. Sleicher, Jr., Trans. ASME, vol. 80, 1958, Table 1, p. 699.

Since $r_{rot} \sim r$

$$\frac{dV(r)}{dr} \frac{1}{r_{rot}} = (1 + \epsilon M/2) \frac{dV(r)}{dr}$$

or

$$\frac{dV(r)}{dr} \frac{1}{r_{rot}} = 1.5 \frac{dV(r)}{dr} \quad y^+ = 8$$

This is only an average case. The situation is more serious at 7000 rpm.

Secondly, a plot of $V(r)$ vs. y although smooth did not close to $y = 0$, but indicated that a probe displacement effect was present. See Fig. 6-3.

Accordingly, the following was done:

Sleicher measured his temperature distributions more accurately than his velocity distributions. Unwilling to give up the quality of his temperature measurements he synthesized a velocity distribution from the data of Reichardt,¹ Deissler,² Laufer³ (but only used those points for $Re = 500,000$) and his

¹H. Reichardt, "Heat Transfer Through Turbulent Friction Layers," NACA TM 1047, 1953.

²R. G. Deissler, "Analytical and Experimental Investigation of Adiabatic Turbulent Flow in Smooth Tubes," NACA TN 2138, 1950.

³J. Laufer, "The Structure of Turbulence in Fully Developed Pipe Flow," NACA TN 2954, 1953.

own data. The synthesized values are presented in the table below, and is taken from Sleicher's¹ previously mentioned ASME paper.

Table 6-1
Experimental Distribution of Velocity Near
a Pipe Wall.

y^+	2	3	4	5	6	8	10	12	14	16	18	20
u^+	2	3	3.9	4.8	5.6	6.9	8.1	9	9.9	10.6	11.2	11.7

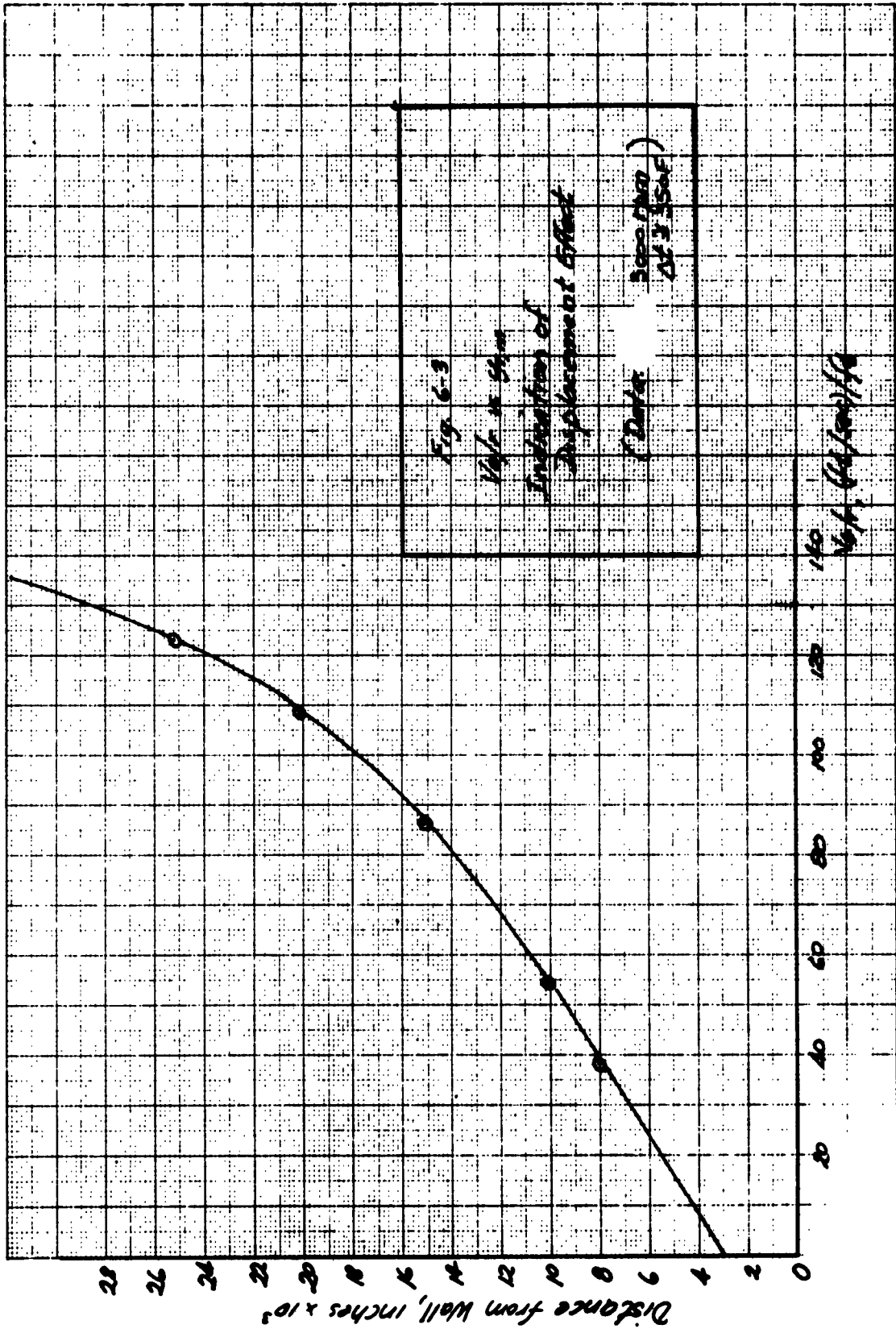
These data are mostly from adiabatic runs but analysis² shows that under greater rates of energy transfer and higher temperatures than encountered in the present experiment u^+ vs. y^+ near the wall does not vary to any extent greater than the experimental error with which one can measure the velocity there. Deviations do not occur until $y^+ = 11$.

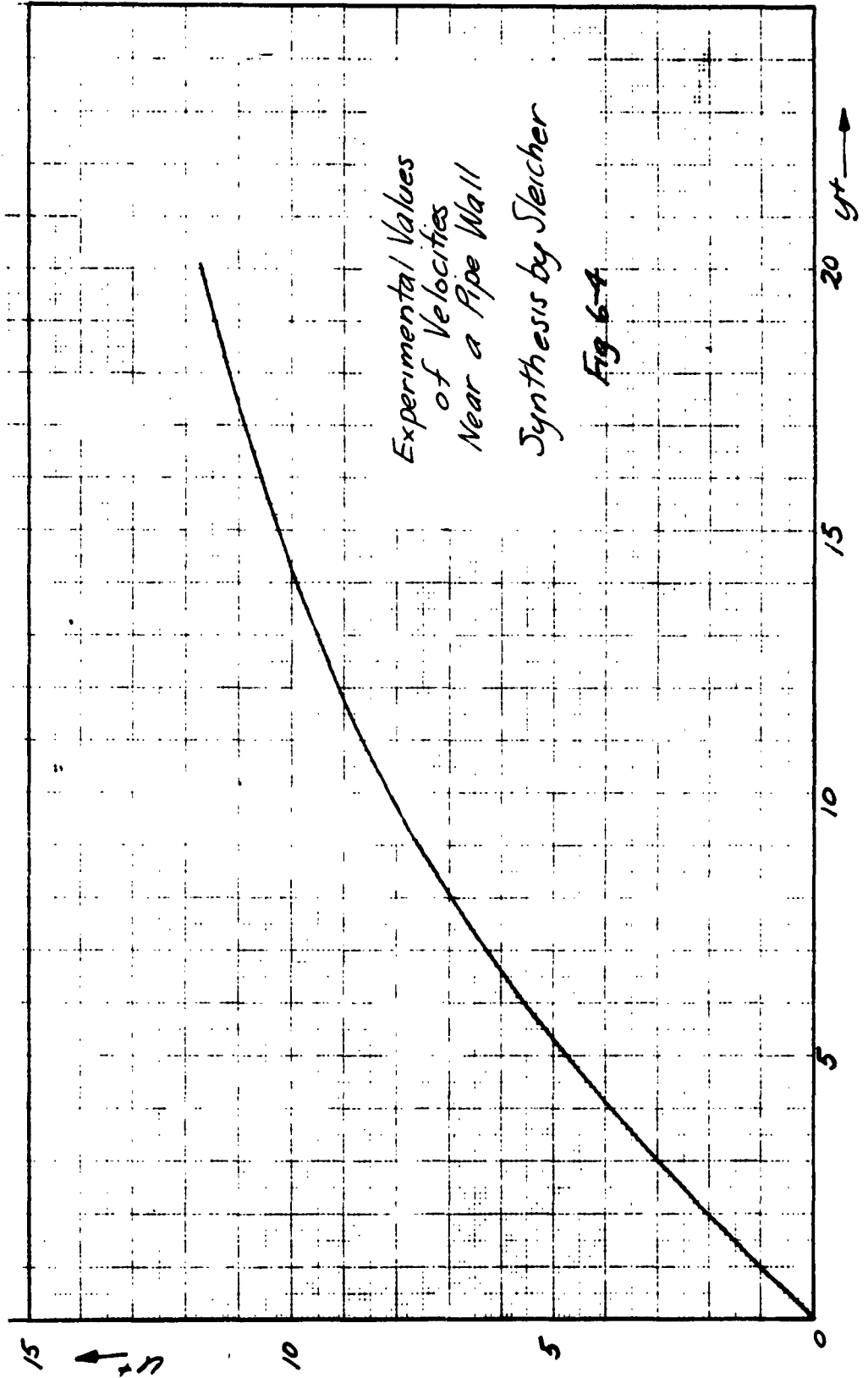
A plot of these values is given in Fig. 6-4. For the present experiment these have been used to determine the value of the shear stress at the wall and the probe displacement by the following scheme:

The data available are $y_{m,i}$ the measured values of y , and $V_{\theta,i}$, the experimentally determined velocities.

¹C. A. Sleicher, Jr., Ph.D. Dissertation, University of Michigan, 1955.

²R. G. Deissler and C. S. Eian, NACA TN 2629, pg. 33, Fig. 4 entitled Predicted generalized velocity distribution for flow of gases with heat addition at Prandtl number 0.73.





*Experimental Values
of Velocities
Near a Pipe Wall
Synthesis by Sleicher
Fig 6-4*

1. Guess a value of u_w
2. Find $V_{\theta,1} = \frac{V_{\theta,1}}{u_w}$
3. From the plot in Fig. 6-4 find the value of y_1^+
4. $y_1^+ = \frac{u_w y_1}{\nu}$
5. $y_1 - y_{m,1} = D_1$, the displacement
6. Find $V_{\theta,2}^+ = \frac{V_{\theta,2}}{u_w}$
7. From the plot find y_2^+
8. Find y_2
9. $y_2 - y_{m,2} = D_2$
10. If $D_2 \neq D_1$, repeat steps 1 - 9.
11. When $D_2 = D_1$, using the value of u_w determined in Step 1, find the value of u_w at the other wall from

$$Pr_{rot,1} Pr_{rot,2}^2 = Pr_{stat,1} Pr_{stat,2}^2$$
12. Find D_1 for the first data point.
13. Find D_2 . This must be the same as D_1 if the functional relationship given in Fig. 6-4 is to hold for the present case.

For the present data one finds that $D_1 = D_2$, and indeed, $D_1 = D_2 = D_3$ on both walls except at the lower temperature high speed runs.

This equality shows that the data follow the functional relation given by the values in Table 1. They have been in no way forced since there are more known quantities than there are equations.

The displacements D_2 never varied from D_1 by more than 0.0005 inches, except for 2 cases at 5000 rpm.

The displacements found over the rotor and stator were in the same general direction as indicated by the references cited in Section 4.3.1.3.2, that is the aerodynamic center of the probe is shifted toward the regions of higher velocity. Thus, velocities measured over the stator are further from the wall than y_m and those over the rotor are closer than y_m .

Thus y is known, u_x is known and V_0^+ vs. y^+ can be calculated.

Consider the application of the method to the data from a run at 7000 rpm, with no heat transfer.

For the stator

$y_{r,m}$	V_0
5	24.53
9	32.66

Try $u_x = 2.9$. The value of u^+ is calculated, y^+ is obtained from Fig. 6-4, and y_r is calculated.

					Displacement in thousandths of inches
Try $u_* = 2.9$					
$y_{T,m}$	u^+	y^+	y_T		
5	8.46	10.7	7.53	2.53	
9	11.27	18.25	12.84	3.84	
Try $u_* = 3.3$					
5	7.43	8.7	5.38	+0.38	
9	9.9	14.1	8.72	-0.28	
Try $u_* = 3.1$					
5	7.91	9.6	6.32	1.32	
9	10.54	15.75	10.36	1.36	

This is satisfactory.

From the principle of Conservation of Angular Momentum

$$u_{*,rotor} = \frac{r_{stator}}{r_{rotor}} u_{*,stator}$$

$$= \frac{2.037}{1.660} \times 3.1 = 3.80$$

For the rotor the data are

$$u_* = 3.8;$$

						Displacement in thousandths of inches
$y_{T,m}$	$(V_{\theta,rotor} - V_{\theta})$	u^+	y^+	y_T		
8	27.87	7.34	8.6	4.62	3.38	
10	35	9.21	12.4	.66	3.34	

The displacement is taken as 3.4 thousandths of an inch.

6.5 The Determination of Friction Factor,

The friction factor is defined as

$$f = \tau_w / \frac{1}{2} \rho V_{\theta c}^2 = 2 u_*^2 / V_{\theta c}^2$$

where V_{gc} is determined from

$$V_{gc} = \frac{V_{g,rotor} r_{rotor}}{2 r_c}$$

$$V_{gc} = \frac{V_{g,rotor} r_{rotor}}{(r_{stator} + r_{rotor})}$$

and is approximately the velocity in the center of the gap.

Therefore,

$$f_{rotor} = \frac{2 U_*^2}{V_{gc}^2}$$

and

$$f_{stator} = f_{rotor} \left[\left(\frac{r_{rotor}}{r_{stator}} \right)^2 \left(\frac{T_{stator}}{T_{rotor}} \right) \right]$$

6.6 The Determination of ϵ_m/z

From equation (2-20)

$$T_B = -\mu r \frac{dV_{gr}}{dr} (1 + \epsilon_m/z) \quad (2-20)$$

All the quantities in this equation have been previously determined except $\frac{dV_{gr}}{dr}$.

To find $\frac{dV_{gr}}{dr}$, V_{gr} was plotted against r . Over the rotor, data points were at $y_r = 8, 10, 15, 20, 25, 35, 45, 60, 85, \text{ and } 185$. Over the stator $y_r = 5, 9, 12, 15, 20, 30, 40, 65, 90 \text{ and } 140$. These are modified by the probe displacement. The points are not evenly spaced. A curve was drawn through the experimental points and every 0.0025 inches of r a value of V_{gr} was taken from the curve.

The derivatives were obtained as outlined in Lanczos.¹ This method places a least-square parable through five evenly spaced points. The derivative is then taken at the central point.

The least-squares parabolas used in the differentiation procedure go through the experimental points with negligible differences except in a few isolated instances. One such instance is presented below.

For example at 5000, $\Delta t \approx 60 R$

<u>Rotor</u>			<u>Stator</u>		
$(y_T)_m$	$(V_{\theta}/r)_m$	(V_{θ}/r) Least squares parabola	$y_{T,m}$	$(V_{\theta}/r)_m$	(V_{θ}/r) Least squares parabola
10	344.06	343.04	5	77.27	73.9
15	297.79	298.25	15	135.13	136.1
20	273.36	273.74	20	154.74	154.07
25	264.58	263.1	30	168.55	168.56
35	250.92	250.89	40	178.03	176.4
45	243.54	243.63			

Although evaluation of ϵ_m/z requires a knowledge of τ_{wall} , the value of $(1 + \epsilon_m/z)/f$ can be found from quantities measured experimentally. See Section 8.5, where $(1 + \epsilon_m/z)/f$ is given as

$$(1 + \epsilon_m/z)/f = - \frac{r_w^2 V_{\theta,c}^2}{2I_w} \left(\frac{\mu_w}{\mu} \right) \frac{1}{r^3 d(V_{\theta}/r)/dr} \quad (8-3)$$

¹C. Lanczos, Applied Analysis (Prentice-Hall, Inc., Englewood Cliffs, New Jersey, 1956), pp. 315-324.

6.7 The Determination of Dimensionless Quantities

6.7.1 Taylor Number

The Taylor Number is defined as

$$Ta = \sqrt{d/r_{rotor}} V_{\theta, rotor} d / \nu_c$$

where ν_c is the kinematic viscosity at temperature

$V_{\theta, rotor}$ is determined from

$$V_{\theta, rotor} = (rpm)(2\pi)r_{rotor}/60$$

6.7.2 $(fTa)_{Lam}$

The quantity $(fTa)_{Lam}$ is formed from the product of the friction factor and the Taylor number for flow at Taylor numbers less than the critical. It is given by

$$(fTa)_{Lam} = 4(d/r_{rotor})^{3/2} r_{stator} / (r_{stator}^2 - r_{rotor}^2)$$

where the friction factor is defined on the basis of rotor velocity.

6.7.3.1 Nusselt Number, Nu

The Nusselt number is given as

$$Nu = hd/k$$

where k is evaluated at $\frac{T_{rotor} + T_{stator}}{2}$

6.7.3.2 (Nusselt Number)_{conducting} = Nu_{cond}

The value obtained for the Nusselt number in laminar flow for the present apparatus is Nu_{cond} and is given as

$$Nu_{cond} = (d/r_{rotor}) / \ln(1 + d/r_{rotor})$$

Chapter VII

Estimates of Errors

In this chapter an attempt is made to estimate the errors in the experiment.

A correction for a determinate systematic error,¹ that caused by the temperature gradient in the quartz windows, has already been made. See Section 4.4.3.2.

There is at least one systematic error which can not be estimated, that caused by neglecting some of the turbulent fluctuating velocities in calculation of the velocity from probe measurements (See Sections 4.3.1.3.3 and 6.2). Another error, in which the personal judgement of the investigator is involved, cannot be evaluated.

This is the case in calculation of $\epsilon_{m/2}$ for $50 < y^+$
 $y^+ < 100$. In the central portion of the gap, velocity measurements were taken at radial intervals of from 0.020 inches to 0.100 inches, as contrasted with intervals of 0.005 inches near the wall. Since the determination of $\epsilon_{m/2}$ required differentiation of the velocity data, as outlined in Section 6.6, a smoothed curve drawn through the data near the central portion of the gap necessarily involved personal judgement.

The effect of the scatter in the data in this region on subsequent calculations is small.

¹Y. Beers, Theory of Errors (2nd ed., Addison-Wesley Publishing Company, Reading Mass., 1957), p. 4.

It is mentioned that in the evaluation of the conduction errors perfect contact is assumed in the installation between the thermocouple, the cement and the sides of the hole. As already stated (see Sec. 6.1.3), the indication of one thermocouple in the rotor differed from the other two by an amount which was flux-dependent, indicating, perhaps an air pocket in the hole in which the thermocouple is immersed.

The estimated conduction errors computed do not include these effects.

Finally, the errors calculated are to be regarded as reasonable, order of magnitude estimates of the errors in the determined quantities.

In evaluating the errors it is assumed that the error of an experimental result can be broken into components determined by the functional relation between the final result and those experimentally determined quantities which enter into the calculation of the final result.

Wilson¹ shows the following:

If the final result y is related to the components x_i as

$$y = F(x_1, x_2, \dots, x_n)$$

then the square of the error in y is

¹E. B. Wilson, Jr., An Introduction to Scientific Research (McGraw-Hill Book Company, Inc., New York, 1952) p. 272.

$$\overline{(\delta y)^2} = \sum_{i=1}^n \left(\frac{\partial F}{\partial x_i} \right)^2 \overline{(\delta x_i)^2}$$

7.1 Overall Heat Transfer

Equation (6-1) defines the overall heat transfer coefficient h as

$$h = Q_c / A_{rotor} (T_{rotor} - T_{stator}) = Q_c / A_{rotor} \Delta T$$

and

$$\overline{(\delta h/h)^2} = \overline{(\delta Q_c/Q_c)^2} + \overline{(\delta A_{rotor}/A_{rotor})^2} + \overline{(\delta \Delta T/\Delta T)^2}$$

7.1.1 The Error in the Determination of Q_c

The quantity $\delta Q_c/Q_c$ in turn can be broken into components

$$\frac{\delta (\text{lbs/hr})_{\text{cooling water}}}{(\text{lbs/hr})_{\text{cooling water}}} + \frac{\delta (\Delta T)_{\text{cooling water}}}{\Delta T_{\text{cooling water}}}$$

Considering first the error in the measurement of the cooling water flow rate,

$$\frac{\delta (\text{lbs/hr})_{\text{cooling water}}}{(\text{lbs/hr})_{\text{cooling water}}} = \frac{\delta (\text{lbs})}{(\text{lbs})} + \frac{\delta (\text{time interval})}{\text{time interval}}$$

The scale used was capable of measuring to within at least 2 oz; that is a 2 oz weight placed on the scale when balanced caused a correct deflection in the lever arm. The weight of water

measured was of the order of 20 lbs. = 320 oz.

A 1/5 second stop watch was used to determine the time interval. Comparison of the stop watch with an electric clock over a thirty minute time interval revealed no discernible error. On the assumption of an error in starting and stopping of 0.4 seconds each, one second is taken as the error in stop watch reading. The time interval over which the weight of water was measured was 15 minutes.

Thus

$$\frac{\delta \text{ (lbs/hr)}}{\text{lbs/hr}} = \frac{2}{320} + \frac{1}{900}$$

The error in the measurement of the cooling water temperature difference can be divided into three parts. They are

1. Conduction errors
 2. Calibration errors
- and 3. Indication errors

Recall that this measurement was made by joining the thermocouples so that the difference in emf was indicated.

The conduction-error was found to be negligible (Section 4.2.5.1).

The calibration error is of no consequence also since the two thermocouples were made from consecutive sections of the same strand of wire.

The error in indication was considered to be a maximum of $1/4$ deg (See Section 4.2.4) the accuracy with which the Portable Precision Potentiometer can be read. The potentiometer was not calibrated during the present experiment. Since it was not mishandled it is assumed that the manufacturers specified accuracy is valid.¹

The error in cooling water determination was then

$$\frac{1/4}{10} = \frac{1}{40}$$

The total fractional error in a_c is

$$\left(\frac{\delta a_c}{a_c}\right) = \frac{2}{320} + \frac{1}{900} + \frac{1}{40}$$

7.1.2 The Determination of $\frac{\delta A_{\text{rotor}}}{A_{\text{rotor}}}$

$$A_{\text{rotor}} = (2 \pi r_{\text{rotor}}) L$$

Measurement of r_{rotor} was made to within 0.001 inches in 1.660 inches; L was measured to within $1/64$ inches in 4.5 inches.

$$\frac{\delta A_{\text{rotor}}}{A_{\text{rotor}}} \text{ is then}$$

$$\frac{\delta A_{\text{rotor}}}{A_{\text{rotor}}} = \frac{1}{1660} + \frac{1}{64 \times 4.5} + \frac{1}{1660} + \frac{1}{288}$$

¹Verbal communication with Mr. Bows, Leeds and Northrup Company (New York); stated accuracy $\pm 0.05\%$ of reading $+0.006$ mv.

7.1.3 The Error in Determination of ΔT

The errors in the determination of ΔT can be classified as

1. Error in determination of stator temperature
 - a. Conduction error
 - b. Placement error
 - c. Calibration error
 - d. Indication error

and

2. Error in determination of rotor temperature, composed of the error in the thermocouple and the error in slip rings.

7.1.3.1 Error in determination of Stator Temperature

- a. Conduction error

This was found to be 0.13 F (Section 4.2.5.1.1)

- b. Placement error

This error was found to be maximum of 0.4 F
a minimum of 0.2 F.

The correction for this has been made in the calculation of

- c. Calibration Error

From the monograph by P. H. Dike, entitled "Thermocouple Thermometry"¹ the nominal limits of error for

¹P. H. Dike, "Thermocouple Thermometry," (Leeds and Northrup Company, Philadelphia, 1954), p. 18.

stock selected chromel-alumel thermocouple wire is 5 degrees in the range 32-600 \bar{F} . Accordingly, since the stator temperature was about 100 degrees the error is 5 F.

d. Indicating error

As with the cooling water thermocouples, this error is 0.25 F.

The total error is $0.13 + 0.25 + 5 = 5.38$ F.

$$\frac{\delta T_{\text{stator}}}{T_{\text{stator}}} = .0538$$

7.1.3.2 Error in Determination of Rotor Temperature

a. Conduction Error

The error was found to be negligible.

(Section 4.2.5.1.2)

b. Placement Error

This error was found to be 1.5 F under maximum conditions of heat transfer (Section 4.2.5.2) and 0.7 under minimum conditions and the correction has already been made in the calculations.

c. Calibration Error

This error is given by Dike as 1% of indication above 500 F. Since the millivolt indication at the highest temperature difference was of the order of 10, this error is of the order of 0.1 millivolt or 3 F at 800 R and 2 F at 600 R.

d. Indicating Error

As with the cooling water thermocouples this error is 1/4 F.

e. Slip Ring Error

As stated in Section 4.2.2.1 this error was found to be 3 F.

The total fractional error in ΔT using the maximum values is

$$\begin{aligned} 0.0538 + 0.0329 &= .0867 \quad \text{max} \\ \text{or } 0.0238 + 0.0131 &= .0669 \quad \text{min} \end{aligned}$$

The error in h is then determined from

$$\frac{\delta Q_c}{Q_c} = \frac{2}{320} + \frac{1}{900} + \frac{1}{40} = 0.032,$$

$$\frac{\delta A_{rotor}}{A_{rotor}} = \frac{1}{1660} + \frac{1}{288} = 0.004,$$

$$\begin{aligned} \frac{\delta \Delta T}{T} &= 0.0867 \quad \text{max} \\ &0.0669 \quad \text{min} \end{aligned}$$

and is calculated as

$$\sqrt{\left(\frac{\delta R}{R}\right)^2} = 8.7\% \quad \text{max to } 6.7\% \quad \text{min}$$

Note that a large part of the error calculated results from the error in the stator thermocouple. Thermocouple readings taken before startup of the equipment after overnight shutdown gave indications for all the thermocouples (cooling water, rotor and stator) which were within one degree F of each other.

The error given here therefore assumed to be on the high side.

7.2 Velocity Distribution

7.2.1 The Error in Determination of V_0

In accordance with the discussion of Section 4.3.1.3.3 the error caused by neglecting turbulent velocity fluctuations (See Section 6.2.1) cannot be estimated.

The accuracy of velocity determination depends on the accuracy of the manometer used.

The velocity is related to the reading on the manometer by

$$V_0 = \sqrt{2g \frac{(R-p)}{\rho}}$$

and

$$\frac{\delta V_0}{V_0} = \frac{1}{2} \frac{\delta(R-p)}{(R-p)}$$

The quantity $\delta(R-p)$ is constant and is estimated to be of the order 0.003 inches of fluid as a maximum, not because of any limitations of the micromanometer but because of the method used to bracket the reading (See Sections 4.3.3, and 5.3).

The minimum value of the quantity $(R-p)$ occurred at $y_{r, \text{stator}} = 5$ at 3000 rpm, $\Delta T = 330 R$ and was of the order 0.020 inches, so an error of

$$\frac{\delta V_0}{V_0} = \frac{1}{2} \frac{0.003}{0.020} = 7.5\%$$

is indicated at that point.

At $y_{r, \text{stator}} = 9$, for the same conditions, $(R-p) = 0.037$ for an error of

$$\frac{1}{2} \times \frac{0.003}{0.037} = 4\%$$

At 7000 rpm, $\Delta T = 330^\circ$, $y_{\text{stator}} = 5$, $(R-p) = 0.064$

and the error is 2.4%.

At $y_T = 9$ for the same run, $(R-p) = 0.140$ and the error is 1.1%.

7.2.2 The Error in Determination of Radial Position, r

The error in radial position r is estimated to be of the order of 0.0005 inches, by the method used for probe location (see Section 4.3.1.2 and Fig. 4-6).

7.2.3 The Error in Determination of $r \frac{dV_e}{dr}$

The quantity $r \frac{dV_e}{dr}$ can be written

$$\frac{dV_e}{dr} - \frac{V_e}{r} = r \frac{dV_e}{dr}$$

If r_1 , r_2 , and r_3 are three evenly spaced radii then a good approximation for the present purposes is

$$\frac{V_{e,3} - V_{e,1}}{r_3 - r_1} \sim \frac{dV_e}{dr} \cdot \frac{1}{2}$$

The error in $\frac{dV_e}{dr}$ is then

$$\frac{\delta V_{e,3}}{V_{e,3}} + \frac{\delta V_{e,1}}{V_{e,1}} + \frac{\delta(r_3 - r_1)}{(r_3 - r_1)}$$

The errors in V_e are generally small in the area of greatest rate of change in $\frac{dV_e}{dr}$ (at about $y_T = 20$) and are taken as 1%.

Further, the accuracy with which the probe can be positioned over an interval is of the order 0.0003 inches, which is the accuracy with which a micrometer can be read, admittedly with some effort. However, if the traverse is always made in the same direction, eliminating the problem of backlash in the micrometer screw and barrel, this estimate of the location error is not unreasonable. The interval $(r_3 - r_1)$ is taken as 0.010 inches.

The accuracy with which $\frac{dV}{dr}$ can be determined is

$$0.01 + 0.01 + 0.03 = 5\%$$

The error in the quantity V_0/r is

$$\frac{\delta V_0}{V_0} + \frac{\delta r}{r} = \frac{\delta V_0/r}{V_0/r}$$

Again $\frac{\delta V_0}{V_0}$ is taken as 1%. The quantity δr is 0.0005 inches, $r = 1.680$.

The experimental error in determining $r \frac{dV_0/r}{dr}$

$$\sqrt{(0.05)^2 + (0.01)^2 + \left(\frac{1}{1.680}\right)^2} = 5\%$$

This value seems somewhat low, but even with the approximations made it does not seem that it could be incorrect by any large amount for the region considered. This is borne out by the results for ϵ_{exp} discussed in the next chapter.

7.2.4 The Error in the Determination of $(1 + \epsilon_m/2)/f$

The quantity $(1 + \epsilon_m/2)/f$ is correlated with y^+ in the next chapter. It is given by the equation

$$\frac{(1 + \epsilon_m/2)}{f} = -\frac{r_w^2 V_{0,c}^2}{22\mu} \frac{\mu_w}{\mu} \frac{1}{\left\{ r^3 \frac{dV_{0,c}}{dr} \right\}}$$

Since, as shown above, the fractional errors in the determination of r are small, the error in $[1 + \epsilon_m/2]/f$ are those resulting from errors in the velocity and the term $r^3 \frac{dV_{0,c}}{dr}$

For
$$\frac{\delta V_{0,c}}{V_{0,c}} = 0.01$$

and
$$\frac{\delta \left(r \frac{dV_{0,c}}{dr} \right)}{r \frac{dV_{0,c}}{dr}} = 0.05$$

The fractional error in $\frac{1 + \epsilon_m/2}{f}$ is

$$\sqrt{(0.02)^2 + (0.05)^2} = 0.054 = 5.4\%$$

7.2.5 The Error in Determination of f

Because of the manner in which the shear stress at the wall was determined (see Sec. 6.4) it is difficult to specify by equation the error in f . An estimate based on the results obtained is 5%. The results are presented in Chapter VIII, Section 8.4.

7.2.6 The Error in Determination of G_m/μ

Combining the results of Sections 7.2.4 and 7.2.5 yields

$$\sqrt{\left(\frac{\delta(G_m/\mu)}{G_m/\mu}\right)^2} = \sqrt{(0.05)^2 + (0.05)^2} = 74\%$$

Again, this is in the region $y^+ = 20$. At $y^+ = 50$ the error is presumed to be greater.

7.3 The Error in Determination of $G_m/\mu = \alpha$

7.3.1 The Error in Determination of $\frac{dT}{dr}$

The error in dT/dr can be estimated in the same manner as the error in dv_0/dr .

Since the variation in p across the gap is negligible so far as a computation of T and ρ is concerned (e.g. 1/2 inch water above atmospheric), $\frac{dT}{T} = -\frac{d\rho}{\rho}$

For three evenly spaced radii, r_1 , r_2 and r_3 , an approximation for $d\rho/dr$ is

$$\frac{d\rho}{dr} = \frac{\rho_3 - \rho_1}{r_3 - r_1}$$

The error in $\rho_3 - \rho_1$ results from errors in measurement of fringe shift, Δ .

From equation (6-8)c

$$\Delta p = 13.1414 \times 10^{-4} \Delta / \Delta_{\text{Fringe}}$$

The measurement of fringe shift Δ , involves the x and y coordinates on the comparator used to evaluate the photographic plates.

Taking as typical the experimental data for 5000 rpm, $\Delta t \cong 160R$, the fringe shift between the points 3 and 1 is 0.021 inches where Δ_3 can be expressed as

$$\Delta_3 = A(x_3 - x_1) + B(y_3 - y_1) + \text{constant}$$

and where x and y are the coordinates measured on the comparator. The values for $(x_3 - x_1)$ and $(y_3 - y_1)$ are 0.0143, and 0.01 respectively. Given x_1 and y_1 the location of x_3 and y_3 on the comparator can be determined to 0.0002 inches without tiring the operator.

The fractional error in Δ_3 is then

$$\delta \Delta_3 / \Delta_3 = \delta(x_3 - x_1) / x_3 - x_1 + \delta(y_3 - y_1) / y_3 - y_1$$

$$= \frac{0.0002}{0.0143} + \frac{.0002}{0.010}$$

$$= 0.014 + 0.02$$

The measurement of Δ_{Fringe} involved only one coordinate on the comparator, and was taken over a span of about ten no-flow fringes. The error is considered negligible.

Therefore

$$\delta \Delta f / \Delta f = \delta \Delta T / \Delta T = 0.034$$

The error in $r_3 - r_1$ is determined from similar considerations. However, since the magnification factor for the interferometric plates was about one-half the error in determination of coordinates x and y for the present calculations is then 0.0004 inches

$$\begin{aligned} \delta(r_3 - r_1) / r_3 - r_1 &= \delta(x_3 - x_1) / x_3 - x_1 + \delta(y_3 - y_1) / y_3 - y_1 \\ &= \frac{0.0004}{0.0143} + \frac{0.0004}{0.010} \\ &= 6.8\% \end{aligned}$$

The fractional error in dT/dr is then

$$\sqrt{\frac{\delta(dT/dr)^2}{(dT/dr)^2}} = \sqrt{(0.034)^2 + (0.068)^2} = 7.6\%$$

The error in α can be determined from equation (2-30) which is repeated here.

$$\alpha P_r = (x/\epsilon_m (1-x) + 1) / x$$

where

$$x = \frac{dT/d(V_0/r)}{\{dT/d(V_0/r)\}_{wall}} (r_w/r)^2$$

or from computation directly from

$$\alpha = \epsilon_H / \epsilon_m$$

The latter is the somewhat simpler procedure since the quantities necessary have been computed.

From equation (2-26)

$$\frac{g_w T_w}{r} = -k \left(1 + \frac{E_H}{\kappa}\right) \frac{dT}{dr}$$

or

$$\frac{E_H}{\kappa} = - \frac{g_w T_w}{r k \frac{dT}{dr}} - 1$$

The fractional error in $\frac{E_H}{\kappa}$ is

$$\frac{\delta E_H/\kappa}{E_H/\kappa} = \frac{\delta g_w}{g_w} + \frac{\delta (dT/dr)}{dT/dr}$$

From Section 7.1.1 the fractional error in g_w

is

$$\begin{aligned} \frac{\delta g_w}{g_w} &\sim \frac{\delta Q_c}{Q_c} = \frac{2}{320} + \frac{1}{900} + \frac{1}{40} \\ &= .006 + .0011 + .025 \\ &= .032 \end{aligned}$$

From the previous section

$$\frac{\delta (dT/dr)}{dT/dr} = 0.076$$

The fractional error in E_H/κ is then

$$\begin{aligned} \sqrt{\left(\frac{\delta (E_H/\kappa)}{E_H/\kappa}\right)^2} &= \sqrt{(0.076)^2 + (0.032)^2} = 0.0825 \\ &= 8-1/4\% \end{aligned}$$

The error in α neglecting the error in

determination of the properties is

$$\sqrt{(\delta\alpha/\alpha)^2} = \sqrt{(\delta\epsilon_m/\epsilon_m)^2 + (\delta\epsilon_H/\epsilon_H)^2}$$

$$= \sqrt{(0.074)^2 + (0.0825)^2} = 11\%$$

7.4 The Error in Determination of Taylor Number, Ta

$$Ta = \sqrt{d/r_{rotor}} V_{0,rotor} d/\nu = \sqrt{d/r_{rotor}} \text{rpm}(2\pi)d r_{rotor}/60\nu$$

$$\overline{(\delta Ta/Ta)^2} = (\delta \text{rpm}/\text{rpm})^2 + (\delta r_{rotor}/r_{rotor})^2 + \frac{3}{2}(\delta d/d)^2 + (\frac{1}{2} \delta r_{rotor}/r_{rotor})^2$$

7.4.1 The Error in Rpm

The rpm as measured with a chronometric tachometer and as kept under continuous observation with a Strobotach was never observed to vary from a given setting by more than 10 rpm over the 6 second time interval of operation of the chronometric tachometer. The chronometric tachometer had been previously calibrated and showed no discernable error. The calibration stand consisted of a shaft directly driven by a synchronous motor. The fractional error in determination of rpm is then

$$\frac{10}{3000} = \frac{1}{300}$$

7.4.2 The Error in Determination of d

The gap width d is

$$r_{\text{stator}} - r_{\text{rotor}}$$

δr_{rotor} and δr_{stator} are taken, as before, as

0.001 inches.

Concentricity of the rotor and stator were established during assembly with "go" and "no-go" gages for which the "no-go" gage was 0.0015 inches greater in diameter than the "go" gage. The concentricity was therefore within 0.002 inches and δd is taken as

$$\delta d = 0.002''$$

Therefore,

$$\delta d/d = 0.053$$

The error in Taylor number is therefore

$$\begin{aligned} \sqrt{(\delta Ta)^2 / Ta^2} &= \sqrt{\left(\frac{1}{300}\right)^2 + \left[\frac{3}{2} (0.053)\right]^2 + \left[\frac{3}{2} \times \frac{0.001}{1.660}\right]^2} \\ &= 6.5\% \end{aligned}$$

Chapter VIII

Experimental Results

In this Chapter, the experimental results are presented and compared with other investigators where possible. The principal results are as follows:

1. That turbulent flow can exist in the gap without an axial flow of air in the range of Taylor number 3000 to 9000.
2. That the correlation offered by Kays and Bjorklund for the heat transfer in the gap, $Nu/Nu_{cond} = 0.175 (Ta)^{1/2}$, can be extended for low temperature differences from Taylor numbers of 2000 to Taylor numbers of 9000. At higher temperature differences the heat transfer is reduced but still varies as $(Ta)^{1/2}$.
3. a. That V_{θ}^+ vs y^+ follows the universal curve for pipe flow out to $y^+ = 10$, and levels off.
b. That V_{θ} in the central portion of the gap is not constant but increases outward toward the stator.
4. That the friction factor follows a relation

$$f_{tm} = \frac{0.3342}{Ta^{0.358}}$$
5. a. That near the walls and out to $y^+ = 50$, two curves, one for the rotor, and one for the stator, suffice to describe Em/h vs. y^+ for $3000 < Ta < 9000$, and for temperature differences of from 60 F to 330 F.

b. That the eddy diffusivity in the middle of the channel can be expressed by the relation

$$(\epsilon_m/\nu + 1) = 0.227 Ta^{0.642} (1 + T_{\text{stator}}/T_{\text{rotor}})$$

6. That the ratio ϵ_H/ϵ_m equals 1.4 for the conditions studied.

and 7. The findings can be used to determine friction factors and overall heat-transfer, given T_{rotor} , T_{stator} , and rpm. This is done in Chapter IX.

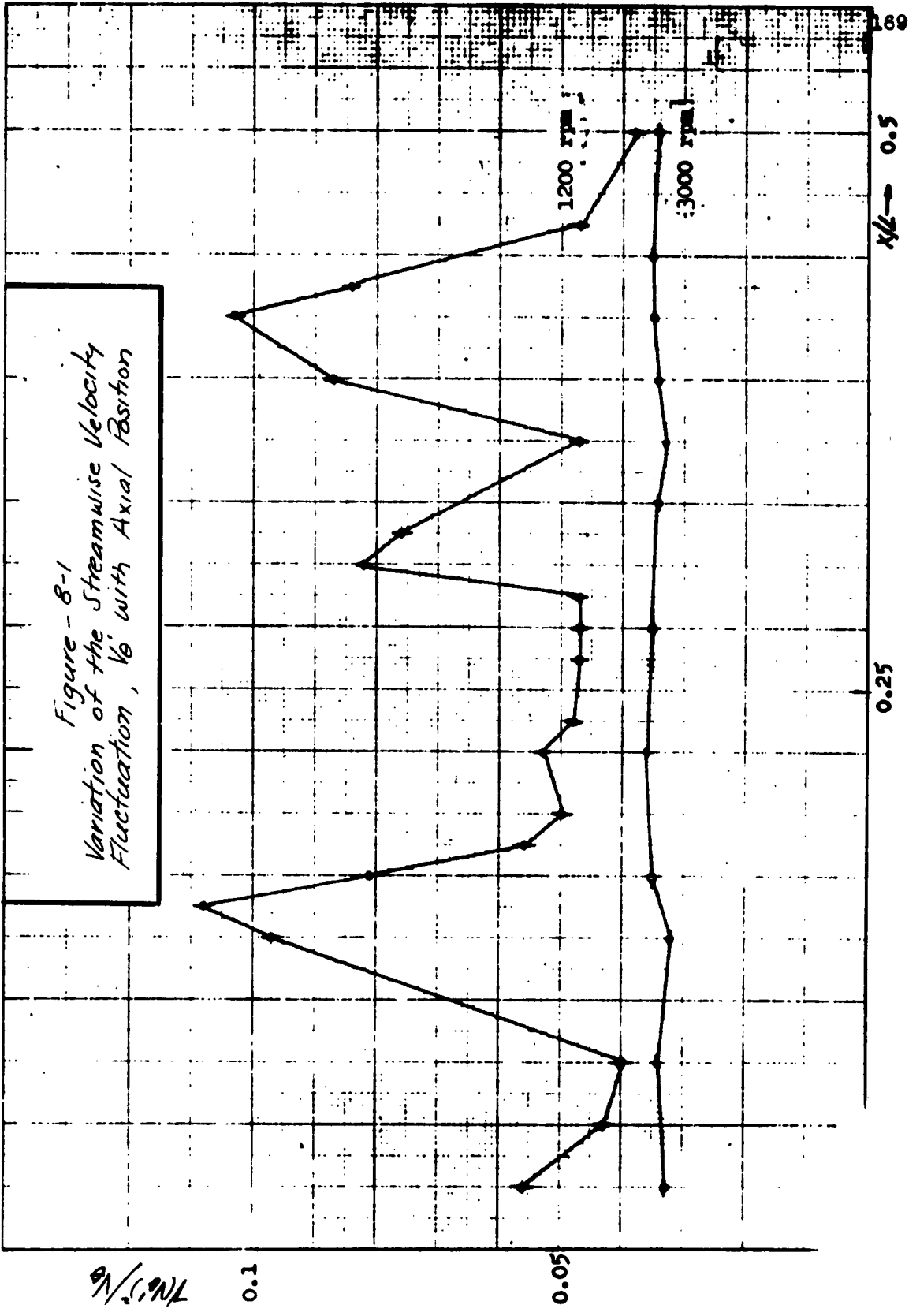
8.1 Hot-wire Measurements to Establish That Turbulent Flow Exists in the Gap

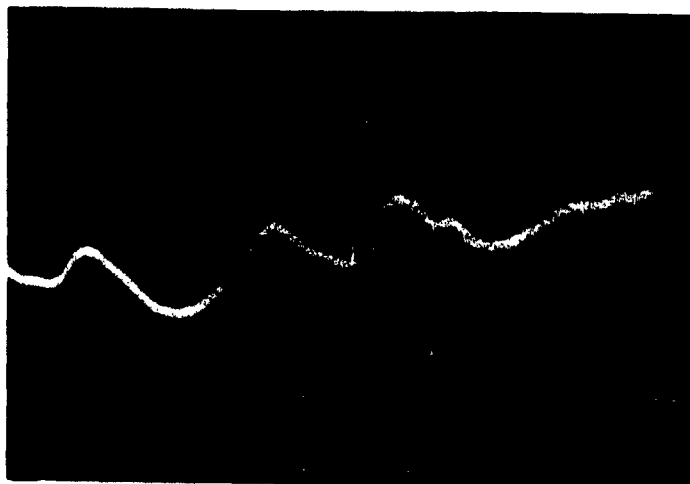
In order to determine whether secondary flows existed in the gap, axial traverses were made in the center of the gap for two rotational speeds; 1200 and 3000 Rpm. The results of these tests are shown in Fig. 8-1 in which are plotted $\sqrt{(V_{\theta}')^2}/V_{\theta}$ for 1200 and 3000 rpm. Shown in Fig. 8-2 are photographs of oscilloscope traces for these runs in which differences in the character of the flows is apparent.

The data demonstrate that two kinds of flow can exist in the gap, those for 1200 rpm showing the existence of secondary flows, and those for 3000 rpm showing the random fluctuations of turbulent motion.

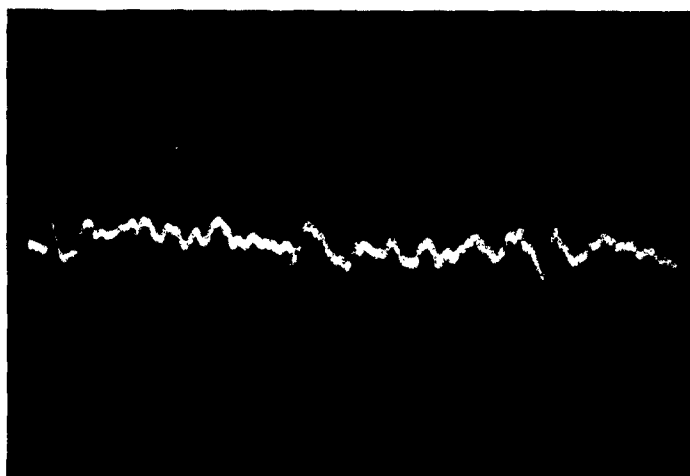
It is interesting that the peaks in $\sqrt{(V_{\theta}')^2}/V_{\theta}$ for 1200 rpm occur at a spacing not too different from 3/8 inches, that predicted by Taylor for the Taylor vortices.

The photographs for 1200 rpm are similar to those





8-2a
Vortical Flow, 1200 RPM



8-2b
Random Turbulence, 3000 RPM

Figure 8-2
Hot-wire anemometer traces at 1200 and 3000 rpm

shown by Kaye and Elgar¹ for turbulent-plus-vortices flow.

The value for the turbulent intensity $\sqrt{v_0'^2}/v_0$ for 3000 rpm in the center of the gap was found to be 3.5%. This compares with the value of 6% found by MacPhail, quoted by Townsend.²

The overall velocity in the center of the channel was checked with the hot wire and agreed to within 1.5%.

Further explorations made with the probe at a fixed axial position and varying speed (from low to high to low values) indicated that at about 1500 rpm a changeover occurs from the secondary type of flow to the turbulent flow.

It appears that the line of demarcation between the turbulent-plus-vortices and turbulent flow regimes as originally hypothesized by Becker³ (see Fig. 1-3 and Section 1.2.1.1) is correct, and turbulent flow can exist in the gap with zero axial velocity.

¹J. Kaye and E. C. Elgar, "Modes of Adiabatic and Diabatic Fluid Flow in an Annulus with an Inner Rotating Cylinder," ASME Paper No. 57-HT-14.

²D. C. MacPhail, Turbulence in a Distorted passage and Between Rotating Cylinders," Ph.D. Dissertation, University of Cambridge, 1941 as reported by A. A. Townsend, The Structure of Turbulent Shear Flow, p. 303, Fig. 12-3.

³K. M. Becker, Sc.D. Dissertation, MIT, 1957.

8.2 Overall Heat Transfer

In Fig. 8-3 are shown the overall heat transfer results for the present experiment. Drawn also is the line $Nu/Nu_{cond} = 0.175(Ta)^{1/2}$ which Kays and Bjorklund suggest as representing their data and those of Becker for $90 < Ta < 2000$. The data of Gazley are also shown.

Gazley's results were obtained from Fig. 8 of his paper¹ noting that $Ta = \frac{7}{10} Re$, and also that the Nusselt number used there is twice that of the present work. Becker, and Kays and Bjorklund have not found any reason for the discrepancy between Gazley's results and theirs although Becker suggests that the fact that Gazley did not account for radiation between the two cylinders may be the cause of the discrepancy.²

¹C. Gazley, Jr., "Heat Transfer Characteristics of the Rotational and Axial Flow Between Rotating Cylinders," ASME Paper No. 56-A-128.

²No data are known concerning the emissivity of the cylinders of Gazley. If an emissivity of 0.36 is assumed and also that the temperature difference was of the order of 100 F, then for a run at a Taylor number of 600, neglecting radiation would account for a discrepancy of 10% as compared to a discrepancy of 60% as reported (e.g., at $Ta = 600$, the line $Nu/Nu_{cond} = .175(Ta)^{1/2}$ yields a value of about 4.4 for Nu/Nu_{cond} as compared with 7 as reported by Gazley).

Thus it does not appear that under the assumptions made, including the effects of radiation heat transfer can account for the difference. It is interesting however that as the Taylor number is reduced the discrepancy is more acute, which is the effect one would expect if radiation effects were the cause, since the radiation heat transfer is constant at constant temperature difference.

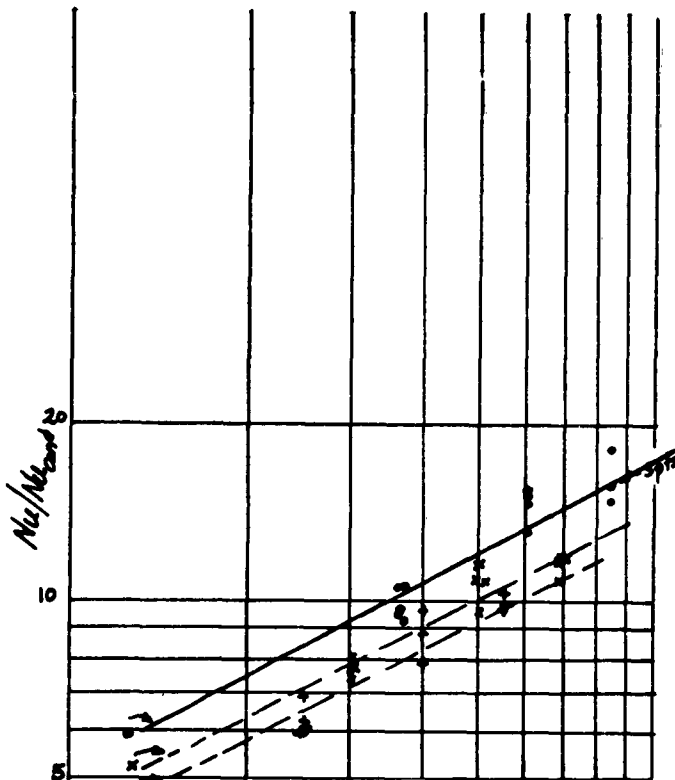


Fig 8-3
Overall Heat Transfer
 Nu/Nu_{conv} vs. Ta

o Trotor \approx 600 R $\Delta T = 80$

x Trotor \approx 720 R $\Delta T = 175$

+ Trotor \approx 880 R $\Delta T = 320$

— Extension of $Nu/Nu_{conv} = 0.175 Ta^{1/2}$

--- Trend of Present Work at higher ΔT

1000 2000 5000 10000 10000

Ta , Taylor Number

As can be seen from Fig. 8-3 the results of the present experiment follow the trend of the curve $Nu/Nu_{cond} = 0.175(Ta)^{1/2}$ but the effects of property variation are clearly in evidence.

At low temperature differences the agreement with the straight line representation of Kays and Bjorklund is good.

However at temperature differences of 330 F, the heat transfer at a given Taylor number is reduced by 30%, and at a given rpm by 20% (e.g. for 7000 rpm, at about 60 F temperature difference, Btu/hr. transferred/degree temperature difference = 3, whereas at about 330 F temperature difference the value is 2.4).

Heat transfer balance between electrical input and heat output in the cooling water was only to within 50%. Study of the problem has shown that

1. A negligible amount of heat is leaking from the rotor to the cooling water through the stator end plates. This is an experimental fact.

2. The difference between electrical energy input and heat abstracted from the cooling water can pass directly from the rotor heater to the stainless steel shaft. This is a calculated result.

Other investigators were not subjected to the same problem by virtue of lower temperature differences. Consequently,

in their designs they were able to use materials of low thermal conductivity such as plastic spacers.

Agreement with their results is noted in the range in which overlap occurs ($Ta \approx 3000$).

8.3 Velocity Distributions

8.3.1 V_{θ}/r versus r

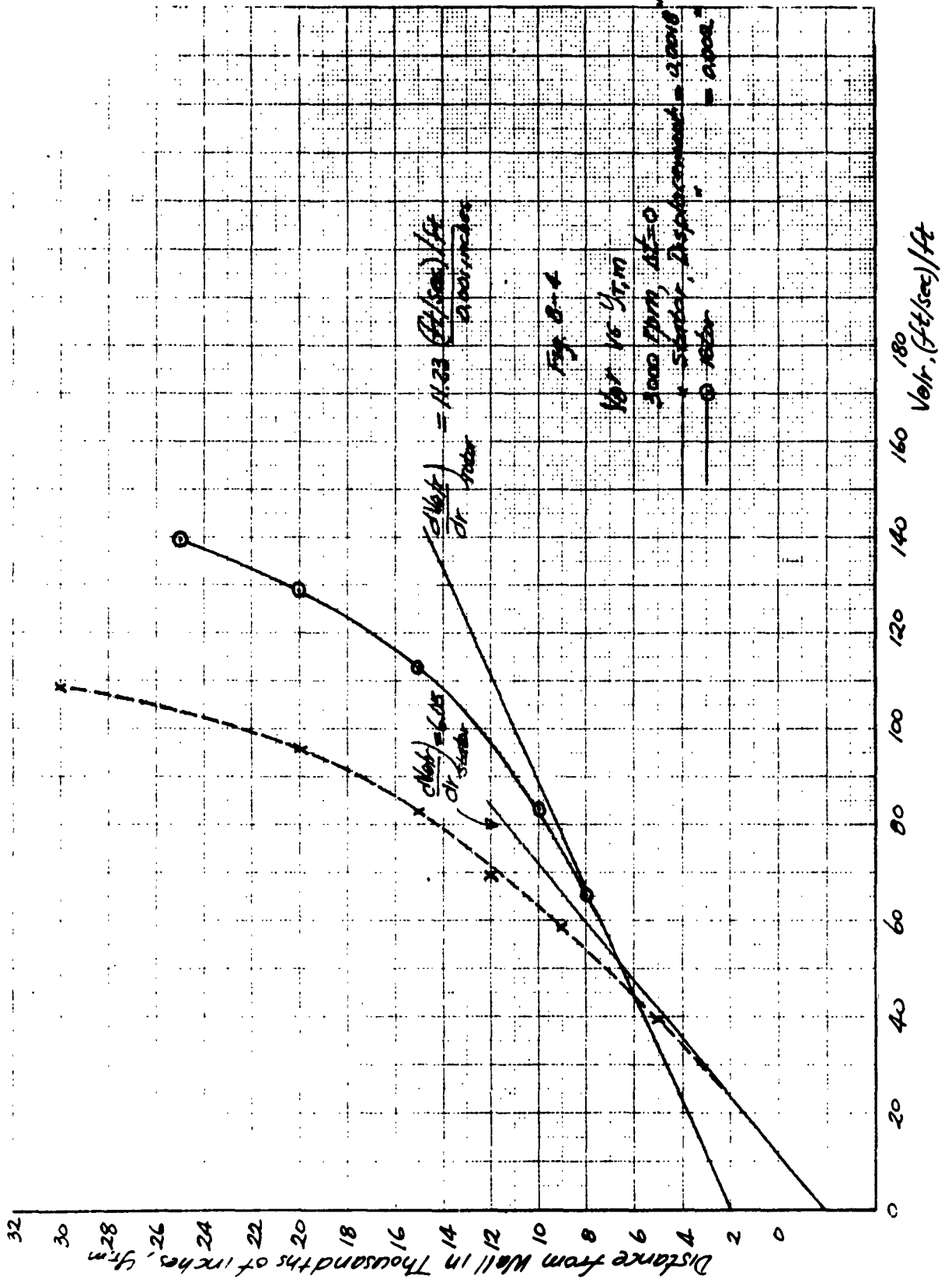
Shown in figures 8-4 to 8-9 are typical velocity distributions, V_{θ}/r versus r , near the rotor and stator obtained for a range of rotational speed 3000 rpm to 7000 rpm ($2500 < Ta < 9000$) and temperature difference ($0 < (T_{\text{rotor}} - T_{\text{stator}}) < 330 \text{ F}$). The distances from the wall have not been adjusted for the displacement effect discussed in Section 6.4. These are the data from which $C_{m\theta}$ was calculated.

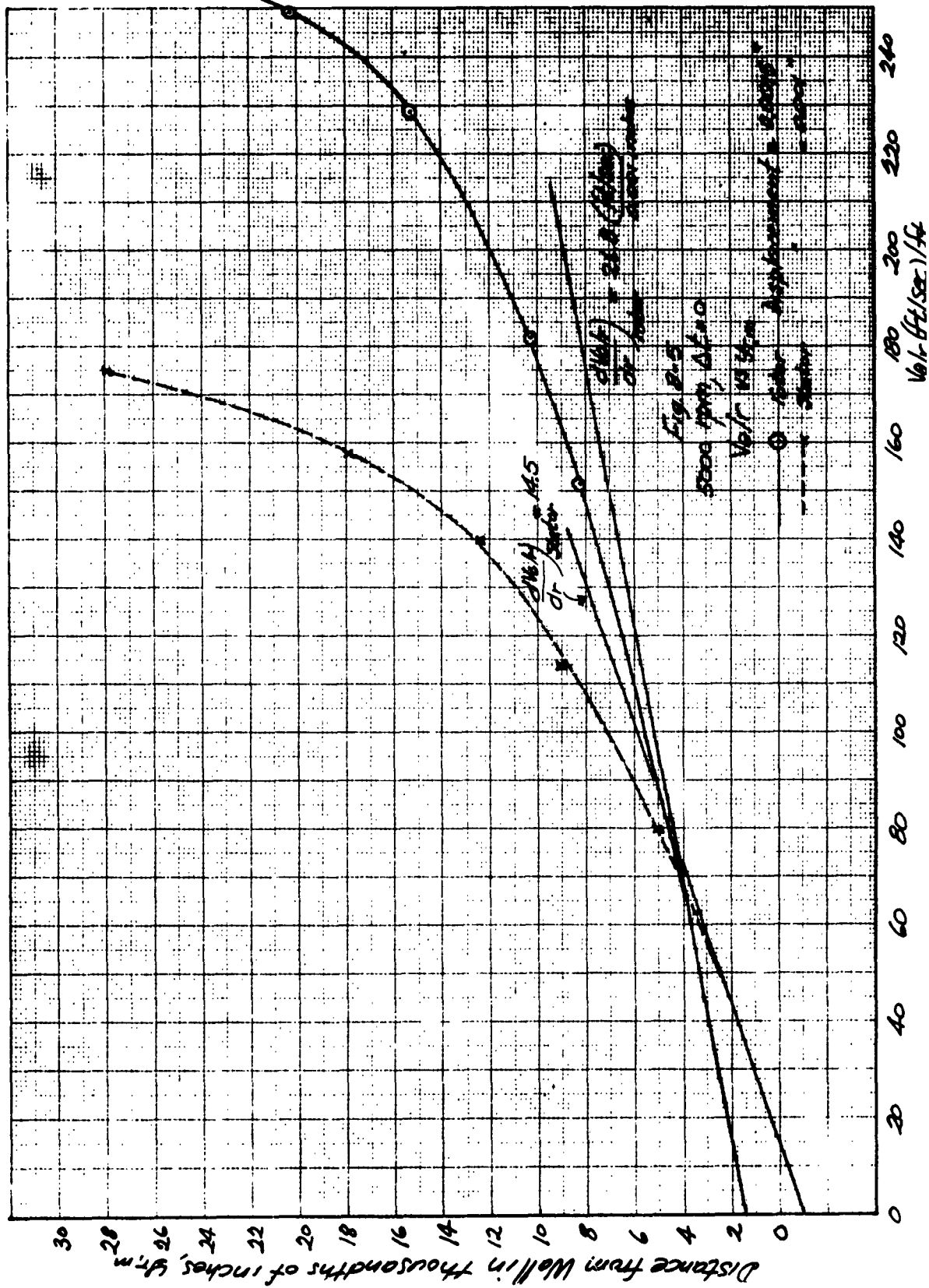
8.3.2 $V_{\theta} r$ versus r

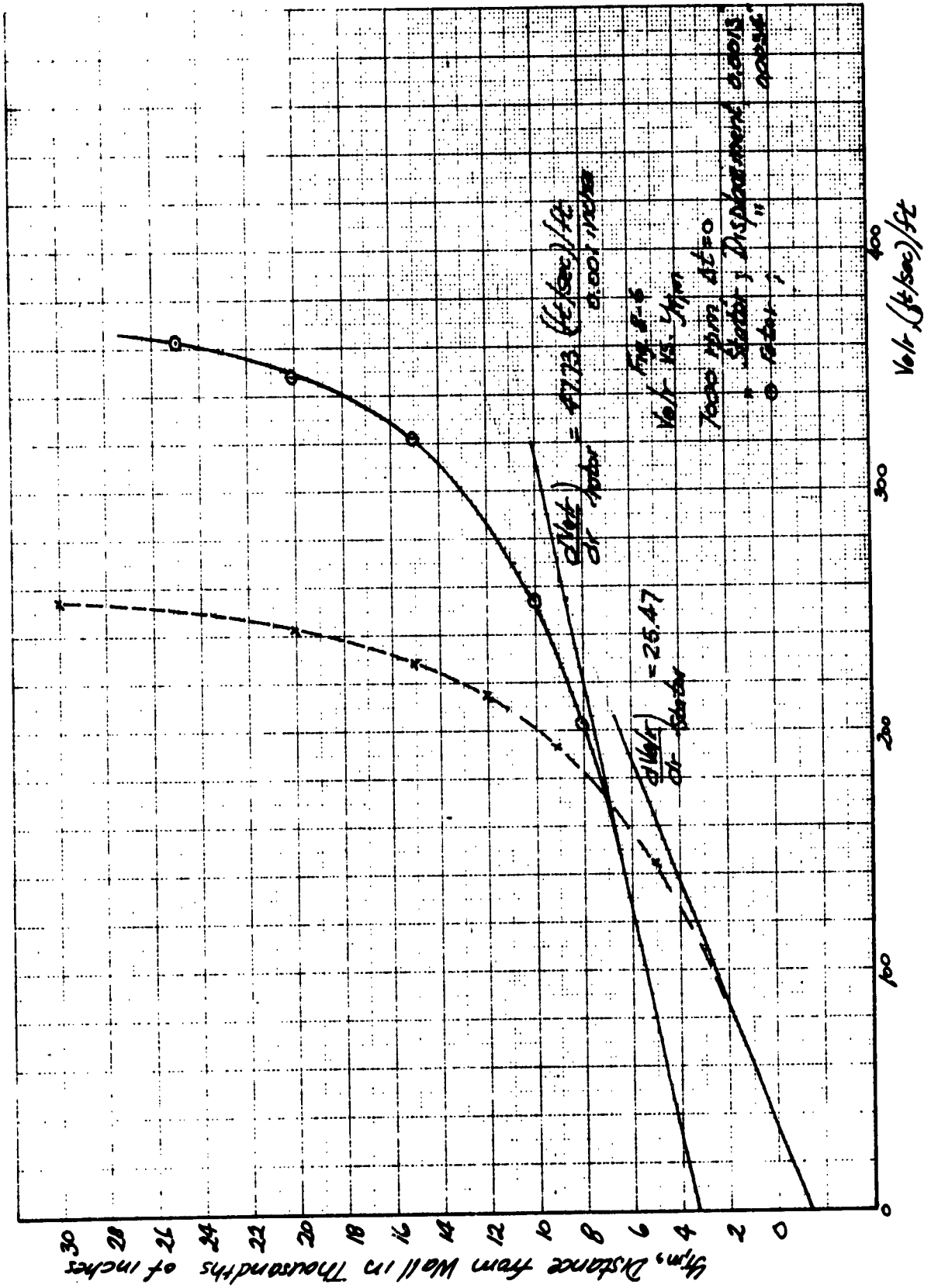
Shown in Fig. 8-10 and 8-11 are typical distributions of $V_{\theta} r$ versus r . As can be seen in the center of the gap $V_{\theta} r$ appears to follow a relation $V_{\theta} r = ar + b$, increasing with r . The variation is small but does exist. This result agrees with Taylor's original data¹ but not his final result obtained from extrapolation of the data to a probe of zero thickness (see Section 1.2.1.3). Pai's² experiments were conducted to test

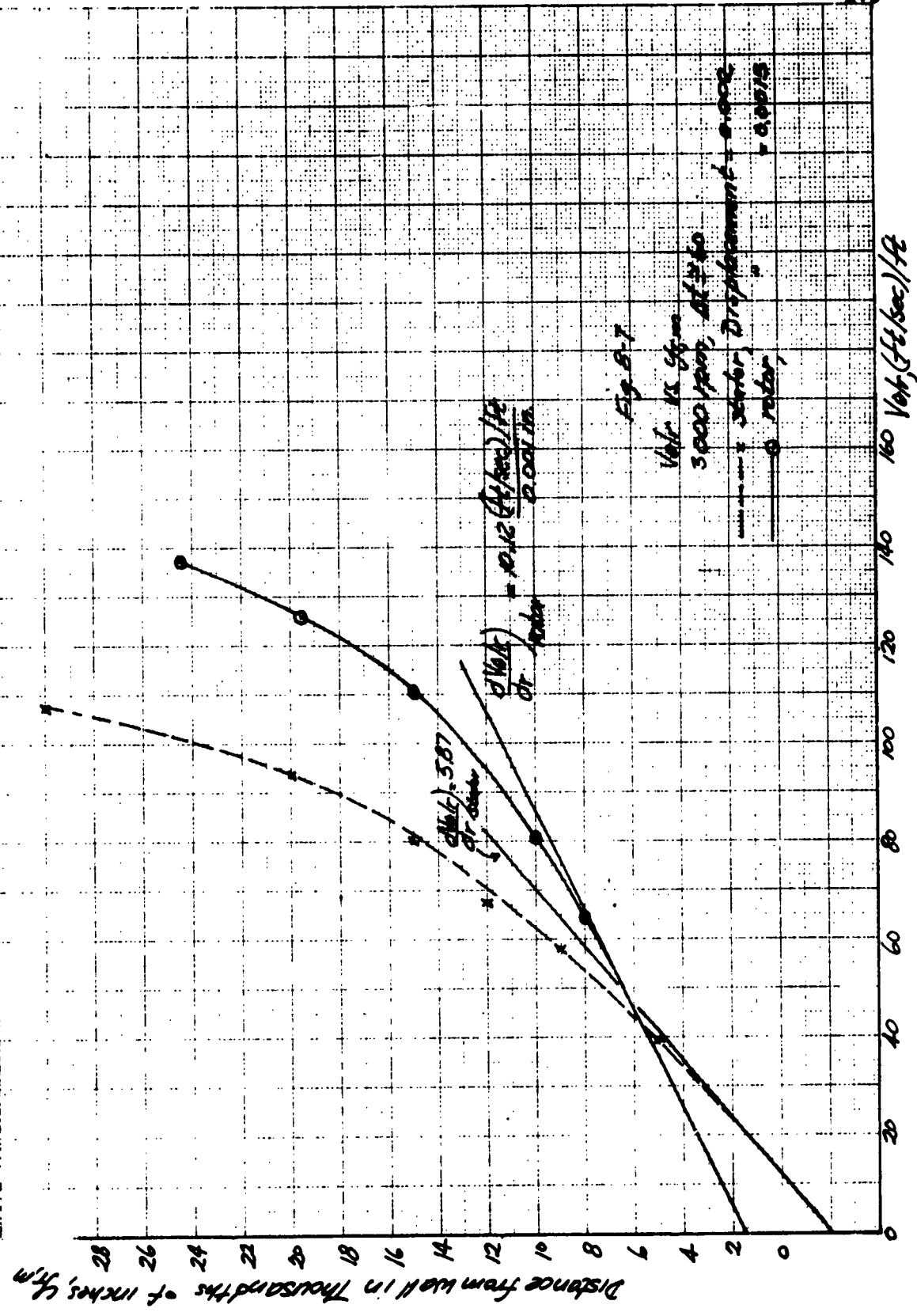
¹G. I. Taylor, Proc. Royal Society of London, ser A, vol. 157, 1936, pp. 492-512.

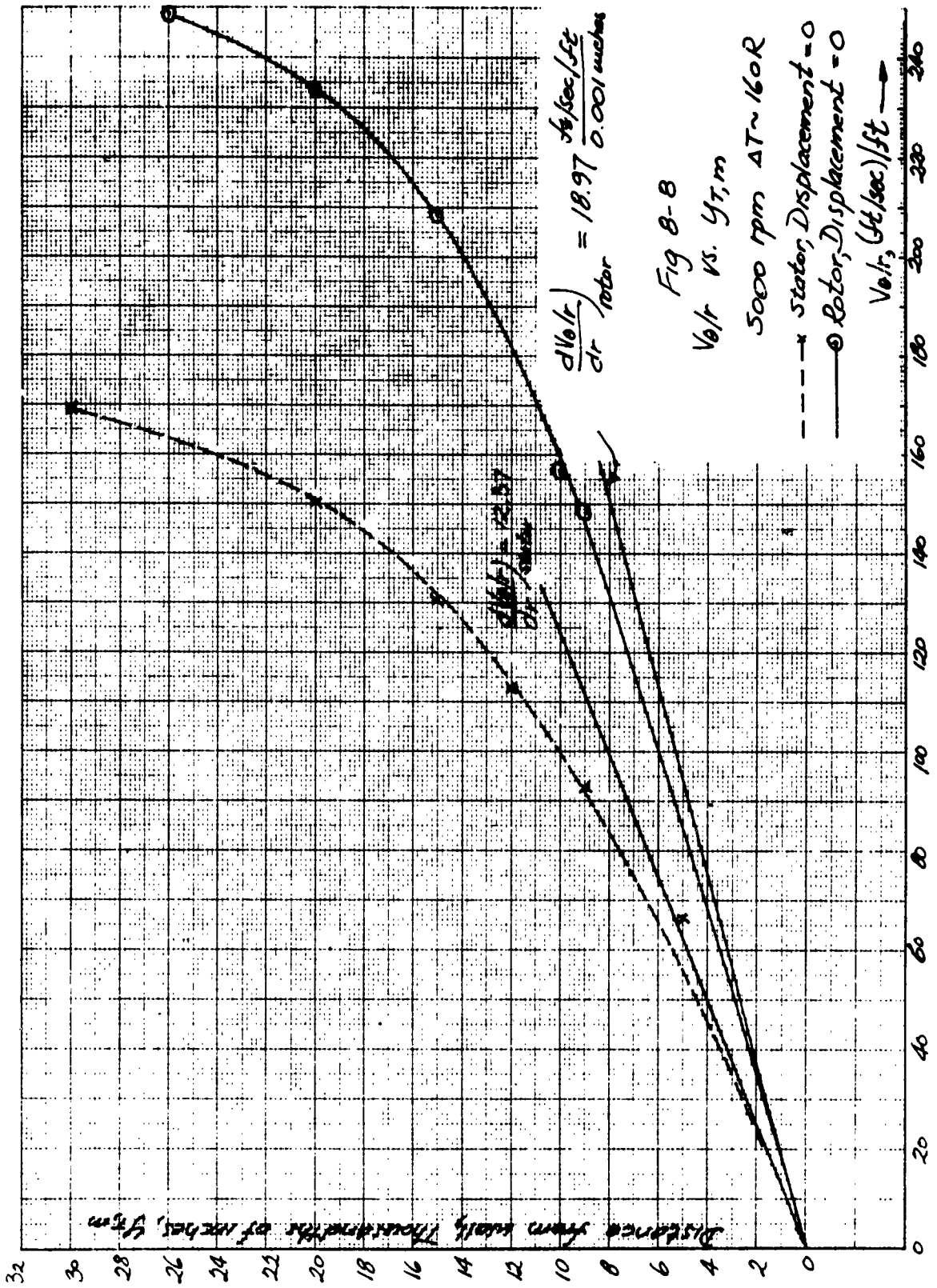
²Pai Shih-I, NACA TN No. 892, p. 2.

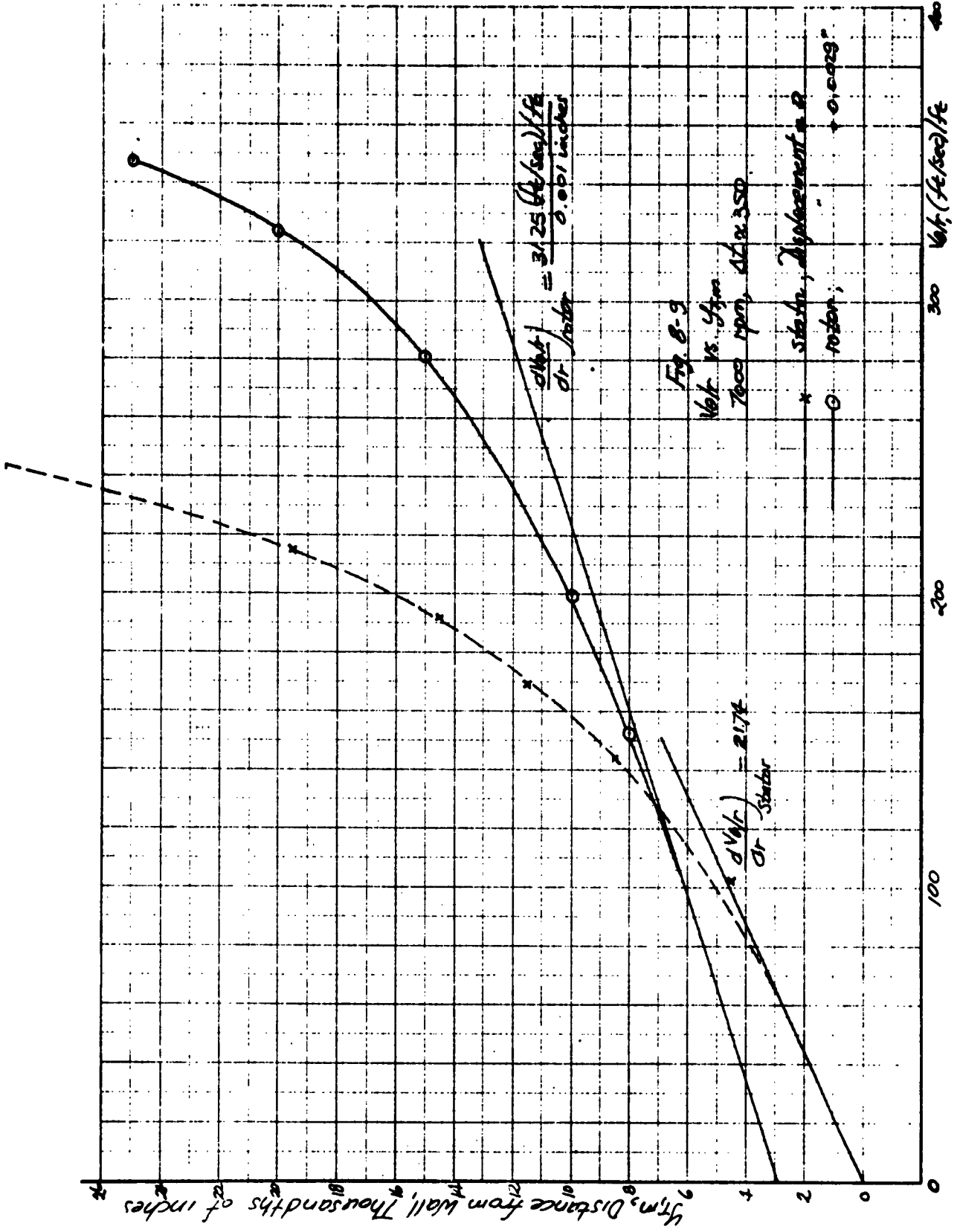












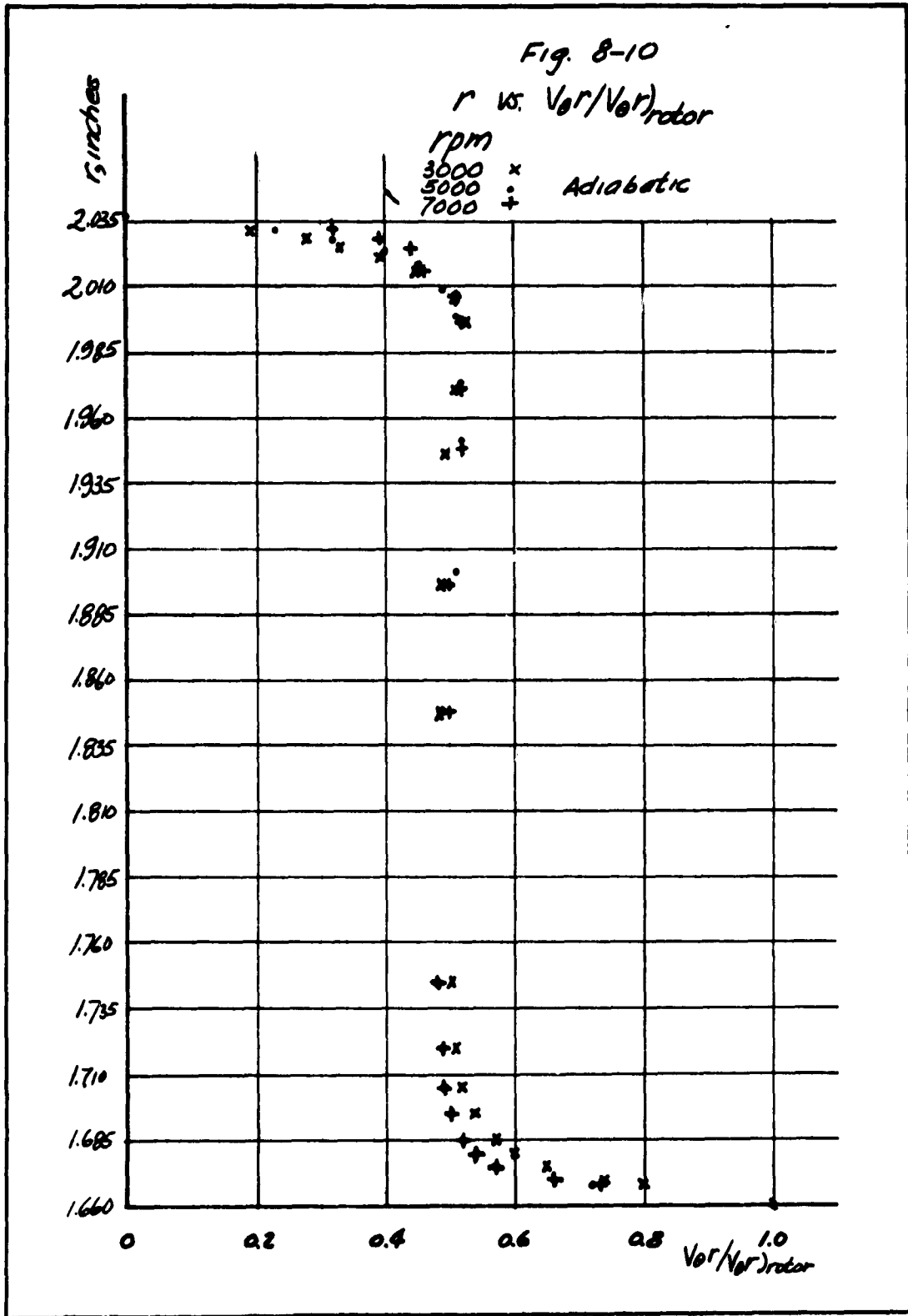
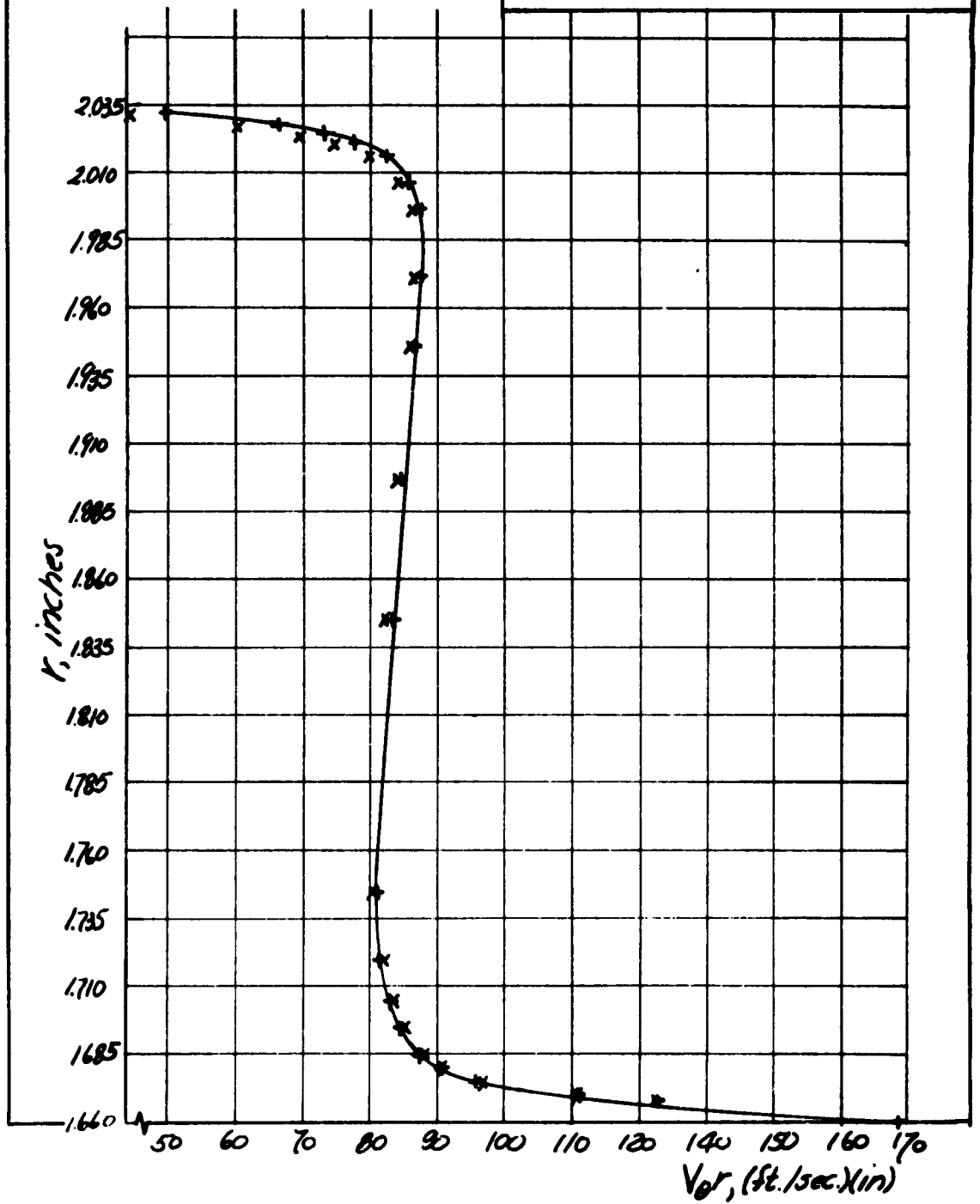
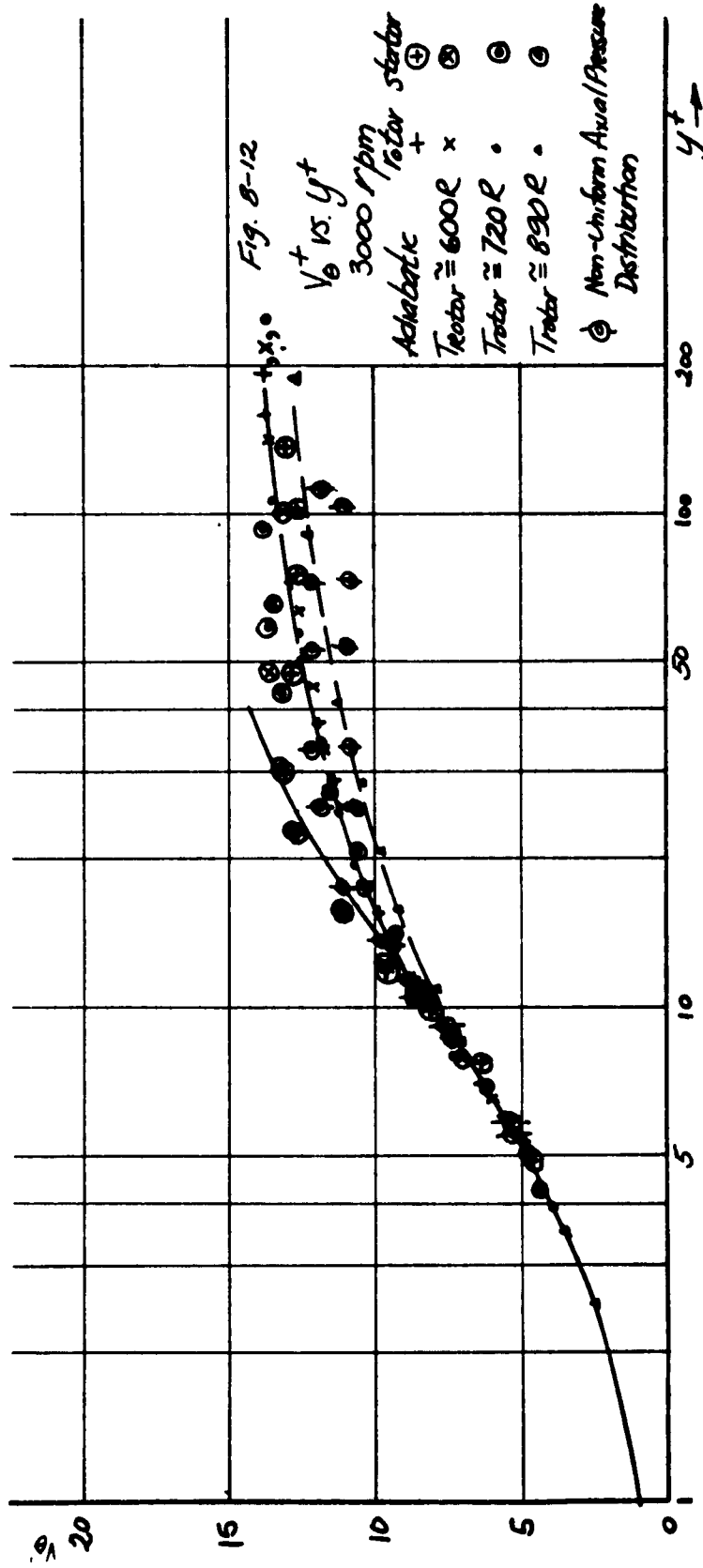
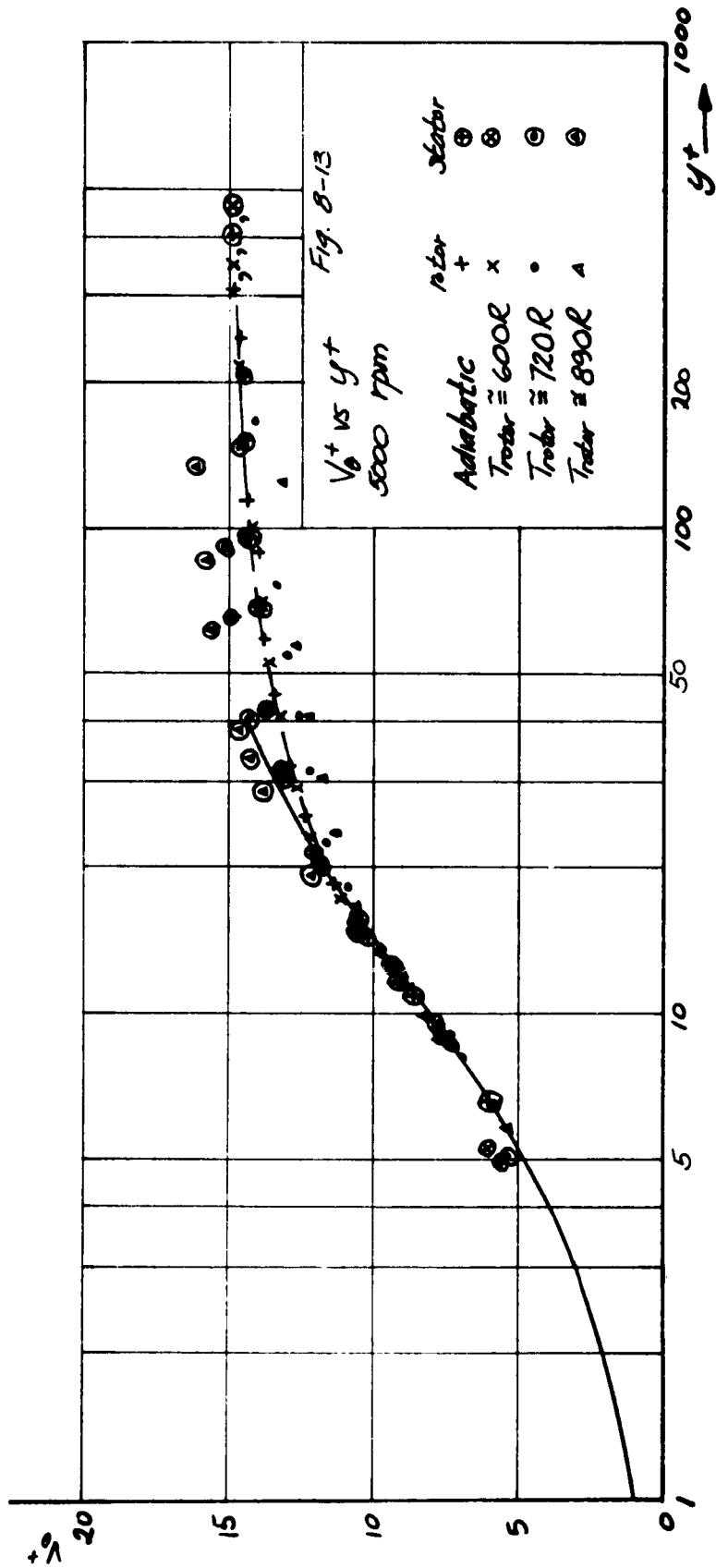
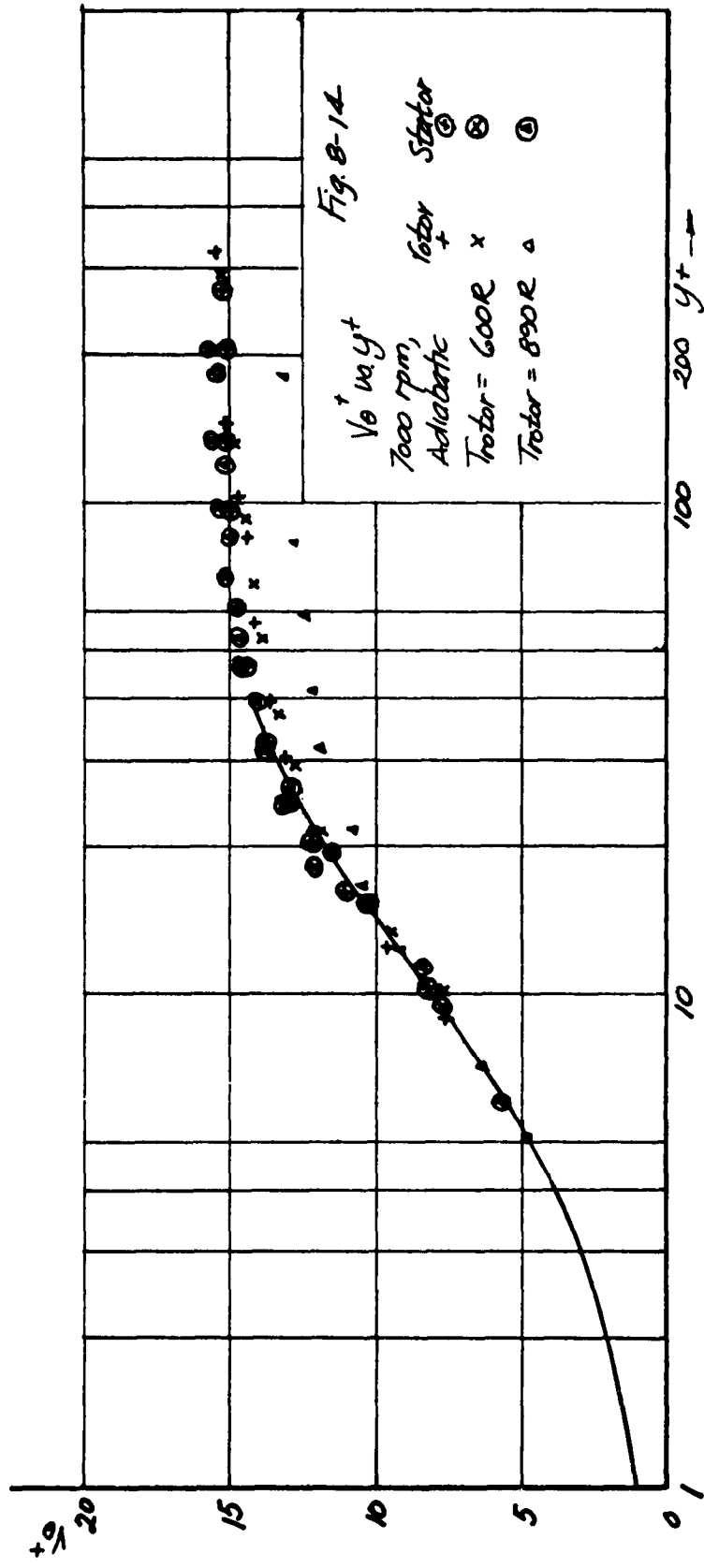


Fig. 8-11
 r vs V_{or}
 7000 rpm, Adiabatic +
 $T_{rotor} = 602.6^\circ X$









the validity of Taylor's extrapolation but in his report he mentions this and then makes no further statement concerning the problem.

Pai's data however show a variation of V_θ r increasing with r. See his Fig. 7 and 9.

Townsend¹ states "A close study of the velocity distribution shows that $Ur[V_\theta r$ in the present notation] is slightly less than its central value near the inner boundary layer and slightly greater near the outer one."

Accordingly, the result for the center of the gap, $V_\theta r = ar + b$ is accepted as correct and was used to determine values of ϵ_m/b in that region.

8.3.3 V_θ^+ vs. y^+

Shown in Fig. 8-12 to 8-14 are curves of V_θ^+ vs. y^+ for the present experiment.

The close agreement to the curve of u^+ vs. y^+ presented by Sleicher for the lower y^+ is understandable (see Sec. 6-4). However, agreement exists beyond the lower y^+ out to $y^+ \cong 10$. At high values the behavior with heat transfer is in agreement with the trend predicted by Deissler²;

¹A. A. Townsend, The Structure of Turbulent Shear Flow (Cambridge at the University Press, 1956), p. 298.

²R. G. Deissler, "Investigation of Turbulent Flow and Heat Transfer in Smooth Tubes, Including the Effects of Variable Fluid Properties," Trans. ASME, vol. 73, 1951, pp. 101-107.

namely, a divergence between the curves for the stator and rotor caused by the effects of cooling on the stator and heating on the rotor.

Wattendorf's¹ reported results for V_{θ}^+ vs r over the rotor only approach the rotor up to a value of y^+ of about 20, so no comparison in that region is possible. Further out in the stream Wattendorf notes a divergence in V_{θ}^+ for the rotor and stator. His Fig. 23 is reproduced as Fig. 8-15.

Such a divergence does not occur in the present experiment. No satisfactory explanation can be offered for the difference. A curious fact, however, is that on page 582 Wattendorf shows two successive equations for the shear stress distribution as

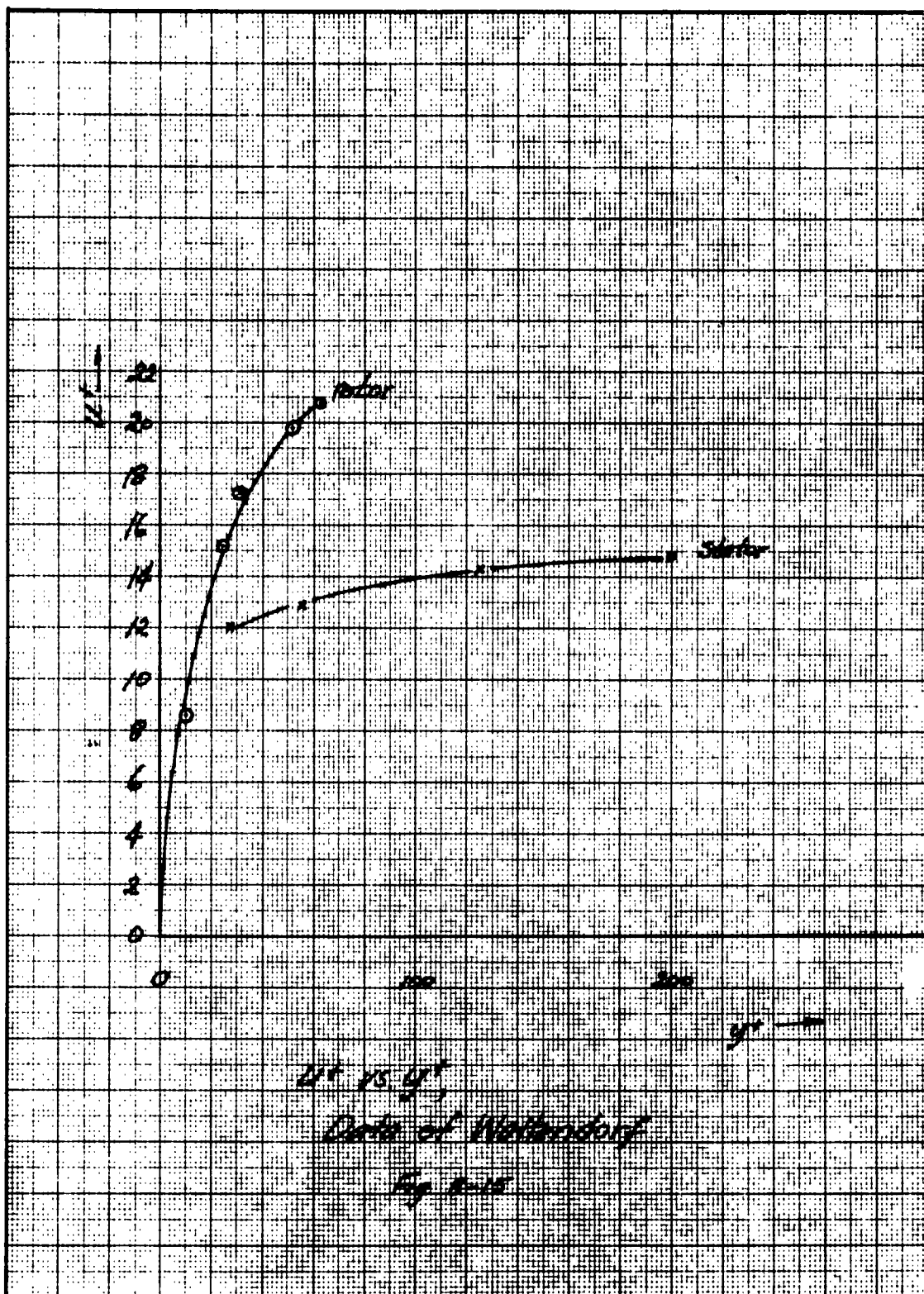
$$\tau_r = \text{constant}$$

and

$$\tau_{inner} = \tau_{outer} r_{outer} / r_{inner}$$

The omission of the power "2" on the radii may be a typographical error. But, if not since Wattendorf measured τ_{outer} , his computation for τ_{inner} would be in error by $\frac{r_{outer}}{r_{inner}} = \frac{25}{20} = 1.25$. Thus, $u_{y,inner} = \sqrt{\frac{\tau_{inner}}{\rho}}$ would be low by 25%. Multiplying Wattendorf's u_{inner}^+ by 0.8, and his y^+ by 1.25 reduces the discrepancy.

¹ F. L. Wattendorf, Proc. Royal Soc. London, ser A, no. 865, vol. 148, Feb. 1935, pp. 565-598.



8.4 Friction Factor

The friction factors found in this experiment have been determined from the values of μ_* obtained from the velocity distributions as outlined in Section 6.4.

For purposes of correlation of the $\epsilon u/\nu$ data the friction factor has been defined as

$$f_{\text{rotor}} = \frac{T_{\text{rotor}}}{\frac{1}{2} \rho_{\text{rotor}} V_{\theta, c}^2}$$

and

$$f_{\text{stator}} = \frac{T_{\text{stator}}}{\frac{1}{2} \rho_{\text{stator}} V_{\theta, c}^2}$$

and not as

$$\frac{T_{\text{rotor}}}{\frac{1}{2} \rho_{\text{avg}} V_{\theta, \text{rotor}}^2}$$

as by Kays and Bjorklund¹.

Thus neglecting property variation

$$f_{\text{rotor}} = 5 f_{\text{Kays and Bjorklund}}^2$$

A plot of f_{rotor} and f_{stator} versus Ta is shown in Fig. 8-16. A least-squares straight line has been calculated for these data and yields the relationship

$$f_{\text{rotor}} = \frac{0.3342}{Ta^{0.358}} \quad (8-1)$$

Apparently, the manner in which fluid properties

¹W. M. Kays and I. S. Bjorklund, ASME Paper No. 58-A-99

²The factor 5 results from the fact that $V_{\theta, c} = 0.45 V_{\theta, \text{rotor}}$ for the dimensions of the present apparatus.

used in the dimensionless ratios are evaluated is beginning to have some influence at $T_{\text{rotor}} = 890 \text{ R.}$

In Fig. 8-17, f_{rotor} is plotted against T_a , with properties based on rotor conditions. Similarly f_{stator} is plotted against T_a with properties based on stator conditions. For the rotor, it is seen that the evaluation of the Taylor number with the kinematic viscosity based on rotor temperature has succeeded in placing the points representing high temperature difference on the correlation curve.

For the stator, the effects of property variation on the correlation have been reduced, since the stator was always at about the same temperature, 80 to 100 F. The obvious conclusion is that the effect of heat transfer has been to reduce the friction by about 20% for the temperature range considered.

Two other efforts in the determination of friction factors have been by Wagner¹ and Taylor.²

Their data were obtained by torque measurements on the stator, Wagner using oil as the fluid and Taylor using

¹E. M. Wagner, "Frictional Resistance of a Cylinder Rotating in a Viscous Fluid Within a Coaxial Cylinder," Thesis for Degree of Engineer, Stanford University, June 1932.

²G. I. Taylor, "Fluid Friction Between Rotating Cylinders," I-Torque Measurements, Proc. Roy. Soc. (London) ser A, vol. 157, 1936, pp. 546-564.

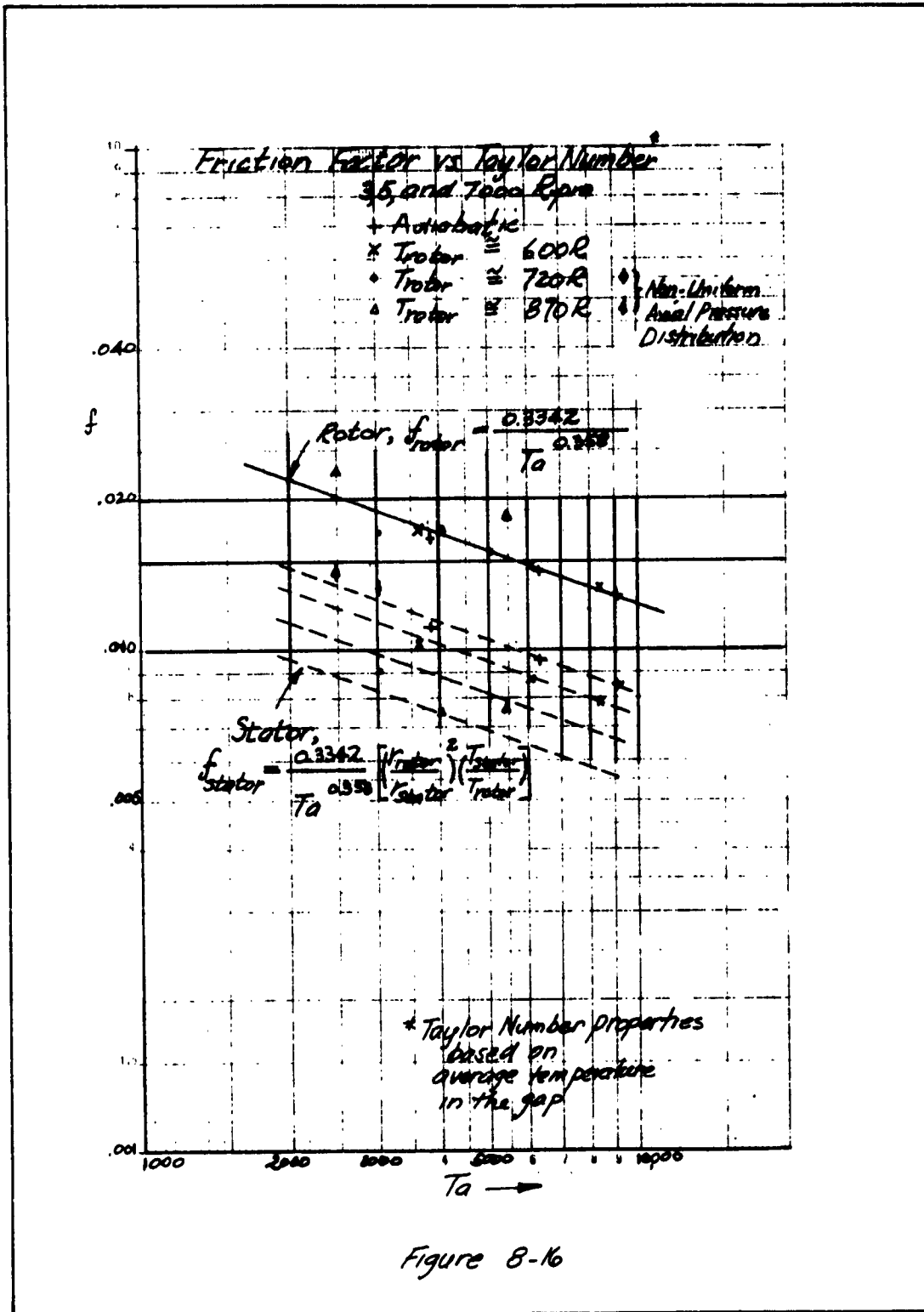
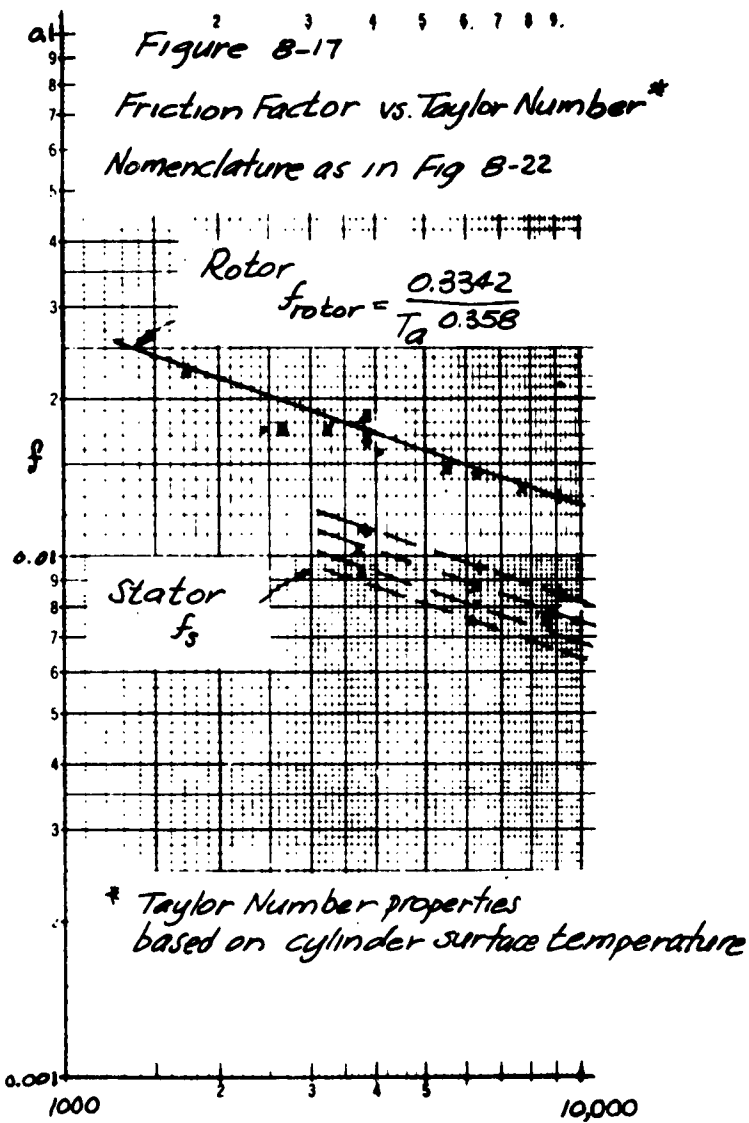


Figure 8-16



water, pentane, glycerine and water, and aviation spirit (18°C) [gasolene?].

Wagner's data have been correlated by Kays and Bjorklund, who have found the relation

$$f_{rotor} Ta / (f_{rotor} Ta)_{lam} = 0.19 Ta^{0.522} \quad (8-2)$$

Agreement of Wagner's data with the correlation is excellent, especially when viewed in the light of the wide variation of f_{rotor} which is d/r_{rotor} dependent. The correlation is achieved by the factor $1 / (f Ta)_{lam}$.

A comparison between the Days and Bjorklund correlation for Wagner's data and the correlation for the present data is shown in Fig. 8-18. Also shown are Taylor's data for $d/r_{rotor} = 0.267$ and Wagner's experimental points for his runs $d = 0.01563$ ft, $d/r_{rotor} = 0.0807$. This was the largest gap he used and d/r_{rotor} was the closest to that of the present experiment (for which $d/r_{rotor} = 0.227$).

The present data, for $d/r_{rotor} = 0.227$, and those of Taylor for $d/r_{rotor} = 0.267$ are lower than the Kays and Bjorklund correlation of Wagner's data.

However, this correlation does well for Taylor's data for $d/r_{rotor} = 0.0278$, 0.0588 , and 0.0108 .

No firm conclusion can be drawn concerning the

adequacy of the correlation, but it appears that at large d/r_{rotor} it is inadequate.

Fig. 8-19 is presented to show the dependence of f_{rotor} on d/r_{rotor} . In this figure, Taylor's data for $d/r_{\text{rotor}} = 0.028$, and 0.267 are included together with Wagner's data for $d/r_{\text{rotor}} = 0.0808$.

It should be noted that

a. The circled points are not Taylor's original data but points taken at convenient places from a smoothed curve of his data as presented in his Fig. 10, pg. 560 in the reference cited, and

b. The shear stress used to compute $\tau/\rho v^2$ in that figure is the stator shear stress.

For small values ^{of} d/r_{rotor} there is little difference between τ_{rotor} and τ_{stator} but for his value $d/r_{\text{rotor}} = 0.267$, $\frac{\tau_{\text{rotor}}}{\tau_{\text{stator}}} = 1.61$. This is mentioned because Gazley¹ in his Fig. 4, "Skin friction on outer cylinder for rotation of inner cylinder and no axial flow", has apparently reported friction factors for Taylor's work based on the shear stress at the rotor rather than the stator.

8.5 Eddy Diffusivity for Momentum, ϵ_M/ν

The quantity ϵ_M/ν can be determined from knowledge

¹C. Gazley, Jr., ASME Paper No. 56-A-128, p. 8.

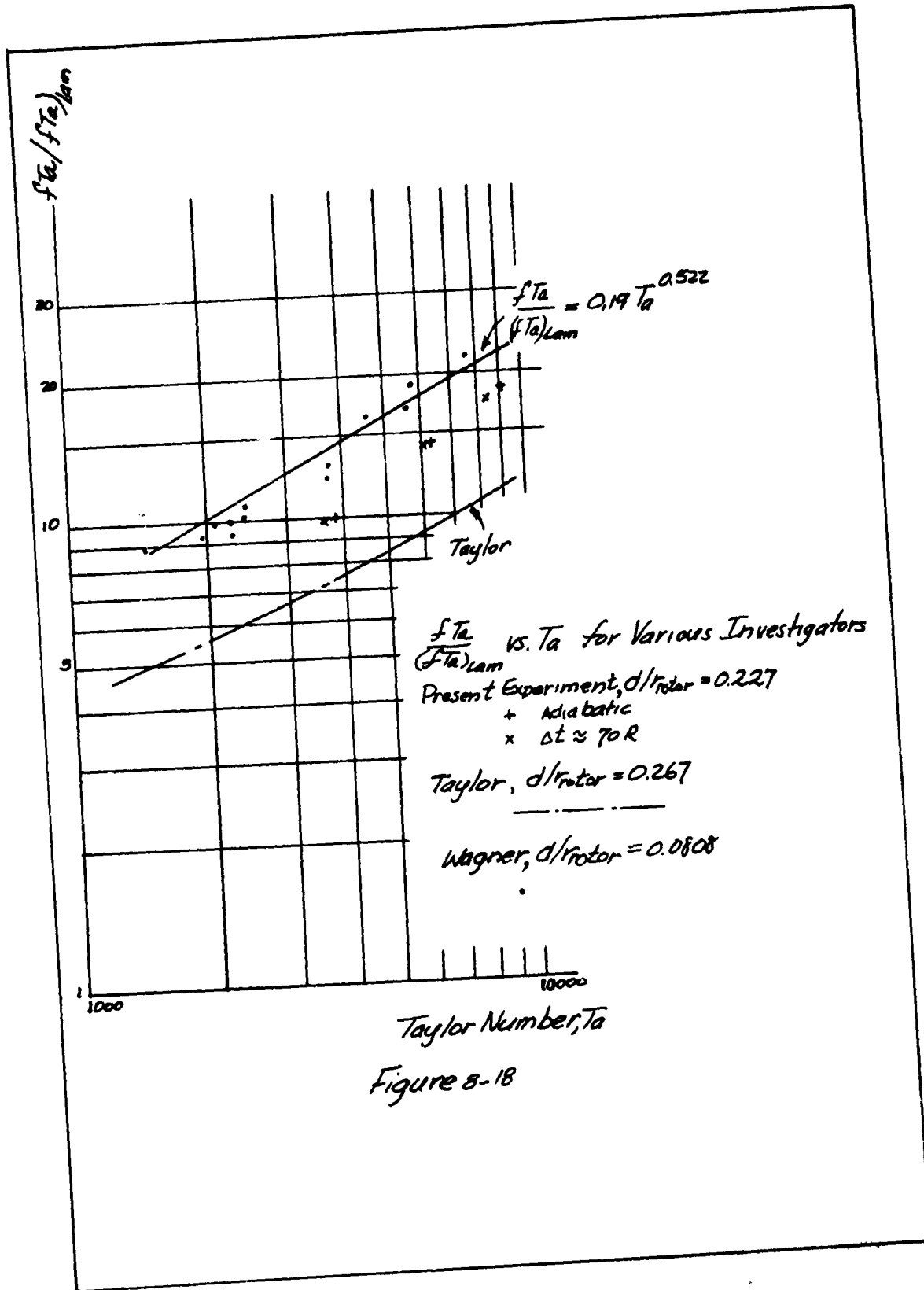
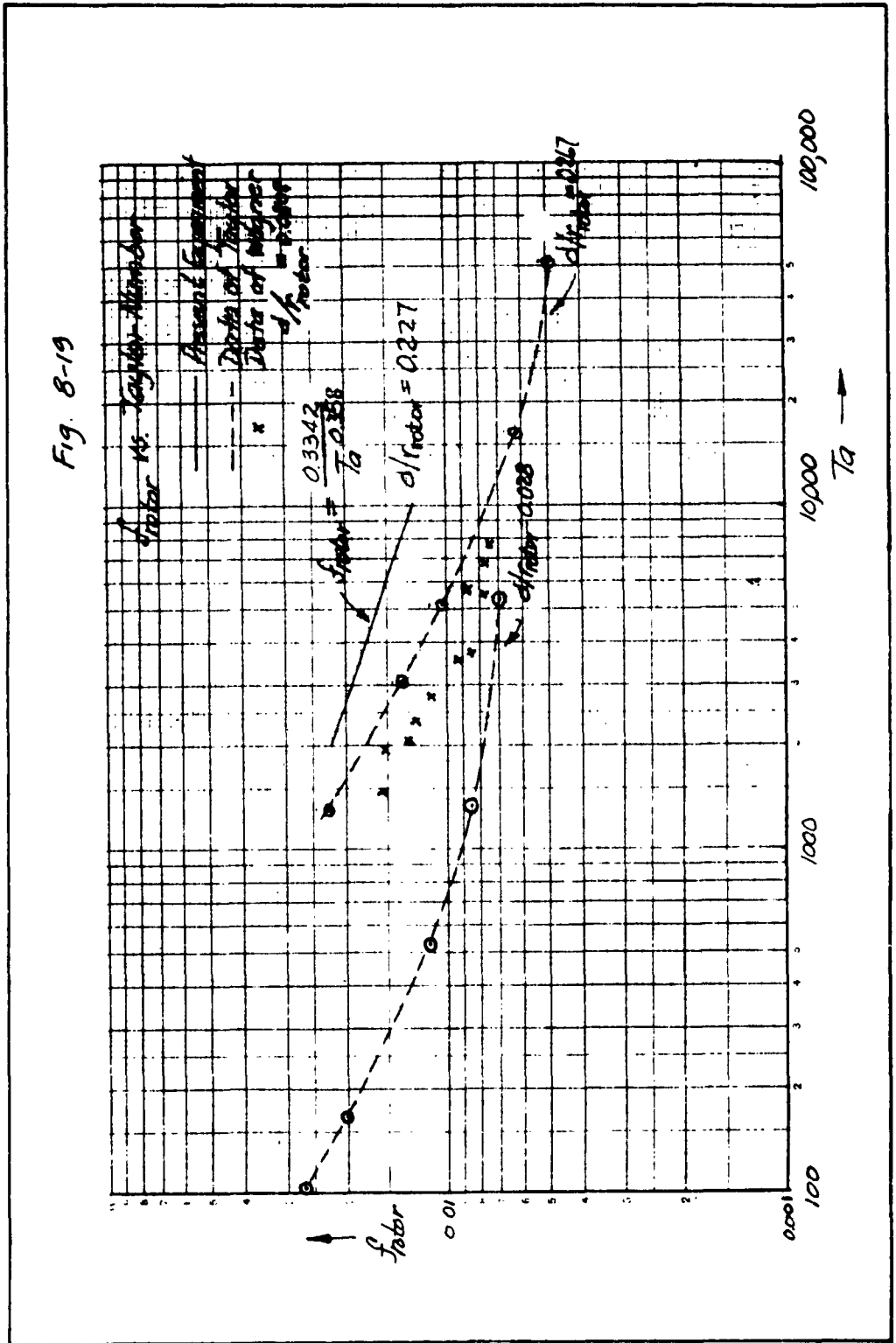


Figure 8-18

Fig. 8-19



of the shear stress, temperature for determination of ϵ_m/ν and dV_e/dr as shown in equation (2-20).

$$\tau_{ro} = -\mu r \frac{dV_e/dr}{dr} (1 + \epsilon_m/\nu)$$

$$\text{Thus } (1 + \epsilon_m/\nu) = -\tau_{ro} / \mu r \frac{dV_e/dr}{dr}$$

The determination of τ_{ro} requires a knowledge of the shear stress at the wall. Before the method for determining u_* at the walls was developed it was decided to present the ϵ_m/ν values in a form which included only experimentally determined quantities. This is accomplished as below:

$$(1 + \epsilon_m/\nu) = -\tau_{ro} / \mu r \frac{dV_e/dr}{dr}$$

Since

$$f = \frac{\tau_w}{\frac{1}{2} \rho_w V_{0c}^2}$$

and

$$\tau_{ro} r^2 = \tau_w r_w^2$$

$$(1 + \epsilon_m/\nu) / f = -\frac{r_w^2 V_{0c}^2}{2 r_w \mu} \left(\frac{\mu_w}{\mu} \right) \frac{1}{r \frac{dV_e/dr}{dr}} \quad (8-3)$$

8.5.1 ϵ_m/ν Near the Wall

In Fig. 8-20 are presented $(1 + \epsilon_m/\nu) / f$ versus y^+ for the various rpm and temperature differences. The correlation is good especially when it is considered that the variation of \mathcal{Z} for the runs presented is from $\mathcal{Z} = 3.8 \times 10^{-4}$ at 890 R to $\mathcal{Z} = 1.6 \times 10^{-4}$ for 540 or 2.4 times.

As $y^+ \rightarrow 0$, $\frac{1.4\epsilon_M/2}{f} \rightarrow \frac{1}{f}$, hence the divergence of the lower ends of the curves in Fig. 8-20.

In an attempt to arrive at a universal correlation it was decided to correlate $\epsilon_M/2$ vs y^+ . These correlations are shown in Fig. 8-21.

In Fig. 8-22 are shown the curves finally selected as representing $\epsilon_M/2$ for the range of speed 3000 rpm to 7000 rpm and the range of temperature of the rotor 890 R to 600 R.

8.5.1.1 Comparison with other Investigators

8.5.1.1.1 Experimental work of Sleicher

For purposes of comparison with the work of Sleicher, values of ϵ_H vs y^+ have been plotted against together with the curve suggested by Sleicher for pipe flow at temperature differences 0 - 20 F and a Reynold's number range of 14,200 to 80,500. This is shown in Fig. 8-23.

The eddy diffusivity for heat, ϵ_H has been plotted rather than ϵ_M since it was this quantity that Sleicher evaluated from his experimentally determined temperature distributions. For the present date, use was made of the experimental fact, not yet discussed, that $\alpha = \epsilon_H/\epsilon_M = 1.4$. Values of $\epsilon_M/2$ were then multiplied by 1.4 to yield $\epsilon_H/2$.

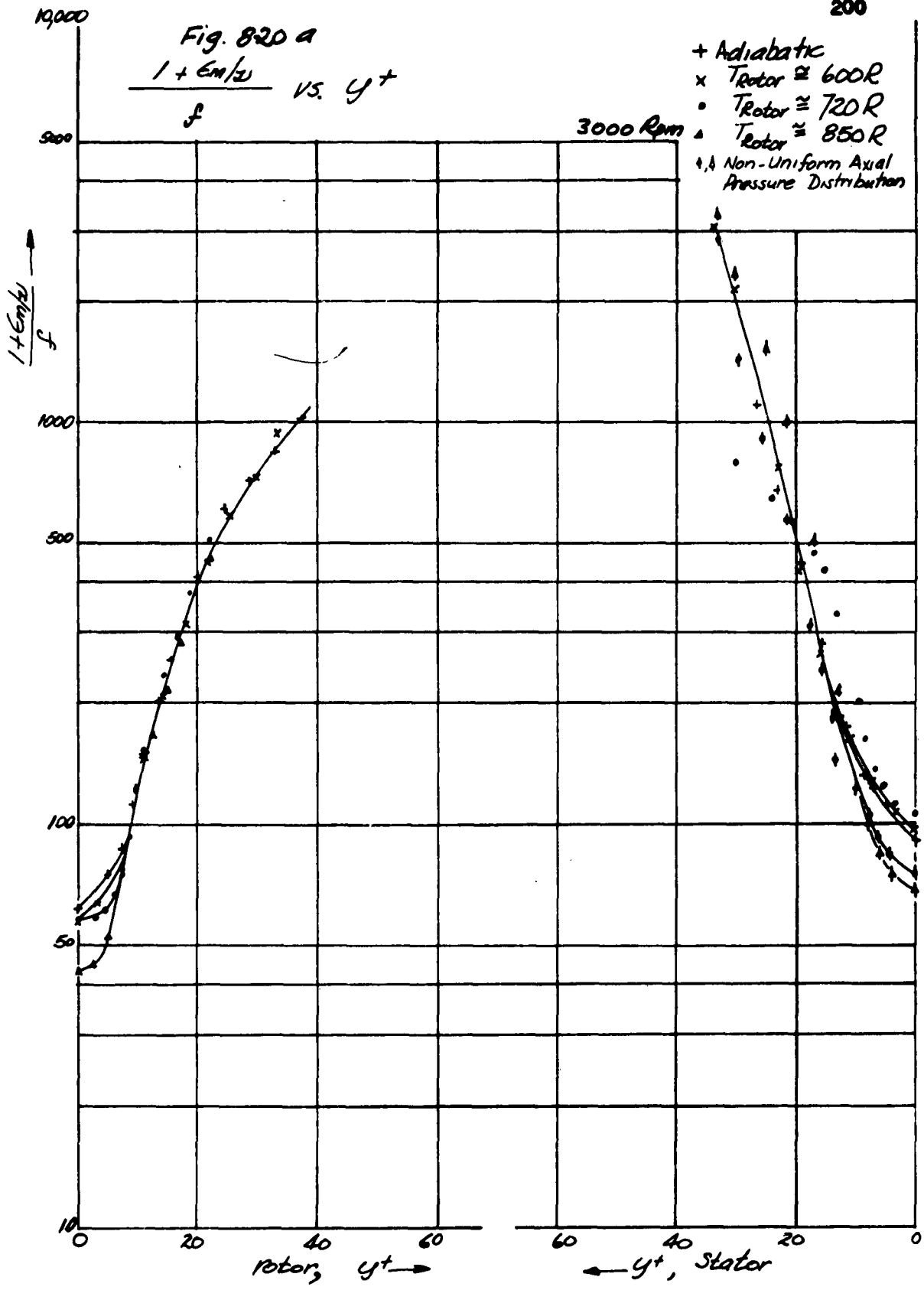
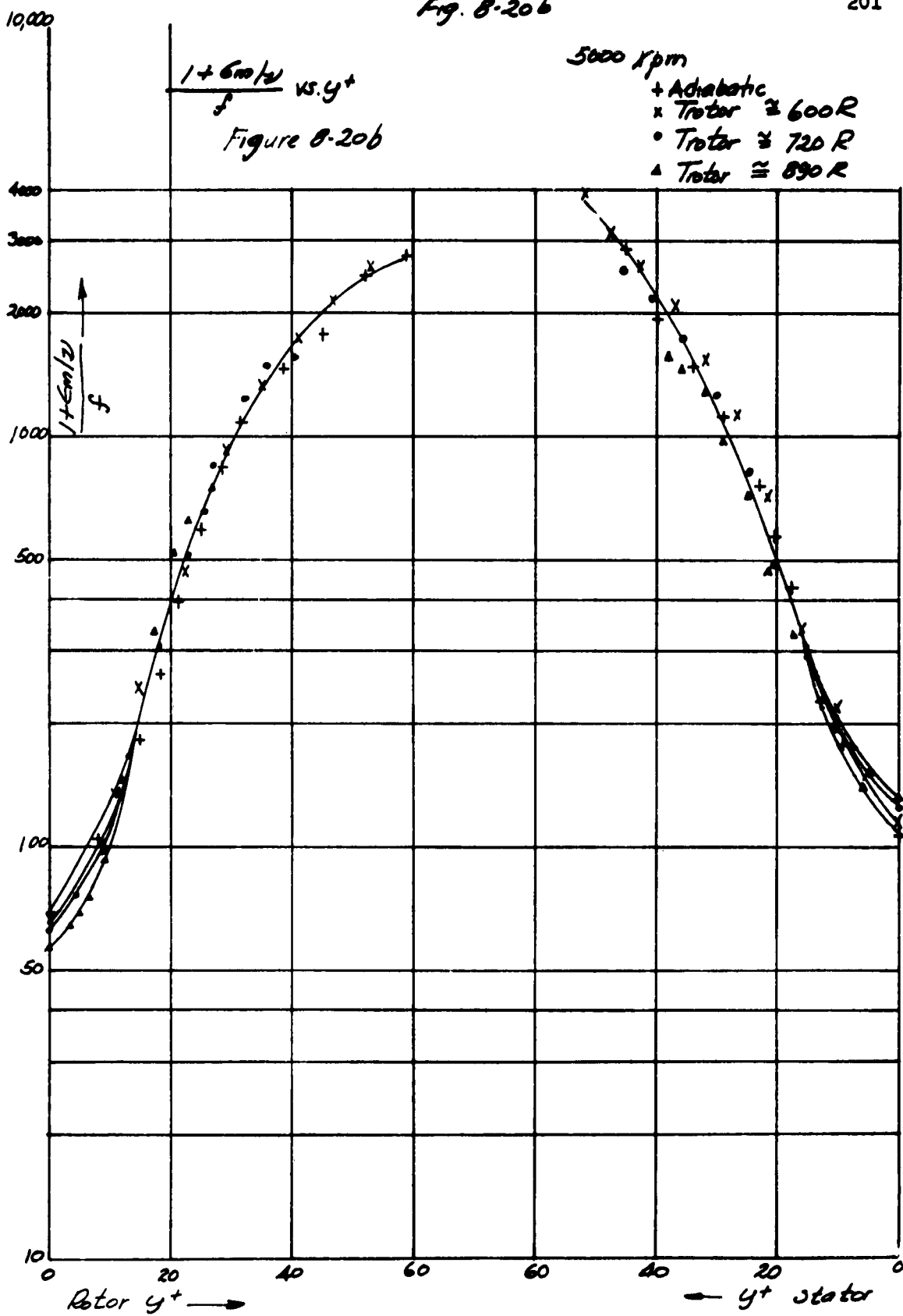
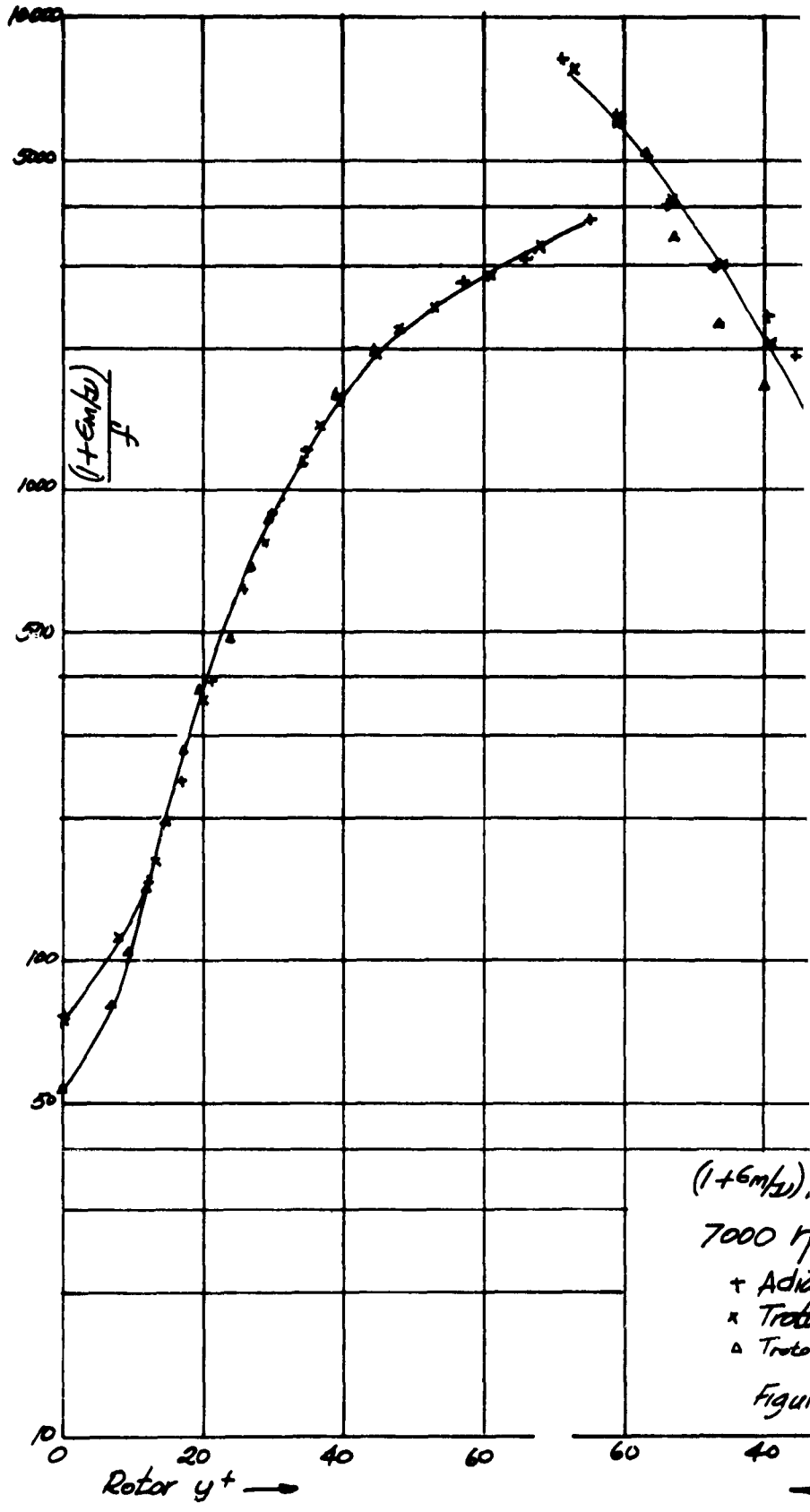
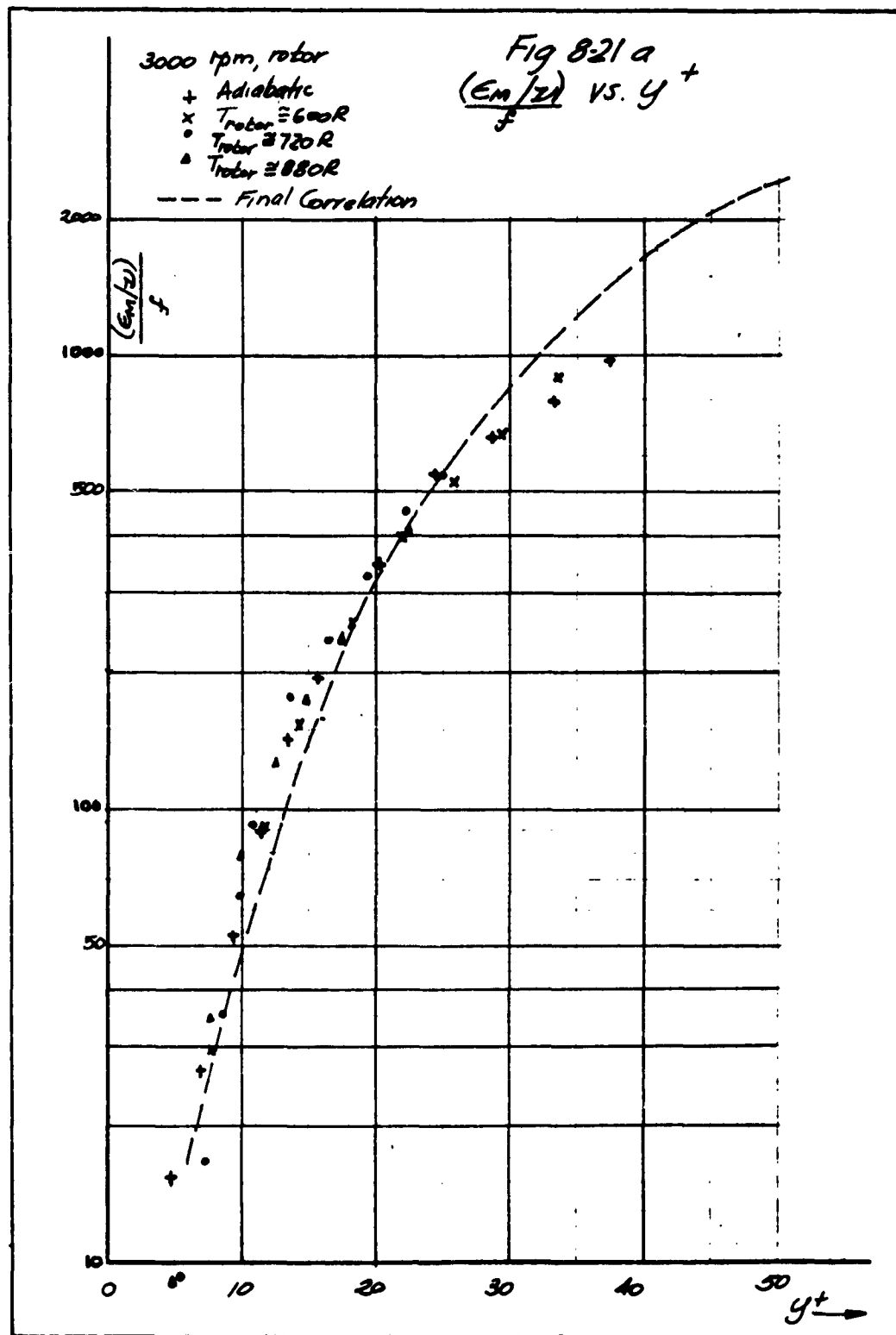
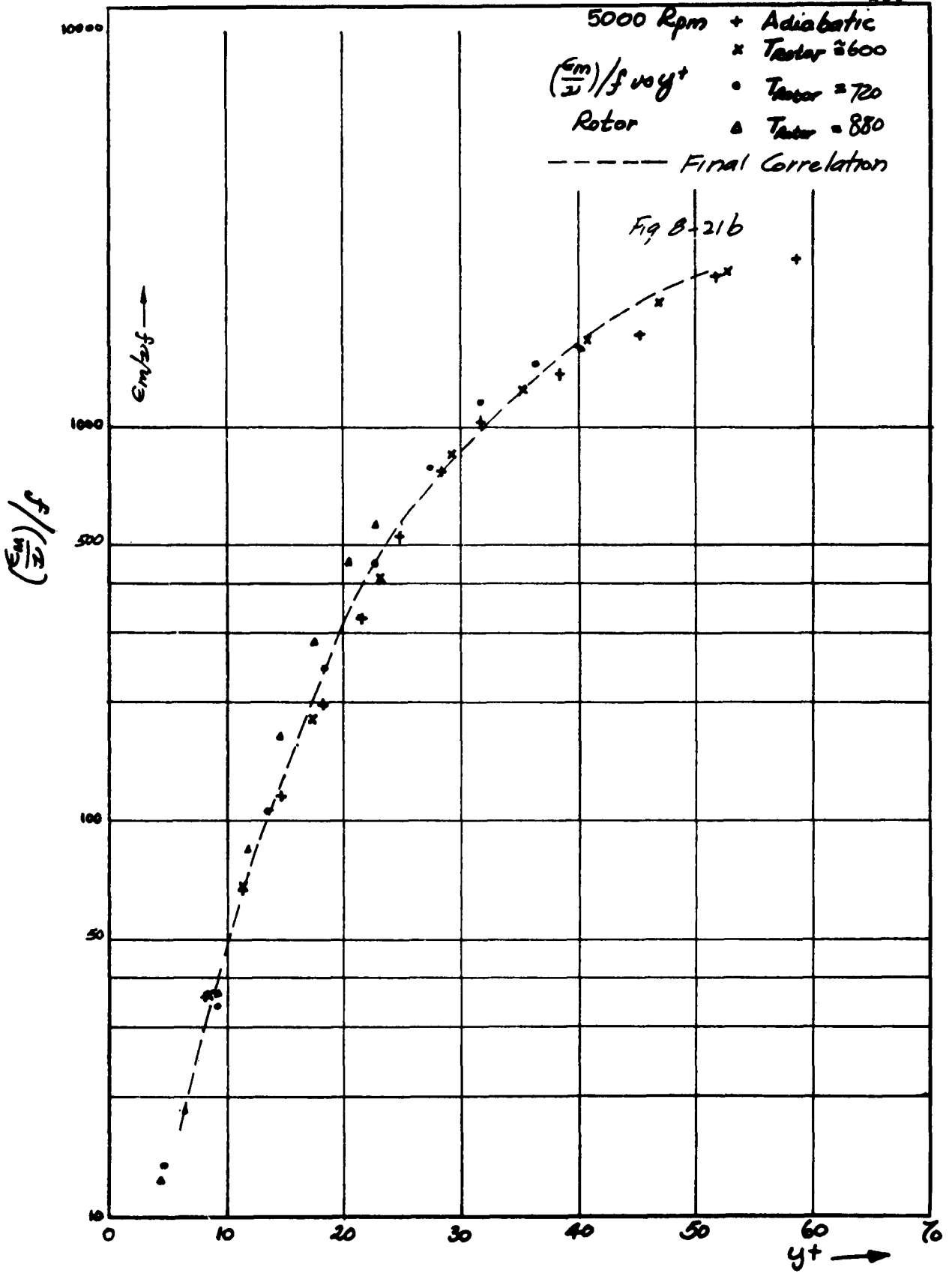


Fig. 8-20b







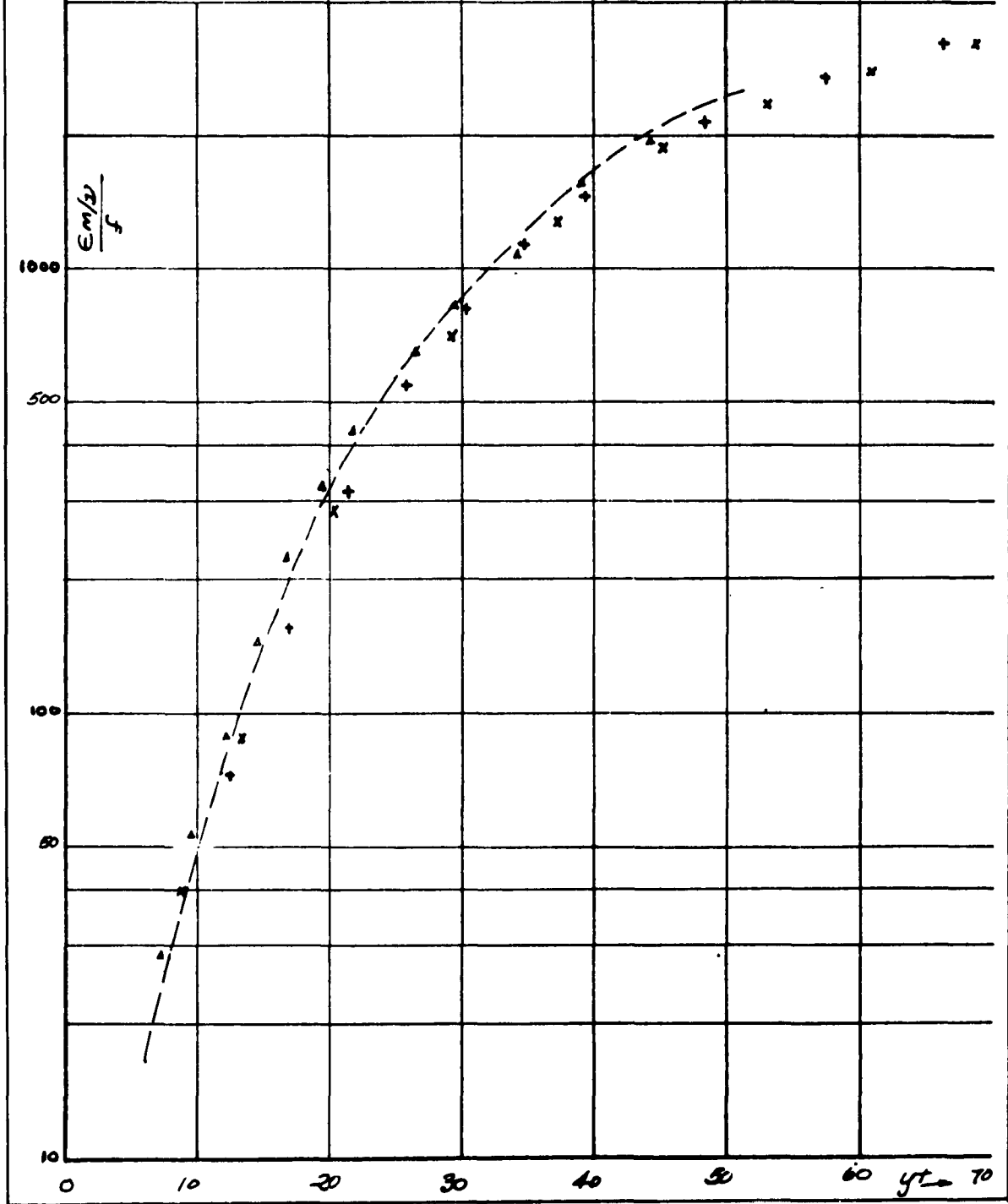


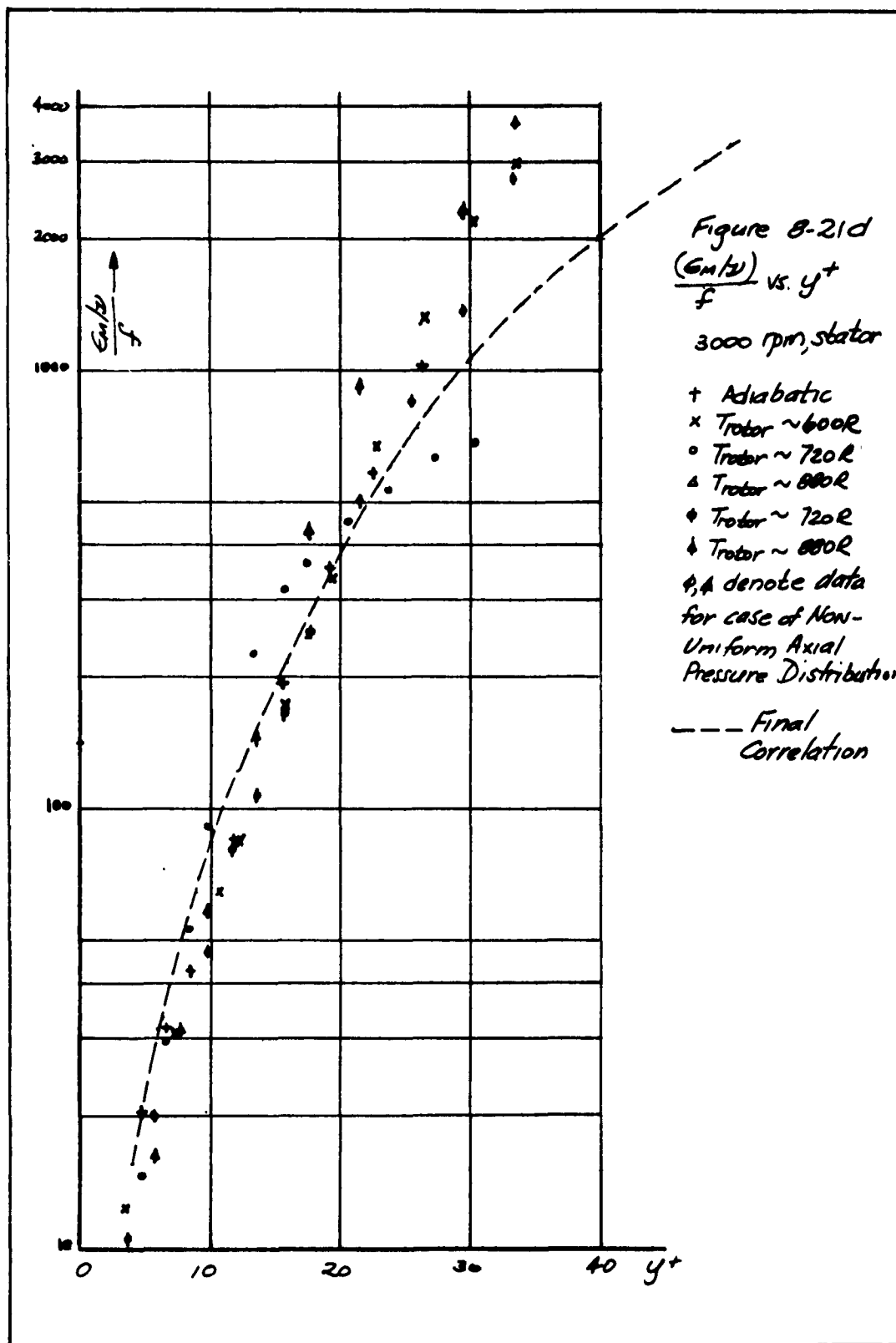
7000 rpm, rotor

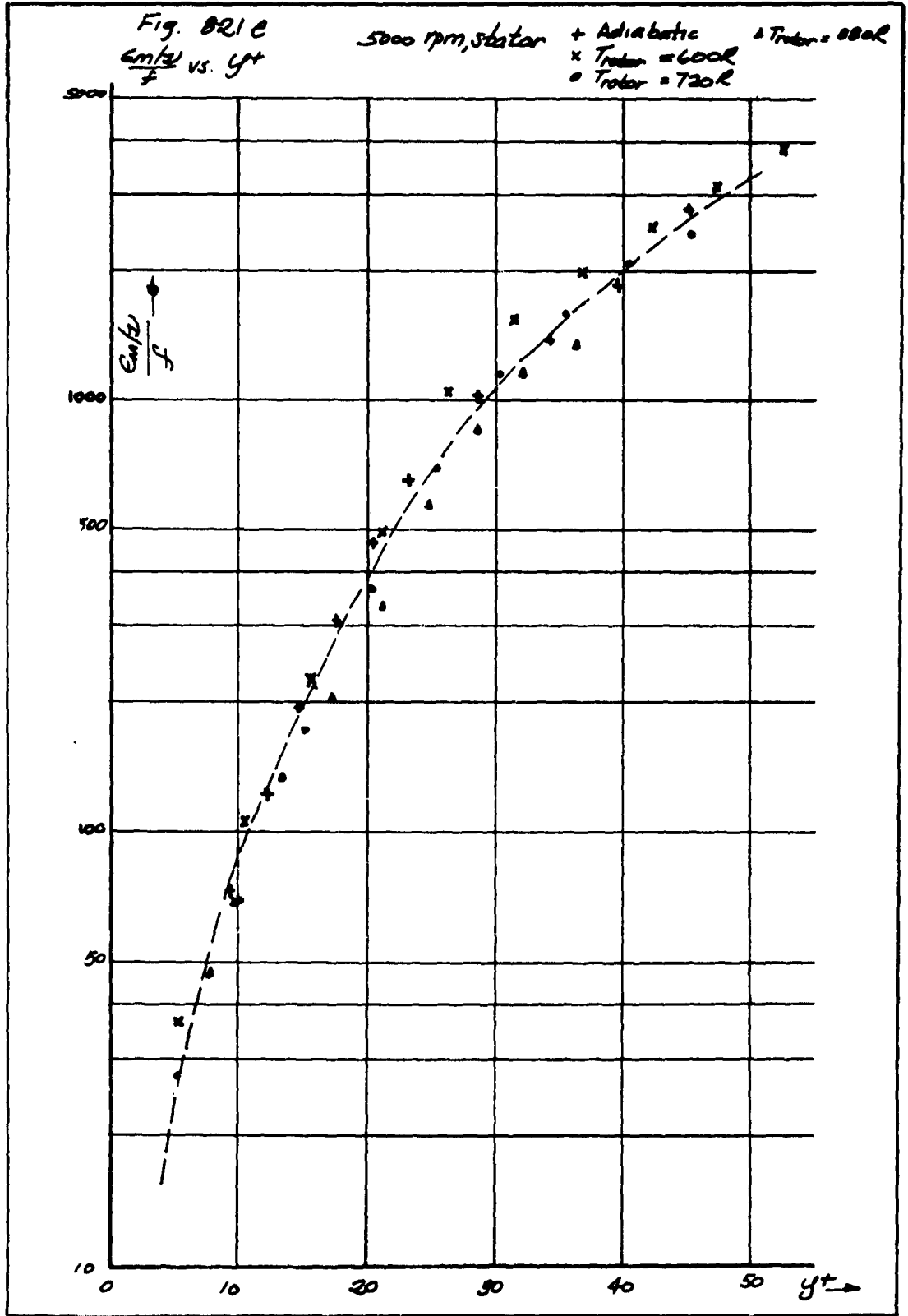
- + Adiabatic
- x T rotor \cong 600R
- o T rotor \cong 720R
- Δ T rotor \cong 890R

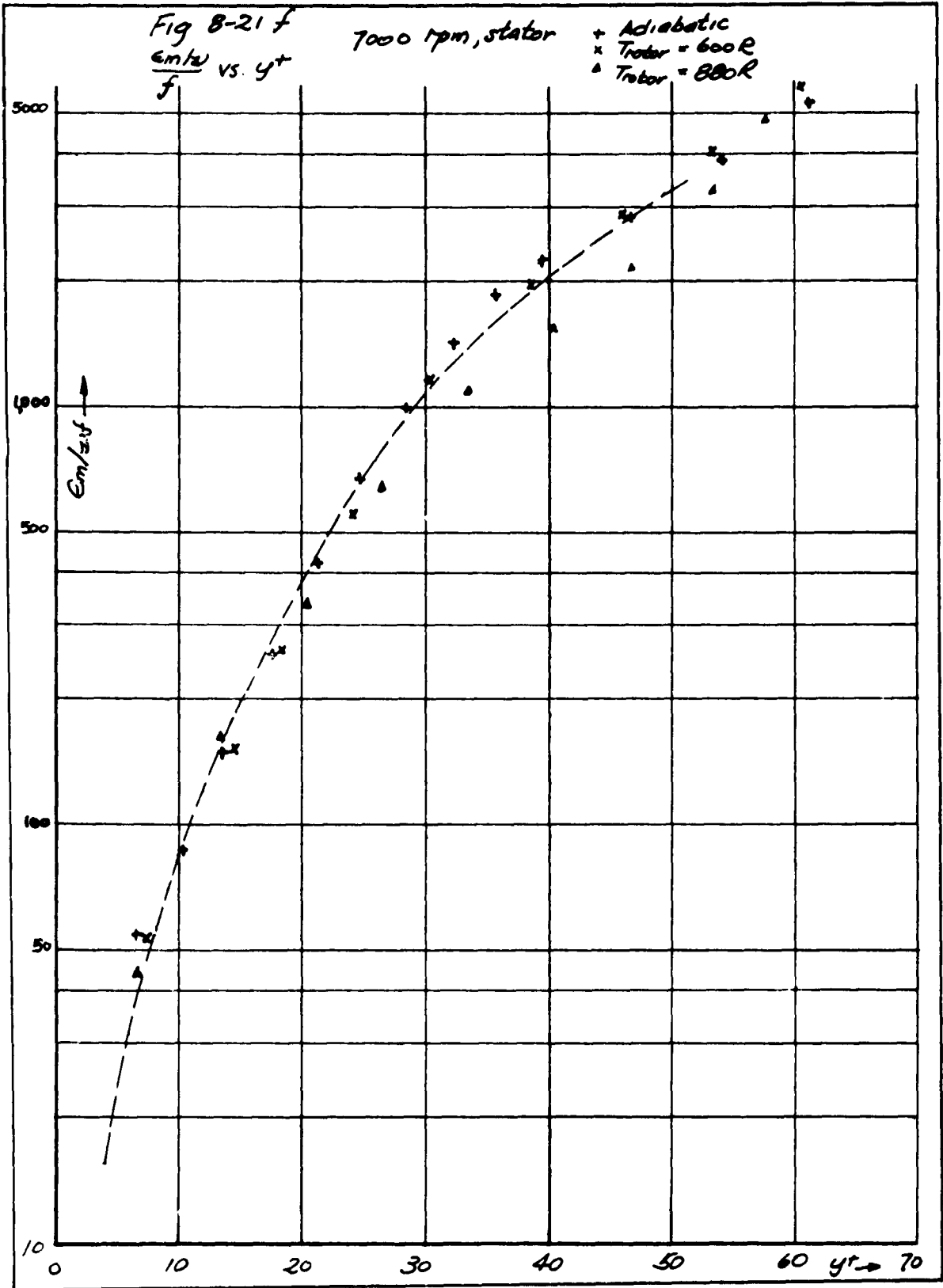
Fig 8-21c
 $\frac{(E_m/w)}{f}$ vs. y^+

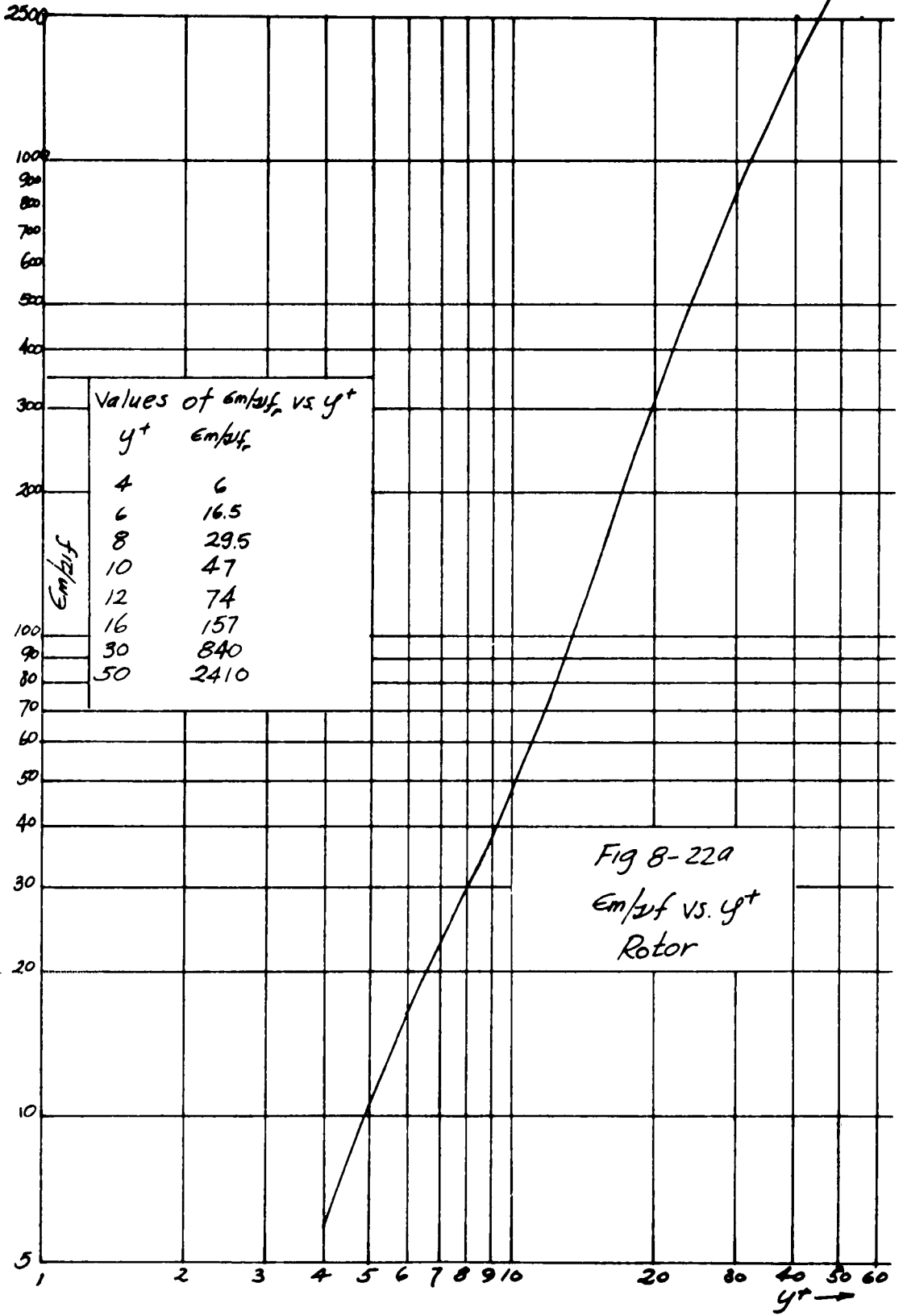
----- Final Correlation

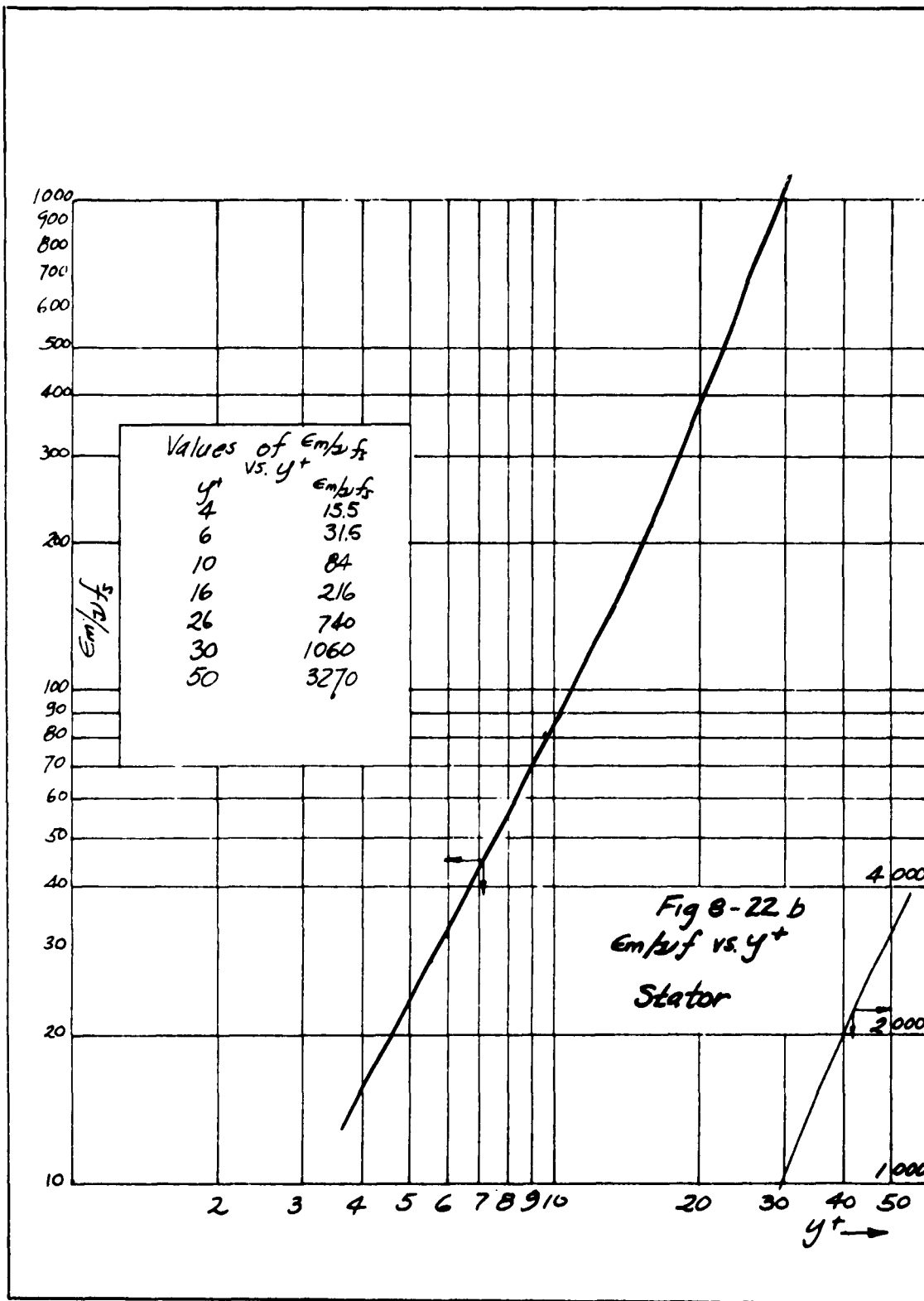


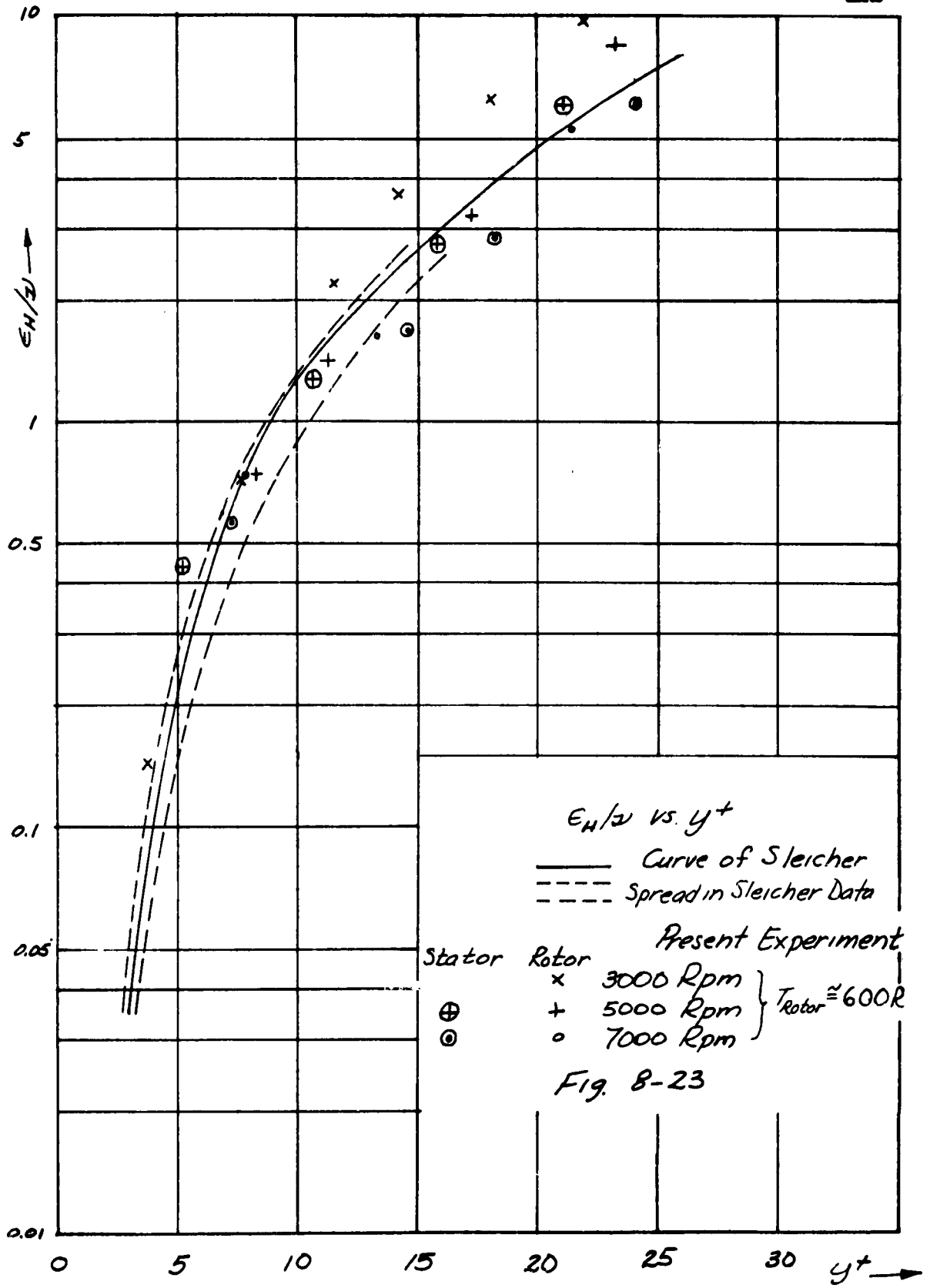


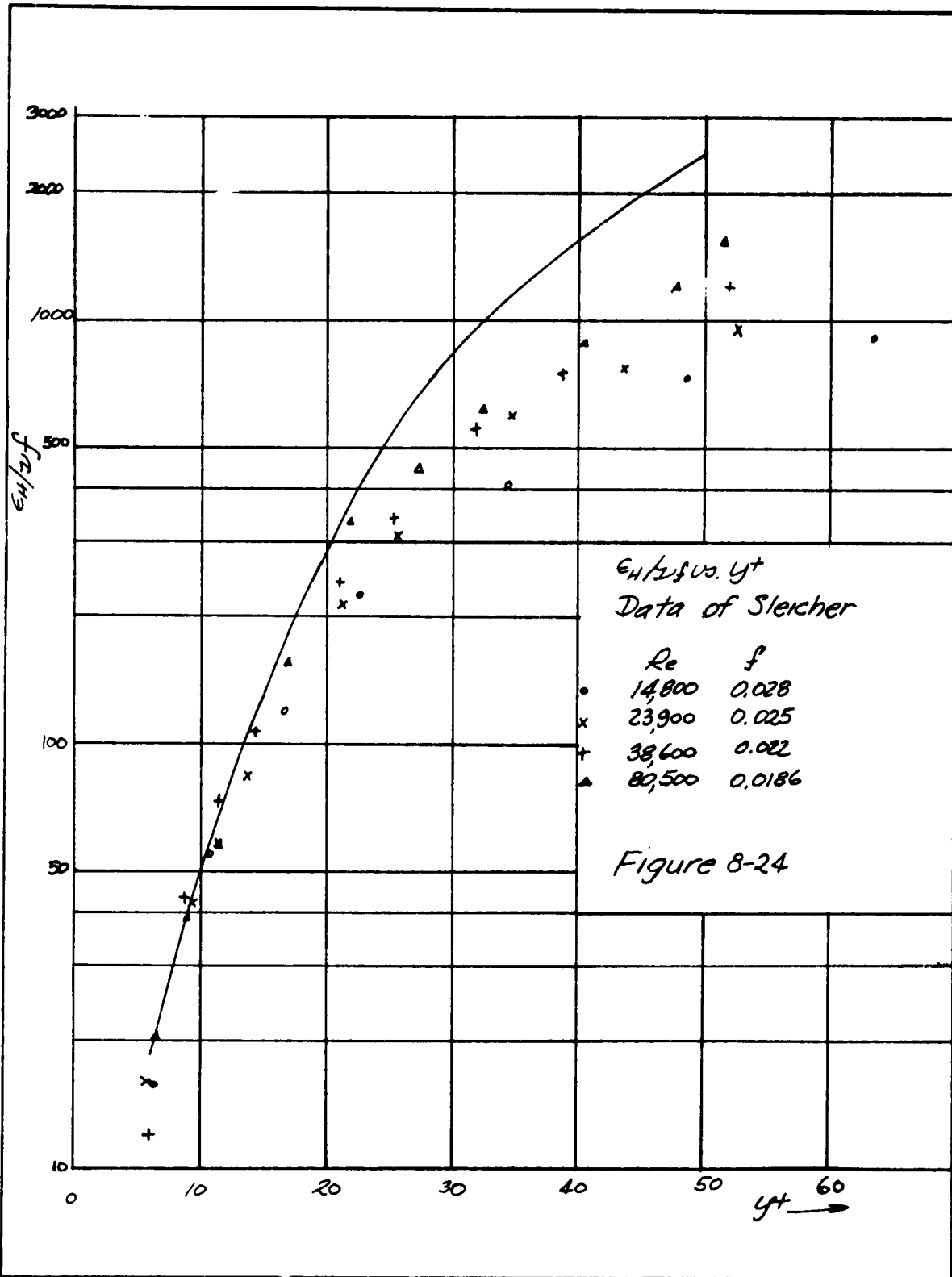












Shown dashed in the figure are lines representing the range of Sleicher's experimental points. The lower dashed line results mostly from data from two runs, those at $Re \approx 80,500$, the highest experimental value of Re at which Sleicher reports data. The Reynolds number for his other runs varied from 14,000 to about 38,000, and these data are closer to his suggested curve.

Referring to the figure, note that a correlation for the present data of ϵ_m/ρ vs. y^+ is not as effective as the one finally selected, of $\epsilon_m/\rho f$ vs. y^+ .

If Sleicher's data are presented on an $\epsilon_m/\rho f$ vs. y^+ basis as in Fig. 8-24 a better correlation is obtained for his data out to y^+ of about 20. Shown also is the relation $\epsilon_m/\rho f$ for the present work shifted in the $\epsilon_m/\rho f$ direction so as to lie with Sleicher's data. The agreement between the shapes of the curves in this region is rather good.

8.5.1.1.2 Comparison With Formulations of Deissler and Van Driest

For the value of eddy diffusivity near the wall Deissler has suggested¹

$$\frac{\epsilon_M}{\nu} = \frac{1}{64} u^+ y^+ \left[1 - e^{-\frac{u^+ y^+}{64}} \right] \quad (8-4)$$

and Van Driest has suggested²

$$\frac{\epsilon_M}{\nu} = \frac{1}{2} \left\{ 1 + 4 K^2 (y^+)^2 \left[1 - e^{-\frac{y^+}{A^+}} \right]^2 \right\}^{-1/2} \quad (8-5)$$

where K and A^+ are experimentally determined constants with the values $K = 0.4$, and $A^+ = 26$.

These relations are plotted in Fig. 8-25 together with the range of values for the present experiment. That is, the universal curve of Fig. 8-22 has been multiplied by the range of friction factors encountered during the experiment, the higher ones for 3000 rpm, and the lower ones for 7000 rpm.

It is seen that the correlation used, ϵ_M/ν vs. y^+ results in a variation in eddy diffusivity for momentum with Reynolds number. Since the original velocity data near the wall were placed on a single curve of V_θ^+ vs. y^+ a small error results in the use of the present correlation. For the

¹C. C. Lin, Turbulent Flows and Heat Transfer (Princeton University Press, Princeton, New Jersey, 1959), Section E, by R. G. Deissler, p. 230.

²E. R. Van Driest, "On Turbulent Flow Near a Wall," Heat Transient and Fluid Mechanics Institute Preprints of Papers, Paper 12, University of California, 1955.

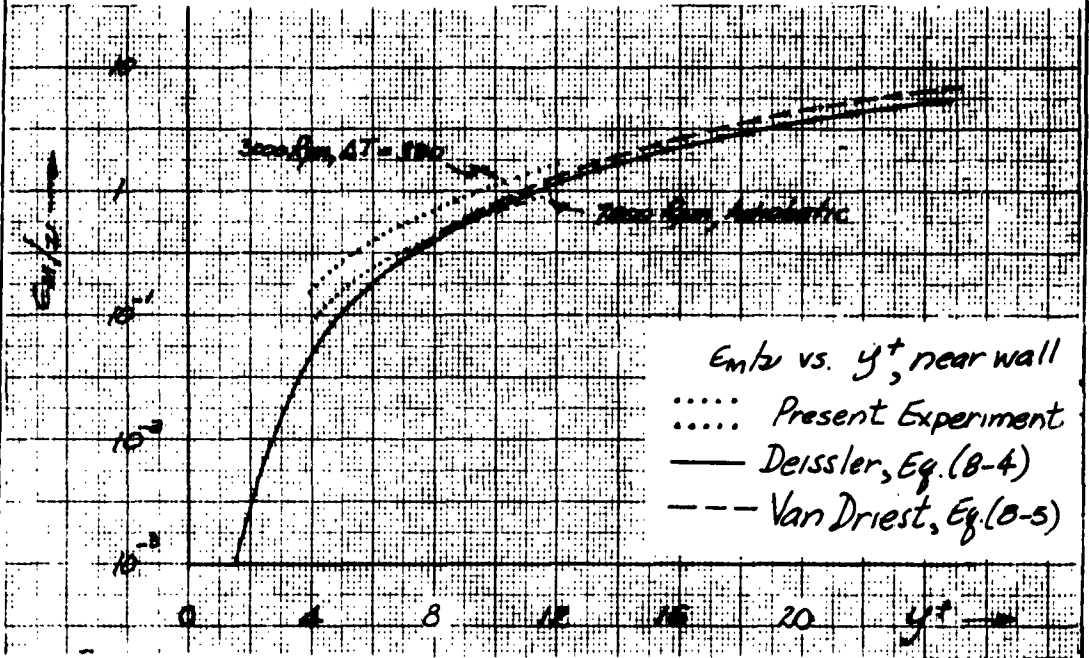


Fig B-25
 Comparison of Present Experiment
 with Formulations of Deissler and
 Van Driest for $Em/2$ near a Wall

range of friction factors found in the present experiment the error in ϵ_m/ν is small at low y^+ being of the order of $\pm 10\%$. This is in a region of y^+ where the eddy diffusivity is very small. Therefore, small error is made in the computations for overall heat-transfer and friction which follows.

It is interesting to note that Sleicher's experimental data show a Reynolds number dependence close to the wall.

8.5.2 ϵ_m/ν in the Center of the Gap

Because the velocities in the center of the gap were not determined at sufficiently close intervals so that eddy diffusivities for momentum in the center of the gap could be determined by the same methods as in Section 8.5.1.1 these quantities were determined as below:

$V_{\theta r}$ was almost, but not quite constant in the middle of the gap. As stated in Section 8.3.2, $V_{\theta r}$ was found to be a function of r according to

$$V_{\theta r} = ar + b$$

Values of $V_{\theta r}$ vs. r for 5000 rpm are given in

Table VIII-1.

Table VIII-I

$V_{\theta r}$ in the Central Region Expressed as a Function

of r , for 5000 rpm, $0.146 < r < 0.156$

rpm	$\Delta t, R$			
5000	0	$V_{\theta r}$	=	$24.9066r + 1.1494$
	60	$V_{\theta r}$	=	$17.9372r + 2.1223$
	160	$V_{\theta r}$	=	$16.8492r + 2.34945$
	360	$V_{\theta r}$	=	$18.9400r + 2.0811$

From these relations $\frac{dV_{\theta}r}{dr}$ can be found and hence ϵ_m/ω .

Typical values for ϵ_m/ω vs. r for various rpm are given in Table VIII-II

In order to develop a relation for ϵ_m/ω in the center of the gap which did not depend on a knowledge of the variation of $V_{\theta}r$ with r , $V_{\theta}r$ was assumed constant in that region.

Thus

$$V_{\theta}r = A$$

and

$$r \frac{dV_{\theta}r}{dr} = -\frac{2A}{r^2}$$

and in the center of the gap

$$= -\frac{2V_{\theta}r c}{r^2} = -\frac{2V_{\theta}c}{r}$$

Using the following

$$(1 + \epsilon_m/\omega) \mu r \frac{dV_{\theta}r}{dr} = T r_0$$

$$f_{rotor} = \frac{2 T r_{rotor}}{r_{rotor} V_{\theta} c^2}$$

$$V_{\theta} c = \frac{V_{\theta, rotor} r_{rotor}}{2r_c}$$

$$T r_{rotor} r_{rotor}^2 = T r^2$$

$$T a = \frac{V_{\theta, rotor} d}{2r_c} \sqrt{\frac{d}{r_{rotor}}}$$

and assuming

$$T_c = 1/2 (T_{\text{rotor}} - T_{\text{stator}})$$

one obtains

$$(1 + \epsilon_m/2)_{\text{center}} = 1/16 (r_{\text{rotor}}/r_c)^2 (1/d/r_{\text{rotor}})^{3/2} f_{\text{rotor}} \left(1 + \frac{T_{\text{stator}}}{T_{\text{rotor}}}\right) Ta$$

The value of $\epsilon_m/2$ obtained from this equation is incorrect because even though the variation in $V_{\theta}r$ is small an error amounting to approximately 60% is introduced by assuming $V_{\theta}r = \text{constant}$ rather than the correct formulation $V_{\theta}r = ar + b$. Accordingly, since the correct values were known the equation above was multiplied by a constant factor adjusted to give the correct value of $\epsilon_m/2$ in the center of the gap. This works rather well and does so because the product of rpm and the slope of the curve $V_{\theta}r$ vs. r is about constant.

The final result for the eddy diffusivity in the central portion of the gap, for $1.75 < r'' < 1.95$, is

$$(1 + \epsilon_m/2) = 0.0894 (r_{\text{rotor}}/r_c)^2 (1/d/r_{\text{rotor}})^{3/2} f_{\text{rotor}} \left(1 + \frac{T_{\text{stator}}}{T_{\text{rotor}}}\right) Ta \quad (8-6a)$$

Making use of the relationship between f_{rotor} and Ta ,

$$f_{\text{rotor}} = \frac{0.3342}{Ta^{0.358}}$$

and the dimensions of the present apparatus, there results

$$(1 + \epsilon_m/2)_{1.75 < r'' < 1.95} = 0.227 Ta^{0.642} \left[1 + \frac{T_{\text{stator}}}{T_{\text{rotor}}}\right] \quad (8-6b)$$

A comparison of this formulation with the values obtained from the velocity distribution is shown in Table VIII-II.

Table 8-2
Values of $\frac{6m}{\lambda}$ in Center of Gap

Rpm	$\Delta T, R$	Value in center of gap computed from $V_{gr} = ar + b$	Computed from eq. (8-6)b
5000	0	138	124.3
	60	113.5	113.8
	160	86	94.6
	360	75	75.9
7000	0	162	157.1
	60	141.5	141.4
	360		

Agreement is acceptable.

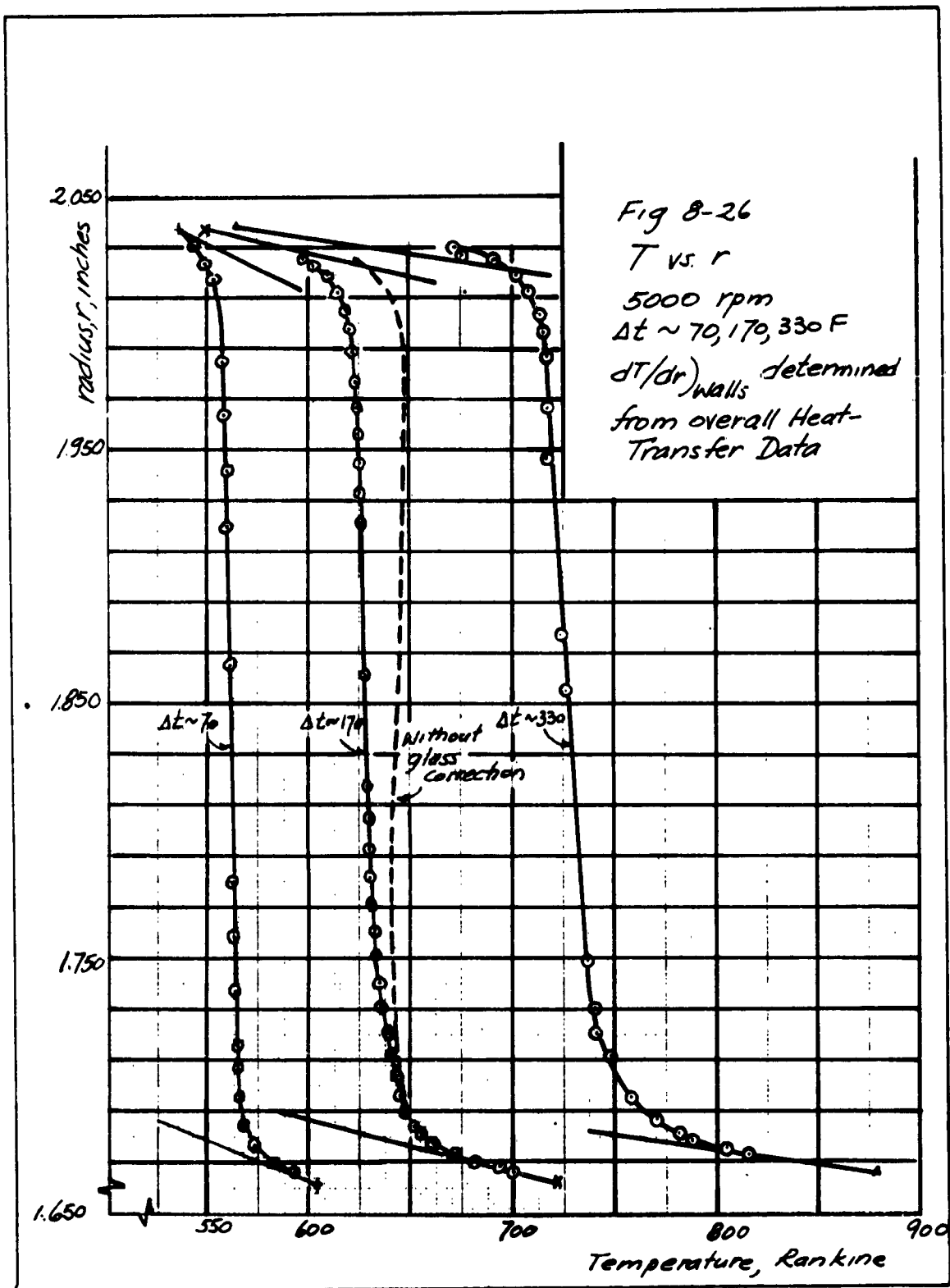
8.6 Temperature Measurements

8.6.1 T vs. r

Representative curves of T vs. r are shown in Fig. 8-26.

Because refractive effects over the cooled stator resulted in an interference similar to Lloyd's mirror interference (see Sec. 5.4.1) data could not be obtained near the rotor. This interference effect is clearly shown in Fig. 8-27a, which is an interferogram from a typical run.

Further although the glass correction was small for



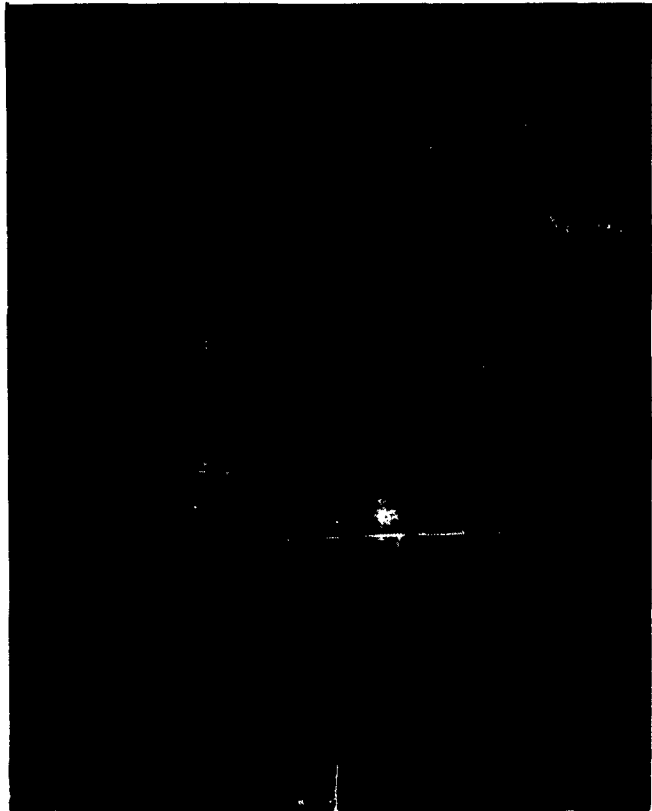


Figure 8-27b
Spark Interferogram

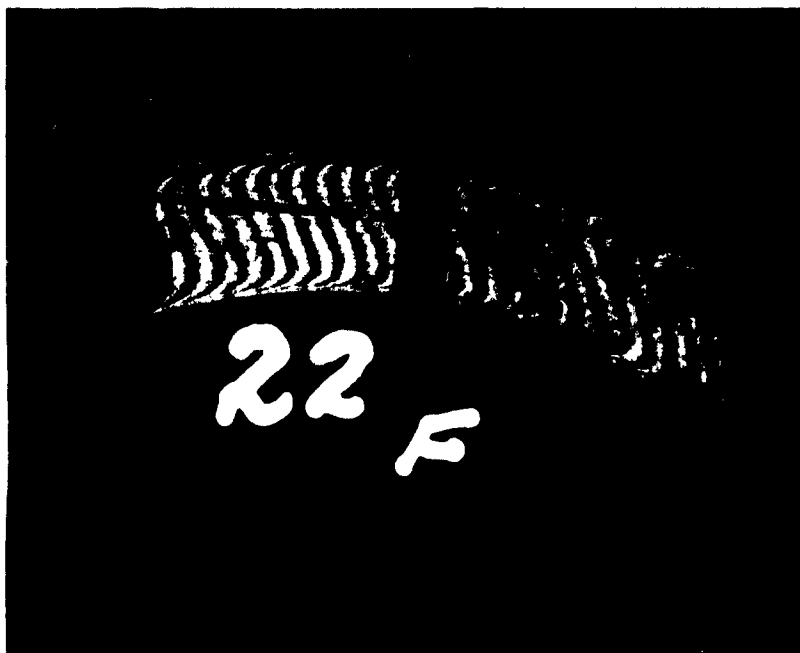


Figure 8-27a
Typical Interferogram
showing
Refractive Effects of Cooled stator

small change in r , the cumulative effect of errors in the correction, which was applied starting at the rotor, over the entire gap width is clearly in evidence.

Also shown is an interferogram taken with a single flash of the mercury vapor lamp. This technique was used at high speeds and density gradients because rotor run-out of 0.0015" caused blurring of the fringes during exposure times required for continuous operation of the lamp.

8.6.2 T vs. V_θ / r ; The Determination of α

Of interest is the variation of T with V_θ / r . Fig. 8-28 shows the variation of T versus V_θ / r in the gap for several runs.

The graphs were prepared in the following manner:

On the rotor surface T_{rotor} is known from thermocouple measurements, and V_θ / r from the speed of the rotor.

The straight line drawn is $(dT/dV_\theta/r)_{\text{wall}}$ and is obtained from $(dT/dr)_{\text{wall}}$, known from overall heat transfer measurements and $(dV_\theta/r/dr)_{\text{wall}}$ known through \mathcal{U}_* . The straight line drawn is independent of interferometer measurements used to obtain T and total pressure measurements used to obtain V_θ / r .

The converse however is not true so far as temperature is concerned because of the manner in which the temperature of

the first measured point on the interferogram was determined (see Section 6.3.1.2). This is considered to have a negligible effect on the results for two reasons. First, although the temperature distribution was "tied" to dT/dr at the wall the first measured velocity occurred at a distance of the order $y/r = 5$ to 8.

On the interferograms however, data is obtained somewhat closer to the wall than this so that the first point shown on the graph T vs. V_θ/r over the rotor is separated from the first measured interferometric point by two or three measurements of temperature, influence not only by $(dT/dr)_{wall}$ but also by the intervening fringe shifts.

Secondly, the distribution measured from an interferogram is Δp vs. r . An incorrect choice of a reference temperature will influence the distribution of ΔT vs. r by a negligible amount. Thus, if an incorrect reference temperature is chosen the level of the T vs. V_θ/r curve is affected in T , but not the shape of the curve. As can be seen in Fig. 8-28, T has a straight line relationship with V_θ/r near the walls.

From equations (2-30) and (2-31), repeated here

$$Rr \alpha = \frac{2/\epsilon m (1-x) + 1}{x} \quad (2-30)$$

$$x = \frac{dT/dV_\theta/r}{\{dT/dV_\theta/r\}_{wall}} \left(\frac{r_w}{r}\right)^2 \quad (2-31)$$

it is seen that since close to the wall $(r_w/r)^2$ is very

nearly unity¹ and since in that region:

$$\frac{dT}{dV/r} = \left\{ \frac{dT}{dV/r} \right\}_{wall},$$

$$x = 1$$

From equation 2-30, for $x = 1$

$$D_r \alpha = 1$$

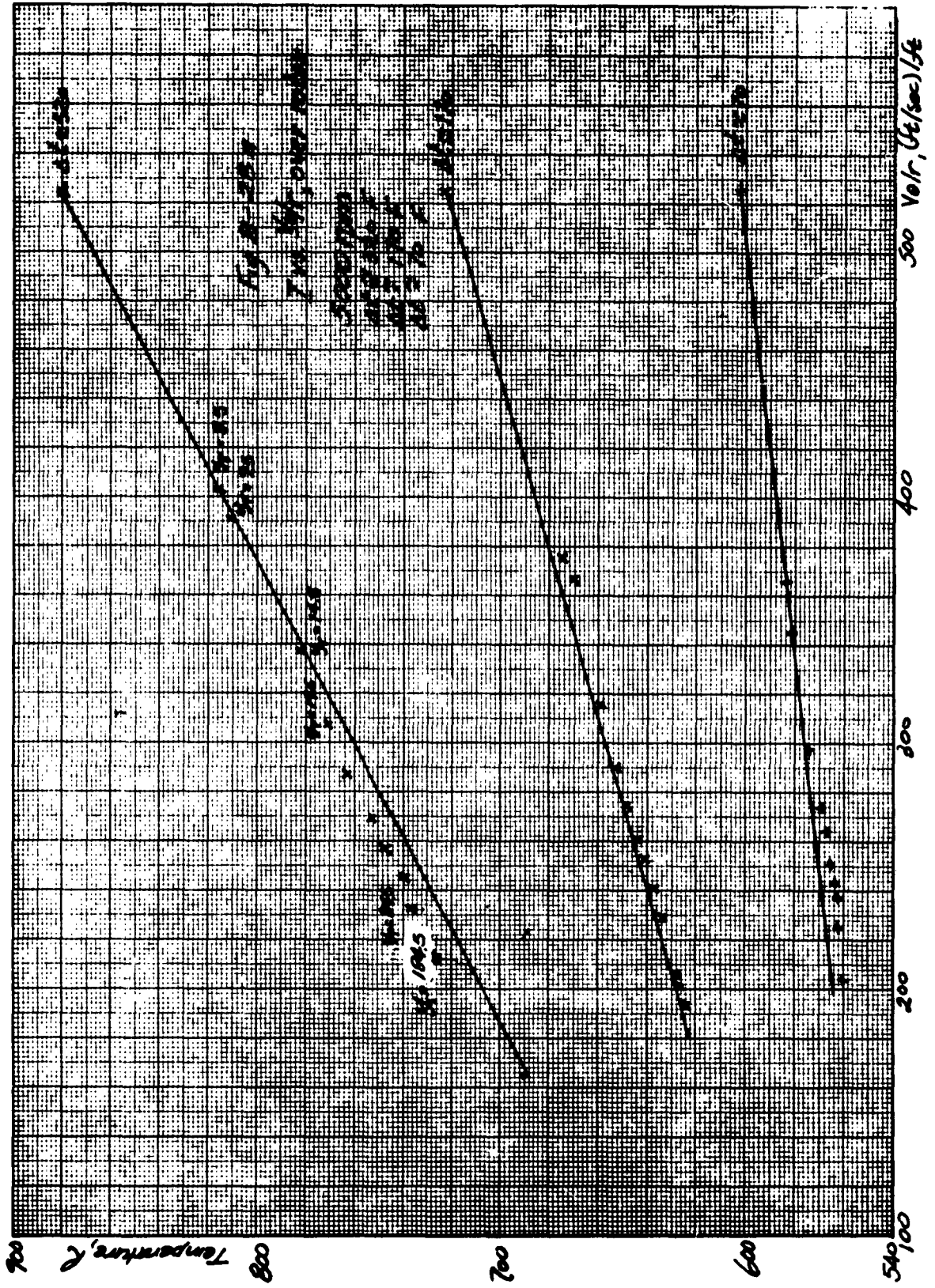
$$\alpha = 1/R$$

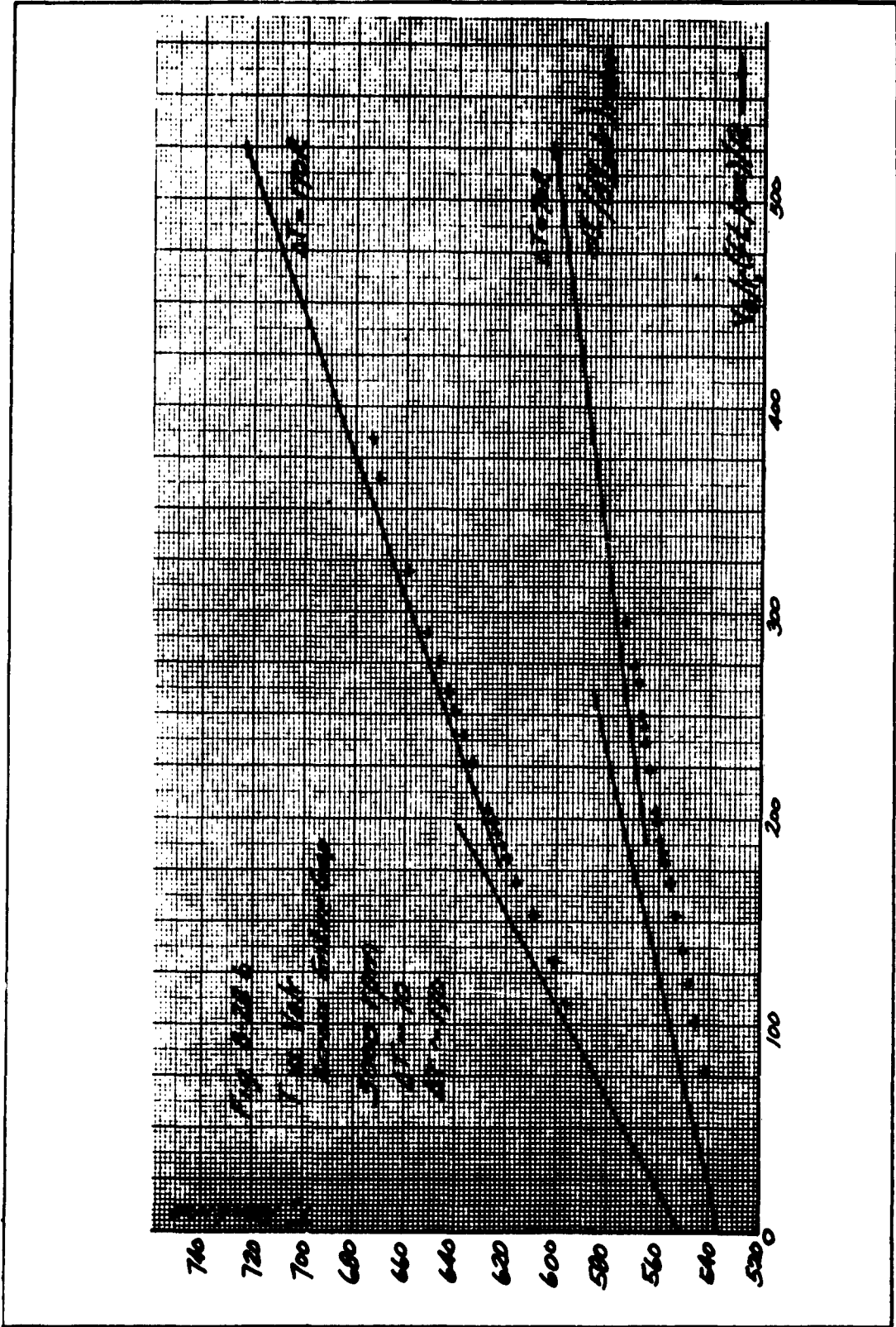
and for air

$$\alpha = 1.4.$$

¹ For example at $y_T = 60$, corresponding to y^+ of the same order $r^+ = 1.720$, and $(r/w)^2 = (1.720/1.66)^2 = (1.035)^2 = 1.07$

so that for $x = 1$, $\frac{dT}{dV/r} = 1.07 \left\{ \frac{dT}{dV/r} \right\}_{wall}$. In fact, this is the means whereby, for $\alpha = 1.4$, the transition is made from the slope at the rotor to that at the stator.





Chapter IX

Reconstruction of Experimental Data and Prediction
of Overall Heat Transfer and Friction Factors

9.1 Introduction

In this chapter it will be demonstrated that the experimental data can be reconstructed using the correlation for em/ku vs. y^+ , and that the correlation can be used to predict values of overall heat transfer and friction factor, knowing T_{stator} , T_{rotor} , rpm and $\alpha = 1.4$.

9.2 Reconstruction of Experimental Data Using the
Correlation em/ku vs. y^+

9.2.1 Derivation of Equations

From equation (2-26)

$$\frac{q}{dr} = -k \left(1 + \frac{em}{k}\right) \frac{dT}{dr} \quad (2-26)$$

which is written

$$= -k \left(1 + \alpha R \frac{em}{2}\right) \frac{dT}{dr}$$

and equation (2-27)

$$\frac{q}{dr} r = \frac{q}{N} N \quad (2-27)$$

Therefore

$$\frac{q}{N} N = -k r \left(1 + \frac{em}{2}\right) \frac{dT}{dr}$$

Integrating, and taking k as

$$k = (1.389 \times 10^{-4}) T^{0.75}$$

¹See Appendix V

$$\int_{T_{stator}}^T k dT = - \dot{q}_w r_w \int_{r_{stator}}^r \frac{dr}{r(1+\epsilon_m/2)}$$

$$\frac{1.389 \times 10^{-4} [T^{1.75} - T_{stator}^{1.75}]}{1.75} = - \dot{q}_w r_w \int_{r_{stator}}^r \frac{dr}{r(1+\epsilon_m/2)} \quad (9-1)$$

Further

$$\dot{q}_w r_w = \frac{-1.389 \times 10^{-4} [T_{rotor}^{1.75} - T_{stator}^{1.75}]}{\int_{r_{stator}}^{r_{rotor}} \frac{dr}{r(1+\epsilon_m/2)}} \quad (9-2)$$

Substitution into equation (9-1) yields

$$\frac{[T^{1.75} - T_{stator}^{1.75}]}{[T_{rotor}^{1.75} - T_{stator}^{1.75}]} = \frac{\int_{r_{stator}}^r \frac{dr}{r(1+\epsilon_m/2)}}{\int_{r_{stator}}^{r_{rotor}} \frac{dr}{r(1+\epsilon_m/2)}} \quad (9-3)$$

From equation (9-2), given T_{rotor} and T_{stator} , and the variation of $\epsilon_m/2$ with r , the overall heat transfer can be calculated.

From equation (9-3), knowing the same yields the variation of T with r .

Comparisons can now be made with two experimentally determined quantities; \dot{q}_w as measured from overall heat transfer results and T vs. r as determined from the interferometer.

The same can be done for the velocity distribution. From equations (2-20) and (2-21)

$$\tau_{ro} = -\mu r \frac{dV_e/r}{dr} (1 + \epsilon m/\omega) \quad (2-20)$$

and

$$\tau_{ro} r^2 = \tau_{wall} r_{wall}^2 = \tau_{stator} r_{stator}^2 \quad (2-21)$$

we find

$$\int_{r_{stator}}^r d(V_e/r) = -\tau_{stator} r_{stator}^2 \int_{r_{stator}}^r \frac{dr}{r^3 \mu (1 + \epsilon m/\omega)} \quad (9-4)$$

The velocity distribution can be reconstructed from this equation.

However, to achieve a more tractable form for computation purposes, consider the following

$$dT/dr = -g_N \tau_w / 2r (1 + \epsilon m/\omega)$$

and

$$(1/r^2) dT/dr = g_N \tau_w \left(\frac{\mu}{2} \right) \left(\frac{1}{\tau_{ro} r^2} \right) \frac{dV_e/r}{dr}$$

so that

$$\int_{r_{stator}}^{r_{rotor}} dV_e/r = \frac{\tau_{stator} r_{stator}^2}{g_N \tau_w} \beta \int_{r_{stator}}^{r_{rotor}} dT/r^2$$

where $\beta = k/\mu = \text{constant}$

Defining a Reynolds number based on the rotor diameter, and \mathcal{D}_{rotor} as

$$Re_{D,rotor} = \frac{V_{e,rotor} D_{rotor}}{\nu_{rotor}}$$

and noting that

$$f_{rotor} = \frac{2 T_{rotor}}{P_{rotor} V_{e,c}^2}$$

equation (9-5) can be put into the following form

$$1 = \frac{\frac{1.75}{16} \left(\frac{T_{rotor}}{T_c}\right)^2 Re_{D,rotor} (T_{rotor})^2}{\left[1 - \left(\frac{T_{stator}}{T_{rotor}}\right)^{1.75}\right] T_{rotor}} f_{rotor} \int_{r_{rotor}}^{r_{stator}} \frac{dT}{r^2} \int_{r_{rotor}}^{r_{stator}} \frac{dr}{r(1+Em/r)} \quad (9-6)$$

The term in the bracket is a constant for a given apparatus speed and temperature difference. The factor 1.75 however results from the variation of k with temperature for air.

If the term on the right is equal to unity then the derived velocity distribution matches the experimental. Call this term G .

$$G = \frac{\frac{1.75}{16} \left(\frac{T_{rotor}}{T_c}\right)^2 Re_{D,rotor} (T_{rotor})^2}{\left[1 - \left(\frac{T_{stator}}{T_{rotor}}\right)^{1.75}\right] T_{rotor}} f_{rotor} \int_{r_{stator}}^{r_{rotor}} \frac{dT}{r^2} \int_{r_{stator}}^{r_{rotor}} \frac{dr}{r(1+Em/r)} \quad (9-7)$$

9.2.2 Reconstruction of Experimental Data

The run chosen for study was one at 5000 Rpm, $T_{rotor} = 722.4$ R, $T_{stator} = 549.4$ R, the measured value of overall heat transfer was $q_{rotor} = 1250$ Btu/hr-Ft².

The value of the friction factor determined from

The same can be done for the velocity distribution. From equations (2-20) and (2-21)

$$T_{ro} = -\mu r \frac{dV_e/r}{dr} (1 + \epsilon m/\omega) \quad (2-20)$$

and

$$T_{ro} r^2 = T_{wall} r_{wall}^2 = T_{stator} r_{stator}^2 \quad (2-21)$$

we find

$$\int_{r_{rotor}}^{r_{stator}} d(V_e/r) = -T_{stator} r_{stator}^2 \int_{r_{rotor}}^{r_{stator}} \frac{dr}{r^3 \mu (1 + \epsilon m/\omega)} \quad (9-4)$$

The velocity distribution can be reconstructed from this equation.

However, to achieve a more tractable form for computation purposes, consider the following

$$dT/dr = -g_N \eta / 2r (1 + \epsilon m/\omega)$$

and

$$(1/r^2) dT/dr = g_N \eta \left(\frac{\mu}{2} \right) \left(1/r_{ro} r^2 \right) \frac{dV_e/r}{dr}$$

so that

$$\int_{r_{stator}}^{r_{rotor}} dV_e/r = \frac{T_{stator} r_{stator}^2}{g_N \eta} \beta \int_{r_{stator}}^{r_{rotor}} dT/r^2$$

$$\text{where } \beta = k_e/\mu = \text{constant}$$

Defining a Reynolds number based on the rotor diameter, and \mathcal{N}_{rotor} as

velocity measurements was $f_{\text{rotor}} = 1.589 \times 10^{-2}$.

From this, f_{stator} can be calculated as $f_{\text{stator}} = 0.805 \times 10^{-2}$.

Other constants required are

$$r_{\text{rotor}} = 1.6633 \text{ inches}$$

$$r_{\text{stator}} = 2.037 \text{ inches}$$

$$r_c = \frac{2.037 + 1.6633}{2} = 1.8502 \text{ inches}$$

$$\nu_{\text{rotor}} = 2.64 \times 10^{-9} \text{ T}^{1.75} = 2.657 \times 10^{-4} \text{ ft}^2/\text{sec}$$

$$\nu_{\text{stator}} = 1.646 \times 10^{-4} \text{ ft}^2/\text{sec}$$

Calculated from the information above are

$$v_{\theta, \text{rotor}} = \text{rpm} \times \frac{2}{60} \times \frac{1.6633}{12} = 72.58 \text{ ft/sec}$$

$$v_{\theta, c} = \frac{72.58 \times 1.6633}{2 \times 1.8502} = 32.63 \text{ ft/sec}$$

$$u_{*, \text{rotor}} = \frac{f_{\text{rotor}}}{2} \quad v_{\theta, c} = 2.907$$

$$u_{*, \text{stator}} = 2.0698$$

from which

$$y_{\tau, \text{rotor}} = 1.0968y^+$$

and

$$y_{\tau, \text{stator}} = 0.9543y^+$$

The first step in the calculation is to determine

$$\int_{r_{\text{stator}}}^{r_{\text{rotor}}} \frac{dr}{r(1 + \epsilon m / \nu)}$$

From the curves for $\epsilon m/\omega$ vs. y^+ in Fig. 8-22 values of $\epsilon m/\omega$ are read off at evenly spaced intervals of y^+ . A convenient interval may be $\Delta y^+ = 5$, for example. These curves can be used for values of y^+ up to 50.

Two integrals can then be evaluated for example by Simpsons' Rule, as r at $y^+ = 50$ and r at $y^+ = 50$

$$\int_{r_{\text{stator}}}^{r} \frac{dr}{(1 + \epsilon m/\omega)r} \quad \text{and} \quad \int_{r_{\text{rotor}}}^{r} \frac{dr}{(1 + \epsilon m/\omega)r}$$

The equation (8-6)a for $\epsilon m/\omega$ in the center of the channel is used for $1.75 < r'' < 1.95$ to evaluate

$$\int_{1.75}^{1.95} \frac{dr}{(1 + \epsilon m/\omega)r}$$

Two areas remain to be evaluated; those for $(r \text{ at } y_{\text{stator}}^+ = 50) < r'' < 1.95$ and $1.75 < r'' < (r \text{ at } y_{\text{rotor}}^+ = 50)$. No expression has been derived for these areas; however, a plot of the function $1/r(1 + \epsilon m/\omega)$ vs. r , as shown for the present example in Fig. 9-1, reveals how small the contribution these areas make to the total integral. To evaluate the unknown integrals the function is plotted in the known areas and for the unknown ones the curve is "faired". The unknown areas are then numerically evaluated using values read from the curve.

The sum of these five areas is the integral $\int_{r_{\text{stator}}}^{r_{\text{rotor}}} \frac{dr}{r(1 + \epsilon m/\omega)}$
From equation (9-2), $g_w r_w$ can now be computed.

The variation of T with r can also be calculated.

$$\left. \begin{aligned} F_{\text{stator}} &\equiv \int_{r_{\text{stator}}}^r \frac{dr}{r(1 + \epsilon m/\omega)} \bigg/ \int_{r_{\text{stator}}}^{r_{\text{rotor}}} \frac{dr}{r(1 + \epsilon m/\omega)} \\ F_{\text{rotor}} &\equiv \int_{r_{\text{rotor}}}^r \frac{dr}{r(1 + \epsilon m/\omega)} \bigg/ \int_{r_{\text{stator}}}^{r_{\text{rotor}}} \frac{dr}{r(1 + \epsilon m/\omega)} \end{aligned} \right\} 9-7a$$

The integral $\int_{r_{rotor}}^r \frac{dr}{r(1+\epsilon m/s)}$ can be read from a desk calculator at each value of y^+ as the evaluation of the total integral proceeds.

Equation (9-3) is then

$$\frac{T^{1.75} - T_{stator}^{1.75}}{T_{rotor}^{1.75} - T_{stator}^{1.75}} = F_{stator}$$

This can be put into the following forms:

$$\frac{T_{stator}}{T} = \left\{ \frac{1}{1 + F_{stator} \left[\left(\frac{T_{rotor}}{T_{stator}} \right)^{1.75} - 1 \right]} \right\}^{1/1.75} \quad (9-8)$$

(OVER THE STATOR)

and

$$\frac{T}{T_{rotor}} = \left\{ 1 - F_{rotor} \left[1 - \left(\frac{T_{stator}}{T_{rotor}} \right)^{1.75} \right] \right\}^{1/1.75} \quad (9-9)$$

(OVER THE ROTOR)

Thus, T vs. r can be evaluated and the integral computed.

$$\int_{rotor}^{stator} \frac{dT}{r^2}$$

All the terms in equation (9-6) are now known and the final check can be made concerning $\Delta V_e/r$ across the channel. For the example chosen the calculation proceeded as follows, for the area over the rotor:

y^+	$\epsilon m/\omega$	$\epsilon m/\omega$	y^+	r''	$r''(1+\epsilon m/\omega)$	$\frac{1}{r''(1+\epsilon m/\omega)}$	$\int_{rotor} \frac{dr}{r''(1+\epsilon m/\omega)}$
0	0	0	0	1.6633	1.6633	0.6012	
5	15	0.238	5.48	1.6688	2.0660	0.4840	2.796×10^{-3}
10	47	0.7468	10.97	1.6743	2.9247	0.3419	5.2630×10^{-3}
15	127	2.018	16.45	1.6797	5.0693	0.1973	
20	294	4.672	21.94	1.6852	9.5585	0.1046	7.5218×10^{-3}
25	532	8.453	27.42	1.6907	15.9822	0.0626	
30	840	13.348	32.92	1.6962	24.3370	0.0411	8.2460×10^{-3}
35	1170	18.591	38.39	1.7017	33.3380	0.03	
40	1570	24.947	43.87	1.7071	44.2941	0.0226	8.5816×10^{-3}
45	1980	31.462	49.36	1.7126	55.9027	0.0179	
50	2410	38.295	54.84	1.7181	65.5127	0.0148	8.781×10^{-3}

Thus $\int_{rotor} \frac{dr}{r(1+\epsilon m/\omega)} = 8.781 \times 10^{-3}$

Similarly over the stator, $\int_{stator} \frac{dr}{r(1+\epsilon m/\omega)} = 7.148 \times 10^{-3}$

For the region $r = 1.75''$ to $r = 1.95''$, $\epsilon m/\omega = 94.6$.

$r(\text{inches})$	$r(1+\epsilon m/\omega)$	$\frac{1}{r(1+\epsilon m/\omega)}$
1.75	167.30	0.0060
1.85	176.9	0.0057
1.95	186.4	0.0054

and

$$\int_{r=1.95''}^{r=1.75''} \frac{dr}{r(1+\epsilon m/\omega)} = 1.140 \times 10^{-3}$$

A plot of $\frac{1}{r(1+\frac{\epsilon m}{2})}$ vs. r is made, as in Fig. 9-1 for the regions in which $\epsilon m/2$ is known. For the regions $1.989 < r < 1.95$ and $1.7181 < r < 1.75$ the curve is faired as shown in the figure. The areas under these portions of the curve are 0.415×10^{-3} and 0.322×10^{-3} respectively.

The total area under the curve is

$$\int_{r_{\text{stator}}}^{r_{\text{rotor}}} \frac{dr}{r(1+\epsilon m/2)} = 17.806 \times 10^{-3}$$

A computation for $\oint_{N/N}$ can now be made.

$$\oint_{N/N} = \frac{1.389 \times 10^{-4}}{1.75} \left[\frac{(722.4)^{1.75} - (549.4)^{1.75}}{17.806 \times 10^{-3}} \right]$$

$$\oint_{N/N} = 0.01708 \times 10^4$$

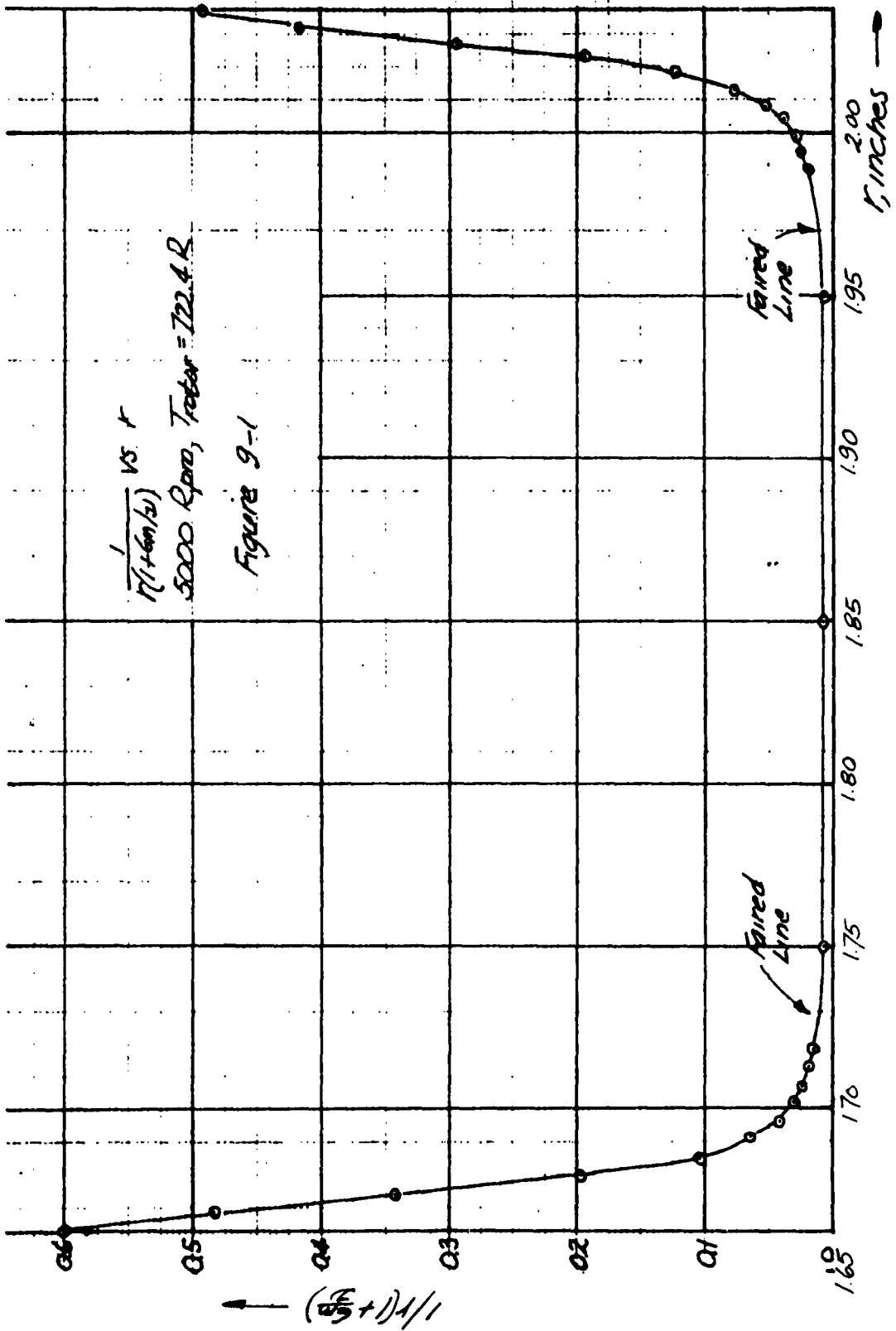
and

$$\oint_{\text{rotor}} = 0.01708 \times 10^4 \times \frac{12}{1.6633} = 1232 \text{ Btu/hr-ft}^2$$

The measured value was 1250 Btu/hr-ft^2 , a difference of 3.2%.

The temperature distribution can now be calculated over the rotor the results are

r	F_{rotor}	T/F_{rotor}	T	$1/r^2$
1.6633	0	1	722.4	0.3615
1.669	0.1671	0.9632	695.8	0.3589
1.674	0.2956	0.9341	674.8	0.3568
1.685	0.4224	0.9047	653.5	0.3522
1.696	0.4631	0.8951	646.6	0.3477
1.707	0.4891	0.8906	643.4	0.3431
1.718	0.4931	0.8880	641.5	0.3388



Over the stator the results are

r	T	$1/r^2$
2.037	549.4	.2410
2.027	590.7	.2434
2.018	690.6	.2456
2.008	617.2	.2480
1.999	620.9	.2503
1.989	623.2	.2528
1.95	627.3	.263
1.85	632.7	.292
1.75	638.3	.327

A plot is now made of T vs. $1/r^2$ as in Fig. 9-2. The area under this curve can be integrated numerically to give

$$\int_{r_{\text{stator}}}^{r_{\text{rotor}}} \frac{dT}{r^2} = 52.162$$

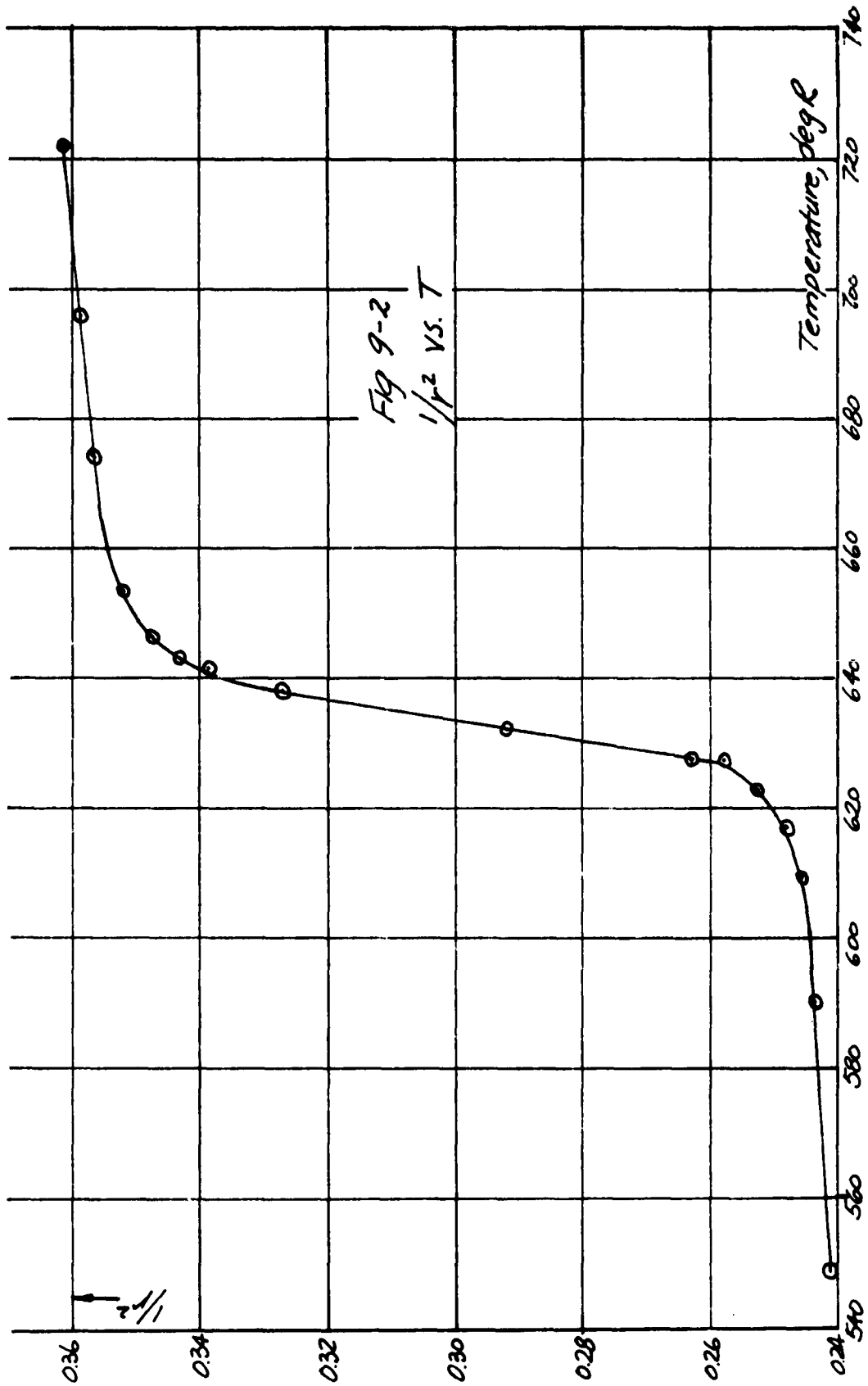
The quantities needed to determine G in equation (9-7) are all known. Recall that G must be unity for agreement between the experimental and calculated velocity distributions.

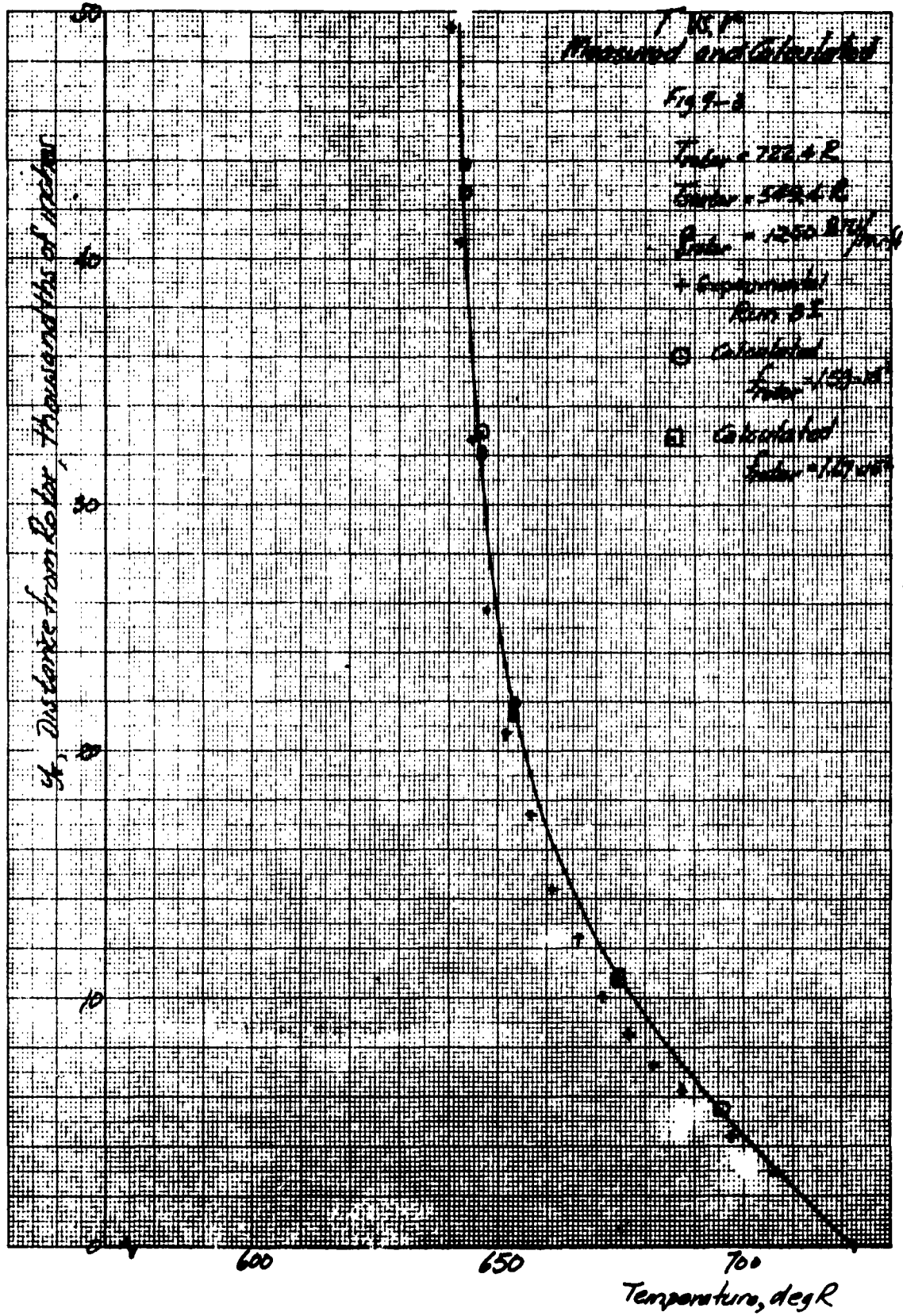
Substitution into equation (9-7) results in

$$1 \stackrel{?}{=} G = 0.9938$$

a difference of 0.62%

In figure 9-3 is shown the temperature distribution over the rotor, as measured and as computed.





9.3 The Use of the Correlation of $\frac{Gm}{\rho f}$ vs. y^+ , to Predict Overall Heat Transfer and Friction Factors

The purpose of this section is to demonstrate the use of the correlation for $\frac{Gm}{\rho f}$ vs. y^+ and the fact that $\alpha = 1.4$ to solve the problem "Given: Rotor Temperature, Stator Temperature and rpm. What is the overall heat transfer and friction factor?"

The procedure is the same as previously, except that in this case a trial friction factor is used until the right hand side of equation (9-6) is equal to unity.

This calculation has been made for the present example. Friction factors f_{rotor} of 1.25×10^{-2} and 1.9×10^{-2} were selected to obtain G . Use was made of the result in the foregoing section. The resulting values for G with various f_{rotor} were

f_{rotor}	$\int_{rotor}^{stator} \frac{dr}{r(1+6m/2r)}$	$\int_{rotor}^{stator} \frac{dT}{r^2}$	G
1.25×10^{-2}	21.998×10^{-3}	51.439	.95190
1.59×10^{-2}	17.806×10^{-3}	52.162	.99368
1.9×10^{-2}	15.132×10^{-3}	52.293	1.0123

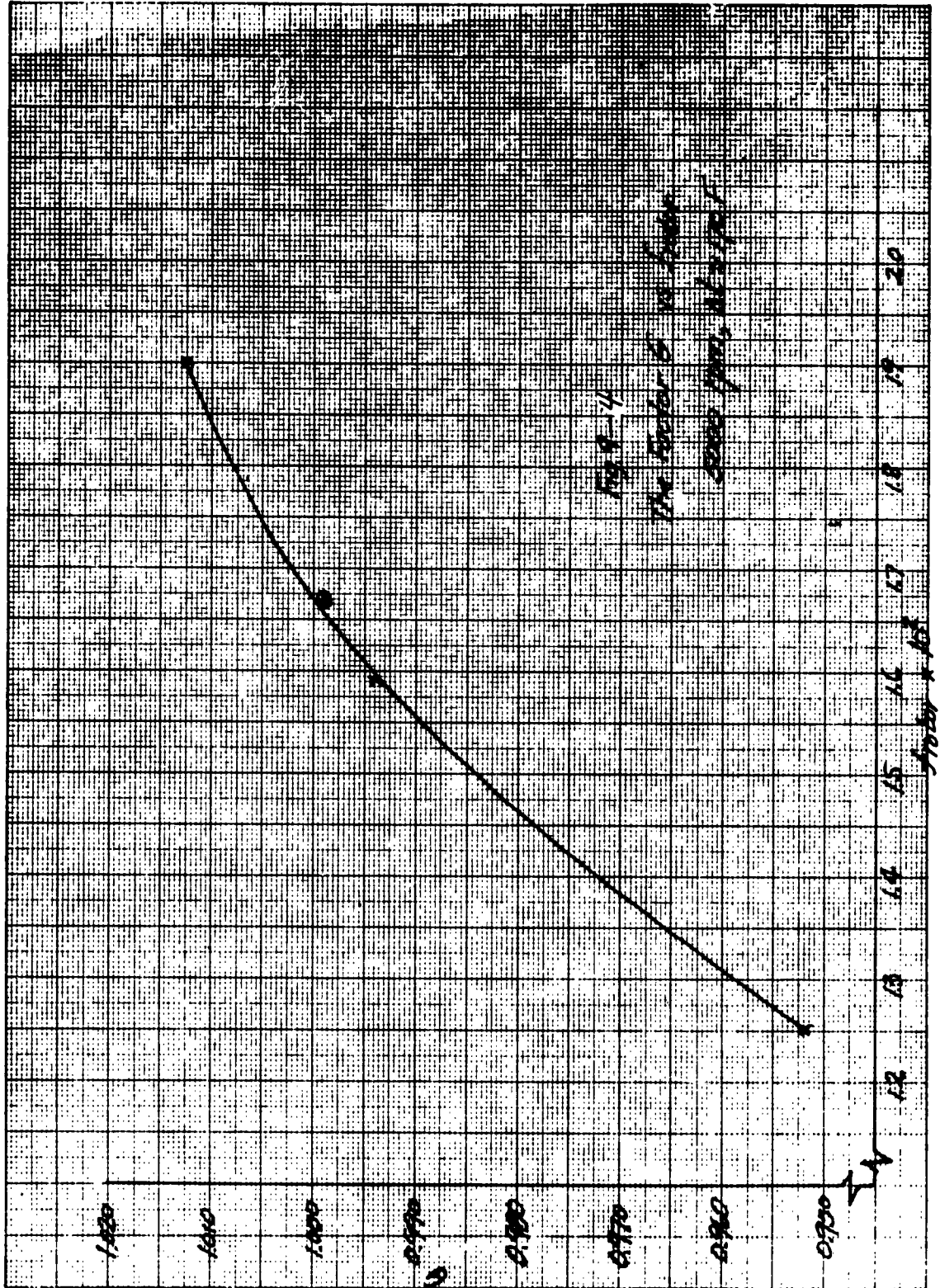
The graph of Fig. 9-4 was then prepared.

The quantity G is unity at $f_{rotor} = 1.67 \times 10^{-2}$

Accordingly, the computation was made with $f_{rotor} = 1.67 \times 10^{-2}$

The value G was found to be 0.9987 and is plotted in Fig. 9-4.

This is considered to be of sufficient accuracy.



The value of f_{rotor} differs from that found from the experimental velocity distributions by 5.1%.

The overall heat transfer computed with $f_{rotor} = 1.67 \times 10^{-2}$ is, a difference of 8% from the experimental value of 1250 Btu/hr-Ft².

The temperature distributions calculated with the trial values of friction factors used in the computation are plotted in Fig. 9-3. Better agreement with experiment is achieved with friction factor 1.67×10^{-2} than 1.589×10^{-2} .

Similar calculations have been made for 5000 rpm for temperature differences $\Delta t = 70, 170, \text{ and } 320 \text{ F}$.

The overall results compared with the experimental values is shown below.

5000 rpm

T_{rotor}, R	T_{stator}, R	Δt	Nu/Nu _{cond}		% diff.	f_{rotor}	
			calc.	exp.		calc.	exp.
604.7	535.7	69	12.8	14.6	12%	0.0139	0.0148
722.4	549.4	173	12.3	11.5	7%	0.0167	0.0159
882.7	564.3	318.4	10.4	9.7	7.2%	0.0195	0.0175

The differences between the calculated and experimental values

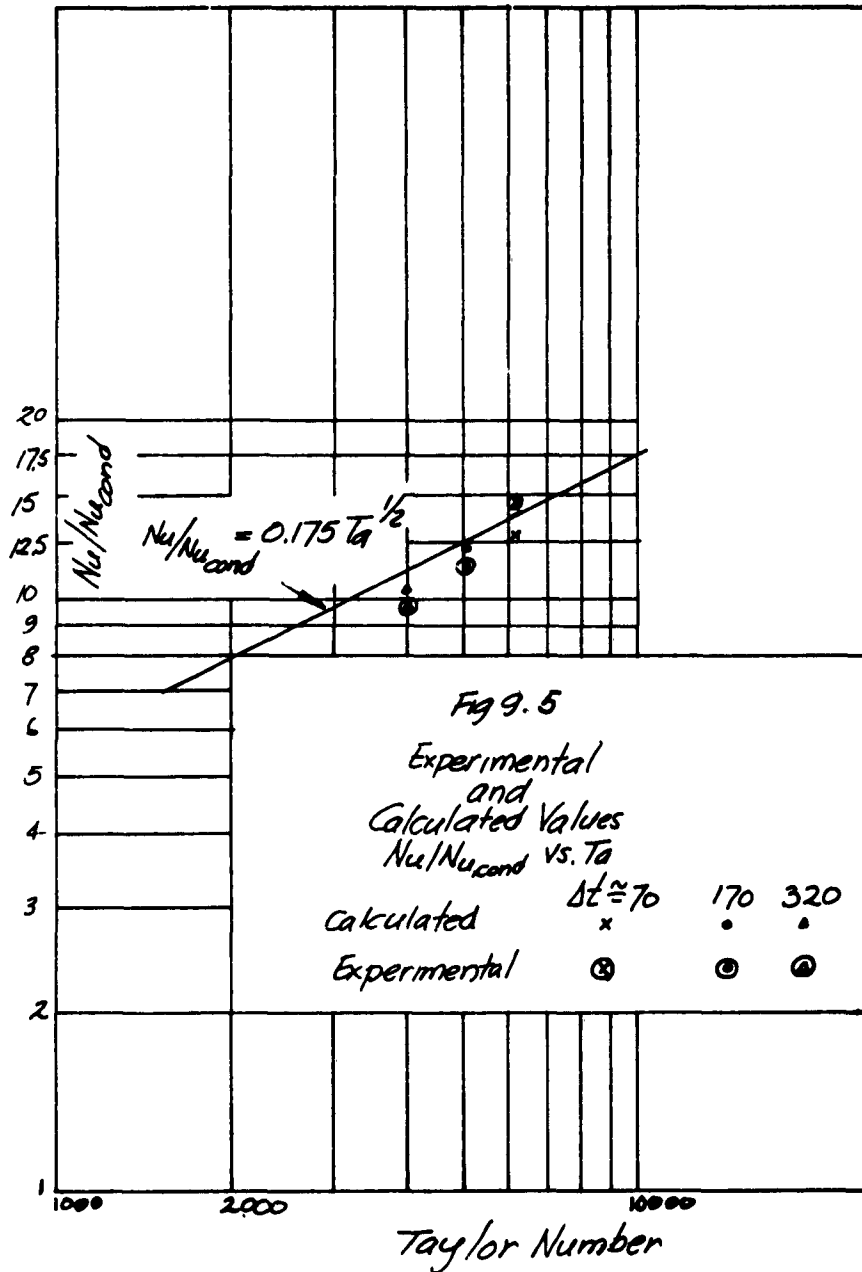
of the heat transfer are about equal to the percentage error calculated for in Chapter VIII for the runs at $\Delta t = 170\text{F}$ and 320F but is higher for the lower temperature run. For this run, agreement between the calculated and experimental Nusselt Number with the extrapolated correlation of Kays and Bjorklund is to within +6.5% for the experimental point and -6.5% for the calculated point.

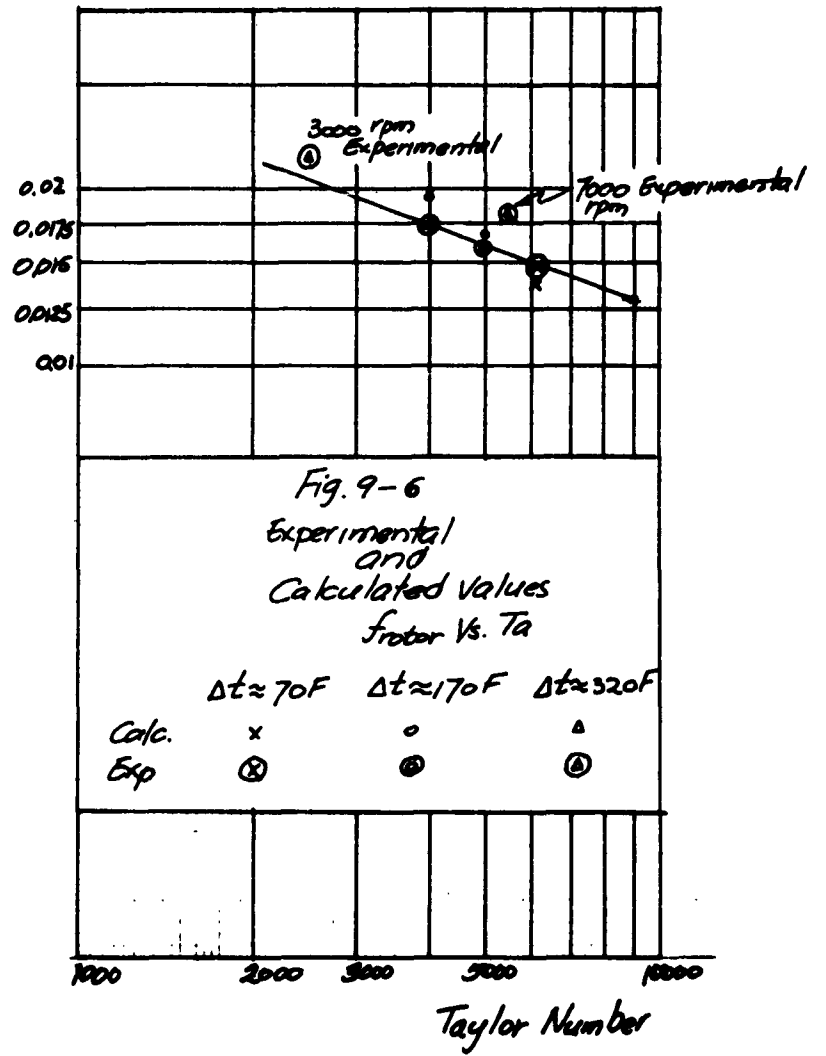
Fig. 9-5 is a plot of $Nu/Nu_{\text{cond.}}$ vs. Ta for the calculated points and the experimental points together with the line $Nu/Nu_{\text{cond.}} = 0.175 Ta^{1/2}$.

The values of the calculated friction factors have been plotted in Fig. 9-6 against Taylor number together with the experimental friction factors.

A trend toward higher friction factors with increased heat transfer is now in evidence for the lower temperature runs as well as for the runs at a temperature difference of 320 F (see Fig. 8-16). Plotted also in Fig. 9-6 are the experimental points for 3000 rpm and 7000 rpm at this temperature difference. The experimental value of f_{rotor} for 5000 rpm, $\Delta t = 320\text{F}$, appeared to be too low compared to f_{rotor} for 3000 and 7000 rpm. The calculated value of f_{rotor} for 5000 rpm is 11% higher than the experimental value, and now appears to be in better relation to the other two points.

The difference between the calculated and experimental friction factors for the lower temperature runs is within 5-1/2%.





The conclusions drawn from the foregoing are that

1. the correlation $\frac{C_{mf}}{C_{mf}}$ vs. y^+ , will reconstruct the experimental data from which it is derived and
2. the correlation can be used to predict overall heat transfer and friction factors for the present apparatus under conditions of property variation when the cylinder temperatures and the speed of the inner cylinder are given.

Appendix I

I.1 Description of operation of a Mach-Zehnder Interferometer

A schematic diagram of a Mach Zehnder interferometer is shown in Fig. I-1. Monochromatic light from a point source is placed at the focal point of a collimating lens *b*, resulting in a beam of parallel light. Beam splitter *c*, a half silvered mirror allows one half the incident light to pass along path I and reflects the other half along path II. Plates *d* and *e* are totally reflecting plane mirrors. The light proceeding along path I is reflected from the mirror *d* and on striking beam splitter *f* is again divided. One half is discarded, and the other half reunites with the light which proceeded along path II.

If one of the mirrors, say *d*, is rotated an angle about an axis perpendicular to the plane of the paper by the laws of incidence and reflection those rays from path I will intersect those of path II at an angle 2δ , as shown in Fig. I-2. In this figure the straight lines drawn beyond the splitting plate *f* mark the wave crests of the individual rays. Each point of intersection between the lines for the light from path I and those for path II marks a line perpendicular to the plane of the paper along which the rays from each path are in phase.

On a screen placed beyond splitting-plate *f*, the line of intersection, appears as a bright band, and an interference pattern is produced as shown. If a region of uniform

density different from that outside the region is placed in path II a light ray along that path will be accelerated or retarded depending on whether the air in the interposed region is less dense or more dense than that outside the region.

This results in a shift of the wave front for these rays by an amount $\epsilon\lambda$ and a shift of the intersecting lines of the wave fronts for the two paths by an amount $\epsilon\lambda/2\delta$. That is, there would be a band shift on the screen an amount $\epsilon\lambda/2\delta$. This is shown in Fig. I-3.

In general, during flow the density in the test section will not be uniform in a plane perpendicular to the light path. Consequently the band shifts will be non-uniform, and the density field must be evaluated on a point by point basis.

I.2 Relationship Between Density and Fringe Shift

The relationship between density and fringe shift is developed as follows:

Let t_1 be the time for a light ray to traverse the length L of the test section during no-flow conditions and t_2 the same during flow conditions.

If V_0 is the velocity of light at room air conditions, and λ_0 the wavelength at room air conditions, the displacement of the wave fronts for the light through the test section is

$$\epsilon\lambda = V_0 (t_2 - t_1)$$

where ϵ is the displacement measured in wavelengths.

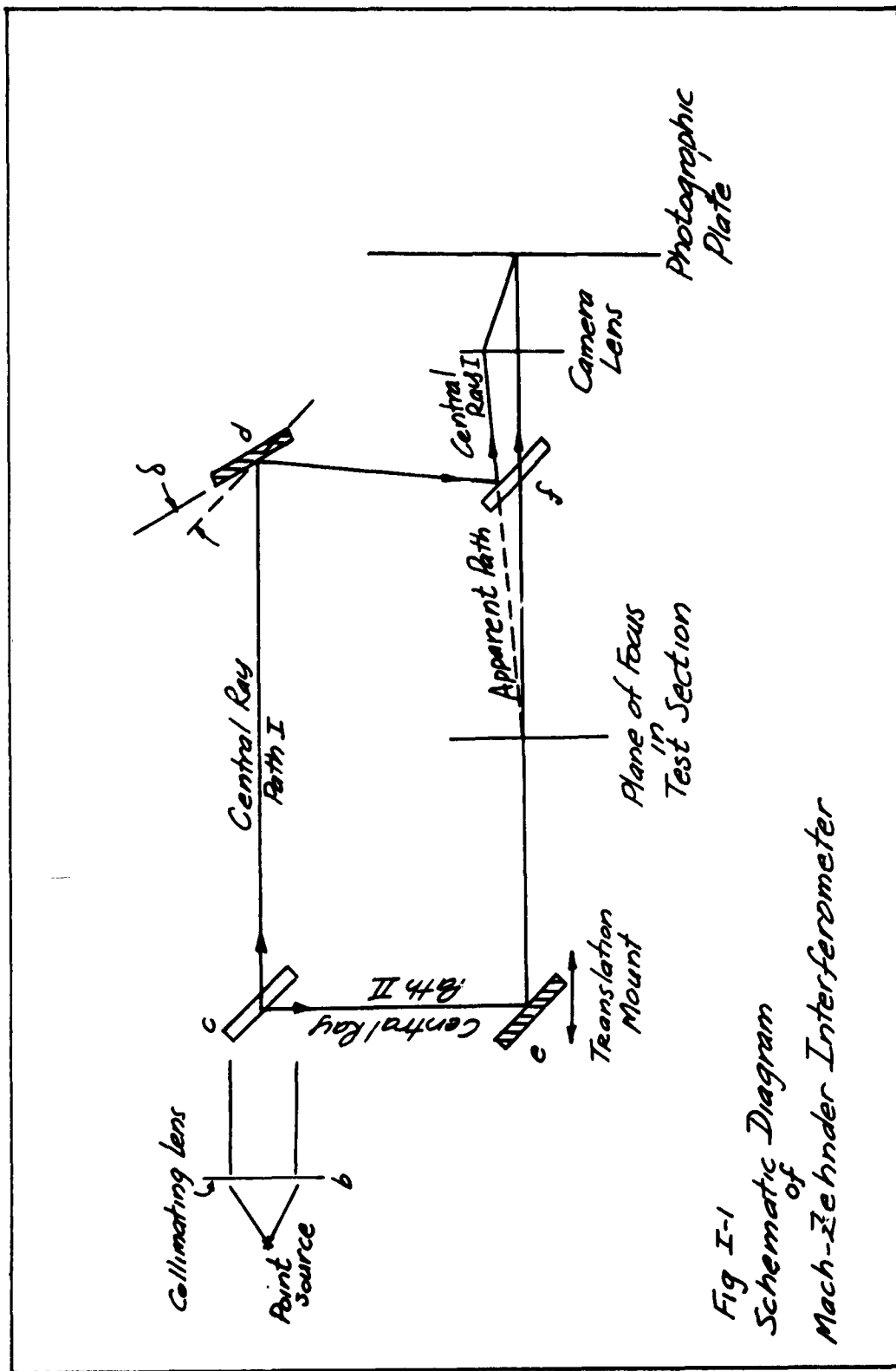
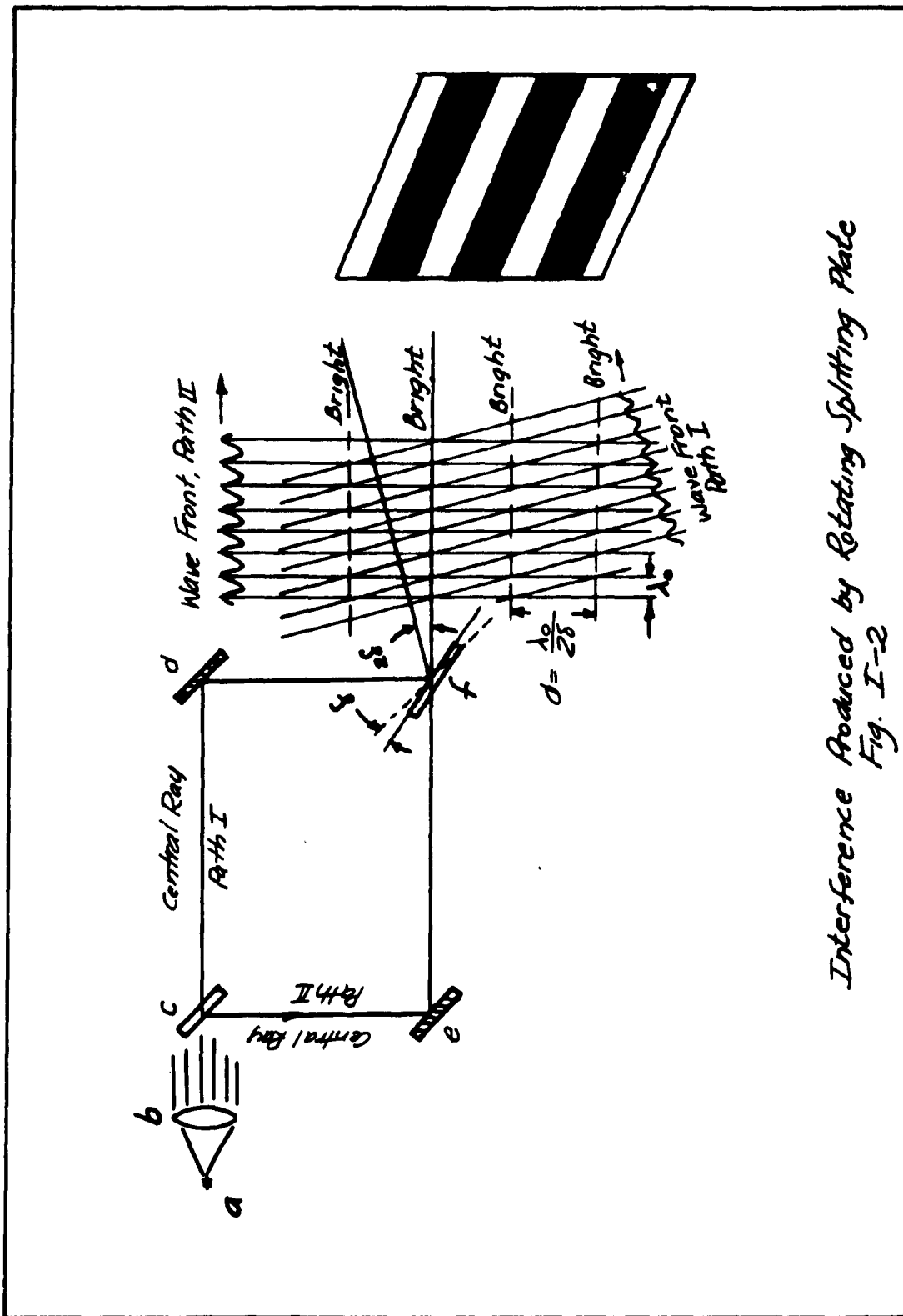
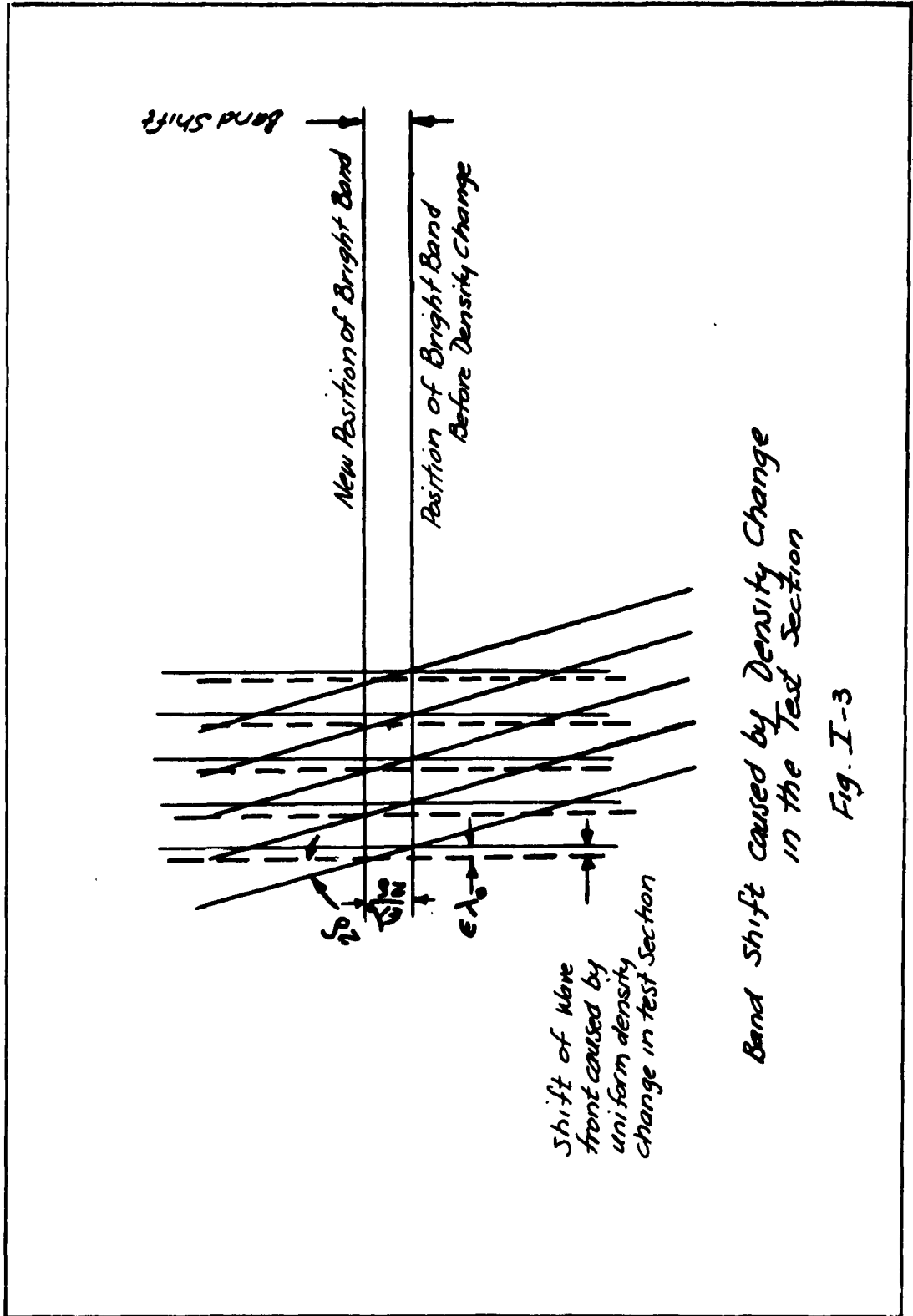


Fig I-1
Schematic Diagram
of
Mach-Zehnder Interferometer



*Interference Produced by Rotating Splitting Plate
Fig. I-2*



Band Shift caused by Density Change in the Test Section

Fig. I-3

The difference in time to traverse the test section between flow and no-flow conditions is

$$t_2 - t_1 = L \left(\frac{1}{V_2} - \frac{1}{V_1} \right)$$

The index of refraction n is defined as

$$n = \frac{V_{\text{vacuum}}}{V}$$

and the frequency of the light, a constant, is given as

$$f = \frac{V}{\lambda}$$

Therefore

$$\epsilon \lambda_{\text{vacuum}} = L(n_2 - n_1)$$

Note that $\epsilon \lambda_{\text{vacuum}}$ is the difference in optical path length between conditions 1 and 2 and can be interpreted not only as the change in optical path length between no-flow and flow conditions, but also as the difference in optical path length between any two points 1, and 2 under flow conditions.

From the Gladstone-Dale Equation

$$n - 1 = K\rho$$

where K is constant for a given gas and wavelength of light over a large range of pressures.¹

¹ Values of K can be obtained from G. M. Edelman and M. H. Bright, "The Specific Refractivity of Gases for Various Wavelengths of Light," Gas Turbine Laboratory Report No. 6, Cambridge Massachusetts: MIT, May 1948.

Thus $n_1 = \kappa \rho_1 + 1$

and $n_2 = \kappa \rho_2 + 1$

Therefore

$$\epsilon \lambda_{\text{vacuum}} = \kappa L (\rho_2 - \rho_1) = \kappa L \Delta \rho$$

or
$$\Delta \rho = \frac{\lambda_{\text{vacuum}} \epsilon}{\kappa L}$$

Knowing ρ_1 allows determination of the density field.

I.3 Adjustment of the Interferometer

Adjustment of the interferometer is accomplished in the following steps:

1. Obtaining a parallel beam of light into the interferometer
2. Adjusting the plates and mirrors to obtain interference fringes
3. Obtaining interference fringes of maximum contrast in focus at the test section.

For alignment of the interferometer with the test section, see Section 5.4.1.

I.3.1 Parallel light into the Interferometer

In order to obtain a parallel beam of light into the interferometer the small opening serving as the effective source must be placed in the focal plane of the collimating lens. This is accomplished by focusing a telescope on a distant object, sighting through the collimating lens with the telescope at the small opening whose position is adjusted

along the lens axis until it is in sharp focus.

I.3.2 Adjusting the plates and mirrors to obtain interference fringes.

For the initial adjustment of the interferometer use was made of the method of Price.^{1,2} The method results in visible interference fringes with monochromatic light. This phase of the adjustment could be the most time consuming but for this method which is described below.

Consider the M-Z arrangement shown in Fig. I-4. For fringe formation the plates and mirrors must be very nearly parallel and the two available path lengths different by not more than a few wavelengths of light.

To accomplish this, place a small plane mirror at B, and a pinhole light at C.

A viewer at the telescope lens sees four primary images of the pinhole light, one for each of the four possible light paths that the light from the pinhole can traverse in proceeding from A to B and back to the telescope lens.

To accomplish the adjustment one rotates the mirrors

¹E. Price, NAVORD Report No. 1182 (1949).

²E. Price, Review of Scientific Instruments, vol. 23, Number 4, April 1951, p. 162.

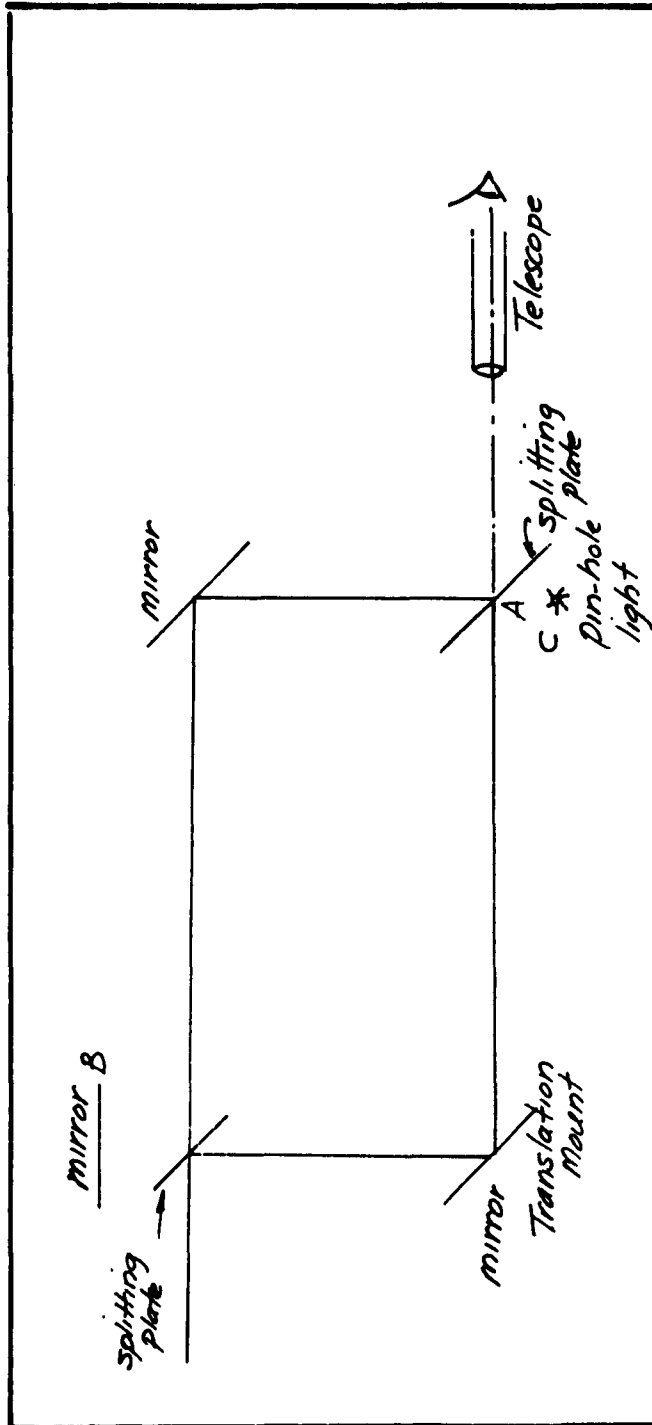


Fig I-4 Preliminary Adjustment According to Method of Price

and plates until the four images are superimposed.

One complication arises because of secondary images resulting from multiple reflections in the splitting plates. In the present apparatus two secondary images were seen for each primary image. The secondary images unfortunately do not differ greatly in brightness from the primary images but one finds in rotating the splitting plates that the images move in sets.

Once the superposition is accomplished, filtered light from the mercury vapor lamp is passed through the interferometer. If no fringes are visible with only the eye, rotation of one of the plates and/or motion of the translation mount will usually result in visible fringes.

I.3.3 Fringes of Maximum Contrast

The fringes now visible are probably not of maximum contrast. If the filter is removed the fringes may disappear. Motion of the translation mount will bring into the field the few fringes about the central band.

To focus the fringes in the plane of interest in the test section, an ordinary 60 watt light bulb can be used in place of the mercury vapor lamp.

Focus a telescope in the plane of interest. Tilt the splitting plates until the fringes come into focus in the telescope. When the bulb is replaced by the mercury lamp, the

fringes now appearing are of maximum contrast. The interferometer is ready for use.

Appendix II

Experimental Determination of Temperature Gradient in the Windows at the Ends of the Gap

To determine the temperature gradient in the windows, narrow, thin strips of Tempilaq of different temperature calibrations were applied to the quartz windows as shown in Fig. II-1.

Tempilaq was selected as the most practical means for determining the temperature gradient. There were two other alternative available. One was drilling holes into the windows and applying thermocouples at selected points. This was rejected as impractical and of questionable accuracy. A second was applying thermocouples at the contact surface between the quartz window and the end plates. This was rejected because only two temperatures on the glass would be known, assuming the temperatures determined were of sufficient accuracy.

Tempilaq is a solution of a substance whose melting point is known and a solvent, the compound being different for different temperature ratings. When the temperature of the Tempilaq reaches the melting point of the compound, melting occurs and on drying a sharp line can be seen between the unaffected Tempilaq and that which has melted and resolidified on cooling.

In general, the applied Tempilaq is slightly opaque, whereas the melted Tempilaq is transparent. There is thus no mistaking the line of demarcation.

The apparatus was operated exactly as during an interferometric run and the pattern of the isotherms emerged on the windows as circles concentric with the rotor.

Measurements were made on the Jones and Lamson Pedestal Comparator to determine the gradient but the size of the correction did not warrant that kind of accuracy so ultimately the isotherms were traced onto a piece of graph paper and the gradients determined.

A diagram of the isotherms for a typical result is shown in Fig. II-1.

In Fig. II-2 is shown the temperature difference in the glass over the gap width versus rpm at different temperature differences across the gap.

Listed below are the experimental results

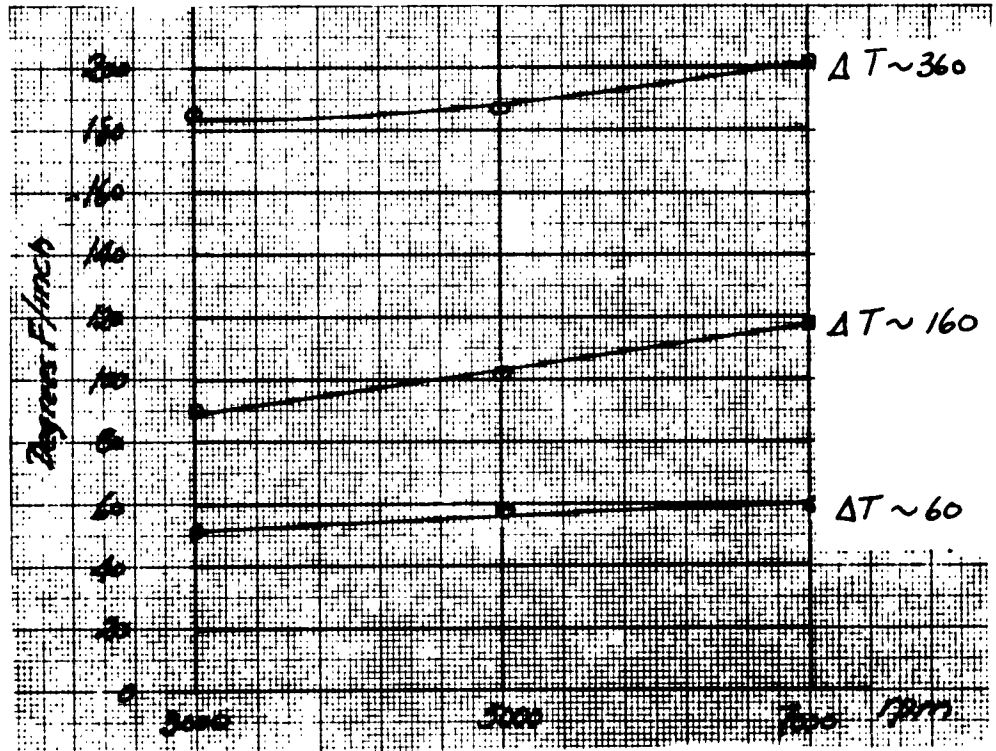
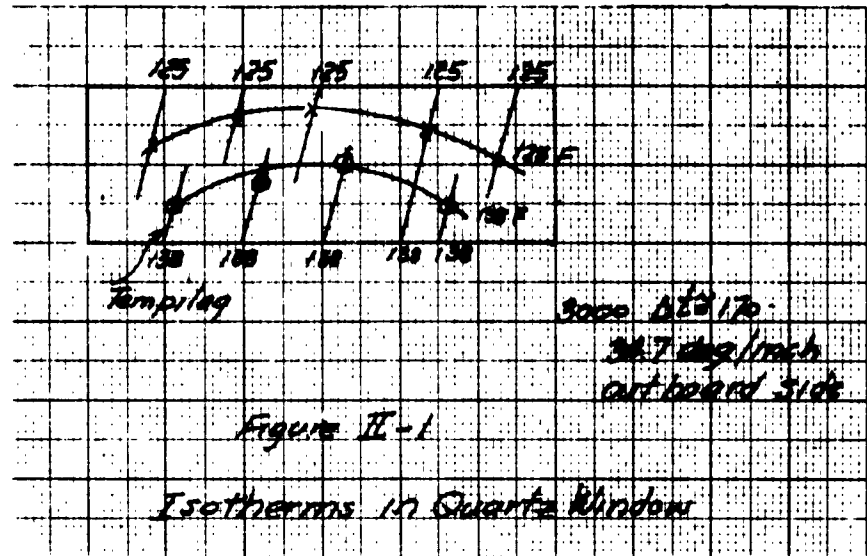
Table II-1

Degrees F/inch versus Rpm at Different $T_{\text{rotor}} - T_{\text{stator}}$

	$(T_{\text{rotor}} - T_{\text{stator}}) \text{ deg F}$		
	60	160	360
RPM			
3000	51.2	90	185
5000	57.6	101.4	187
7000	59.2	117.5	202

A simple fin analysis on the window shows that convective effects on the surface of the glass play only a

small part in determining the gradient in the glass.



Appendix III

Experiments Performed to Determine the Accuracy
of the Slip-Ring Assembly

The sequence of tests performed to determine the accuracy of indication of the slip-ring assembly was as follows:

Test #1. To determine the error caused by frictional heating of the rings when the brushes were in continuous contact with the rings.

Test #2. To determine the reduction in error when cooling air is passed over the slip rings.

Test #3. To determine the reduction in error when cooper lead wire is introduced between the rotor thermocouples and the slip rings.

Test #4. To determine the slip ring error with the circuit arranged as in Test #3, with cooling air passing over the slip rings, with the brushes in momentary contact during a reading and with current in the heater.

This comprises the final slip-ring arrangement. A description of these tests together with the results obtained follows.

Test #1.

a. Arrangement as shown in Fig. 4-2. except that iron-constantan leads from the rotor thermocouples are soldered directly to the silver slip rings.

b. Brushes in continuous contact with the slip-rings.

c. No heater current.

With no heater current the error in emf is the difference between the emf indicated with no rotation and the emf indicated with rotation (since frictional heating effects on the rotor are negligible).

Result: The slip-ring error after steady state conditions are reached at 4000 and 5000 rpm is of the order of 60 F.

Test #2.

Conditions the same as in Test #1 except that cooling air was passed over the slip rings. The effect of passing compressed air over the slip-rings was to reduce the error of indication to an order of 10 F for the thermocouple slip rings closest to the heater slip rings.

The errors resulting were considered to be too high, and the slip ring assembly was altered so as to interpose copper wire between the rotor thermocouples and the silver slip rings. Only three thermocouples were connected in this manner. The copper wires issuing from the two slip-rings closest to the heater were joined. Any indication from this circuit was due mainly to slip ring error.

Two further tests were then conducted.

Test #3.

This test was conducted under exactly the same conditions as Test #1, except for the copper leads between the rotor thermocouples and the slip-rings. See Fig. 4 -2.

With the brushes in continuous contact, no current in the heater, and no cooling air over the slip-rings, the errors in indication were of the order of 1 to 2 deg F for speeds in steps of 1000 rpm up to 6000 rpm for 20 minutes at each speed.

Test #4.

This test was conducted with the slip ring assembly in its final arrangement.

Cooling air was passed over the rings, the brushes were only in intermittent contact with the rings, and heater current was passed through the rings as during the subsequent experiments.

The reading obtained from the set of rings adjacent to the heater rings, which were joined as in Test #3, should have read in the absence of ring error, the temperature of the compensating junction in the circuit.

An independent thermocouple was placed near the stationary, compensating thermocouple.

The indication from the independent thermocouple agreed with the indication from the two rings adjacent to the heater rings to within 3 F at conditions approximating those met during the subsequent experiment.

The slip ring assembly is thus considered to be capable of indicating rotor temperature to within 3 F under conditions of the experiment.

Appendix IV A

Overall Heat Transfer

Run #	RPM	T_{rot} , degR	T_{stat} , degR	ΔT	Q_{rot} , BTU/hr	Q_c , BTU/hr	T_c , degR	Taylor Number	Nu/ Nu _{cond}
4 _a	OHT 3000	140.5	74.8	65.7	120.1	114.1	567.1	3744	9.31
7	OHT 3000	145.1	71.1	74	152.9	146.7	568.1	3722	10.62
11	OHT 3000	155	79.4	75.6	135	129	577.2	3639	9.52
4I	3000	145	77.2	67.8	129	123.2	571.1	3659	9.68
11I	3000	143.6	75.4	68.2	141.1	135.4	569.5	3659	10.58
4 _b	OHT 3000	266.5	81.4	185.1	312.3	290.3	634	3047	7.74
7I	3000	258.2	83.1	175.1	295.7	276.2	630.6	3061	7.74
15I	3000	261.8	93	168.8	273.9	256	637.4	3047	7.44
22I	3000	263.5	90	173.5	303.1	285	636.8	3047	8.1
6	OHT 3000	391.4	89.6	301.8	467.1	417.5	700.5	2540	6.25
10	OHT 3000	391.7	90.2	301.5	448.6	399.1	701	2540	5.98
17I	3000	393.2	95.9	297.3	521.6	461.6	704.5	2520	7
25I	3000	389.4	99	290.4	460.8	400.8	704.2	2530	6.2

Appendix IV A (Continued)

Overall Heat Transfer

Run #	RPM	$T_{p_{out}}$, degR	$T_{p_{in}}$, degR	ΔT , degR	Q_{tot} , BTU/hr	Q_c , BTU/hr	T_c , degR	Taylor Number	Nu/ Nu _{cond}
4	OHT 5000	147.9	79	68.9	189.4	183.4	573.5	6099	14.2
5	OHT 5000	146.7	77.9	68.8	175	169	572.3	6099	13.1
5	I 5000	148	78.8	69.2	204.2	198.2	573.4	6099	15.24
10	I 5000	143.8	75.7	68.1	191.8	186	569.8	6099	14.55
3	OHT 5000	272.7	89	183.7	429	411.7	640.9	4938	10.9
12	OHT 5000	271.7	87	184.7	385.3	362.6	639.3	5007	9.58
8	I 5000	260.4	89.4	170	417.3	397	634.9	5078	11.46
12	I 5000	252.4	84.9	167.4	387.3	368	628.6	5176	10.85
6	OHT 5000	426.2	93.8	332.8	648.9	588.9	720.2	4009	7.82
16	I 5000	422.7	104.3	318.4	758.6	698.7	723.5	4009	9.7
26	I 5000	419.4	102.7	316.7	688.1	628.8	721.1	4009	8.78
5	OHT 7000	144.8	79.4	65.4	199.8	193.8	572.1	8538	15.79
11	OHT 7000	152	82.1	69.9	213.05	207.1	577.1	8538	15.8

Appendix IV A (Continued)

Overall Heat Transfer

Run #	RPM	T_{Hot} , degR	T_{Cold} , degR	ΔT	Q_{HT} , BTU/hr	Q_c , BTU/hr	T_{avg}	Taylor Number	Nu/Nu_{end}
6I	7000	144.9	79.8	65.1	196.7	191.2	572.4	8538	15.64
18I	7000	148.2	85.3	63.6	221.6	215.6	576.8	8538	18.15
20I	7000	155.7	92.1	63.6	185.8	180.4	584	8258	14.93
12 OHT	7000	271.7	92.1	179.6	464.7	442.6	641.9	6913	11.96
9I	7000	261.2	91.6	169.6	434.3	413.4	636.4	7109	11.96
21I	7000	262.6	95.5	167.1	406.5	374.5	639.1	6977	10.93
24I	7000	256.8	87.6	169.2	467	445.3	632.2	6977	11.9
6 OHT	7000	432.4	99.1	333.3	809.2	747.9	725.75	5592	9.87
10 OHT	7000	437.5	103.6	333.9	798.3	736.3	730.6	5509	9.65
19I	7000	422	104.4	317.6	769.9	707.9	723.2	5592	9.86
23I	7000	430.8	108.8	322	825.4	763.4	729.8	5509	10.4

Appendix IV B
Velocity Distributions
 V_θ versus r

Run 54 V

3000 rpm

Adiabatic, $t = 80$ F

Stator			Rotor		
$y_{T,m}$	r , inches	V_θ , ft/sec	$y_{T,m}$	r , inches	V_θ , ft/sec
0	2.037	0	0	1.660	(43.45)
5	2.032	6.68	8	1.668	34.60
9	2.028	9.85	10	1.670	32.11
12	2.025	11.67	15	1.675	28.13
15	2.022	13.94	20	1.680	25.94
20	2.017	16.08	25	1.685	24.53
30	2.007	18.23	35	1.695	23.14
40	1.997	19.02	45	1.705	22.19
65	1.972	18.56	60	1.720	21.40
90	1.947	18.30	85	1.745	20.74
140	1.897	18.37	185	1.845	18.89

Appendix IV B
Velocity Distributions
 V_{θ} versus r

Run 55 V

3000 rpm

$T_{\text{rotor}} = 606.1 \text{ R}$

$T_{\text{stator}} = 538.2 \text{ R}$

$\Delta T = 67.9 \text{ R}$

Stator

Rotor

y, m	r, inches	V_{θ} , ft/sec	y, m	r, inches	V_{θ} , ft/sec
0	2.037	0	0	1.6613	43.49
5	2.032	6.68	8	1.6693	34.91
9	2.028	9.83	10	1.6713	32.72
12	2.025	11.41	15	1.6763	28.56
15	2.022	13.51	19.5	1.6808	26.38
20	2.017	15.75	24.5	1.6858	24.85
30	2.007	18.00	34.5	1.6958	23.24
40	1.997	18.63	44.5	1.7058	22.11
65	1.972	19.12	59.5	1.7208	21.51
90	1.947	18.90	84.5	1.7458	20.69
140	1.897	18.52	184.5	1.8458	18.77

Appendix IV B
Velocity Distributions
 V_θ versus r

Run 58 V

3000 rpm

$T_{\text{rotor}} = 725.73 \text{ R}$

$T_{\text{stator}} = 546.22 \text{ R}$

$\Delta T = 179.51 \text{ R}$

Stator

Rotor

$y_{r,m}$	r, inches	V_θ , ft/sec	$y_{r,m}$	r, inches	V_θ , ft/sec
0	2.037	0	0	1.6634	(43.54
5	2.032	5.94	8	1.6714	36.22
9	2.028	8.26	10	1.6734	34.61
12	2.025	9.91	15	1.6784	29.91
15	2.022	11.15	20	1.6834	27.28
20	2.017	12.35	25	1.6884	25.90
30	2.007	14.01	35	1.6984	23.92
40	1.997	15.31	45	1.7084	22.86
65	1.972	17.63	60	1.7234	21.72
90	1.047	18.11	85	1.7484	20.54
140	1.897	18.48	185	1.8484	18.73

Appendix IV B
Velocity Distributions
 V_{θ} versus r

Run 59 V

3000 rpm

$T_{\text{rotor}} = 847.9 \text{ R}$

$T_{\text{stator}} = 555.4 \text{ R}$

$\Delta T = 292.5 \text{ R}$

Rotor

y_{rm}	r, inches	V_{θ} , ft/sec
0	1.6654	43.6
8	1.6734	38.71
10	1.6754	36.27
15	1.6804	31.87
20	1.6854	28.81
25	1.6904	26.83
35	1.7004	24.37
45	1.7104	22.86
60	1.7254	21.66
85	1.7504	19.90
185	1.8504	17.55

Appendix IV B
Velocity Distributions
 V_θ versus r

Run 46 V

5000 rpm

Adiabatic, $t = 81$ F

Stator

Rotor

$y_{r,m}$	r , inches	V_θ ft/sec	$y_{r,m}$	r , inches	V_θ ft/sec
0	2.037	0	0	1.660	(72.4)
5	2.032	13.5	8.3	1.6683	51.73
9	2.028	19.25	10.3	1.6703	47.57
12.4	2.0246	23.56	15.3	1.6753	41.18
17.9	2.019	26.53	20.3	1.6803	38.38
27.9	2.009	29.28	25.3	1.6853	37.32
37.4	1.9996	30.73	35.3	1.6953	35.58
62.4	1.9746	31.58	45.3	1.7053	34.79
86.4	1.9506	32.03	60.3	1.7203	34.06
136.4	1.9006	32.18	85.3	1.7453	32.96
188.9	1.8481	32.09	185.3	1.8453	32.11

Appendix IV B
Velocity Distributions
 V_{ϕ} versus r

Run 47 V

5000 rpm

$T_{\text{rotor}} = 606.2 \text{ R}$

$T_{\text{stator}} = 526.4 \text{ R}$

$\Delta T = 79.8 \text{ R}$

Stator

Rotor

$y_{r,m}$	r, inches	V_{ϕ} ft/sec	$y_{r,m}$	r, inches	V_{ϕ} ft/sec
0	2.037	0	0	1.6613	(72.49)
5	2.032	13.08	8	1.6693	50.75
9	2.028	16.93	10	1.6713	47.92
12	2.025	20.21	15	1.6763	41.60
15	2.022	22.77	20	1.6813	38.30
20	2.017	26.01	25	1.6863	37.18
30	2.007	28.19	35	1.6963	35.47
40	1.997	29.63	45	1.7063	34.63
65	1.972	30.04	60	1.7213	33.90
90	1.947	31.08	85	1.7463	32.74
140	1.897	31.37	135	1.8463	31.44

Appendix IV B
Velocity Distributions
 V_θ versus r

Run 48 V

5000 rpm

$T_{\text{rotor}} = 725.8 \text{ R}$

$T_{\text{stator}} = 549.9 \text{ R}$

$\Delta T = 179.5 \text{ R}$

Stator

Rotor

y, m	r, inches	V_θ , ft/sec	y, m	r, inches	V_θ , ft/sec
0	2.037	0	0	1.6632	72.49
5	2.032	11.30	9	1.6722	52.29
9	2.028	15.71	10	1.6732	51.18
12	2.025	18.99	15	1.6782	44.07
15	2.022	22.06	20	1.6832	40.64
20	2.017	25.34	25	1.6882	38.66
30	2.007	28.30	35	1.6982	36.85
40	1.997	29.62	45	1.7082	35.81
65	1.972	30.98	60	1.7232	34.62
90	1.947	31.86	85	1.7482	33.30
140	1.897	31.75	185	1.8482	32.74

Appendix IV B
Velocity Distributions
 V_{θ} versus r

Run 49 V

5000 rpm

 $T_{\text{rotor}} = 880.5 \text{ R}$ $T_{\text{stator}} = 559.7 \text{ R}$ $\Delta T = 320.8 \text{ R}$

Stator			Rotor		
$Y_{T,m}$	r, inches	V_{θ} , ft/sec	$Y_{T,m}$	r, inches	V_{θ} , ft/sec
0	2.037	0	0	1.6656	(72.7)
5	2.032	11.48	9	1.6746	56.2
9	2.028	14.81	10	1.6756	54.6
12	2.025	18.08	15	1.6806	47.1
15	2.022	20.75	20	1.6856	43.1
20	2.017	24.22	25	1.6906	40.4
30	2.007	27.74	35	1.7006	38.1
35	2.002	28.67	45	1.7106	36.6
40	1.997	29.28	60	1.7256	35.1
65	1.972	31.28	85	1.7506	33.8
90	1.947	31.69	185	1.8506	32.4
140	1.897	32.21			

Appendix IV B
Velocity Distributions
 V_θ versus r

Run 51 V

7000 rpm

$T_{\text{rotor}} = 606.7 \text{ R}$

$T_{\text{stator}} = 540.2 \text{ R}$

$\Delta T = 66.5 \text{ R}$

Stator

Rotor

$y_{T,m}$	r , inches	V_θ , ft/sec	$y_{T,m}$	r , inches	V_θ , ft/sec
0	2.037	0	0	1.6614	(101.49)
5	2.032	21.74	8	1.6694	73.21
9	2.028	29.71	10	1.6714	66.33
12	2.025	34.52	15	1.6764	57.52
15	2.022	37.09	20	1.6814	54.03
20	2.017	39.67	25	1.6864	52.17
30	2.007	41.95	35	1.6964	50.13
40	1.997	43.11	45	1.7064	48.96
65	1.972	43.90	60	1.7214	47.75
90	1.947	44.23	85	1.7464	46.40
140	1.897	44.62	185	1.8464	44.81

Appendix IV B
Velocity Distributions
 V_θ versus r

Run 50 V

7000 rpm

Adiabatic, $t = 80$ F

Stator			Rotor		
$y_{T,m}$	r , inches	V_θ , ft/sec	$y_{T,m}$	r , inches	V_θ , ft/sec
0	2.037	0	0	1.660	101.4
5	2.032	24.53	8	1.668	73.53
9	2.028	32.66	10	1.670	66.40
12	2.025	36.29	15	1.675	57.26
15	2.022	38.48	20	1.680	57.77
20	2.017	40.75	25	1.685	51.88
30	2.007	42.71	35	1.695	49.95
40	1.997	43.87	45	1.705	48.74
65	1.972	44.46	60	1.720	47.58
90	1.947	44.66	85	1.745	46.58
140	1.897	44.65	185	1.8455	45.34

Appendix IV B
Velocity Distributions
 V_θ versus r

Run 53 V

7000 rpm

$T_{\text{rotor}} = 888.7 \text{ R}$

$T_{\text{stator}} = 564.8 \text{ R}$

$\Delta T = 323.9 \text{ R}$

Stator

Rotor

$y_{T,m}$	r, inches	V_θ , ft/sec	$y_{T,m}$	r, inches	V_θ , ft/sec
0	2.037	0	0	1.6654	0
4.5	2.032	17.36	8	1.6734	80.99
8.5	2.028	24.34	10	1.6754	74.49
11.5	2.025	28.52	15	1.6804	63.24
14.5	2.022	32.34	20	1.6854	57.50
19.5	2.017	36.14	25	1.6904	54.35
29.5	2.007	40.55	35	1.7004	50.98
39.5	1.997	42.55	45	1.7104	49.53
64.5	1.972	43.60	60	1.7254	48.23
89.5	1.947	44.51	85	1.7504	46.46
139.5	1.897	44.36	185	1.8504	44.78

Appendix IV C

Frictionless Velocity, U_{*} , and Probe Displacement

RPM	Rotor		Displacement, inches x 10^3	$U_{*, \text{rotor}}$	$U_{*, \text{stator}}$	Stator	
	ΔT , deg F	$U_{*, \text{rotor}}$				Displacement	Displacement
3000	0	1.78	2	1.45	1.8		
5000	0	2.75	1.5	2.24	1.0		
7000	0	3.67	3.4	2.97	1.3		
3000	67.9	1.82	1.5	1.40	2.0		
5000	79.8	2.8	0.4	2.15	0		
7000	66.5	3.72	1.5	2.85	1.5		
3000	179.5	1.82	1.0	1.33	1.5		
5000	179.5	2.91	0	2.07	0		
3000	292.5	2.1	3.0				
5000	320.8	3.06	0.5	2.0	0.25		
7000	323.9	4.4	2.9	2.82	0		

Appendix IV D
Friction Factor, f^1 and Taylor Number²

rpm	ΔT	$f_{rotor} \times 10^2$	$f_{stator} \times 10^2$	Taylor Number
3000	0	1.665	1.105	3829
5000	0	1.430	0.949	6385
7000	0	1.299	0.870	9092
3000	67.9	1.735	1.027	3621
5000	79.8	1.479	0.872	6035
7000	66.5	1.332	0.793	8400
3000	179.5	1.728	0.916	3018
5000	179.5	1.589	0.805	5030
3000	292.5	2.291		2496
5000	320.8	1.747	0.748	4003
7000	323.9	1.85	0.77	5450

$$1 \quad f_{rotor} = \frac{P_{rotor}}{\frac{1}{2} \rho V_{rotor}^2 d}$$

$$2 \quad Ta = \sqrt{\frac{d}{f_{rotor}}} \frac{V_{rotor} d}{\nu_{rotor}}$$

Appendix IV - E

 $(1 + \epsilon_m/\omega)/f$, and $(\epsilon_m/\omega)/f$, versus y^+

3000 rpm, Adiabatic

$$f_{\text{rotor}} = 1.665 \times 10^{-2}$$

$$f_{\text{stator}} = 1.105 \times 10^{-2}$$

Rotor			Stator		
y^+	$(1 + \epsilon_m/\omega)/f$	$(\epsilon_m/\omega)/f$	y^+	$(1 + \epsilon_m/\omega)/f$	$(\epsilon_m/\omega)/f$
4.8	75.52	15.45	4.83	110.95	20.43
6.98	86.63	26.56	6.61	122.28	31.76
9.16	112.37	52.30	8.39	133.23	42.71
11.34	149.53	89.46	11.94	176.06	85.54
13.52	200.58	140.51	15.5	282.81	192.29
15.7	254.96	194.89	19.05	447.14	356.62
20.07	406.55	346.48	22.61	676.15	585.63
24.43	606.74	546.67	26.16	1109	1018.5
28.79	719.3	659.23			
33.15	854.7	794.63			
37.52	1039	978.9			

Appendix IV - E

 $(1 + \epsilon_m/\omega)/f$, and $(\epsilon_m/\omega)/f$, versus y^+

3000 rpm

$$T_{\text{rotor}} = 606.1 \text{ R}$$

$$T_{\text{stator}} = 538.2 \text{ R}$$

$$\Delta T = 67.9 \text{ R}$$

$$f_{\text{rotor}} = 1.735 \times 10^{-2}$$

$$f_{\text{stator}} = 1.027 \times 10^{-2}$$

Rotor			Stator		
y^+	$(1 + \epsilon_m/\omega)/f$	$(\epsilon_m/\omega)/f$	y^+	$(1 + \epsilon_m/\omega)/f$	$(\epsilon_m/\omega)/f$
3.85	63.54	5.91	3.58	109.77	12.37
7.7	87.13	29.5	7.16	128.12	30.72
11.55	148.25	90.62	10.74	161.93	64.53
14.25	208.97	152.34	12.17	182.15	84.75
18.1	315.46	257.83	15.75	269.32	171.92
21.95	453.24	395.61	19.33	433.3	335.9
25.8	582.94	525.31	22.91	768.1	670.7
29.6	726.96	669.33	26.49	1422.3	1324.9
33.5	955.3	897.67	30.07	2286.1	2188.7
			33.65	3096.5	2999.1

Appendix IV - E

$(1 + \epsilon_m/\omega)/f$, and $(\epsilon_m/\omega)/f$, versus y^+

3000 rpm

$$T_{\text{rotor}} = 725.7 \text{ R}$$

$$T_{\text{stator}} = 546.2 \text{ R}$$

$$\Delta T = 179.5 \text{ R}$$

$$f_{\text{rotor}} = 1.728 \times 10^{-2}$$

$$f_{\text{stator}} = 0.916 \times 10^{-2}$$

Rotor

Stator

y^+	$(1 + \epsilon_m/\omega)/f$	$(\epsilon_m/\omega)/f$	y^+	$(1 + \epsilon_m/\omega)/f$	$(\epsilon_m/\omega)/f$
2.84	58.74	.87	3.27	113.11	3.93
4.26	60.36	2.49	4.9	123.8	14.62
5.68	67.24	9.37	6.53	138.72	29.54
7.10	74.74	16.87	8.17	162.41	53.23
8.52	93.17	35.30	9.8	200.24	91.06
9.94	122.33	64.46	13.07	333.61	244.43
10.79	150.41	92.54	15.68	426.85	317.67
13.63	237.38	179.51	17.32	474.24	365.06
16.47	293.23	235.36	20.59	565.57	456.39
19.31	383.81	325.94	23.86	647.73	538.55
22.15	517.69	459.8	27.13	745.56	636.38
24.99	599.92	542.05	30.40	795.62	686.44

Appendix IV - E

$(1 + \epsilon_m/z)/f$, and $(\epsilon_m/z)/f$, versus y^+

3000 rpm

$$T_{rotor} = 847.9 R$$

$$T_{stator} = 555.4$$

$$\Delta T = 292.5 R$$

Rotor

y^+	$(1 + \epsilon_m/z)/f$	$(\epsilon_m/z)/f$
2.49	44.5	0.85
4.97	52.6	9.00
7.46	78.5	34.9
9.98	122.6	78.95
12.43	169.8	126.2
14.91	218.2	174.6
17.40	280.34	236.7
22.37	447.73	404.1

Appendix IV - E

 $(1 + \epsilon_m/\psi)/f$, and $(\epsilon_m/\psi)/f$, versus y^+

5000 rpm adiabatic

$$f_{\text{rotor}} = 1.430 \times 10^{-2}$$

$$f_{\text{stator}} = 0.949 \times 10^{-2}$$

Rotor			Stator		
y^+	$(1 + \epsilon_m/\psi)/f$	$(\epsilon_m/\psi)/f$	y^+	$(1 + \epsilon_m/\psi)/f$	$(\epsilon_m/\psi)/f$
8.09	105.85	35.93	9.35	178.5	73.1
11.46	137	67.1	12.1	226.77	121.4
14.83	185.5	115.6	14.85	299.79	194.4
18.2	265.1	195.2	17.6	415.15	309.8
21.59	396.2	326.3	20.35	571.78	466.4
24.94	595.2	525.3	23.1	757.92	652.5
28.31	835.1	765.2	28.6	1116.5	1011.1
31.68	1082.6	1012.7	34.1	1482.44	1377
38.42	1437.7	1367.8	39.6	1927.34	1821.9
45.16	1777.2	1707.3	45.1	2893.28	2787.9
58.64	2761.5	2691.6			

Appendix IV - E

$(1 + \epsilon_m/\omega)/f$, and $(\epsilon_m/\omega)/f$, versus y^+

5000 rpm

$$T_{\text{rotor}} = 606.2 \text{ R}$$

$$T_{\text{stator}} = 526.4 \text{ R}$$

$$\Delta T = 79.8 \text{ R}$$

$$f_{\text{rotor}} = 1.479 \times 10^{-2}$$

$$f_{\text{stator}} = 0.872 \times 10^{-2}$$

Rotor			Stator		
y^+	$(1 + \epsilon_m/\omega)/f$	$(\epsilon_m/\omega)/f$	y^+	$(1 + \epsilon_m/\omega)/f$	$(\epsilon_m/\omega)/f$
8.41	103.9	36.3	5.27	151.1	36.4
11.37	135.8	68.2	10.54	220.7	106.
17.28	247.8	180.2	15.81	341.1	226.4
23.2	478.4	410.8	21.08	611.7	497.
29.12	918.3	850.7	26.35	1152.3	1037.6
35.04	1315.2	1247.6	31.62	1639.7	1525.
40.96	1748	1680.4	36.89	2105.1	1990.4
46.88	2157.2	2089.6	42.16	2622.2	2507.8
52.81	2563.8	2496.2	47.43	3232.5	3117.8
			52.7	3953.9	3839.2

Appendix IV - E

$(1 + \epsilon n/\omega)/f$, and $(\epsilon n/\omega)/f$, versus y^+

5000 rpm

$$T_{\text{rotor}} = 725.8 \text{ R}$$

$$T_{\text{stator}} = 549.9 \text{ R}$$

$$\Delta T = 179.5 \text{ R}$$

$$f_{\text{rotor}} = 1.589 \times 10^{-2}$$

$$f_{\text{stator}} = 0.805 \times 10^{-2}$$

Rotor			Stator		
y^+	$(1 + \epsilon n/\omega)/f$	$(\epsilon n/\omega)/f$	y^+	$(1 + \epsilon n/\omega) f$	$(\epsilon n/\omega)/f$
4.52	75.4	13.5	5.07	151.5	27.3
9.04	96.7	33.8	10.15	193.4	69.2
13.56	168.6	105.7	15.22	295.7	171.5
18.08	307.6	244.7	20.29	487.5	363.3
22.61	515.1	452.2	25.37	815.2	691.
27.13	854	791.1	30.44	1273.2	1149.
31.65	1242	1179.1	35.51	1719.5	1595.3
36.17	1513.4	1450.5	40.59	2186.3	2062.1
40.69	1554.8	1491.9	45.66	2537.9	2413.7

Appendix IV - E

 $(1 + \epsilon\eta/\rho)/f$, and $(\epsilon\eta/\rho)/f$, versus y^+

5000 rpm

$$T_{\text{rotor}} = 880.5 \text{ R}$$

$$T_{\text{stator}} = 559.7 \text{ R}$$

$$\Delta T = 320.8 \text{ R}$$

$$f_{\text{rotor}} = 1.747 \times 10^{-2}$$

$$f_{\text{stator}} = 0.748 \times 10^{-2}$$

Rotor			Stator		
y^+	$(1 + \epsilon\eta/\rho)/f$	$(\epsilon\eta/\rho)/f$	y^+	$(1 + \epsilon\eta/\rho)/f$	$(\epsilon\eta/\rho)/f$
3.75	64.4	7.2			
5.12	69.6	12.4	5.92	139.9	6.2
6.49	75.6	18.4	7.81	181.5	47.8
9.22	93.9	36.7	9.71	202.5	68.8
11.96	141.9	84.7	13.5	266.6	132.9
14.69	222.3	165.1	17.3	333.9	200.2
17.42	344.2	287	21.1	465.3	331.6
20.15	511.7	454.5	24.9	705.3	571.6
22.88	618	560.8	28.6	987.5	853.8
25.62	659.6	602.4	32.4	1277.9	1144.2
26.98	723	665.8	36.2	1464.8	1331.1
			38.1	1506.1	1372.4

Appendix IV - E

$(1 + \epsilon_m/z)/f$, and $(\epsilon_m/z)/f$, versus y^+

7000 rpm Adiabatic

$$f_{\text{rotor}} = 1.299 \times 10^{-2}$$

$$f_{\text{stator}} = 0.87 \times 10^{-2}$$

Rotor			Stator		
y^+	$(1 + \epsilon_m/z)/f$	$(\epsilon_m/z)/f$	y^+	$(1 + \epsilon_m/z)/f$	$(\epsilon_m/z)/f$
12.52	149.5	72.5	6.55	170.1	52.45
17.	233.5	156.5	10.22	204.2	86.6
21.5	393.2	316.2	13.87	267.5	149.9
25.9	617.8	540.8	17.52	371.5	253.9
30.4	894.2	817.2	21.17	537.6	420
34.9	1205.3	1128.3	24.82	788.1	670.5
39.4	1534.5	1457.5	28.47	1115.7	998.1
48.3	2216.6	2139.6	32.12	1530	1412.4
57.3	2777.3	2700.3	35.77	1967	1849.4
66.2	3281.8	3204.8	39.42	2359	2241.4
75.1	3742.3	3665.3	46.72	2919	2801.4
			54.02	3963.8	3846.2
			61.32	6341.8	6224.2
			68.62	8796.3	8678.7

Appendix IV - E

 $(1 + \epsilon n/\omega)/f$, and $(\epsilon n/\omega)/f$, versus y^+

7000 rpm

$$T_{\text{rotor}} = 606.7 \text{ R}$$

$$T_{\text{stator}} = 540.2 \text{ R}$$

$$\Delta T = 66.5 \text{ R}$$

$$f_{\text{rotor}} = 1.332 \times 10^{-2}$$

$$f_{\text{stator}} = 0.79 \times 10^{-2}$$

Rotor			Stator		
y^+	$(1 + \epsilon n/\omega)/f$	$(\epsilon n/\omega)/f$	y^+	$(1 + \epsilon n/\omega)/f$	$(\epsilon n/\omega)/f$
7.91	114.8	39.7	7.3	179.7	51.8
13.45	163.7	88.6	14.6	279.4	151.5
21.36	361.2	286.1	18.25	388	260.1
29.27	775.2	700.1	24.1	681.1	553.2
37.18	1362.6	1287.5	31.39	1301.7	1173.8
45.09	1953.4	1878.3	38.69	2092.1	1964.2
53	2422.8	2347.7	45.99	3019	2891
60.91	2871.5	2796.4	53.29	4186.6	4058.7
68.82	3277.9	3202.8	60.59	5897.2	5769
			67.89	7779.6	7651.7

Appendix IV - E

 $(1 + \epsilon_m/\omega)/f$, and $(\epsilon_m/\omega)/f$, versus y^+

7000 rpm

$$\begin{aligned} T_{\text{Rota}} &= 809.8 R \\ T_{\text{stator}} &= 568.9 R \end{aligned}$$

Stator			Rotor		
y^+	$(1 + \epsilon_m/\omega)/f$	$(\epsilon_m/\omega)/f$	y^+	$(1 + \epsilon_m/\omega)/f$	$(\epsilon_m/\omega)/f$
6.69	175.29	45.29	7.1	82.3	28.3
13.37	292.86	162.86	9.56	107.9	53.9
20.06	463.77	333.77	12.03	143.8	89.8
26.74	778.70	648.7	14.49	198.2	144.2
33.43	1228.21	1098.2	16.96	279.7	225.7
40.11	1642.73	1512.73	19.42	376.1	322.1
46.80	2242.2	2112.2	21.88	491.4	437.4
53.48	3441.6	3311.6	26.81	711.	657.
56.83	5120.4	4990.4	29.28	868.	814.
			34.2	1153.	1099.
			39.1	1643.	1589.
			44.1	2018	1964

Appendix IV - F
 Typical Temperature Distribution, T versus r
 Run 8 I

5000 rpm
 Trotor = 722.4 R
 Tstator = 549.4 R
 T = 173.0 R

r _{plate} , inches	r _{true} , inches	$\rho_{\text{measured}} \text{ \#/ft}^3$	$\rho_{\text{corrected}} \text{ \#/ft}^3$	T, deg R
.7669	1.6633	0.056184	0.056184	722.4
.7664	1.6662	0.056283	0.056275	706.87
.7668	1.6651	0.056436	0.056434	705.73
.7666	1.6659	0.056626	0.056621	703.74
.7671	1.6655	0.056760	0.056763	701.42
.7676	1.6666	0.056904	0.056915	699.66
.7679	1.6677	0.057061	0.056915	697.79
	1.6683		0.057077	695.81

Appendix IV - F

Typical Temperature Distribution, T versus r

Run 8 I (Continued)

r_{plate} , inches	r_{true} , inches	ρ_{measured} #/ft ³	$\rho_{\text{corrected}}$ #/ft ³	T, deg R
.7681	1.6688	0.057233	0.057242	693.81
.7678	1.6681	0.057446	0.057461	691.16
.7686	1.6695	0.057756	0.057783	687.31
.7689	1.6705	0.058215	0.058247	681.83
.7695	1.6718	0.058665	0.058707	676.49
.7702	1.6733	0.059120	0.059173	671.16
.7713	1.6757	0.059532	0.059603	666.32
.7722	1.6777	0.059996	0.060001	661.02
.7737	1.6809	0.060395	0.060505	656.39
.7751	1.6840	0.060821	0.060953	651.56
.7774	1.6890	0.061149	0.061318	647.69
.7806	1.6959	0.061375	0.061596	644.76
.7843	1.7040	0.061535	0.061815	642.48

Appendix IV - F

Typical Temperature Distribution, T versus r

Run 8 I (Continued)

r_{plate} , inches	r_{true} , inches	ρ_{measured} #/ft ³	$\rho_{\text{corrected}}$ #/ft ³	T, deg R
.7883	1.7127	0.061667	0.062012	640.44
.7925	1.7218	0.061776	0.062188	638.63
.7968	1.7311	0.061866	0.062348	636.99
.8012	1.7407	0.061938	0.062491	635.53
.8061	1.7513	0.061963	0.062595	634.47
.8106	1.7611	0.062030	0.062734	633.07
.8152	1.7711	0.062088	0.062866	631.74
.8200	1.7815	0.062108	0.062963	630.76
.8252	1.7928	0.062067	0.063006	630.33
.8309	1.8052	0.61999	0.063030	630.09
.8362	1.8167	0.061954	0.063070	629.69
.8577	1.8634	0.061768	0.063199	628.41
.8843	1.9212	0.061556	0.063447	625.95
.8899	1.9334	0.061484	0.063466	625.77

Appendix IV - F

Typical Temperature Distribution, T versus r

Run 8 I (Continued)

r _{plate} , inches	r _{true} , inches	$\rho_{\text{measured}} \#/\text{ft}^3$	$\rho_{\text{corrected}} \#/\text{ft}^3$	T, deg R
.8952	1.9449	0.061443	0.063510	625.33
.9003	1.9560	0.061430	0.063579	624.65
.9051	1.9664	0.061450	0.063676	623.70
.9150	1.97771	0.061476	0.063781	622.67
.9151	1.9881	0.061468	0.063856	621.94
.9194	1.9975	0.061558	0.064015	620.40
.9231	2.0055	0.061746	0.064262	618.01
.9262	2.0123	0.062014	0.06580	614.97
.9285	2.0172	0.062417	0.065020	610.81
.9293	2.0190	0.062588	0.065204	609.09
.9301	2.0207	0.062774	0.065403	607.23
.9305	2.0216	0.063030	0.065666	604.80
.9300	2.0222	0.063127	0.065767	603.87

Appendix IV - F

Typical Temperature Distribution, T versus r

Run 8 I (Continued)

r _{plate} , inches	r _{true} , inches	$\rho_{\text{measured}} \text{ \#/ft}^3$	$\rho_{\text{corrected}} \text{ \#/ft}^3$	T, deg R
.9311	2.0227	0.063257	0.065901	602.64
.9322	2.0242	0.063471	0.066126	600.59
	2.0253	0.063830	0.066493	597.23

Appendix IV - G

V_f / r and Temperature versus r

3000 rpm	y_f	r , inches	T, deg R	V_f / r , (ft/sec)/ft
$\Delta \approx 70F$	Distance from Surface,			
	Thousandths of inches			
rotor	0	1.6613	603.8	314.16
	6.5	1.6678	590.3	251.7
	8.5	1.6698	587.8	235.50
	13.5	1.6748	582.3	204.8
	18	1.6793	579.2	188.7
	23	1.6843	576.6	177.
	33	1.6943	572.	164.6
	43	1.7043	569.7	155.7
	58	1.7193	567	150.1
	83	1.7443	564	142.3
	183	1.8443	557	122.1

Appendix IV - G

V_{ϕ}/r and Temperature versus r (Continued)

3000 rpm	y_T	r , inches	T, deg R	V_{ϕ}/r , (ft/sec)/ft
$\Delta T \approx 70^{\circ}\text{F}$ stator	Distance from Surface			
	Thousandths of inches			
	142	1.895	578.6	117.20
	92	1.945	576.2	116.61
	67	1.970	573.5	116.47
	42	1.995	570.5	112.06
	32	2.005	568.6	107.73
	22	2.015	563.5	93.8
	17	2.020	559.5	80.26
	14	2.023	557.2	67.68
	11	2.026	553.3	58.22
	7	2.030	547.2	39.49
	0	2.037	535.4	0

Appendix IV - G

		V /r and Temperature versus r (Continued)			
3000 rpm	γ_T	r, inches	T, deg R	V_f /r , (ft/sec)/ft	
$\Delta T = 170^\circ F$	Distance from Surface				
	Thousandths of inches				
	184	1.8474	637.7	121.57	
	84	1.7474	640.5	140.96	
	59	1.7224	643	151.23	
	44	1.7074	646	160.54	
	34	1.6974	649.4	168.98	
	24	1.6874	657.4	184.03	
	19	1.6824	663	194.45	
	14	1.6774	671.3	213.83	
	9	1.6724	687.6	248.22	
7	1.6704	695.2	260.05		
0	1.6634	722	314.16		
rotor					

Appendix IV - G

V_{θ}/r and Temperature versus r (Continued)

3000 rpm	V_{θ}/r	r , inches	T, deg R	V_{θ}/r , (ft/sec)/ft
$\Delta T \approx 170^{\circ}\text{F}$	Distance from Surface			
	Thousandths of inches			
stator	0	2.037	549.3	0
	6.5	2.0305	574.1	35.28
	10.5	2.0265	583.	48.97
	13.5	2.0235	593.6	58.95
	16.5	2.0205	601.3	66.46
	21.5	2.0155	611.9	73.77
	31.5	2.0055	622.4	83.95
	41.5	1.9955	628.3	92.19
	66.5	1.9705	633.6	107.85
	91.5	1.9455	636.5	111.70
	141.5	1.8955	637.5	117.

Appendix IV - G

V_{θ}/r and Temperature versus r (Continued)

3000 rpm	r_T	r , inches	T, deg R	V_{θ}/r , (ft./sec)/ft
475 3002 rotor	Distance from Surface			
	Thousandths of inches			
	0	1.6654	847.8	314.16
	5	1.6704	819	275.6
	7	1.6724	810	259.8
	12	1.6774	793	227.6
	17	1.6824	781	205.1
	22	1.6874	767	190.5
	32	1.6974	757	171.9
	42	1.7074	750	160.4
	58	1.7224	745	150.6
	83	1.7474	736.8	136.4
	103	1.8474		113.8

Appendix IV - G

5000 rpm	V_{θ}/r	γT	V_{θ}/r and Temperature versus r (Continued)	r , inches	T , deg R	V_{θ}/r , (ft/sec)/ft
$\Delta T = 70^{\circ}F$	Distance from Surface	Thousandths of inches				
stator	0	2.037	535.6		0	
	5	2.032	541.7		77.27	
	9	2.028	545.1		100.18	
	12	2.025	547.1		119.76	
	15	2.022	549.3		135.13	
	20	2.017	552.1		154.74	
	30	2.007	555.2		168.55	
	40	1.997	556.6		178.03	
	65	1.972	557.8		182.8	
	90	1.947	558.7		191.6	
	140	1.897	560.1		198.4	

Appendix IV - G

V_g/r and Temperature versus r (Continued)

5000 rpm	y_T	r , inches	T, deg R	V_e/r , (ft/sec)/ft
$\Delta T \approx 70F$	Distance from Surface			
	Thousandths of inches			
rotor	184.6	1.8459	560.7	204.31
	84.6	1.7459	562.9	224.98
	59.6	1.7209	564	236.33
	44.6	1.7059	564.9	243.54
	34.6	1.6959	565.7	250.92
	24.6	1.6859	567.4	264.58
	19.6	1.6809	569.2	273.36
	14.6	1.6759	573.6	297.79
	9.6	1.6709	580.1	344.06
	7.6	1.6689	583.6	364.82
	0	1.6613	603.3	523.6

Appendix IV - G

V_{θ}/r and Temperature versus r (Continued)

5000 rpm $\Delta T \cong 170^{\circ}\text{F}$	y_T	r , inches	T, deg R	V_{θ}/r , (ft/sec)/ft
	Distance from Surface			
	Thousandths of inches			
stator	0	2.037	549.4	0
	5	2.032	573.5	66.71
	9	2.028	589.	92.94
	12	2.025	598.	112.51
	15	2.022	604.5	130.89
	20	2.017	611.3	150.74
	30	2.007	616.9	169.19
	40	1.997	620.5	177.96
	65	1.972	623.2	188.53
	90	1.947	625.2	193.3
	140	1.897	627.	200.82

Appendix IV - G

V_{θ}/r and Temperature versus r (Continued)

5000 rpm	y_T	r , inches	T, deg R	V_{θ}/r , (ft/sec)/ft
$\Delta T \approx 170^{\circ}F$ rotor	Distance from Surface			
	Thousandths of inches			
	0	1.6632	722.4	523.6
	9	1.6722	675.	375.26
	10	1.6732	671.5	367.09
	15	1.6782	660.1	315.12
	20	1.6832	653.	289.76
	25	1.6882	648.5	274.82
	35	1.6987	644.2	260.37
	45	1.7082	641.4	252.13
	60	1.7232	638.4	241.07
	85	1.7482	634.8	228.56
	185	1.8482	628.8	206.06

Appendix IV - G

5000 rpm $\Delta T \approx 320^\circ\text{F}$		V_θ / r and Temperature versus r (Continued)	V_θ / r , (ft/sec)/ft
y_T	r, inches	T, deg R	
Distance from Surface			
Thousands of inches			
0	1.6656	879.	523.6
8.5	1.6741	816.	402.9
9.5	1.6751	811	391.2
14.5	1.6801	784.1	336.6
19.5	1.6851	771.	307.03
24.5	1.6901	763.	286.9
34.5	1.7001	755.	269.02
44.5	1.7101	748.	257.03
59.5	1.7251	741.	244.45
84.5	1.7501	737.	231.91
184.5	1.8501	726.	210.15

Appendix IV - G

5000 rpm		V_{ϕ}/r and Temperature versus r (Continued)	r , inches	T , deg R	V_{ϕ}/r , (ft/sec)/ft
$\Delta T \cong 320^{\circ}\text{F}$	y_r	Distance from Surface			
	Thousandths of inches				
stator	0		2.037	564.5	0
	5.25		2.0318		67.80
	9.25		2.0278	677.	87.64
	12.25		2.0248	694.	107.2
	15.25		2.0218	701.	123.2
	20.25		2.0168	705.5	144.1
	30.25		2.0068	712.	165.9
	35.25		2.0018	714.5	171.9
	40.25		1.9968	716.	178
	65.25		1.9718	717.5	190.4
	90.25		1.9468	716.5	195.3
	140.25		1.8968	720.5	203.8

Appendix IV - G

V_{ϕ} / r and Temperature versus r (Continued)

7000 rpm	y_T	r , inches	T, deg R	V_{ϕ} / r , (ft/sec)/ft
$\Delta T = 70^{\circ}\text{F}$ rotor	Distance from Surface			
	Thousandths of inches			
	0	2.037	531.2	0
	6.5	2.0305	553.	128.48
	10.5	2.0265	555.5	175.93
	13.5	2.0235	557.1	204.71
	16.5	2.0205	558.5	220.28
	21.5	2.0155	560.5	236.19
	31.5	2.0055	562.8	251.01
	41.5	1.9955	563.5	259.24
	66.5	1.9705	563.9	267.34
	91.5	1.9455	564.9	272.81
	141.5	1.8955	565.5	282.48

Appendix IV - G

V_b/r and Temperature versus r (Continued)

7000 rpm $\Delta T \cong 70F$	y_T Distance from Surface Thousandths of inches	r , inches	T, deg R	V_b/r , (ft/sec)/ft
stator	0	1.6613	602.6	733.04
	6.5	1.668	581.1	526.25
	8.5	1.670	579.2	476.22
	13.5	1.675	576.4	411.74
	18.5	1.680	574.7	385.61
	23.5	1.685	573.3	371.23
	33.5	1.695	571.1	354.61
	43.5	1.705	569.9	344.38
	58.5	1.720	569.5	332.87
	83.5	1.745	568.5	318.83
	183.5	1.845	566.6	291.23

Appendix IV - G

V_{ϕ} / r and Temperature versus r (Continued)

7000 rpm $\Delta T \approx 320F$	V_T	r , inches	V_{ϕ} / r (ft/sec)/ft	T , deg R
	Distance from Surface			
	Thousandths of inches			
rotor	0	1.6654	733.04	889.8
	5.1	1.6705	580.78	
	7.1	1.6725	533.53	834.
	12.1	1.6775	451.61	809.
	17.1	1.6825	409.4	791.
	22.1	1.6875	385.83	780.
	32.1	1.6975	359.77	769.
	42.1	1.7075	347.5	762.
	57.1	1.7225	335.44	753.
	82.1	1.7475	318.51	747.
	182.1	1.8475	290.40	737.

Appendix IV - G

V_{ϕ}/r and Temperature versus r (Continued)

7000 rpm $\Delta T \approx 320^{\circ}\text{F}$	y_T Distance from Surface Thousandths of inches	r , inches	V_{ϕ}/r (ft/sec)/ft	T , deg R
stator	0	2.037	0	568.9
	4.5	2.0325	102.49	
	8.5	2.0285	143.99	
	11.5	2.0255	168.97	
	14.5	2.0225	191.88	
	19.5	2.0175	214.96	662.
	29.5	2.0075	242.39	704.
	39.5	1.9975	255.62	715.
	64.5	1.9725	265.25	725.
	89.5	1.9475	274.26	729.
	139.5	1.8975	280.54	733.

Appendix V

Fluid Properties of Air Used in the Computations

For evaluation of the integrals in Chapter IX containing as factors the fluid properties k and ν , it was desirable to express both these quantities as functions of the absolute temperature T .

Values of k and μ obtained from Keenan and Kaye, Gas Tables¹, Table 2, Air at Low Pressures, p. 34 were plotted on log-log coordinates as in Fig. V-1.

If constant Prandtl number and constant specific heat are assumed, then k and μ vary in the same manner with temperature.

As can be seen from the figure, the curves for k and μ are slightly divergent. A straight line was drawn representing the average slope between the two curves. This line varies as $T^{0.75}$.

From McAdams, Heat Transmission,² 2nd edition, the thermal conductivity of air at 212°F, from the data of Moser, Dissertation, Berlin 1913, is given as 0.0183 Btu/hr-ft²-degF/ft. A line varying as $T^{0.75}$ was passed through this point resulting in

$$k = 1.389 \times 10^{-4} T^{0.75}$$

¹J. H. Keenan and J. Kaye, Gas Tables (1st ed., John Wiley and Sons, Inc., New York, New York, 1956), p. 34.

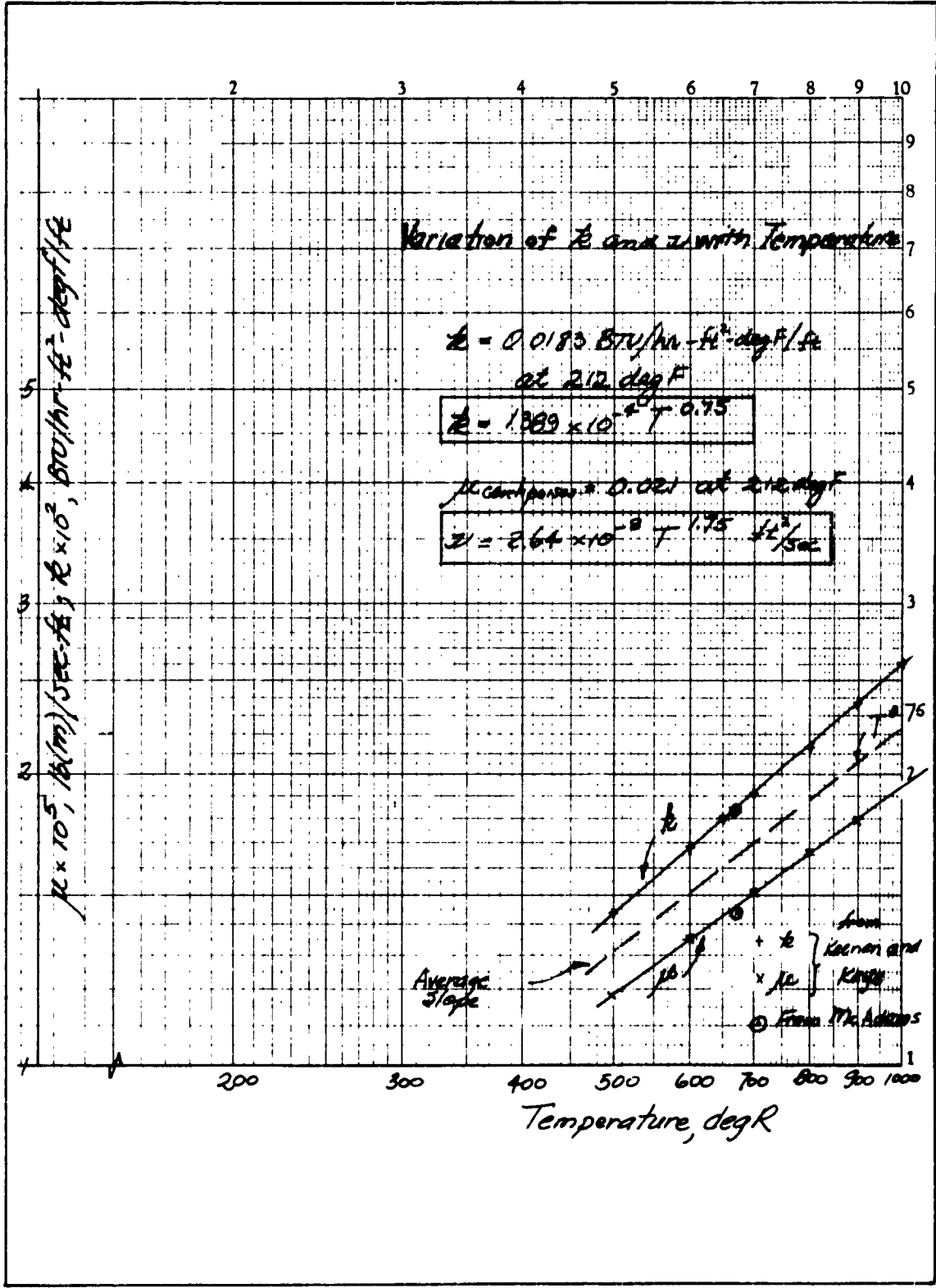
²McAdams, Heat Transmission, p. 391.

The kinematic viscosity ν varies with T as $T^{1.75}$ under the assumptions made.

Using a value of μ centipoises from McAdams, Fig. 204 of

μ centipoises = 0.021 at (100 C = 212 F)
a relationship for ν is obtained as

$$\nu = 2.64 \times 10^{-9} T^{1.75}$$



Bibliography

	Page	Footnote
	No.	No.
Chapter I		
Becker, Kurt, "An Experimental and Theoretical Study of Heat Transfer in an Annulus with an Inner Rotating Cylinder," Sc. D. Thesis, Massachusetts Institute of Technology, Aug. 1957.	8	1
Becker, K. M., and J. Kaye, "Measurements of Diabatic Flow in an Annulus with an Inner Rotating Cylinder," ASME Paper No. 61-SA-19, August, 1961.	8	2
Bjorklund, I. S., and W. M. Kays, "Heat Transfer between Concentric Rotating Cylinders, ASME Paper No. 58-A-99, 1958.	10	3
Brown, H. E., B. H. Amstead, and B. E. Short, "The Transfer of Heat and Momentum in a Turbulent Stream of Mercury," Trans. ASME, Vol. 79, 1957, pp. 279-285.	18	1
Corocoran, W. H., F. Page, Jr., W. G. Schlinger, and B. H. Sage, "Temperature Gradients in Turbulent Gas Streams," Industrial and Engineering Chemistry, vol. 44, 1952, pp. 410-430.	18	3
Corrsin, S., and M. S. Uberoi, NACA TN 2124, 1950	19	2

	Page	Footnote
	No.	No.
Elias, F., "Heat Transfer from a Heated Plate to Flowing Air," NACA TM 614, originally published in 1930.	17	2
Deissler, R. G., "Analysis of Turbulent Heat Transfer, Mass Transfer and Friction in Smooth Tubes at High Prandtl and Schmidt Numbers," NACA TN 3145, 1954.	16	3
Deissler, R. G. and C. S. Eian, "Analytical and Experimental Investigation of Fully Developed Turbulent Flow of Air in a Smooth Tube with Heat Transfer with Variable Fluid Properties," NACA TN 2629, 1952.	16	2
Deissler, R. G. and M. F. Taylor, "Analysis of Turbulent Flow and Heat Transfer in Non-Circular Passages," NACA TN 4384, 1958.	16	4
Gazley, Carl, Jr., "Heat Transfer Characteristics of Rotational and Axial Flow between Concentric Cylinders," ASME Paper No. 56-A-128, 1956.	10	2
Goldstein, S., <u>Modern Developments in Fluid Mechanics</u> (Oxford at the Clarendon Press, 1938) vol. I, pp. 209-214.	15	2
Hinze, J. O., <u>Turbulence</u> , McGraw-Hill Book Company, Inc., New York, 1959, p. 394.	16	1

	Page	Footnote
	No.	No.
Isakoff, S. E. and T. B. Drew, "Heat and Momentum Transfer in Turbulent Flow of Mercury," General Discussion on Heat Transfer, The Institution of Mechanical Engineers, London, 1951, pp. 405-409.	17	3
Kaye, J., and E. C. Elgar, "Modes of Adiabatic and Diabatic Fluid Flow in an Annulus with an Inner Rotating Cylinder," ASME Paper #57-HT-14, 1957.	6	1
Lewis, J. W., "An Experimental Study of the Motion of a Viscous Liquid Contained Between Two Coaxial Cylinders," Proc. Roy Soc. London, Ser. A, 117, pp. 388-407 (1927-1928).	5	1
Lyon, R. N., "Liquid Metal Heat Transfer Coefficients," Chemical Engineering Progress, vol. 47, 1951, pp. 75-79.	16	5
Pai, Shih-I, "Turbulent Flow between Rotating Cylinders," NACA TN-892, March 1943.	5	2
Prandtl, L., <u>Essentials of Fluid Dynamics</u> (Hafner Publishing Company, Inc., New York, 1952), p. 117-121.	15	1
Reichardt, H., "The Principles of Turbulent Heat Transfer," NACA TM 1408, 1957.	17	2

	Page	Footnote
	No.	No.
Seban, R. A. and T. T. Shimazaki, "Temperature Distribution for Air Flowing Turbulently in a Smooth Heated Pipe," General Discussion on Heat Transfer, The Institution of Mechanical Engineers, London, England, 1951, pp. 122-126.	18	2
Sleicher, Jr., C. A., "Experimental Velocity and Temperature Profiles for Air in Turbulent Pipe Flow," Trans. ASME, vol. 80, 1958, pp. 693-704.	18	4
Stewart, R. W., "A New Look at the Reynolds Stresses," Canadian Journal of Physics, vol. 34, 1956, pp. 722-725.	15	3
Taylor, G. I., "Stability of a Viscous Fluid Contained between Two Rotating Cylinders," Philosophical Trans. of the Royal Society of London, series A, vol. 223, 1923, pp. 289-343.	4	1
Taylor, G. I., "Distribution of Velocity and Temperature between Concentric Rotating Cylinders," Proc. Royal Society of London, ser. A, vol. 157, no. 892, Dec. 2, 1936, pp. 494-512.	13	1
Wattendorf, F. L., "A Study of the Effect of Curvature on Fully Developed Turbulent Flow," Proc. Royal Society of London, ser. A, no. 865, vol. 148, Feb. 1935, pp. 565-598.	13	3

	Page	Footnote
	No.	No.
Chapter II		
Deissler, R. G. and A. L. Loeffler, Jr., "Turbulent Flow and Heat Transfer on a Flat Plate at a High Mach Number with Variable Fluid Properties," ASME Paper Number 55-A-33, 1955, p. 20.	30	2
Li, Ting-Yi, and H. T. Nagamatsu, "Effect of Density Fluctuations on the Turbulent Skin Friction on a Flat Plate at High Supersonic Speeds," Guggenheim Aeronautical Laboratory, California Institute of Technology, Pasadena, California, Memorandum No. 11, Nov. 1, 1952, p. 4.	27	1
Chapter III		
Baker, H. D., E. A. Ryder, and N. H. Baker, <u>Temperature Measurement in Engineering</u> (New York: John Wiley and Sons, 1953), Vol. I.	40	1
Chapter IV		
Barker, M., "On the Use of Very Small Pitot Tubes for Measuring Wind Velocity," <u>Proc. Royal Soc.</u> London, A101, (1922), pp. 435-445.	82	1
Chaplin, R., "Multichannel Slip Rings for Stress and Temperature Measurement," National Gas Turbine Establishment, Pyestock, Hants, Great Britain, Memorandum Number M.289, (December, 1956), p. 7.	65	1

	Page	Footnote
	No.	No.
Davies, P. O. A. L., "The Behaviour of a Pitot Tube in Transverse Shear," Aeronautical Research Council, (December, 1957), F. M. 2619, Fluid Motion Sub-Committee, (December, 1957).	85	3
Dean, R. C., Jr., <u>Aerodynamic Measurements</u> (Boston; Eagle Enterprises, 1953), p. 60.	92	2
DeFrate, L. A., "Application of the Interferometer to the Study of Boundary Layers," Sc.D. Dissertation, M.I.T., 1950.	104	1
Deissler, R. G., "Analytical and Experimental Investigation of Adiabatic Turbulent Flow in Smooth Tubes," NACA, TN 2138, (July, 1950).	80	3
Hall, I. M., "The Displacement Effects of a Sphere in Two Dimensional Shear Flow," <u>Journal of Fluid Mechanics</u> , Vol. 1, Part 2, (July, 1956), 142-162.	85	1
Horton, B. M., "Sliding Contacts to Transmit Signals," <u>Rev. Sci. Insts.</u> , Vol. 20, Number 12, (December 1949), pp. 930-932.	65	2
Hurd, C. W., K. P. Chesky, and A. H. Shapiro, "Influence of Viscous Effects on Impact Tubes," J. Appl. Mech., Vol. 20, (1953), pp. 253-256.	82	3
<u>International Critical Tables</u> (first ed., McGraw-Hill Book Company, New York, 1929) Vol. IV, p. 21, Vol. VI, p. 341, p. 342.	107	1

	Page	Footnote
	No.	No.
Ladenburg, R. and D. Bershader, "Optical Studies of Boundary Layer Phenomena on a Flat Plate at Mach Number 2.35," Final Technical Report for Contracts NRO61 and N6pri-105, Task II, Palmer Physical Laboratory, Princeton, New Jersey, Dec. 15, 1952. See Chapter VIII, The Refraction Error by G. P. Wachtell.	103	1
Ladenburg, R. W., B. Lewis, R. N. Pease, H. S. Taylor, <u>Physical Measurements in Gas Dynamics and Combustion</u> (Princeton, New Jersey: Princeton University Press, 1954), pp. 112-118.	82	2
Lighthill, M. J., "Contributions to the Theory of Pitot-Tube Displacement Effect," <u>Journal of Fluid Mechanics</u> , Vol. 2, Part 5, (July 1957), pp. 493-512.	85	1
Livesey, J. L., "Design of Total Pressure Probes for Minimum Interference with Measured Flow," J. Aero. Sci., Vol. 21, (Sept., 1954), p. 641.	85	2
MacMillan, F. A., "Experiments on Pitot Tubes in Shear Flow," Aeronautical Research Council, R and M 3028, (Feb., 1956).	86	1
MacMillan, F. A., "Liquid Manometers with High Sensitivity and Small Time Lag," <u>J. Sci. Instr.</u> , V. 31, 1954, p. 17.	91	2

	Page	Footnote
	No.	No.
MacMillan, F. A., "Viscous Effects on Flattened Pitot Tubes at Low Speeds," Aeronautical Research Council, Fluid Motion Sub-Committee, FM2081a, Oct. 1954.	82	4
Matting, F. W., D. R. Chapman, J. R. Nyholm and A. G. Thomas, "Turbulent Skin-Friction at High Mach Numbers and Reynolds Numbers in Air and Helium," NASA Technical Report R-82, 1961.	87	2
Staff of the Aerodynamics Division, N.P.L., Ministry of Aviation, "On the Measurement of Local Surface Friction on a Flat Plate by Means of Preston Tubes," Aeronautical Research Council R and M No. 3185, May 1958, Published 1961.	87	1
Rayle, R. E., "An Investigation of the Influence of Orifice Geometry on Static Pressure Measurements," MIT, SM Thesis, Dep't. of Mech. Engr., (1949).	90	1
Smith, A. M. O., J. S. Murphy, "Micromanometer for Measuring Boundary Layer Profiles," <u>Rev. Sci. Inst's.</u> , Vol. 26, Number 8 (Aug., 1955).	90	3
Tanner, L. H., "The Design and Use of Interferometers in Aerodynamics," Aeronautical Research Council, R and M No. 3131, Sept., 1957.	93	3
Tanner, L. H., "The Optics of a Mach-Zehnder Interferometer," Aeronautical Research Council R and M 3069, Oct. 1956.	93	2

	Page	Footnote
	No.	No.
Taylor, G. I., "Measurements with a Half-Pitot Tube," Proc. Roy. Soc. (London), Ser. A, Vol. 166, 1938, pp. 475-481.	87	3
Von Doenhoff, A. E., "Investigation of the Boundary Layer About a Symmetrical Airfoil in a Wind Tunnel of Low Turbulence, NACA WR-L-507, 1940.	87	4
Wachtell, G. P., "Refraction Error in Interferometry of Boundary Layer in Supersonic Flow Along a Flat Plate," Ph.D. Dissertation Princeton University, 1951.	103	2
Young, A. D. and J. N. Maas, "The Behaviour of a Pitot Tube in a Transverse Total Pressure Gradient," Aeronautical Research Council, R. and M. 1770 1936.	85	1
Chapter V		
DeFrate, L. A., "Application of the Interferometer to the Study of Boundary Layers," Sc.D. Dissertation, M.I.T., 1950.	115	1
Howes, W. L. and D. R. Buchele, "Practical Considerations in Specific Applications of Gas Flow Interferometry," NACA TN 3507, July, 1955	115	3
Jenkins, F. A. and H. E. White, <u>Fundamentals of Optics</u> (2nd ed; McGraw-Hill Book Company, Inc., 1950), pp. 238-239.	115	4
Wachtell, G. P., "Refraction Error in Interferometry of Boundary Layer in Supersonic Flow Along a Flat Plate," Ph.D. Dissertation, Princeton University, 1951.	115	1

	Page	Footnote
	No.	No.
Chapter VI		
Edelman, G. M., and M. H. Bright, "The Specific Refractivity of Gases for Various Wavelengths of Light," Gas Turbine Laboratory Report, No. 6, Cambridge Massachusetts, M.I.T., May, 1948, p. 5.	127	1
Lanczos, C., <u>Applied Analysis</u> (Prentice-Hall, Inc., Englewood Cliffs, New Jersey, 1956), pp. 315-324.	146	1
Lauffer, J., "The Structure of Turbulence in Fully Developed Pipe Flow," NACA TN 2954, 1953.	139	3
Lin, C. C., Turbulent Flows and Heat Transfer (Princeton University Press, Princeton, New Jersey, 1959), Section E, by R. G. Deissler, p. 230.		1
McAdams, W. H., Heat Transmission, (2nd ed; McGraw-Hill Book Company, Inc., New York, 1942), Table XIII, p. 59.	122	1
Sleicher, Jr., C. A., Trans. ASME, vol. 80, 1958, Table 1, p. 699.		2
Sleicher, Jr., C. A., Ph.D. Dissertation, University of Michigan, 1955.	139	1

	Page	Footnote
	No.	No.
Chapter VII		
Dike, P. H., "Thermocouple Thermometry," (Leeds and Northrup Company, Philadelphia, 1954), p. 18.	154	1
Wilson, Jr., E. B., <u>An Introduction to Scientific Research</u> (McGraw-Hill Book Company, Inc., New York, 1952), p. 272.	150	1
Chapter VIII		
MacPhail, D. C., Turbulence in a Distorted Passage and Between Rotating Cylinders," Ph.D. Dissertation, University of Cambridge, 1941, as reported by A. A. Townsend, <u>The Structure of Turbulent Shear Flow</u> , p. 303, Fig. 12-3.	171	2
Townsend, A. A., <u>The Structure of Turbulent Shear Flow</u> (Cambridge at the University Press, 1956), p. 298.	171	1
Van Driest, E. R., "On Turbulent Flow Near a Wall," Heat Transient and Fluid Mechanics Institute Preprints of Papers, Paper 12, University of California, 1955.	214	2
Taylor, G. I., "Fluid Friction Between Rotating Cylinders," I-Torque Measurements, Proc. Roy. Soc. (London) ser. A, vol. 157, 1936, pp. 546-564.	191	2

	Page No.	Footnote No.
Wagner, E. M., "Frictional Resistance of a Cylinder Rotating in a Viscous Fluid Within a Coaxial Cylinder," Thesis for Degree of Engineer, Stanford University, June 1932.	191	1
Appendix I		
Price, E.,-NAVORD Report No. 1182 (1949).	254	1
Price, E., Review of Scientific Instruments, vol. 23, Number 4, April 1951, p. 162.	254	2